Where we are tells us where we are going: the role of allocentric location cues in the visual guidance of walking

Danlu Cen

A Thesis Submitted to Cardiff University for the Degree of Doctor of Philosophy

2017

DECLARATION

This work has not been submitted in substance for any other degree or award at this or any other university or place of learning, nor is being submitted concurrently in candidature for any degree or other award.

Signed ……..... (candidate) Date ……28/09/2017……

STATEMENT 1

This thesis is being submitted in partial fulfillment of the requirements for the degree of ……(insert MCh, MD, MPhil, PhD etc, as appropriate)

Signed ……..... (candidate) Date ……28/09/2017……

STATEMENT 2

This thesis is the result of my own independent work/investigation, except where otherwise stated, and the thesis has not been edited by a third party beyond what is permitted by Cardiff University's Policy on the Use of Third Party Editors by Research Degree Students. Other sources are acknowledged by explicit references. The views expressed are my own.

Signed ……..... (candidate) Date ……28/09/2017……

STATEMENT 3

I hereby give consent for my thesis, if accepted, to be available online in the University's Open Access repository and for inter-library loan, and for the title and summary to be made available to outside organisations.

Signed ……..... (candidate) Date ……28/09/2017……

STATEMENT 4: PREVIOUSLY APPROVED BAR ON ACCESS

I hereby give consent for my thesis, if accepted, to be available online in the University's Open Access repository and for inter-library loans **after expiry of a bar on access previously approved by the Academic Standards & Quality Committee.**

Signed ……..... (candidate) Date ……28/09/2017……

Summary

Does location information play any role in the visual guidance of walking towards a target? So far, the human walking literature has focused on two cues: optic flow (the pattern of motion at the eye) and the egocentric direction of the target. In stark contrast, in the related areas of animal navigation, the role of location information has been found to be particularly important. To address this gap, this thesis explored the role of allocentric location cues in visually guided walking.

In a series of experiments, participants were asked to walk to a target wearing prisms or "virtual prism" which introduced an offset between their visual direction and walking direction. The salience of allocentric location cues was manipulated and the relative use of cues was evaluated by the curvature of the trajectories.

Chapter 3 demonstrates the role of allocentric location cues. Trajectories were examined in four virtual environments with varying amount of optic flow and allocentric location cues. The pattern could not be explained by the richness of optic flow but is better captured by allocentric location cues. In addition, the pattern of heading judgements in the same environments was a poor predictor of the trajectories. Following this, Chapter 4 considers the impact of the target location on the walking trajectories.

Chapter 5 uncovers a role of prior experience with the environment in the guidance of walking. The effect is robust when the availability of visual cues is limited in the environment. To further explore the use of prior knowledge, Chapter 6 aims to replicate an earlier study which has shown an effect of an allocentric representation on steering (Andersen & Enriquez, 2006).

Taken together, the results in this thesis provide evidence for an important role of allocentric location cues and prior experience with the environment in the visual guidance of walking.

Acknowledgements

My heartfelt thanks

To Simon and Seralynne

for guidance, dedication, inspiration and patience.

I'm so lucky to have had you as my supervisors

To John

for being a wonderful mentor.

To My Family

for all the love and support.

To My Friends

Jiangyi, Danying, Jilu, Phoebe, Zoe, Beth, Kait, Stephanie, Katja

for making my life so enjoyable

To those who in any way helped this project

Dave, Yulia, Matt, Keven, Den, Scot, and all my participants

Thank you!

Table of Contents

1 General Introduction

1.1 Introduction

Imagine you are enjoying a visit to the Charlottenburg Palace. You come to the Green Room and would like to have a look at the fireplace at the end of this room (**Figure 1.1**). What visual information would you use to guide yourself walking to it? The question is interesting as the same strategy (or strategies) might be used by our prehistoric ancestors when they were approaching a prey, reaching a tree bearing fruits or walking towards their shelters.

Figure 1.1 *A view of inside of a room in Charlottenburg Palace. The fireplace is on the wall opposite to the view.*

Nearly seventy years ago, Gibson proposed that *optic flow* is what we use in visually guiding our locomotion (Gibson, 1950, 1958, 1979). As shown in **Figure 1.2a**, when we move forward, the relative motion of the surrounding scene projects a radial pattern at our eye. The expansion originates from a singularity, the *focus of expansion* (FoE), which corresponds to the point in the environment toward which we are moving. Therefore, by keeping the FoE aligned with your target (the fireplace in the example) while walking, you will ultimately reach it (**Figure 1.2b**).

Alternatively, as proposed by Rushton and colleagues (Rushton, Harris, Lloyd, & Wann, 1998), you could just walk to the target (i.e. the fireplace) by keeping it aligned with your perceived straight-ahead (**Figure 1.2c - d**). As this strategy utilises the direction of the target relative to the midline of your body, it is termed as *egocentric direction* strategy.

A third strategy is to use your location (position and orientation) with respect to the environment, namely *allocentric location information*. If you are walking in an enclosed environment as in the example, based on information such as the perspective shape of the walls and distance to the walls, you may have a strong sense of where you are and where you are heading with respect to the environment. Relying on the allocentric information about your location, you could steer your locomotion to approach the target (**Figure 1.2e-f**).

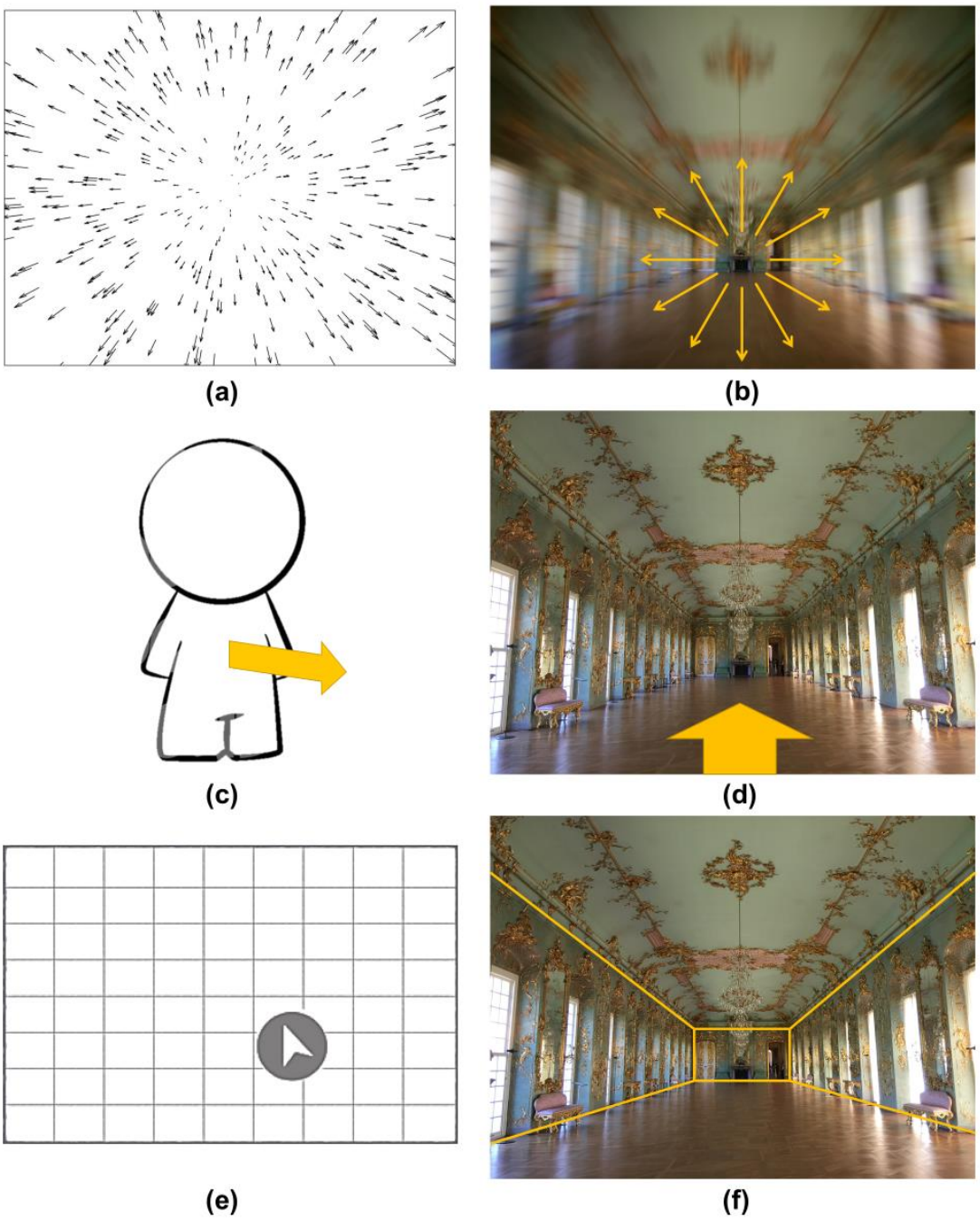

Figure 1.2 (a) *Radial optic flow field, the pattern projected at the eye of an observer by a translational forward movement.* ***(b)*** *By keeping the centre of the flow field, or the focus of expansion (FoE) over the target (i.e. fireplace), an observer would ultimately reach it.* ***(c)*** *Egocentric direction, the direction of an object relative to the perceived midline of the body.* ***(d)*** *By keeping the perceived straight-ahead pointing at the target (i.e. fireplace), an observer would ultimately reach it.* ***(e)*** *Position and orientation of an observer with respect to the environment, or allocentric position and orientation.* ***(f)*** *Geometric information and other features of the room can inform an observer about his/her allocentric position and orientation. Based on this information, the observer would ultimately reach the target (i.e. fireplace).*

So far, the literature on human walking has exclusively focused on the first two cues, optic flow and egocentric direction, and there has been an ongoing debate as to which one is the primary cue in the visual guidance of walking (Fajen & Warren, 2000; Rushton, 2008; Wann & Land, 2001; Warren, Kay, Zosh, Duchon, & Sahuc, 2001). In stark contrast, in the field of spatial learning and navigation, an accumulating body of work has demonstrated the key role of *allocentric location cues*. Thus, there appears to be a gap between the two fields. To address this gap, this thesis will take on the task to explore the role of allocentric location cues in the visual guidance of walking.

In this chapter, I will first briefly review optic flow and egocentric direction hypotheses before introducing allocentric location cues. At the end of the chapter, an overview of the thesis will be outlined.

1.2 Optic flow

The idea of optic flow comes from research on landing an aircraft. During landing, the pilot will see the image of the runway expanding outward with the visual speed of elements of the image scaling with inverse distance and eccentricity. The origin from which the image expands, or the *focus of expansion* (FoE), corresponds to the point at which the plane is flying (see **Figure 1.3**). The significance of such expanding flow patterns in the guidance of landing aircraft was first recognised by Grindley. In his report to the Air Ministry in the early 40s, Grindley described the information from such expanding patterns as *velocity cues* and concluded that 'a pilot could land an aeroplane safely *on the basis of velocity cues along*' (as quoted in Mollon, 1997). In 1950, Gibson took the idea and introduced it to the academic world in his influential books and articles (Gibson, 1950, 1958, 1979). At the same time, another scholar from an engineering background also formed similar ideas about the utility of optic flow in landing an aircraft (Calvert, 1950, 1954).

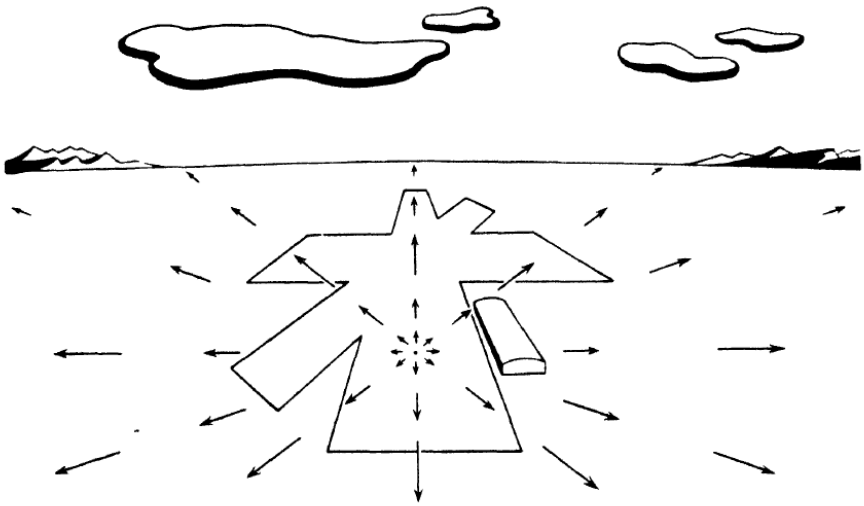

Figure 1.3. *An illustration for the landing of an aircraft using optic flow. The arrows represent the image motion at the pilot's eye during the landing glide. Taken from Gibson's book "The Perception of the visual world" (1950).*

The idea of optic flow was then generalised by Gibson to the guidance of other types of locomotion including walking. That is, the walking observer first recovers the direction of the self-motion, or heading[1], which is specified from the FoE; then by aligning the FoE with the intended target, the observer will reach it.

1.2.1 Optic flow in heading perception

Thus far, the concept of optic flow has stimulated a substantial body of work encompassing psychophysical, neurophysiological, computational modelling and computer vision (for an excellent review see Lappe, Bremmer, & van Den Berg, 1999). Most of the attention has been paid on heading perception. A typical paradigm used in empirical works is to present a simulated movement on a computer screen and to ask subjects to indicate the direction of the movement relative to the target. In their study, Warren, Morris, & Kalish

[1] The meaning of *heading* is ambiguous. In the visual research literature, the word is used to refer the current direction of travel, or *aimpoint*. In vehicular control and aircraft/watercraft navigation, *heading* is used to refer the facing direction of the vehicle (static or mobile). The moving direction of the vehicle, however, is called the *course* or *track* in the flying or *bearing* in the sailing. Due to existence of crosswinds or crosscurrents, the vehicle often moves in a direction different from its facing direction. To maintain agreement with the visual research literature, we use *heading* to designate the instantaneous travel direction.

(1988) simulated a translational forward movement[2] through a world consisting of a plane of randomly positioned points and manipulated the number of the dots systematically. The accuracy of heading perception was found to be considerably high (1° ~ 2°), within the critical range required for safe control of locomotion (Cutting, Springer, Braren, & Johnson, 1992). The accuracy remained high even when the number of the dots on the display was down to 10 and regardless of stimuli speed, suggesting a robust heading perception during pure forward translation based on optic flow.

1.2.1.1 Heading perception during eye (and/or head) rotation

Our eyes (and head) seldom remain static during natural walking. In such cases, more complicated flow patterns are painted at the retinal, called *retinal flow*, in which the FoE does no longer correspond to the actual walking direction. Instead, it coincides with the place that we are looking at (Regan & Beverley, 1982; see **Figure 1.4**).

How to determine heading under such a complicated situation? The approaches that have been proposed so far mainly focus on reconstruction of the FoE from the complicated pattern of retinal flow. Because the movement of the eye can be described by a combination of translation and rotation, the pattern of retinal flow can be considered to consist of two components that respectively correspond to the translation and rotation of the eye movement

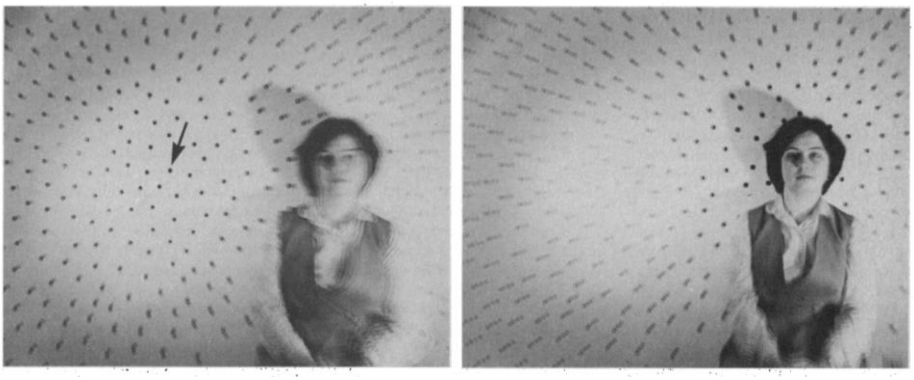

Figure 1.4. *Retinal flow patterns with eye rotations. Right panel shows the pattern resulting from looking at the womans's head while moving towards her. In this case, the FoE corresponds to the heading. Left panel shows the pattern resulting from looking at a point on one side of the woman while moving towards her. In this case, the FoE does not coincide with the heading. Instead, it corresponds to the direction of the gaze. Taken from Regan and Beverly (1982).*

[2] Here I only discuss the situations that involve a translational movement. For situations of curvilinear movements, interested readers are directed to (Lee & Lishman, 1977; Wann & Land, 2000; Wann & Swapp, 2000; Warren, Mestre, Blackwell, & Morris, 1991).

(Koenderink & van Doorn, 1981; Longuet-Higgins & Prazdny, 1980). The translational component coincides with optic flow and the FoE corresponding to the moving direction; whereas the rotational component is superimposed on the translational component and shifts the FoE. Therefore, to determine heading in this case, one could subtract the rotational component from the retinal flow pattern and reconstruct the FoE from the translational component.

How to detect and subtract the rotational component then? One solution is to use non-visual extraretinal signals that accompany the eye or head movements. These extraretinal signals include proprioceptive and vestibular signals or an efference copy of the motor command to the eye and/or neck muscles (Banks, Ehrlich, Backus, & Crowell, 1996; Thomas Charles Augustus Freeman, Champion, Sumnall, & Snowden, 2009; Souman & Freeman, 2008). They are used to compensate for the rotational component of the retinal flow and to reconstruct the FoE. Another solution suggests that retinal flow itself contains sufficient information to separating the rotational and translational components (Gibson, 1950).

A typical approach to address the relative contribution of visual and extraretinal information is to compare the accuracy of heading judgements with and without extraretinal cues (Cutting, 1986; Rieger & Toet, 1985). While fixating a stable point on the screen, participants are shown a retinal flow pattern that is normally experienced during translational movement with eye rotations. As the participants' eyes remain stationary, the extraretinal information that would be available during real eye movements is absent. By doing this a "conflict condition" is created, in which visual and extraretinal signals are put into conflict. Conversely, a situation where the participants are making a real pursuit eye movement during the presentation of pure optic flow is called "non-conflict" condition. In this condition, extraretinal cues are available and congruent with visual cues.

In the conflict situation, results are variable. Warren and Hannon (1988, 1990) found the heading judgements were still accurate (mean heading error = 1.5°) with the conflict. However, they only tested situations where rotation rates were slow (< 2°/s). Banks and colleagues have examined situations with higher rotation rates and found poorer performance with larger errors (Banks et al., 1996; Royden, Banks, & Crowell, 1992; Royden, Crowell, & Banks, 1994). They thus concluded that, when rotations rates are higher than 1°/s, extraretinal signals are required. However, other researchers found reasonable performance at rotation rates up to 16°/s, supporting the hypothesis of visual decomposition (Cutting, Vishton, Flückiger, Baumberger, & Gerndt, 1997; Rieger & Toet, 1985; Stone & Perrone, 1997; van

den Berg, 1992). Li and Warren (2000) later proposed that heading could be accurately determined on the basis of retinal flow alone given that dense motion parallax is present.

In the non-conflict situation when extraretinal information is available from real eye rotation, performance is overall higher than in the conflict condition without extraretinal information (Banks et al., 1996; Royden, Crowell, & Banks, 1994; van den Berg, 1992; van den Berg, 1996; Warren & Hannon, 1990), suggesting that extraretinal information is used in compensation for eye rotation. Interestingly, small errors still occurred in the non-conflict condition – participants' responses were displaced to a small degree in the direction of eye rotation. When asked to make pursuit eye movements to a sinusoidally moving target while a forward translational movement was simulated, participants reported that they perceived self-motion oscillating at the same frequency as the pursuit eye movement, a phenomenon called the *slalom illusion* (Freeman, Banks, & Crowell, 2000). The illusion provides further support for the use of extraretinal information in the perception of self-motion.

Other researchers argued that decomposition of the retinal field is not required for heading perception, and some alternative approaches have been proposed (see Warren & Hannon, 1990 for a more complete list and discussion of theories). For example, the heading can be detected using the relative motion and velocities of near and far objects against the fixated target, namely *motion parallax*. Based on this, Cutting and colleagues (1992) proposed two sources of information that could be used to estimate heading. The first is called *differential motion parallax* (DMP). When a moving observer fixates and pursues a target object, the objects nearer than the target will normally appear to move faster than and in the opposite direction from those objects that are further than the target. Therefore, the observer can detect the heading by looking in the opposite direction to the most rapid flow in the retinal array. To test DMP, heading judgements with DMP violations can be compared to those without. Using this paradigm, Cutting et al. (1992) found that the heading judgements were highly accurate without DMP violations (95% performance for a gaze-movement angle of 2° and considerably got worse with DMP violations. The results provided evidence for DMP as a source of information for heading judgements. In addition, there is neurophysiological evidence from other species suggesting that visual system is able to pick up DMP information (Allman, Miezin, & McGuinness, 1985; Bridgeman, 1972; Frost & Nakayama, 1983; Judge, 1990; Nakayama, 1985; Roy & Wurtz, 1990). Further, DMP-like schemes have also been developed in machine vision (Rieger & Lawton, 1985). The second source is called *inward motion* (IM), which refers to the distant object beyond the fixated object moving slowing towards the fovea. The velocity of this inward movement indicates

how far the gaze is from the point where the observer is heading. There is some neurophysiological evidence for the existence of cortical neurons that respond to IM information (Perrett, Harries, Mistlin, & Chitty, 1990).

1.2.1.2 Other cues in heading perception

In addition to optic flow, other cues have been demonstrated to play a role in the determination of heading. For example, Beusmans (1998) has shown that the change of perspective shape of an object can provide information about an observer's heading. The author put optic flow and configural information in conflict by using a Mach-Ames house. In the experiment, the outline of the Mach-Ames house was a concave corner but would be misleadingly perceived as a convex house. Consequently, if moving towards the left of the Mach-Ames house, the observer would believe that the movement was towards the right (for illustration see **Figure 1.5**) which was opposite to the direction that would be perceived from optic flow.

Another line of research has focused on scene-based strategy in determining heading. In the study by Hahn, Andersen and Saidpour (2003), participants were able to judge the

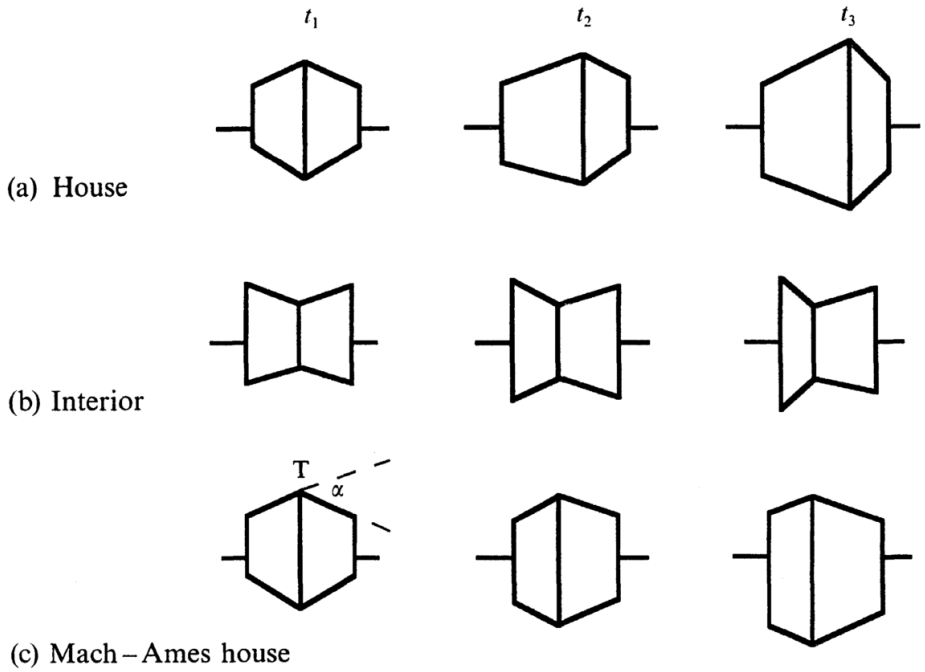

Figure 1.5. *Schematic sample views of an observer's movement towards the left of the exterior of a house* ***(a)****, the interior of a house* ***(b)*** *and the Mach-Ames house* ***(c)****. In* ***(a)*** *and* ***(b)*** *it can be clearly seen that the movement is to the left of the object. However, in* ***(c)*** *the direction of the movement appears to be towards the right. From Beusmans (1998).*

heading from a sequential presentation of static real-world scenes. The interval between the two frames was deliberately set to be large in order to eliminate apparent motion. However, the authors found that the process of heading judgement from static scenes had a coarse spatial resolution (i.e., the large displacement between frames) and was capacity limited. Cutting and colleagues proposed that heading is determined on the basis of the spatial displacement of objects in the scene (Vishton & Cutting, 1995). Similar to Hahn et al.'s (2003), the authors presented the stimuli in an intermittent way in order to remove motion information (Vishton & Cutting, 1995, Experiment 4 & 5). They found that the performance of heading was adequate as required by the criteria for safe locomotion (<3.3° at 22m/s), given that the stimuli were identifiable. They concluded that it is the spatial displacement of objects from the previous location, rather than the flow field, that specifies heading.

1.2.1.3 Neuronal mechanisms underlying heading perception from optic flow

Numerous neurophysiological and neuroimaging studies have been carried out on monkeys and humans to understand neural mechanisms underlying heading perception by optic flow.

In monkeys, neurons have been found in several cortical areas to be selective for optic flow stimuli including the medial superior temporal (MST) area (especially the dorsal region), the ventral intraparietal (VIP) area, the area 7a, the anterior superior temporal polysensory (STPa) area, the caudal portion of area PE (PEc) and the motor cortex (see Lappe, 2000 and Raffi & Siegel, 2004 for a review). Among these areas, area MST has received most attention (see Duffy, 2000 for a review). Neurons in this area have shown several functional features that make area MST an ideal candidate for the analysis of optic flow fields. First, MST neurons have large receptive fields and could support processing global visual motion (Komatsu & Wurtz, 1988b; Tanaka et al., 1986). Second, MST neurons respond to elements of optic flow stimuli such as planar, radial and circular patterns (Tanaka, Fukada, & Saito, 1989; Tanaka & Saito, 1989), and the responses form a continuum for different types of optic flow stimuli (Duffy & Wurtz, 1991) and are tuned for the position of FoE (Duffy & Wurtz, 1995). Third, MST neurons are sensitive to speed gradients in the optic flow stimuli which reflects the three-dimensional structural layout of the visual environment (Duffy & Wurtz, 1997; Duffy, 2000) Moreover, applying electrical microstimulation on area MST during the heading discrimination task biased the monkey's decisions about the heading, suggesting that area MST is directly involved in computation of heading from optic flow (Britten & van Wezel, 1998).

With regards to perception of optic flow during eye-movement, a number of studies have shown that MST neurons also respond to pursuit eye movements (Erickson & Thier, 1991; Ilg & Thier, 2003; Komatsu & Wurtz, 1988a, 1988b; Kurkin, Akao, Shichinohe, Fukushima, & Fukushima, 2011; Newsome, Wurtz, & Komatsu, 1988). These findings suggest that MST neurons may play a role in compensating for the rotation induced by eye movements (Bradley, Maxwell, Andersen, Banks, & Shenoy, 1996; Page & Duffy, 1999; but see Andersen, Shenoy, Crowell, & Bradley, 1999).

In humans, related changes in regional cerebral blood flow (PET) or blood oxygenation (fMRI) are monitored during the heading discrimination task. Like in monkeys, studies on humans also show several areas that are sensitive to flow patterns. These areas include the human MT+ complex which is the homologue of monkey MT and MST areas (Dukelow et al., 2001; Huk, Dougherty, & Heeger, 2002; Morrone et al., 2000; Peuskens, Sunaert, Dupont, Van Hecke, & Orban, 2001; Smith, Wall, Williams, & Singh, 2006), the V3a and KO/V3b areas (Dupont et al., 1997; Pitzalis et al., 2010; Rutschmann, Schrauf, & Greenlee, 2000; Seiffert, Somers, Dale, & Tootell, 2003; Smith, Greenlee, Singh, Kraemer, & Hennig, 1998; Tootell et al., 1997; Van Oostende, Sunaert, Van Hecke, Marchal, & Orban, 1997), the V6 area (Cardin, Hemsworth, & Smith, 2012; Cardin & Smith, 2010; Pitzalis et al., 2006, 2010), the anterior portion of the intraparietal sulcus (VIP) and cingulate sulcus visual area (CSv) (Wall & Smith, 2008).

1.2.2 Optic flow in the guidance of walking

As outlined above, a substantial body of studies has been inspired by Gibson's optic flow theory. The great majority of the research effort, however, has focused on heading perception. It raised the question of what people actually do in the guidance of locomotion (Nakayama, 1994). Using a perturbation paradigm (Rushton, Harris, Lloyd, & Wann, 1998) that will be described below, some evidence for the use of optic flow in the online guidance of walking was obtained (Warren et al., 2001; Wood, Harvey, & Young, 2000). Especially in Warren et al. (2001), a conclusion was made that the contribution of optic flow is proportional to its richness. The findings by Warren et al. (2001) has been widely cited as the strongest evidence for the use of optic flow in the visual guidance of walking. However, as we will discuss in Chapter 3, the contribution of other cues was not isolated in their study. We will return to the details of this study after introducing the logic behind the standard perturbation paradigm that they used in the following section.

1.3 Egocentric direction of target

Rushton and colleagues have challenged the view that optic flow has a central role in the visual guidance of human walking. They proposed that walking is guided by the egocentric direction of the target (Rushton et al., 1998). The idea is simple – if you walk to keep the target at your perceived straight ahead then you will reach it by a straight-line trajectory. In this case, the recovery of heading is not needed.

Unlike optic flow, the first evidence for the egocentric direction hypothesis came directly from a walking experiment, which was inspired by a peculiar walking pattern of a patient with unilateral visual neglect, W.V. When walking to an intended target, W.V.'s trajectory veered, which was not compatible with the optic flow theory. Instead, the trajectory was better captured by the egocentric direction hypothesis – the direction of the target was misperceived in W.V.'s case and could result in a curved trajectory. Motivated by this observation, Rushton and colleagues conducted a study on healthy participants to see whether similar trajectories could be obtained by perturbing the participants' perceived direction.

In this experiment, Rushton and colleagues use wedge prisms to displace the participants' perceived straight ahead. Prism laterally rotates the whole visual field. For example, if the prism rotates the visual field to the right, a target that is actually straight ahead will appear to the right. If the observers rely on the egocentric direction of the target to guide their walking, they would take a distinctively curved trajectory to the target (see Chapter 2 for more details). Importantly, prisms shift the whole visual field and thus should not interfere with the use of optic flow to guide walking. Therefore, if the observer relying on optic flow he or she would take a straight line to the target (after an initial step in the wrong direction). Results showed that the observers took curved trajectories that are characteristic of the sole use of egocentric direction.

The findings of Rushton et al. (1998) have been replicated and extended by follow-up studies using both prisms (Harris & Carré, 2001; Rogers & Allison, 1999; Rogers & Dalton, 1999; Wood, Harvey, & Young, 2000) and virtual reality technologies (Saunders et al., 2011; Warren et al., 2001; see Chapter 2 for details about implementing prisms effects using VR).

The view of using egocentric direction challenged the dominance of the flow-based theories in the field of locomotion control. To confront the challenge, Warren and colleagues (2001) conducted the study that we have mentioned above. In this study, the same perturbation paradigm was employed using virtual reality (VR) techniques. They created four

different virtual worlds that varied in visual complexity and displaced the walking direction specified by optic flow from the actual walking direction. They found that the walking trajectories became straighter as the visual complexity of the virtual world increased. The authors interpreted this trend of straightening as being due to the increase in the observer's reliance on optic flow. They thus concluded that egocentric direction is always used but the role of optic flow becomes dominant when its richness increases in the environment. Now it is generally agreed that both perceived egocentric direction and optic flow are used in the visual guidance of walking, but the debate about which one is the primary cue has still been going on (Fajen & Warren, 2000; Harris, 2001; Harris & Rogers, 1999; Harris & Carré, 2001; Lappe, Bremmer, & van Den Berg, 1999b; Rushton, 2008; Rushton & Salvucci, 2001; Wann & Land, 2001).

1.3.1 Target drift

Before Rushton et al. (1998), Llewellyn (1971) brought about a related idea that change of the egocentric direction of a target provides a source of information about the observer's walking direction, namely *target drift*. The strategy is thus based on a temporal derivative of target direction.

When heading straight towards a target, the target will appear to remain at the straight ahead of the observer. However, if the observer deviates off course, the target will appear to move in a direction opposite to the observer's deviation at each step (see **Figure 1.6** for illustration). Therefore, the apparent drift of the target informs about the walking direction of the observer. The magnitude of the drift is proportional to step size, the distance from the straight ahead and the distance from the target (Rushton, 2004). To reach the target, the observer can walk to cancel the drift. Mathematically, if an observer walks to cancel the target drift by keeping it in a fixed

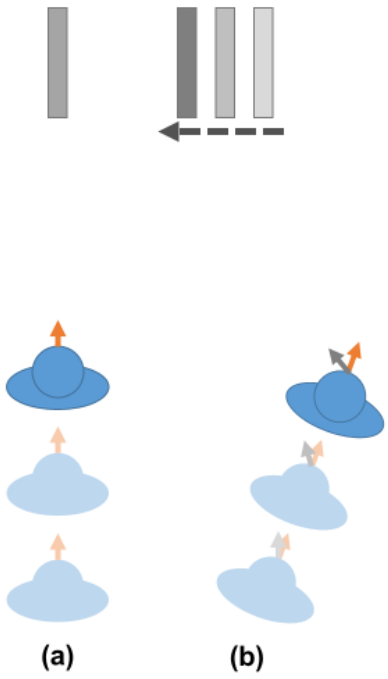

***Figure 1.6**. Illustration of Llewllyn's (1971) target drift hypothesis. **(a)** If an observer walks directly towards the target, the target will not appear to drift. **(b)** If an observer walks to the right side of the target, the target will appear to drift to the left relative to the observer.*

direction other than the straight ahead, he or she will end up with an equal-angular spiral to the target (Rushton & Harris, 2004; Rushton, Wen, & Allison, 2002). As computationally demonstrated by Rushton and Harris (2004), if the observer overcompensates for the target drift by walking to the direction of the drift (e.g., left in **Figure 1.6**), the trajectory will become straighter.

1.3.2 Neuronal underpinnings of egocentric direction

The parietal areas, especially the posterior parietal cortex, have a well-established role in supporting both perception and action in an egocentrically represented space (i.e., with reference to the position of the eye, head or body). The most compelling evidence comes from single-unit recordings in monkeys and lesion cases in humans.

1.3.2.1 Single-unit recordings in monkeys

In monkeys, neurons in the posterior parietal cortex have been found to encode visual space in egocentric coordinates that are centred on eyes, head and potentially body. A typical research is to train monkeys to fixate a visual target on the screen while ignoring a secondary stimulus flashed briefly at a different location on the screen. The receptive field of a neuron is mapped by recording the neuron's response to the secondary stimulus at various locations on the screen. After the receptive field of the neuron is mapped, the monkey's gaze is shifted to another location on the screen while the secondary stimulus is placed at the peak location of the response profile of the neuron. As the monkey's head is fixed, if the neuron encodes the stimulus in eye-centred coordinated, the response of the neuron will change when the monkey's gaze is directed to different places; otherwise, the neuron may encode the stimulus in at least head-centred coordinated. Andersen and colleagues found that, for neurons in the area 7a, the receptive field remains retinotopic but the magnitude of the response is modulated by eye position in the orbit (Andersen, Essick, & Siegel, 1985). This gaze-dependent response is well captured by a neural network model that simulates calculation of visual space in head-centred coordinates (Andersen & Zipser, 1988). Based on the findings, Andersen and colleagues proposed a model that visual space is indirectly encoded in head-centred coordinates at the population level by the distributed activity of neurons.

The gaze-dependent response has also been found in other parietal regions, including the lateral intraparietal area (LIP) (Andersen, Bracewell, Barash, Gnadt, & Fogassi, 1990), ventral intraparietal area (VIP) (Duhamel, Bremmer, Ben Hamed, & Graf, 1997) and the anterior bank of the parieto-occipital sulcus (PO) (Galletti, Battaglini, & Fattori, 1993).

In addition to the gaze-dependent response, cells whose response is modulated by the head orientation have also been found in the posterior parietal cortex (Brotchie, Andersen, Snyder, & Goodman, 1995). In their study, Brotchie and colleagues manipulated the monkey's eye position and head orientation separately and found that the responses of the neurons in the posterior parietal cortex were modulated by gaze direction regardless of whether the gaze was directed by the eyes or head.

In addition to the indirect coding model, Galletti, Battaglini and Fattori (1993) propose a direct coding model that stimuli can be encoded in head-centred coordinates at a single cell level. They found a small number of cells in the area V6 and PO that have responses not modulated by gaze direction. The receptive fields of these neurons remained the same spatial location regardless of eye position. The authors named these neurons as 'real-position' cells and proposed that the visual space is *directly* encoded in head-centred coordinates by these cells. The signals from these heading-centred cells can be combined to encode the spatial location of stimuli in body-centred coordinates.

The findings of the gaze-dependent effect and 'real-position' cells suggest that the posterior parietal cortex encode visual space in at least head-centred coordinates at both population level and single cell level and probably in body-centred coordinates.

1.3.2.2 Lesion cases and neuroimaging studies in humans

In humans, damage to the parietal areas produces deficits including distorted spatial attention, disorientation and spatial memory loss. The most compelling case is the neglect of the space at the contralateral side to the lesion (Chokron, 2003; Darling, Pizzimenti, & Rizzo, 2003; Rousseaux, Honoré, & Saj, 2014). Many patients show a syndrome of ignoring objects or the content of a scene in the half of their visual field contralateral to the lesion side (see Andersen, 2011 for a review). Of particular relevance is the view that such parietal neglect reflects a deviation of egocentric space representation to the ipsilesional side (Bisiach, Perani, Vallar, & Berti, 1986; Ferber & Karnath, 1999; Karnath, 1997).

In keeping with the neuropsychological data, neuroimaging studies were conducted on healthy participants, asking them to judge the location (or movement) of a visual stimulus with respect to the body. A network of frontoparietal areas has been found to be associated with the egocentric judgments, including the superior parietal lobule, intraparietal sulcus, inferior parietal lobule, precuneus and premotor areas (Darling et al., 2003; Galati et al., 2000; Saj et al., 2014; Vallar et al., 1999). Together, the results suggest a role of these areas in the representation of egocentric space.

1.4 Allocentric location cues

1.4.1 Behavioural evidence

In the field of spatial navigation, substantial attention has been placed on how animals and humans acquire an accurate sense of location and direction within the surrounding environment, which is essential for successful navigation through the environment. The location and direction can often be estimated by identifying environmental properties, which has been distinguished into two types: featural and geometric cues (Gallistel, 1990). Featural cues are non-geometric cues. They could be the colour of the wall or discrete landmarks. Geometric cues provided by the shape of the environment have been found to play a predominant role. As first demonstrated by Cheng (1986), rats were trained to find food hidden in a corner of a rectangular arena. Despite the presence of the distinctive landmarks in each corner, rats made rotational errors by visiting the geometrically correct corners. The preferential use of geometric cues has been demonstrated in other species including birds (e.g., Bingman, Erichsen, Anderson, Good, & Pearce, 2006; Kelly, Spetch, & Heth, 1998; Tommasi & Polli, 2004), fish (e.g., Sovrano, Bisazza, & Vallortigara, 2003), nonhuman primates (e.g., Gouteux, Thinus-Blanc, & Vauclair, 2001), ants (e.g., Wystrach & Beugnon, 2009), as well as in infant humans (e.g., Wang, Hermer, & Spelke, 1999) and adult humans (e.g., Hermer & Spelke, 1996). The capacity of animals to find a hidden goal using geometric cues has also been shown in an arena in the shape of a kite (Pearce, Good, Jones, & McGregor, 2004), a parallelogram (Tommasi & Polli, 2004), a triangle with a curved base (Pearce, Ward-Robinson, Good, Fussell, & Aydin, 2001), and an outline of a house (McGregor, Jones, Good, & Pearce, 2006).

Based on the information obtained from landmarks and geometric cues, a detailed internal spatial representation of the surrounding environment, a *cognitive map* could be formed, which enables the animal to take a novel route or short-cut to a destination (O'Keefe & Nadel, 1978; Tolman, 1948).

1.4.2 Neuronal substrates

Limbic system structures especially the hippocampus has been thought to play a crucial role in supporting spatial representations in an allocentric frame of reference. The most compelling evidence comes from single-unit recordings in freely-moving rats, and from lesion studies that examine how damages to the area impair the animal's performance in a spatial task.

1.4.2.1 Single-unit recordings

In these studies, the activities of neurons were recorded in an awake, freely-moving animal. The correlation between the firing rates of the neurons and the spatial relationship between the animal and the surrounding environment was examined. Three major functionally dedicated cell types have been discovered in the hippocampus and neighbouring areas. They are *place cells*, *head-direction cells* and *grid cells*. Each of these cell types shows the property of signalling an aspect of the spatial relationship between the animal and its environment. *Place cells* signal the animal's allocentric location, *head direction cells* inform about the animal's facing direction and *grid cells* tell how far the animal has travelled and in what direction.

Place cells were first found in the CA1 field of the anterior dorsal hippocampus by O'Keefe and Dostrovsky (1971). These cells fire maximally when the animal occupies or passes a particular place in the environment and become virtually silent when the animal is at another location. The region within which the neuron shows high firing rate is called the neuron's 'place field'. Each place cell has a place field at a different area of the environment (O'Keefe, 1979; O'Keefe & Conway, 1978; O'Keefe & Nadel, 1978). Collectively, a population of place cells can represent the entire surface of an environment, and such an internal representation can provide information about the animal's position with respect to the environment (O'Keefe, 1976; O'Keefe & Nadel, 1978; Wilson & McNaughton, 1993).

Head-direction (HD) cells, first discovered by James Ranck (1984), have been found in several limbic system areas including the postsubiculum (Taube, Muller, & Ranck, 1990a, 1990b), anterior thalamus (Blair & Sharp, 1995; Taube, 1995), entorhinal cortex (Sargolini et al., 2006) and lateral mammillary nucleus (Blair, Cho, & Sharp, 1998; Stackman & Taube, 1998). The firing rate of HD cells is a function of the animal's head orientation within the horizontal plane in the environment. Each HD cell is tuned to a single preferred direction. Only when the head of the animal faces this direction, the cell fires maximally, and the firing rate of the cell decrease linearly as the head deviates from the preferred direction. The recorded HD cells also showed a uniform distribution of the preferred directions that covered a 360° range (Taube et al., 1990a). In this manner, HD cells can be seen as a collection of internal compasses that point to different directions, and thought to have a functional role in informing the animal about the direction of its head orientation relative to landmarks the surrounding environment (see Taube, 1998 for a review).

Grid cells, discovered in the medial entorhinal cortex, have a firing pattern that is different from that of place cells and HD cells. Instead of responding to a single location or direction, grid cells fire at multiple discrete locations. In other words, each grid cell has more than one firing field. The spatial structure of the firing fields forms a hexagonal grid-like pattern covering the entire surface available to the animal in the environment (Fyhn, Molden, Witter, Moser, & Moser, 2004; Hafting, Fyhn, Molden, Moser, & Moser, 2005). The firing patterns of neighbouring cells are similar in terms of size, spacing and orientation, but differ in phases. As a result, the firing fields of a few cells can fully cover the environment. For a given grid cell, the distances between the firing fields are similar across environments. These properties allow grid cells to provide the animal with a measure of distance travelled from a reference point and the direction in any environment (see Rowland, Roudi, Moser, & Moser, 2016 for a review on the properties of grid cells). By interacting with other types of cells in the medial entorhinal cortex, e.g., HD cells, speed cells (signalling the moving speed of the animal) and border cells (signalling the distance to the boundary of the environment), grid cells can provide a representation of the animal's current position (Kropff, Carmichael, Moser, & Moser, 2015; Sargolini et al., 2006; Savelli, Yoganarasimha, & Knierim, 2008; Solstad et al., 2008) .

The firing fields of place, grid and head direction cells has been shown to be similarly affected by environmental cues (Hafting, Fyhn, Molden, Moser, & Moser, 2005; Muller & Kubie, 1987; O'Keefe & Conway, 1978). For example, the signals of the three spatial cell types are also strongly influenced by the geometry of the environment. For example, scaling up the size of a cylinder arena or changing a square arena into a rectangle, the firing fields of place cells frequently expand correspondingly to the change in the environment or separate into two components to represent two locations (Muller & Kubie, 1987; O'Keefe & Burgess, 1996). Similarly, the preferred firing direction of head direction cells show dramatic shifts when the shape of the environment is changed (Golob, Stackman, Wong, & Taube, 2001; Taube, Muller, & Ranck, 1990b; see Dudchenko, 2007 for a review). For example, when the rat foraged in a trapezoid-shaped environment, rotating the environment by 90° produced a corresponding shift in the firing direction of the head direction cells. The shifts, however, was more variable if the rat was in a rectangular environment, which could be due to the ambiguity in the symmetric shape of the environment (Clark, Harris, & Taube, 2012). For grid cells, it has been shown that the grid pattern rescales with changes in the size and shape of a familiar environment (Barry, Hayman, Burgess, & Jeffery, 2007). A more recent study has shown the shape of the environment to have a dramatic effect on grid patterns. When rats

are tested in irregular environments (e.g. trapezoids) the hexagonal pattern of the grid cells is broken and becomes more inhomogeneous (Krupic, Bauza, Burton, Barry, & O'Keefe, 2015).

In addition to the three types, the existence of other spatially modulated neurons have been suggested or found in the limbic system, including border cells as mentioned above. Although their properties and functional roles are less understood than the three major types, they may be by no means less important (see Grieves & Jeffery, 2017 for a review). Together, these cells can form a complex system that animals rely on for navigation.

1.4.2.2 Lesion studies

Lesions studies on rats provide converging evidence for the role of the limbic system in navigation based on the geometric information. For example, rats with hippocampal lesions were found to be impaired at finding the hidden platform in a pool with reference to the shape of the environment (McGregor, Hayward, Pearce, & Good, 2004; Pearce, Good, Jones, & McGregor, 2004). Rats with lesions within the head direction system (e.g., anterior thalamic nuclei and lateral mammillary nucleus) were impaired on similar tasks that required animals to use the shape of the environment to navigate (Aggleton, Poirier, Aggleton, Vann, & Pearce, 2009; Vann, 2011).

Navigation appears to be supported by the same network of brain structures across species. Patient studies and neuroimaging studies have highlighted the importance for a number of brain regions in humans including the hippocampus (Burgess, 2008; Maguire et al., 2000; Maguire, Intraub, & Mullally, 2015), the parahippocampal region (Aguirre, Detre, Alsop, & D'Esposito, 1996; Maguire et al., 1998; Spiers & Barry, 2015) and retrosplenial cortex (Auger, Zeidman, & Maguire, 2017; Epstein & Vass, 2014; Marchette, Vass, Ryan, & Epstein, 2014; Vann, Aggleton, & Maguire, 2009; Wolbers & Büchel, 2015). Furthermore, evidence for place and grid cells in humans has been found from studies using functional MRI (fMRI; Doeller, Barry, & Burgess, 2010; Ekstrom et al., 2003) and single-cell recordings in epilepsy patients (Jacobs et al., 2013; Miller et al., 2013).

1.4.3 A hint of use of allocentric location cues in guiding walking

As highlighted above, there is a stark contrast between the human walking literature and spatial navigation literature. While the latter has generated a substantial body of evidence

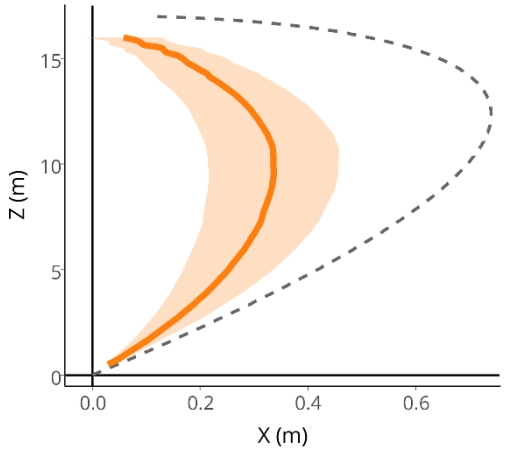

Figure 1.7 *Mean walking trajectory replotted from the data in Herlihey's study (2010). The dashed line represents the trajectory predicted by purely using egocentric direction. The solid line represents the mean walking trajectory. The shaded area corresponds to 95% confidence interval.*

for the use of spatial information in guiding the organism's navigation, the former has been exclusively focusing on optic flow and egocentric direction. A recent study has shown some intriguing results that are not compatible with either of the two strategies (Herlihey, 2010). In this study, the authors asked participants to walk to a target while wearing prism glasses. For each step, they were required to follow the process: close their eyes, take a step forward, stop and bring their feet together, open their eyes for a moment, close their eyes again and take another step forward. They were asked to repeat the process until they reached the target. By doing this, optic flow was removed. Therefore, in the absence of optic flow, walking trajectories in this condition should be fully curved as predicted by sole use of egocentric direction (as indicated by the dashed line in **Figure 1.7**). However, the observed walking trajectories were remarkably straighter (as indicated by the solid line in **Figure 1.7**).

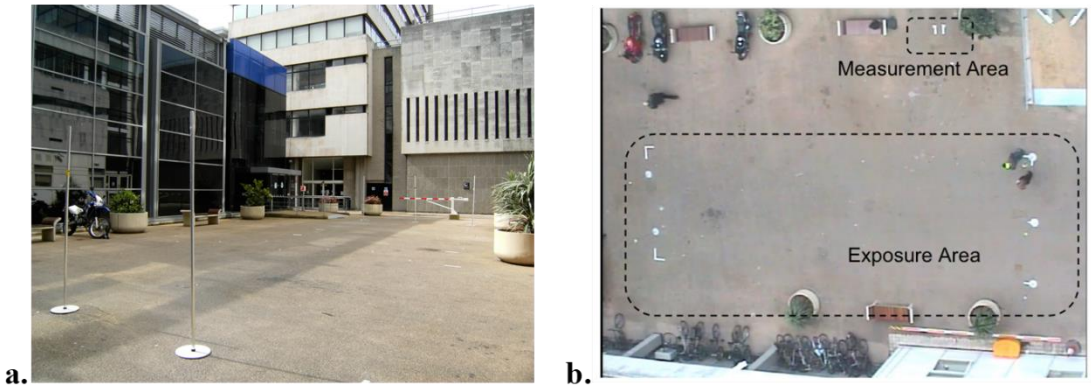

Figure 1.8 (a) *A perspective view of the testing area in Herlihey's study (2010).* ***(b)*** *A bird view of the testing area in Herlihey's study (2010). Taken from Herlihey (2010).*

The findings cannot be explained by either the egocentric direction hypothesis or the optic flow hypothesis. They suggest a potential use of a previously unrecognised type of cues. Like optic flow, these cues are not affected by prismatic displacement and hence produce a relatively straight trajectory.

What are these cues? One possibility may lie in the testing environments used in the study. In Herlihey's (2010), the testing area was a rectangular-shaped parking area bounded by buildings (see **Figure 1.8b**), which is reminiscent of the arena used in animal studies (e.g.,Cheng, 1986). As highlighted above, such a regular environment provides a strong source of information about the participants' location within it. As such, a number of visuospatial cues could be used by the participants to guide their walking. For example, if you are walking to the fronto-parallel wall or a corner, any change in the perspective shape of the wall(s) would signal a change in your walking direction, as demonstrated in Beusmans (1998) (see **Figure 1.5** for illustration). To maintain a walking trajectory, you can walk to keep the perceived shape of the wall(s) constant. Furthermore, the distances (or the ratio of the distances) to the walls would also be a source of information about the walking direction, as suggested by O'Keefe and Burgess (1996). Because these potential cues can inform about the observer's location (position and orientation) with respect to the surrounding environment, we call them collectively as *allocentric location cues.*

1.5 Exploring allocentric location cues in the guidance of walking

The results by Herlihey (2010) point to a gap between the human walking literature and research on spatial navigation. As pointed out by Vishton & Cutting (1995), the two literatures have '*made no contact*' (p.991). In this thesis, we attempt to bridge the gap

between the two literatures by exploring the role of allocentric location cues in the visual guidance of walking.

1.6 Overview of the thesis

As highlighted above, it is widely assumed that optic flow controls the guidance of walking and the contribution of optic flow is proportional to its richness. In Chapter 3, we set out to test this assumption by showing a role of allocentric location cues in the guidance of walking. Using a similar design as in Warren et al.'s (2001), we examined the walking trajectories in four virtual environments (VEs) that vary in the richness of optic flow and allocentric location cues. The pattern of trajectories is not commensurate with the optic flow hypothesis, but more compatible with the allocentric hypothesis. Then we go on to test another important assumption of the optic flow theory that the heading judgement taps the same process as walking. We assessed performance on heading judgment in the same four VEs. We found that precision of heading judgments is a poor predictor of straightness of walking trajectories, suggesting differences in the underlying processes between heading judgements and walking.

Chapter 4 explores whether the location of the target has an impact on the walking trajectory. In Experiment 4.1, the target location was manipulated so that the salience of perspective symmetry cues varied. In Experiment 4.2, the target was either near or far from the starting point so that the salience of target drift and motion parallax differed between conditions. In both experiments, we found a trend of influence of target location on the walking trajectories.

Chapter 5 provides further evidence for the allocentric location hypothesis by examining whether prior experience with the walking environment plays a role in the visual guidance of walking. In four experiments, the participants' prior experience was manipulated so that they were either familiar or unfamiliar with the test room before the experiment started. Across the four experiments, access to visual cues was manipulated by changing the illumination in the test room (i.e., dark, stroboscopic and fully lit) and/or on target (i.e., continuously and intermittently) as well as restricting the participants' visual field. We found a clear effect of prior experience when the access to visual cues was limited. The results also reinforce our findings of the role of allocentric location cues and revealed a role of target drift in the guidance of walking.

Leading on from this, Chapter 6 investigates whether knowledge about the environment can be acquired and contributed to the guidance of walking "on-the-fly" based

on the configuration of a landmark array. We sought to replicate the results of a study using a desktop steering task in active walking (Andersen & Enriquez, 2006). We manipulated the stability of a landmark array in VE so that the layout either remained constant (either viewpoint-dependent or viewpoint-independent) or randomly changed from trial to trial. Participants could form a mental representation when the layout was constant but could not do so when the layout was randomly changed. Therefore, according to Anderson & Enriquez's (2006) finding, trajectories should be straighter in the constant conditions. In conflict to Andersen & Enriquez (2006), we did not find any evidence for the use of a mental representation. Possible reasons for the discrepancy was discussed.

2 General methodology

This chapter gives a general introduction to the methodologies employed in this thesis. I will start by describing the typical paradigm that distinguishes the contribution of the cues. Next, I will introduce the equipment that was used, including the motion-tracking and virtual reality (VR) system. Last, I will describe how the data were pre-processed and analysed. Some technical issues such as smoothing, normalising and time course analysis will be discussed in more details.

2.1 Distinguishing the relative contribution of the cues

Normally, regardless of which cue is used, be it optic flow, egocentric direction or allocentric location cues, the resultant trajectory is a straight line to the target. How to disentangle the relative contribution of these cues? A typical paradigm is to insert an error by displacing the direction seen by the viewer from his or her actual walking direction by a quantifiable degree. As I will show in the following section, such an error produces walking trajectories in different shapes depending on the relative use of cues.

2.1.1 The use of prisms

Rushton et al.'s (1998) is the first study to employ this standard perturbation paradigm to investigate the role of optic flow and egocentric direction in the visual guidance of walking. They perturbed the visual direction by placing in front of the observer a pair of glasses containing wedge prisms (**Figure 2.1a)**. The prisms rotate the image of the scene by a specifiable degree. For example, consider viewing through base left prisms placed in front of your eyes. The doorway that stands in front of you will appear to be on the right side of its actual position, as shown in **Figure 2.1a** and **Figure 2.1d**. If at this point, you turn to face the doorway in the apparent direction of the doorway and take a step (**Figure 2.2b-c)**, you will end up heading to the right of your intended target (**Figure 2.2c**). If you continue to follow the apparent direction of the target (i.e., the egocentric direction of the target) in each step you make, there will always be an offset between the correct direction to the target and your concurrent heading. Ultimately, you will take an equiangular spiral to the target (see **Figure 2.2h**). This is the resultant trajectory that is predicted by sole use of egocentric direction of the target.

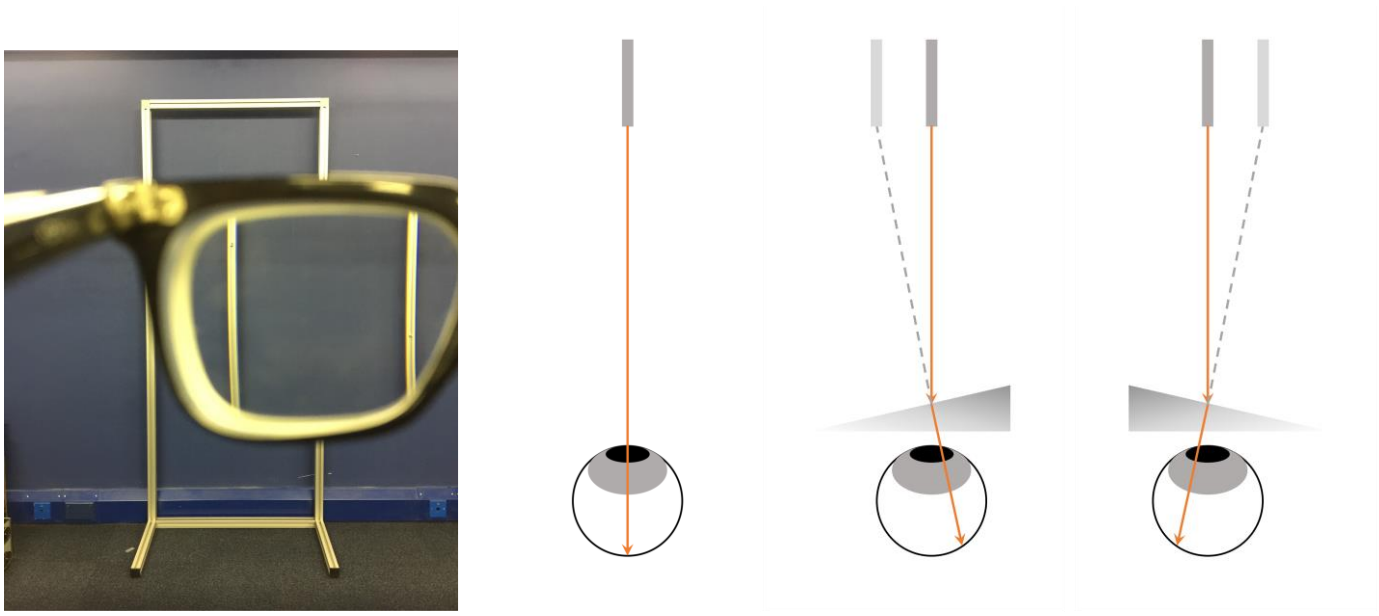

(a) (b) (c) (d)

Figure 2.1. (a) *Sample view seen through a base right, leftward deflecting prism. The frame is in front of the viewer, but seen through the prism it appears to be on the left.* ***(b)*** *Schematic illustration of viewing a target without prisms.* ***(c)*** *Schematic illustration of viewing a target through a base right, leftward deflecting prism.* ***(d)*** *Schematic illustration of viewing a target through a base left, rightward deflecting prism.*

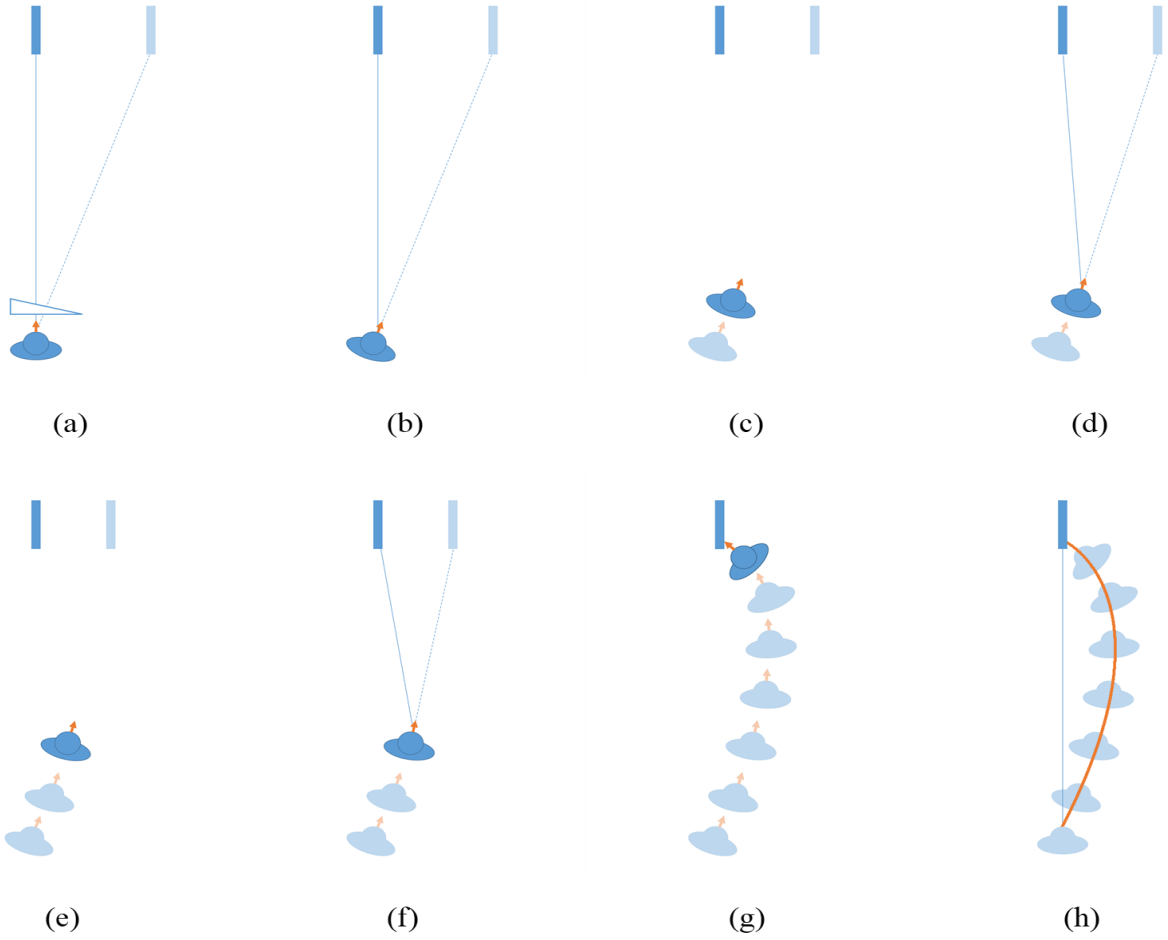

Figure 2.2. *Schematic illustration of the strategy used by an observer relying on* ***egocentric direction****. Dark blue square represents the target. Light blue represents the image of the target seen through the prism. (a) The prism shifts the image of the target to the right. (b) Align the body to the direction of the image of the target. (c) Make a step forwards but in the direction of the target image. (d) Realign the body to the target image. (e) Make another step forwards. (f) Realign the body to the target image again. (g) Repeat the procedure until reach the target. (h) The resultant trajectory is a curved path to the target.*

What about the trajectory predicted by the use of optic flow? Before making the first step, you are static. In that case, there is no optic flow at this point. As a result, the first step is to the apparent direction of the target (**Figure 2.3a-c**). After the first step, you have started moving. Therefore, optic flow becomes available. If you rely on optic flow after the first step, you will walk to the target by aligning the focus of expansion (FoE) with the image of the target. Note that, since the prisms shift the view as a whole, the relationship between the FoE and the image of the target remains intact. Therefore, FoE will still indicate the actual

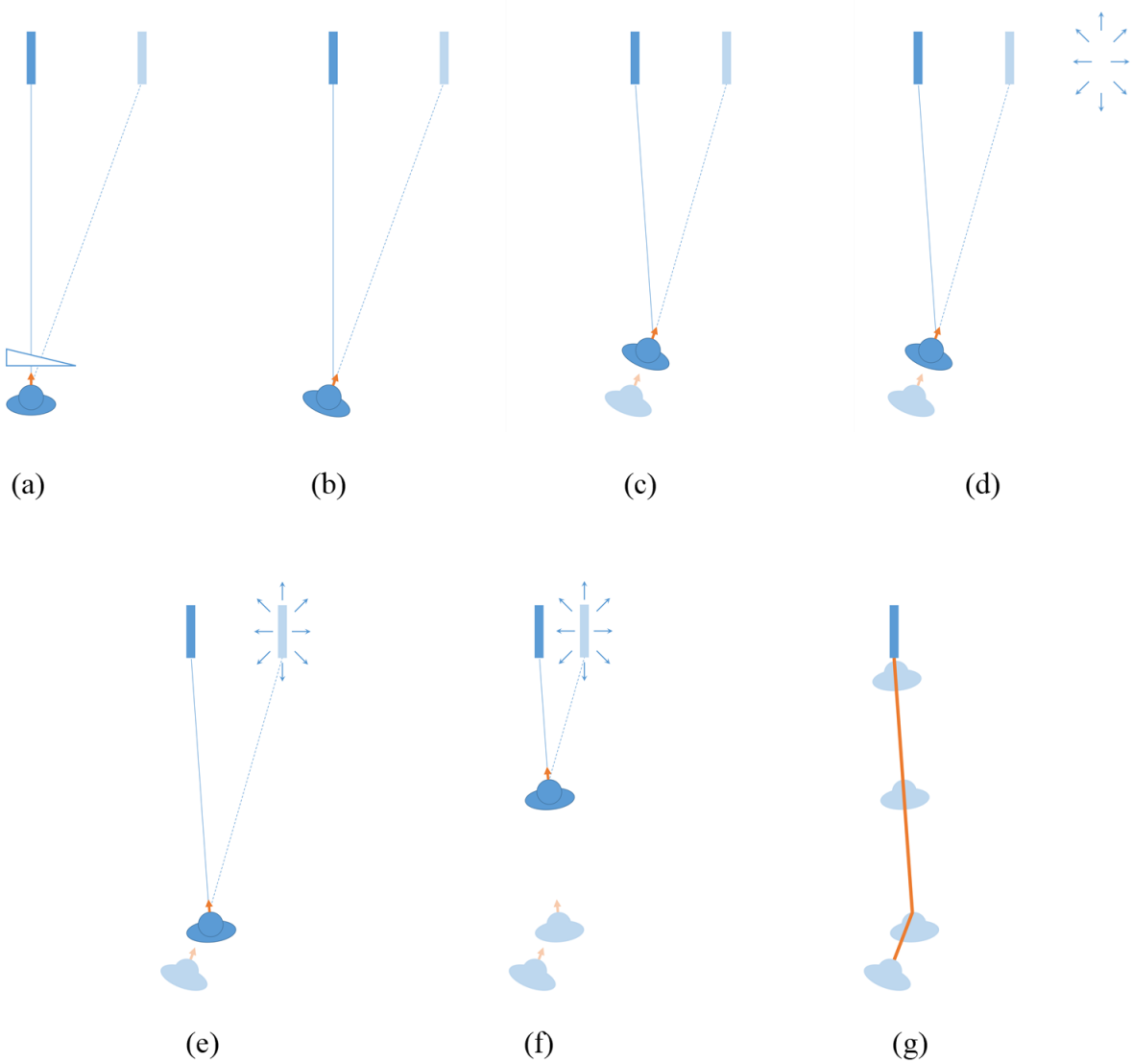

Figure 2.3. *Schematic illustration of the strategy used by an observer relying on* ***optic flow****. Dark blue square represents the target. Light blue represents the image of the target seen through the prism.* ***(a)*** *The prism shifts the image of the target to the right.* ***(b)*** *Align the body to the direction of the image of the target.* ***(c)*** *Make a step forwards but in the direction of the target image.* ***(d)*** *The FoE is not aligned with the image of the target.* ***(e)*** *Adjust the walking direction so that the FoE is aligned with the image of the target.* ***(f)*** *Walk to keep the FoE aligned with the target image.* ***(g)*** *The resultant trajectory is a relatively straight path to the target.*

heading of your movement. Consequently, if you keep walking with the FoE aligned with the target (**Figure 2.3d-f**), the trajectory will be a straight line to the target (**Figure 2.3g**).

The straightness of a trajectory thus provides us with an index of the relative contribution of cues. As shown in **Figure 2.4**, if egocentric direction is the sole cue used, the trajectory would be fully curved trajectory. As the contribution of optic flow (and/or other cues as will be discussed in the following chapters) increases, the straightness of the trajectory increases. In other words, the straightness of the trajectory is proportional to the contribution of the cues other than egocentric direction.

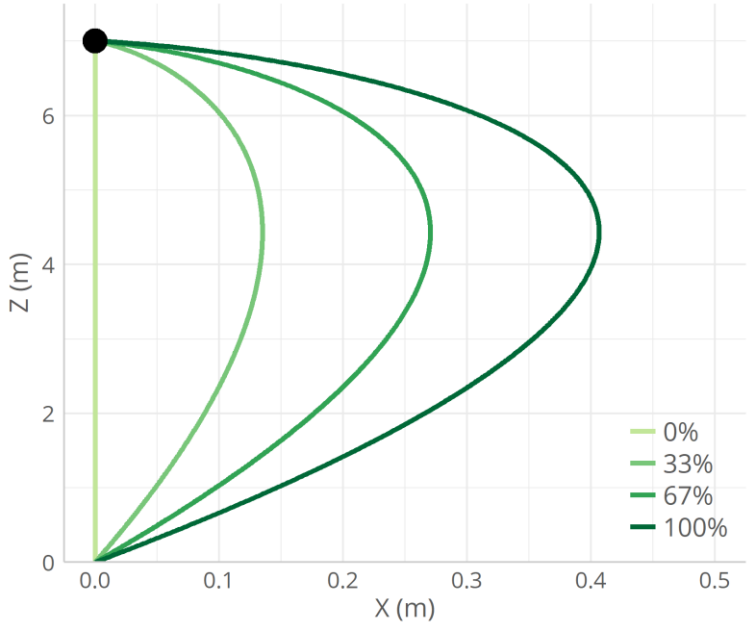

Figure 2.4 *Illustration of the straightness of a trajectory and the relative contribution of egocentric direction. Black filled circle represents the target. Darkest green line indicates a full curvature that is predicted by the sole use of egocentric direction with a 10° offset. Lighter green lines represent the trajectories with intermediate curvatures. Increase in straightness suggests use of cues other than egocentric direction.*

2.1.2 The use of virtual reality techniques

In addition to using prisms, displacing the perceived and physical moving direction can also be achieved using immersive virtual reality techniques (VR; e.g. Warren et al. 2001). The VR technology has become an increasingly popular experimental tool in recent year as it allows for an unprecedented control over the manipulation of stimuli. Normally, the VR techniques involve building a virtual environment (VE), tracking the position and orientation of the participant's head, rendering the image of the VE from a viewpoint based on the head's position and orientation, and presenting the image to the participant in real time (e.g., through a head-mounted display or HMD). In many cases, the display presents binocular

(stereoscopic) visual imagery that contributes to the perception of depth in the VE. As a result, participants experience a compelling sense of immersion within the VE.

To mimic the effect of real wedge prisms, an "error" is inserted between the physical direction and the visual direction by rotating visual space relative to physical space by 10°. That is, if you make a step forward in the real world, you will see yourself end up making a step to the right (or left) side in the virtual world (see **Figure 2.5**).

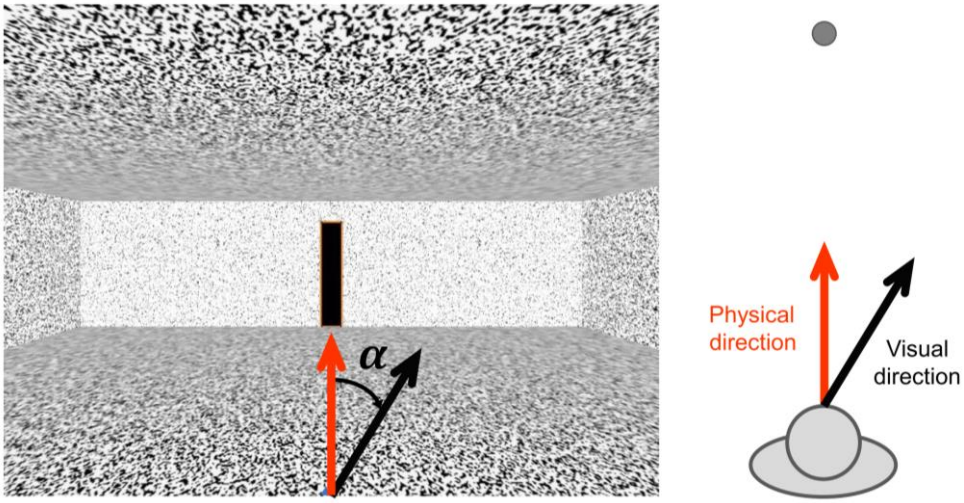

Figure 2.5. *Illustration of "virtual prism" with perspective (left) and top-down view (right). Red arrow indicates the physical direction. Black arrow indicates the visual direction that the observer sees in the virtual environment. The visual direction is rotated rightward by α. If the observers make a step forward in the physical world, they would see themselves heading to the right.*

2.1.3 Evaluation of the methods

2.1.3.1 Prisms

Some researchers argue that prism distorts the optic flow pattern and consequently forces the observer to use an alternative cue (i.e., egocentric direction) (Warren et al., 2001). However, studies have shown that human participants are able to determine heading with high accuracy when seeing through regular prisms (Vernon Odom, Ghude, & Humble, 2006) or even fisheye lenses (Kim, Fajen, & Turvey, 2000).

Another criticism of prism is that the flow field is confined by the frame of the spectacles. Such restrictions might deny an observer's access to relevant parts of an optic flow field such as foreground flow (Harris & Carré, 2001). Indeed, prisms used in earlier studies had a very low field of view (FoV; e.g., Redding, Clark, & Wallace, 1985 used a FoV of only 20°) which might limit the access to the flow information. However, Harris and Carré

(2001) found that increasing foreground flow by asking participants to look downwards while walking had no significant effects on walking trajectories – the trajectories were still curved as predicted according to the prismatic displacement. Moreover, Crowell and Banks (1993) found that effect of retinal eccentricity on heading judgements was small and less consistent. That is, the visual system is able to specify heading accurately from a variety of retinal regions.

Together, we consider prisms as a valid tool to investigate the visual guidance of walking in this thesis.

2.1.3.2 VR

The most obvious advantage of using VR is that it offers experimenters unprecedented control over the environment that is presented to participants. However, the technique has possible limitations. One concern is the latency between the movement of the observer and the updated change in the image seen by the observer. If this latency is longer than 50ms, it will reduce the observer's sense of immersion in the VE and even cause nausea (Carmack, 2013). The latency of the VR system used in our experiments was measured using a method similar to those reported by Morice, Siegler, & Bardy (2008) and Niehorster, Li, and Lappe (2017). In the Oculus Rift HMD (refreshing at 75Hz) a colourful scene was displayed with the view updated by the movement of the motion trackers on a helmet. The helmet was moved in an oscillation motion by a person. Both the change of view in the HMD display and the movement of the helmet was filmed simultaneously by a GoPro camera (Hero 2) at 120fps. The latency was measured by finding the time difference between frames containing the maxima of the helmet motion and updated display, which was about 42ms. In addition, no perceivable latency was reported from participants.

Another issue concerns the limited spatial and temporal resolutions of the HMD. For instance, the HMD used in Warren et al.'s (2001) had a resolution of only 640 × 480 and refreshed at 60Hz. However, the technology has been advanced greatly for the past decade. The HMD used in our experiments is 960 × 1080 *per eye*, and refreshes at 75Hz, considerably higher than those used in earlier studies.

A third issue concerns the restricted FoV in the HMD. For instance, the FoV of the HMD was only 60° horizontally in Warren et al.'s (2001). However, the HMD used in our experiments offers a FoV of 80° (horizontally) and 100° (diagonally), which is substantially improved from those used in earlier studies.

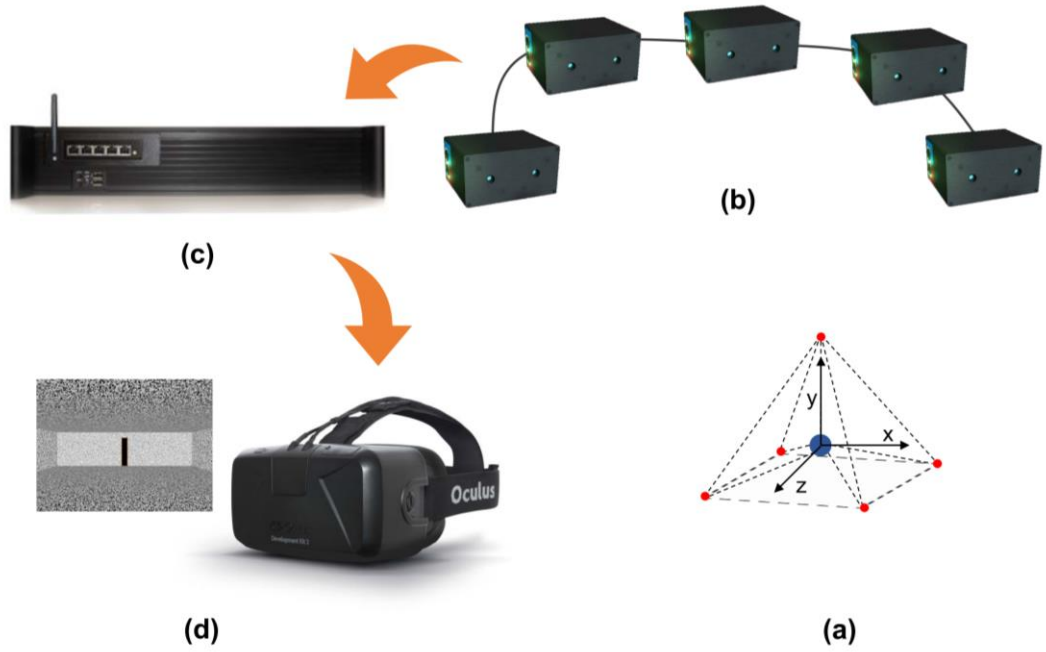

Figure 2.6. *Schematic illustration of the motion-tracking process.* ***(a)*** *Five LED markers constituted a rigid body for the head. Red dots represent LED markers. Blue and green circles respectively represent the centroid of head. Dashed lines indicate the distances among the markers and between the markers and centroids. Arrows indicate the local xyz axes. Signals from the LED markers are captured by the motion-tracking cameras* ***(b)****, and then sent back to the hub* ***(c)****. The signals are calculated and transformed to position and orientation information by the hub. The position and orientation information is then reflected in the virtual environment that is displayed on the HMD* ***(d)****.*

Despite the limitations, VR has a great potential in offering the researchers an unprecedented control over the environmental stimuli. Moreover, the fast advance in technologies in recent years have reduced, and in some cases, overcome some of the limitations. Further, when considering the visual guidance of walking, results of studies with prisms (e.g., Rushton, Harris, Lloyd, & Wann, 1998) and VR techniques (e.g., Guterman, Allison, & Rushton, 2007; Saunders et al., 2011) are often in good agreement. Therefore, VR is also considered a valid and effective tool in our studies, especially when priority is placed on control over the environmental stimuli.

In sum, both prisms and VR techniques are regarded as valid and effective tools and were used in the thesis.

2.2 Experimental setup and apparatus

In this thesis, except Experiment 3.2 which involved a heading judgement task, all experiments involved walking to a seen target. All the walking experiments employed the

standard perturbation design as described above to disentangle the contribution of cues. Both prisms and VR techniques were used. All walking experiments were carried out in a square room (8.3m × 8.3m × 3.4m) with position tracked by an Impulse X2 motion capture system (PhaseSpace Inc., the United States). This system contains 16 cameras (3600 × 3600 resolution at 480Hz with 60° camera field of view). The cameras were mounted on the ceiling to maximise the capture coverage.

LED markers were attached on participants so that the system could track their movement. It is necessary to obtain both position (x, y, z) and orientation (yaw, pitch, roll). However, a single LED marker only provides position data (x, y, z). In order to acquire orientation data, it is necessary to create a rigid body that consists of more than 3 LED markers which are fixed relative to one other. For a rigid body, the position data are calculated based on the position of the centre of mass (or centroid). To calculate the orientation of the rigid body, a local coordinate system (*xyz* axes) that lies within and moves with the rigid body is defined when creating the rigid body. The orientation data are calculated on the basis of the orientation of the local *xyz* axes relative to the rigid body.

Five LED markers formed a rigid body for the head (see **Figure 2.6a**). The position and orientation of the rigid bodies were captured by the motion-tracking cameras. The data were then sent back to the hub and streamed in real-time over a wireless local network using the virtual-reality peripheral network protocol (VRPN; Taylor II et al., 2001) so that client programs within the local network could receive the data.

A custom program was written in Vizard (WorldViz Inc., the United States) and run on a desktop PC to receive and record the position and orientation data from the hub (sampled at 60Hz). The program was also used to control the experimental procedure.

In the experiments that involved walking within a VE, a wireless setup was implemented to allow participants to walk freely in the lab without the confinement or distraction of attached wires. The VE was generated in a custom program (written in Vizard) running on a laptop (Dell, USA) and displayed on an HMD (Oculus Rift, USA) that was connected to the laptop. The laptop was securely placed in a rucksack that was carried on the back of the participants. The position and orientation data were streamed to the Vizard program running on the laptop via the wireless local network using VRPN protocol. Visual images were rendered based on the position and orientation data and displayed on the HMD at 75Hz.

In the experiments that involved walking with prisms, participants wore a pair of prism glasses that are of high quality and offer minimal distortions and the same FoV as

regular spectacles (**Figure 2.7**). They wore either a pair of rightward shifting glasses (white-framed) or leftward shifting glasses (black-framed). For both glasses, the prism lenses produce an angular deflection of 9° and in turn a navigational error of the same magnitude (see the data in Chapter 5 for evidence). Although the two pairs of glasses differ in the colour of their frames, there was no difference in the use of them. As we will show in the chapters that follow, no statistical difference was found in the straightness of trajectories between the participants who wore the white-framed glasses and those who wore the black-framed glasses. The setup of motion tracking and data recording was the same as in the VR experiments.

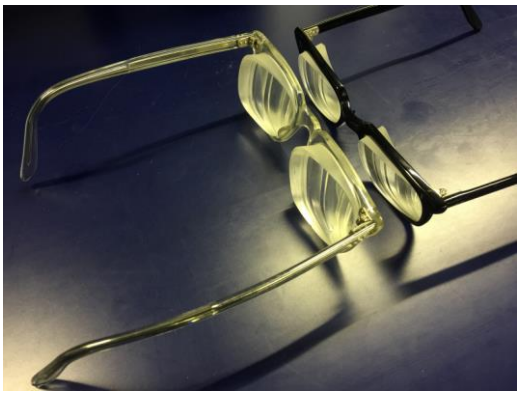

(a)

(b)

(c)

Figure 2.7. (a) *Glasses with white frame are mounted with base left, rightward shifting prisms. Glasses with black frame are mounted with base right, leftward shifting prisms. Both were used in the walking experiments of this thesis.* ***(b)*** *Seeing through the base right prisms.* ***(c)*** *The image taken through the base right prisms.*

2.3 Measures of trajectory curvature

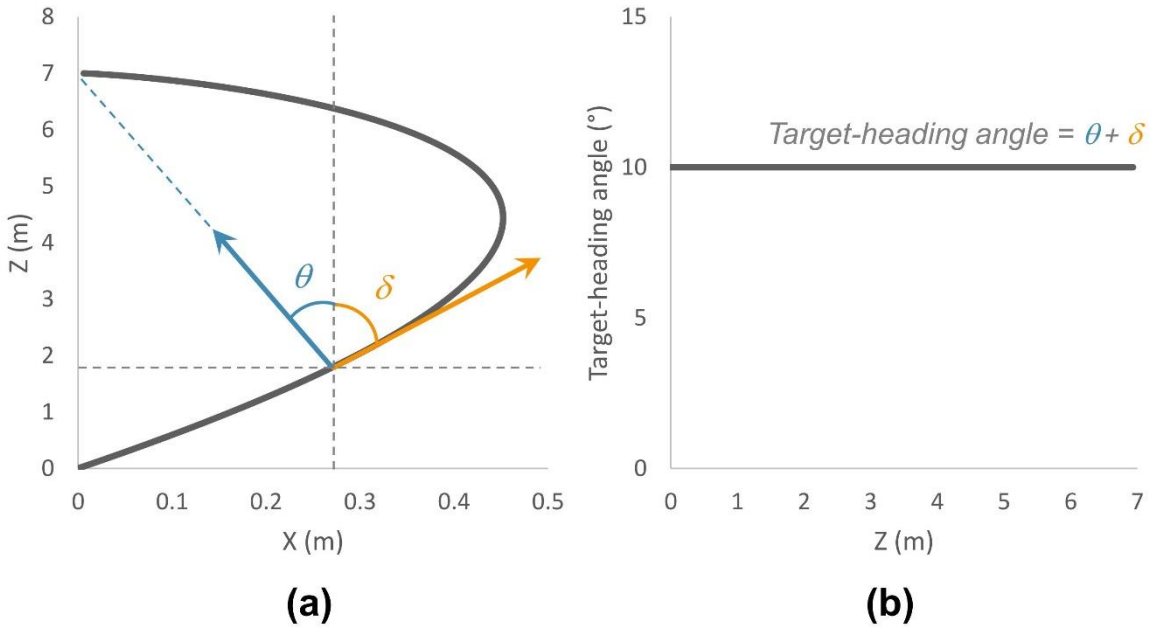

Figure 2.8. *Schematic illustration of how target-heading angles are calculated.* ***(a)*** *Black solid line indicated the predicted trajectory that only the egocentric direction cue is used when the target is shifted by an angular deflection (e.g., 10°). Blue arrow indicates the correct direction to the actual target represented. Yellow arrow indicates the instantaneous heading. The angle between the two arrows corresponds to target-heading angle. Its value is calculated by summing* θ *and* δ*.* ***(b)*** *Black solid line at 10° shows the target-heading angle calculated at each point of the trajectories in* ***(a)****. Because only the egocentric direction cue is used, the magnitude of target-heading angle corresponds to the magnitude of the angular deflection (i.e. 10°). Any trajectory straighter then the predicted trajectory in* ***(a)*** *corresponds to a series of target-heading angle smaller than those in* ***(b)****. Note the difference in the scale and label of the x- and y-axis.*

As noted above, from the curvature of the walking trajectory we can infer the relative contribution of the cues in the guidance of walking. Therefore, the curvature of the walking trajectory provides a behavioural measure that we used for all the walking experiments in this thesis. How to quantitatively measure the curvature? One way[3] is to calculate the angle between the instantaneous heading and the direction to the actual target, which is referred to as "target-heading angle" in this thesis (see **Figure 2.8** for details about the calculation). For a

[3] Alternatively, one can use lateral deviation along the trajectory. This was used in Warren et al. (2001). However, this measure reflects an accumulative curvature, whereas target-heading angle corresponds to an instantaneous curvature and thus is more sensitive to the change of curvature. Moreover, compared to lateral deviation, target-heading angle is not affected by the initial position at the beginning of the trajectory.

fully curved trajectory, the corresponding target-heading angle will be equivalent to the degree of the displacement throughout the trajectory.

To index the overall straightness of a trajectory as a whole, a mean target-heading angle can be calculated by averaging over the whole distance. To reflect the time course of the straightness of a trajectory, for example, the change of straightness as a function of distance, the target-heading angles along the distance can be examined as time series.

2.4 Analysis of walking data

2.4.1 Pre-processing

2.4.1.1 Smoothing

Before submitting to analysis, the data should be smoothed to remove oscillating noise resulting from the sway of walking. A conventional approach used in previous studies (Bruggeman, Zosh, & Warren, 2007; Saunders & Ma, 2011; Warren et al., 2001) is to apply a Butterworth low-pass filter on the walking data, using a fixed cut-off frequency. The value of the cut-off frequency is usually determined on the basis of the average walking speed (i.e., 1.4m/s), assuming that all participants walk at the average speed throughout the experiment and have similar sway frequency. However, in practice, these assumptions are difficult to hold.

Take Experiment 3.1 for example. The average speed was 0.73m/s, which was significantly slower than the normal speed of 1.4m/s. Moreover, there was a large variability both within and between participants. The largest speed was 1.07m/s, whereas the slowest was 0.32m/s. The speed also increased over the course of the experiment, as the participants became more familiar with the setup. Furthermore, the sway frequency does not only depend on the walking speed but also on the step size. That is, at the same speed, the sway frequency increases as the step size decreases. Therefore, even walking at the same speed, there may be a large variability in sway frequency between participants. As a consequence, the use of a fixed cut-off frequency may result in under-smoothing (for most cases) or over-smoothing (for a few cases).

In this thesis, we designed a 2^{nd}-order Butterworth low-pass filter for the data of each trial and for each participant. The frequency of walking sway was determined using Fourier transformation, which was then employed in the Butterworth filter as the cut-off frequency. Doing this should remove most of the noise due to walking sway (see Supplementary Materials 8.1 for more details).

2.4.1.2 Normalising

As described above, the position and orientation data were recorded at 60Hz. On the other hand, participants walked at various speeds and thus took different lengths of time to finish each trial. As a result, the length of data varied. In order to combine the data across trials and participants, the data were normalised. To do so, the data of each trial was segmented along the z-axis (from 0.5m to 6m) into 100 bins with equal lengths. Then, a mean was calculated for each bin by averaging the data within the bin. To combine the data (e.g. to calculate a mean trajectory), the mean was calculated at each bin across the trials and participants.

Then the data in the trials with base right prisms (left-shifted image) were flipped around so that they were on the same side with those trials with base left prisms (right-shifted image).

2.4.2 Statistical analysis

In this thesis, we took two steps to analyse the walking data. The first step was to reveal the general effects of the cues on the overall straightness of walking trajectories. That is, we compared the overall mean target-heading angles that were averaged over the distance between conditions, using standard general linear model (GLM) analyses such as analysis of variance (ANOVA) or t-tests. When Levene's test indicated unequal variances, Welch's t-test was used instead of Student's t-test.

The second step was to further probe the fine-grained detail of the trajectory straightness over the course of walking. In this step, two approaches could be employed on the time course data (i.e., mean target-heading angle as a function of trial or as a function of distance). The first approach is to examine the effect of cues on the *linear* rate of change in the straightness of trajectories using *growth modelling* (Mirman, 2014; Singer & Willett, 2003). This approach could answer the question of which cues would lead to faster straightening of trajectories. The second approach is a *nonlinear* time course analysis using an in-house routine combining *nonparametric permutation tests* (Nichols & Holmes, 2003) and *cluster-based decisions* (Ashby, 2011). This approach could answer the question of where the walking trajectories become significantly straighter in a certain condition than another.

2.4.2.1 Growth modelling

As reported previously, walking behaviours may change over the course of walking (Bruggeman et al., 2007; Herlihey & Rushton, 2012; Warren et al., 2001). For example, trajectories may straighten up both within (showing a trend of online adjustment) and across trials (showing a trend of adaptation or learning). Thus, different rates of change of walking behaviours could reflect different temporal dynamics of cue use.

There are two approaches that have been commonly used for examining the rate of change. One approach is to compute a repeated-measures ANOVA on the data across a series of time windows (e.g. trials). In this model, time is treated as a within-subject categorical factor with levels corresponding to the individual time window. Significant interactions between time and experiment manipulation would indicate various effects of cues on the time course of the data. An alternative method is the ordinary least squares (OLS) approach. The walking data are first regressed against the temporal factor (e.g. trial or distance) at the individual level. The parameters (e.g., intercepts and slopes) estimated from each individual regression are then submitted to further analysis to reveal the effect of experimental manipulation on these parameters. For instance, a significant difference in the slopes would indicate impacts of experimental manipulation on the rate of change in the walking behaviour.

In this thesis, I use an approach that is novel for analysing walking data, namely *growth modelling*. This approach builds on techniques designed to evaluate change over time (Singer & Willett, 2003). These techniques have been widely used on longitudinal behavioural data in the developmental literature. Here, I apply the approach to the walking data which are treated as longitudinal data collected on a fast time scale. The most prominent advantages of using growth modelling over the two aforementioned approaches are that it takes individual differences into account and that it can account for autocorrelation and capture heteroscedasticity of residuals over time (see Mirman, Dixon, & Magnuson, 2008 for a detailed discussion on advantages of using growth modelling).

2.4.2.1.1 Structure of a growth model

The approach of growth modelling is quite similar to the OLS approach but is different in important ways. Unlike the OLS approach, a growth model contains two (or more) sub-models that are hierarchically related. The *level*-1 sub-model captures the effect of time. As in the OLS approach, level-1 sub-models are calculated by regressing the walking data against a time factor (e.g. trial or distance) for each individual participant (Eq. 2.1).

Here, a linear equation is used for the level-1 sub-model as we are interested in the rate of change against time. By doing so, the level-1 sub-model forces participants to differ only in the values of the individual intercept and slope parameters.

$$Y_{ij} = \alpha_{0i} + \beta_{1i} \times Time_{ij} + \varepsilon_{ij} \quad (2.1)$$

The subscript *i* indexes individuals and *j* indexes measurement occasions (e.g., trials or distance bins). As in OLS models, there is an intercept α_{0j}, a slope β_{1i}, and an error term ε_{ij}. However, unlike OLS models, the intercept and the slope in the growth model are allowed to vary across individuals around the population average values. The variation is captured in *level*-2 sub-models. That is, for each parameter of the level-1 sub-model, there is a level-2 sub-model that describes the corresponding level-1parameter in terms of population means, fixed effects and random effects. For example, the level-2 sub-model for the intercept is: $\alpha_{0i} = \gamma_{00} + \zeta_{0i}$, where γ_{00} denotes the population average intercept and ζ_{0i} the individual deviation from γ_{00}. Similarly, the level-2 model for the slope is: $\beta_{1i} = \gamma_{10} + \zeta_{1i}$, where γ_{10} denotes the population average slope and ζ_{1i} the individual deviation from γ_{10}. Note that the residual terms ζ_{0i} and ζ_{1i} allow the individual intercept and slope parameters α_{0i} and β_{1i} to vary around the population average intercept γ_{10} and slope γ_{10} respectively.

To capture the effects of experimental manipulations, structural terms can be included into the level-2 sub-models. This gives us a new level-2 sub-model for intercept α_{0i} (Eq.2.2) and a new level-2 sub-model for slope β_{1i} (Eq.2.3):

$$\alpha_{0i} = \gamma_{00} + \gamma_{0C} \times C + \zeta_{0i} \quad (2.2)$$

$$\beta_{1i} = \gamma_{10} + \gamma_{1C} \times C + \zeta_{1i} \quad (2.3)$$

Here *C* denotes some experimental condition. The term γ_{0C} indexes the effect of the condition *C* on the intercept and γ_{1C} the effect of the condition *C* on the slope. These two parameters address the question of what is the difference in the average intercept and slope associated with experimental manipulation. Thus, these two parameters are of primary interest for the analyses included this thesis. If there are more than two categorically distinct conditions, one of the conditions would be treated as a baseline, and the parameters are estimated relative to the baseline for the other conditions. Together with γ_{00} and γ_{10}, the four parameters in the level-2 sub-models are also called *fixed effects*.

The error terms ζ_{0i} and ζ_{1i}, also called *random effects*, allow for individual (or individual × condition) variation around the relevant population averages. These terms capture the portion of variation in the data that is not explained by the fixed effects.

To see how a growth model captures heteroscedasticity of residuals over time, we can combine Eq. 2.1, Eq. 2.2 and Eq. 2.3:

$$Y_{ij} = \gamma_{00} + \gamma_{0C} \times C + (\gamma_{10} + \gamma_{1C} \times C) \times Time_{ij} + (\varepsilon_{ij} + \zeta_{0i} + \zeta_{1i} \times Time_{ij}) \quad (2.4)$$

Now the error term is the sum of three components. Among these components, the product term $\zeta_{1i} \times Time_{ij}$, allows error to be heteroscedastic within each individual. That is, as ζ_{1i} is multiplied by Time, the magnitude of the product error term can differ over time.

In sum, by introducing random effects into the model, growth modelling is able to account for individual difference and heteroscedasticity in residuals. More importantly, the growth model approach is more precise than the OLS approach in estimating parameters. The reasons are: (1) that the growth model approach, unlike the OLS approach, takes into account information about the individual growth parameter estimates' precision; (2) that the growth model approach calculates parameter estimates using weighted averages of the OLS and population average growth parameters which yields a more precise estimate; and (3) that the growth model approach requires estimation of fewer parameters assuming that individual participants shared the same level-1 residual variance.

2.4.2.1.2 Estimation of model parameters

Maximum likelihood methods are used to estimate the parameters in a growth model. The basic idea of the maximum likelihood estimation is to guess the values of the unknown population parameters that can maximise the probability of observing the sample of data that we have obtained from experiments. This is done through maximising numerically the log-likelihood function, namely the logarithm of the joint likelihood of observing all the data obtained in the experiment. The process yields a number for the magnitude of the log-likelihood function for the observed data and parameter estimates together, called *sample log-likelihood* statistic. Then deviance statistic is calculated by multiplying the log-likelihood by -2. The deviance statistic gives an index for the goodness of the fit of the model.

2.4.2.1.3 Procedure for model building

To address our research questions, it is necessary to build a model with all relevant predictors included and to examine their contributions. The procedure of model building involves two steps: (1) model comparisons for testing whether a predictor has a statistically

significant effect and (2) evaluation of individual parameter estimates for more information about the fixed effects.

For model comparisons, we followed a standard path, namely a *taxonomy* of statistical models (Singer & Willett, 2003). This path starts from a simple model with only an intercept. This model describes the scenario that the change of trajectory straightness is a flat line at the individual means. The simple model serves as a baseline against which we could evaluate the significance of predictors by adding them sequentially into the model. This process of adding predictors results in a systematic sequence of models, i.e. a taxonomy of statistical models.

The decision about the significance of a predictor is made based on whether including the predictor to the current model would increase the fit as compared to the model before adding the predictor. This can be determined from the change in the deviance statistic, or ΔD, which is distributed as χ^2 with degrees of freedom equal to the number of coefficients added. If adding the predictor into the model significantly improves the model fit, it will be considered as having a significant effect.

After model comparisons, if the predictor in question has an effect, we evaluate the related individual parameter estimates in the model. In principle, this is a one-sample *t*-test assessing whether the estimated parameter is different from 0. The *t*-value is computed by dividing the parameter estimate using its standard error. Because (1) here time course data have a large number of observations as compared to the number of fixed effect parameters in the model and (2) the *t* distribution converges to the normal distribution when the number of degrees of freedom is large, it is possible to estimate the associated *p*-value using the normal distribution as an approximation for the *t*-value (Mirman, 2014).

All growth modelling analyses were carried out in R version 3.24 using the `nlme` package (Pinheiro, Bates, DebRoy, Sarkar, & R Core Team, 2017). In cases when there were more than two discrete conditions for a predicter, *multcomp* package in R (Hothorn, Bretz, & Westfall, 2008) was used for simultaneous comparisons of differences between conditions.

2.4.2.2 Permutation test using cluster-based decisions

In this thesis, we are not only interested in the effects of the experimental manipulation on the average walking behaviour or the linear rate of change, but also in the question of where along the trajectory the walking behaviour differs significantly between two conditions. In order to address this question, it would be useful to devise a way of looking at the dynamic aspect of cue use.

A way to do this was to calculate t-statistic at each point along the distance, yielding a statistical parametric "line". From this line, inferences are drawn by locating points where an effect is present. The procedure is akin to the statistical analysis of functional magnetic resonance imaging (fMRI) data where a statistical parametric map is constructed and voxels with stronger response are located (SPM, Friston, Ashburner, Kiebel, Nichols, & Penny, 2007). Therefore, this approach faces the same problem as the fMRI data analysis. The problem is what criterion should be used to decide whether the t-statistic at any given point is sufficiently large and can be considered as a significant effect.

One big problem with determining significance is the high likelihood of false positives due to multiple comparisons. This problem is especially prominent given the large number of data points (n = 100). On the other hand, there is a positive spatial correlation between the adjacent data points, especially after smoothing. That is, if the t-value at a single data point is high, it is very likely that the t-values of the adjacent data points are also high. Such correlations, along with the large number of data points, renders conventional correction methods (e.g., Bonferroni) overly stringent.

To solve the multiple comparisons problem, a non-parametric permutation test is used to analyse the time course data. In addition, significance decisions are made on clusters of data points. This would not only reduce the number of comparisons but also account for the spatial corrections of the walking data.

The algorithms are as follows.

Step 1 Calculate a t-value at each data point along the distance to produce a t-line. The t-line contains 100 observed t-values.

Step 2 Calculate $T = 50\% \times$ mean of observed t-values. This is to set an arbitrary threshold.

Step 3 Randomly shuffle the data. Calculate t-values on the shuffled data to produce a new t-line.

Step 4 Repeat Step 3 a total of N times with a new random shuffle on each repetition. Choose a large value for N (e.g., 250 million). At the end of this step, a permutation distribution of N different t-lines will exist. Each t-line contains 100 t-values.

Step 5 Find the cluster that is 10 data points long (approximately 1 step) that had the largest sum of observed t-values. Call the sum of observed t-values s_{obs}.

Step 6 Calculate the sums of the t-values from the permutation distribution for the same cluster. At the end of this step, a distribution of N sums of t-values will exist, S_T.

Step 7 Calculate $p_{cluster} = P(S_T \geqslant s_{obs})$.

Step 8 If $p_{cluster} < 0.05$, expand the cluster by including an adjacent data point whichever had a larger observed t-value.

Step 9 Repeat Step 8 until $p_{cluster} > 0.05$, the cluster has included all 100 data points or the lowest t-value in the cluster is $< T$. The last criterion is to avoid any unintuitive result, e.g. small or even negative t-values are included into a significant cluster. Such a scenario usually appears at two ends of the trajectory.

At the end of the algorithms, location information of the significant cluster (if there is any) on the distance and the *p*-value will be given. The location of the cluster provides information about where the two conditions significantly differed. For instance, if the trajectory in Condition A is significantly more curved than in Condition B but catches up later on, a significant cluster should be expected in the early part of the trajectory.

3 Do allocentric location cues play a role in the visual guidance of walking?

Warren and colleagues (2001) introduced an offset between the visual and physical moving directions and examined the walking trajectories in four virtual environments that varied in visual complexity. They found that the trajectories straightened with the increase in the visual complexity. Hence, they conclude (1) that the guidance of walking is controlled by a combination of egocentric direction and optic flow and (2) that optic flow becomes dominant as the richness of it increases. The two points are reflected in the model they proposed: $\frac{d\phi}{dt} = -k(\beta + wv\alpha)$, where ϕ denotes the walking direction, β the egocentric direction of the target, v is the moving velocity of the observer and α the visual angle between the focus of the optic flow pattern and the target. The relative contribution of optic flow and egocentric direction is mainly determined by w, which represents the visual richness of the walking environment.

Warren et al.'s model, however, does not hold for the results of a recent study (Herlihey, 2010). As highlighted in Chapter 1, Herlihey (2010) demonstrated that even in a condition without optic flow ($w = 0$), the walking trajectories are as straight as those in the condition with rich optic flow ($w > 0$). The results, therefore, suggest that other cues (e.g., allocentric location cues) could also play a role in the visual guidance of walking and yields a relatively straight path.

Comparing the environmental stimuli between the two studies revealed a potential confound in Warren et al.'s (2001) study. The rich environments in Warren et al. (2001) consisted of surfaces like floor, ceiling and walls. These environments resemble the test environment in Herlihey's (2010) (see **Figure 1.8** in Section 1.4.3), which was a rectangular area surrounded by buildings. As discussed in *General Introduction*, such enclosed environments with regular shapes provide not only plenty of optic flow but also a large amount of spatial information about the location of the observer with respect to the environment (i.e., allocentric location cues). Therefore, the increase in the straightness of walking trajectories in the rich environments in Warren et al. (2001) might not be due to the increase in the richness of optic flow but to the increase in the richness of allocentric location cues (or the combination of both).

In Experiment 3.1, we evaluate the contribution of optic flow and allocentric location cues using a similar design as Warren et al. (2001). In Experiment 3.2, we go on to examine

the relationship between heading judgements and walking trajectories. To anticipate the results, we found that both the richness of optic flow and heading judgements did not capture the pattern of walking trajectories well. However, the pattern of walking trajectories was better predicted by the availability of allocentric location cues.

3.1 Experiment 3.1 Is the richness of optic flow a good predictor of walking trajectories?

As in Warren et al. (2001), we had participants walk in four virtual environments that varied in the richness of optic flow and allocentric location cues respectively. The simplest and richest environments were adopted from Warren et al. (2001) with minor changes. The simplest environment (*Line*; **Figure 3.1a**) contained only a post target in empty space. The richest environment (*Room*; **Figure 3.1b**) was a square room with solid surfaces all painted with a random-noise pattern. Two additional environments were created to separate optic flow and allocentric location cues. The *Cloud* environment was generated by adding a cloud of white dots in the *Line* environment (**Figure 3.1c**). The white dots filled up the same volume as the *Room*. This environment should provide richer optic flow than the *Room* condition does for two reasons. First, the dots should generate larger vectors surrounding the FoE and thus make the FoE easier to locate. Second, the dots were distributed throughout the 3-dimensional space and thus motion parallax cues are richer than the *Room* condition. More detailed analysis and comparison of optic flow between the *Cloud* and *Room* conditions is included in Supplemental Material 8.2.1.1. The edges of the cloud may provide minimal allocentric locational cues. The *Outline* condition was created by adding a set of red lines at the edges of the *Room* and then removing the surfaces (**Figure 3.1d**). It provides minimal optic flow but contains a large amount of allocentric location cues. Because the surfaces were removed, the amount (or salience) of allocentric location cues in the *Outline* condition should be less than in the *Room* condition. As a result, the four environments can be ordered in terms of optic flow as *Cloud* > *Room* > *Outline* > *Line*, or in terms of allocentric location cues as *Room* > *Outline* > *Cloud* > *Line*.

If the guidance of walking relied solely on optic flow, one should expect to observe an order of *Cloud* > *Room* > *Outline* > *Line* in the straightness in the walking trajectories. Alternatively, if the guidance of walking relied solely on allocentric location cues, the order of straightness would be expected to be: *Room* > *Outline* > *Cloud* > *Line*.

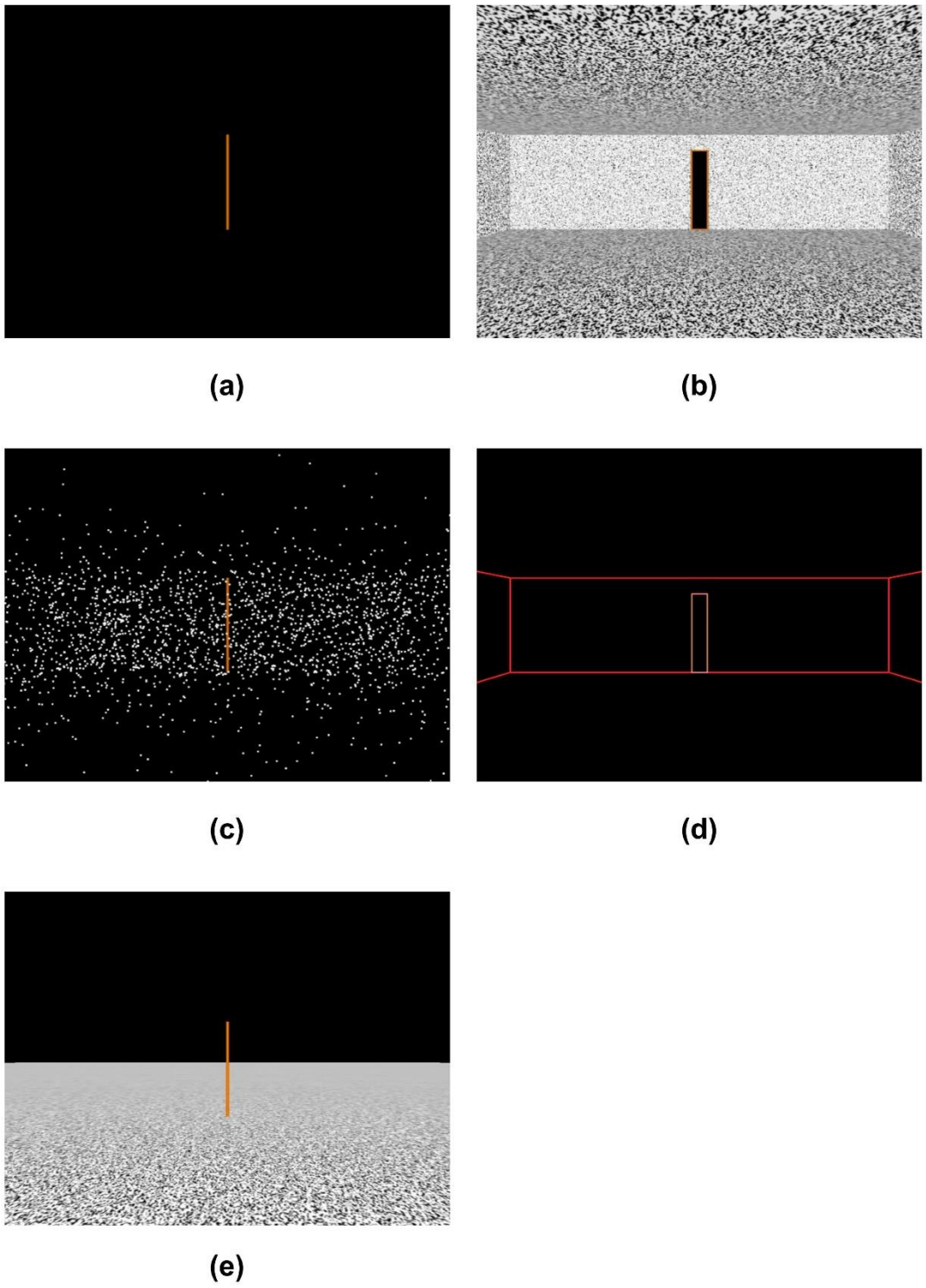

Figure 3.1 *Virtual environments:* ***(a) Line*** *environment, only a post target visible;* ***(b) Room*** *environment, a room with all the walls, floor and ceiling painted random-noise pattern and a doorway on the front wall to serve as the target;* ***(c) Cloud*** *environment, a post target surrounded by dots that filled up the whole volume of the room in the Room condition;* ***(d) Outline*** *environment, a red outline of the room and a doorway target as in the Room condition.* ***(g) Baseline*** *environment, an environment used in the baseline blocks.*

3.1.1 Method

3.1.1.1 Participants

Participants were recruited until, after necessary exclusions, we had a counterbalanced sample, forty-eight in total. In order to obtain these numbers, it was necessary to recruit fifty-six participants. Reasons for exclusion were technical faults during the experiment (n = 4), not following instruction (n = 1) and being outliers (n = 3; see Data analysis 3.1.1.5 for full details of exclusion).

The demographic statistics of the forty-eight participants that were included in the analysis were mean age = 19.54, SD = 1.34, range: 18 ~ 23; 7 males. All participants had self-reported normal vision or vision that was corrected to normal with contact lenses[4]. None reported impairments of stereo or colour vision or hearing. The pupillary distance of each participant was measured and used to adjust the position of the HMD to obtain a stereo view of the environment. All participants provided informed written consent in accordance with the requirements of the School of Psychology research ethics committee that approved the research. All were naïve to the actual purposes of the study.

3.1.1.2 Virtual environments

Four virtual environments were created in Vizard: *Line*, *Cloud*, *Outline*, *Room*. As mentioned above, the *Line* and *Room* were modelled on those corresponding scenes in Warren et al. (2001), and the *Cloud* and *Outline* were constructed on the basis of the *Line* and *Room* respectively. In all environments, the distance between the starting point and the walking target was 7m.

Figure 3.1a gives an example view of the *Line* environment from the starting point. It contained only a post target (height = 3m, radius = 2cm) surrounded by a black void. The bottom of the target was at ground level in the virtual environment (VE); ground level in the VE had been matched to the floor of the physical laboratory.

As shown in **Figure 3.1b**, the *Room* was a square room (12m × 12m × 3m) with the walls, floor and ceiling painted with a random-noise pattern. On the wall opposite to the

[4] When we recruited participants, we explicitly required those participants who needed vision correction to wear contact lenses on the test day. The reason was that they would wear prism glasses and the HMD during the experiments. Wearing optical spectacles would be difficult for them to put on experimental equipment.

starting point there was a doorway (2.5m high and 0.5m wide) that consisted of lines (2.5cm in radius). This doorway served as the walking target.

The *Cloud* was constructed on the basis of the *Line* by adding a total of 5250 white dots (**Figure 3.1c**). These dots were all fixed in two pixels in diameter, and uniformly distributed in a volume of space the same dimensions as the *Room*. In order to discourage that participants from using direction information specified from tracking a single dot, each dot had a life time of 37 frames (approximately 0.5s at 75 frames/s).

The *Outline* was constructed by placing red lines at each of the edges of the room in the *Room* and then removing all the surfaces (i.e., walls, floor and ceiling). The width of the red lines was fixed to 2 pixels. The doorway remained as the walking target (**Figure 3.1d**).

In addition to the four test environments, a baseline environment was also created to be used in the baseline blocks (see Section 3.1.1.3.1 below). This environment contained a flat ground place with a horizon at 100m which was painted with a random-noise pattern (**Figure 3.1e**). A homogeneous black "sky" was rendered with the border at the horizon. The same post target as in the *Line* was used as the walking target.

3.1.1.3 Design

3.1.1.3.1 Experimental conditions

The experiment was a within-subject design. Each participant walked back and forth along the diagonal axis of the room 18 times, yielding 36 trials in total. The 36 trials were evenly grouped into 9 blocks. Among the nine blocks, the even-numbered blocks were test blocks and the odd-numbered blocks baseline blocks.

Each test blocks presented one of the four test environments. A "virtual prism" of 10° was added in the participant's head orientation in the VE (see Section 2.1.2). That is, the visual direction was shifted by 10° from the walking direction in the VE. The direction of the "virtual prism" was alternated between the test blocks. The order of the test environments was counterbalanced and randomised across the participants.

In all baseline blocks, the baseline environment was displayed (**Figure 3.1e**) without a "virtual prism". The first baseline block served as a practice session so that the participants could familiarise themselves with walking in a VE and the experimental procedure. At the end of the practice block, all participants reported that they were confident about walking in a VE and ready to start the actual experiment. For the rest of the baseline blocks, each of them followed a test block. Hence, the baseline blocks could serve two purposes: (1) to examine

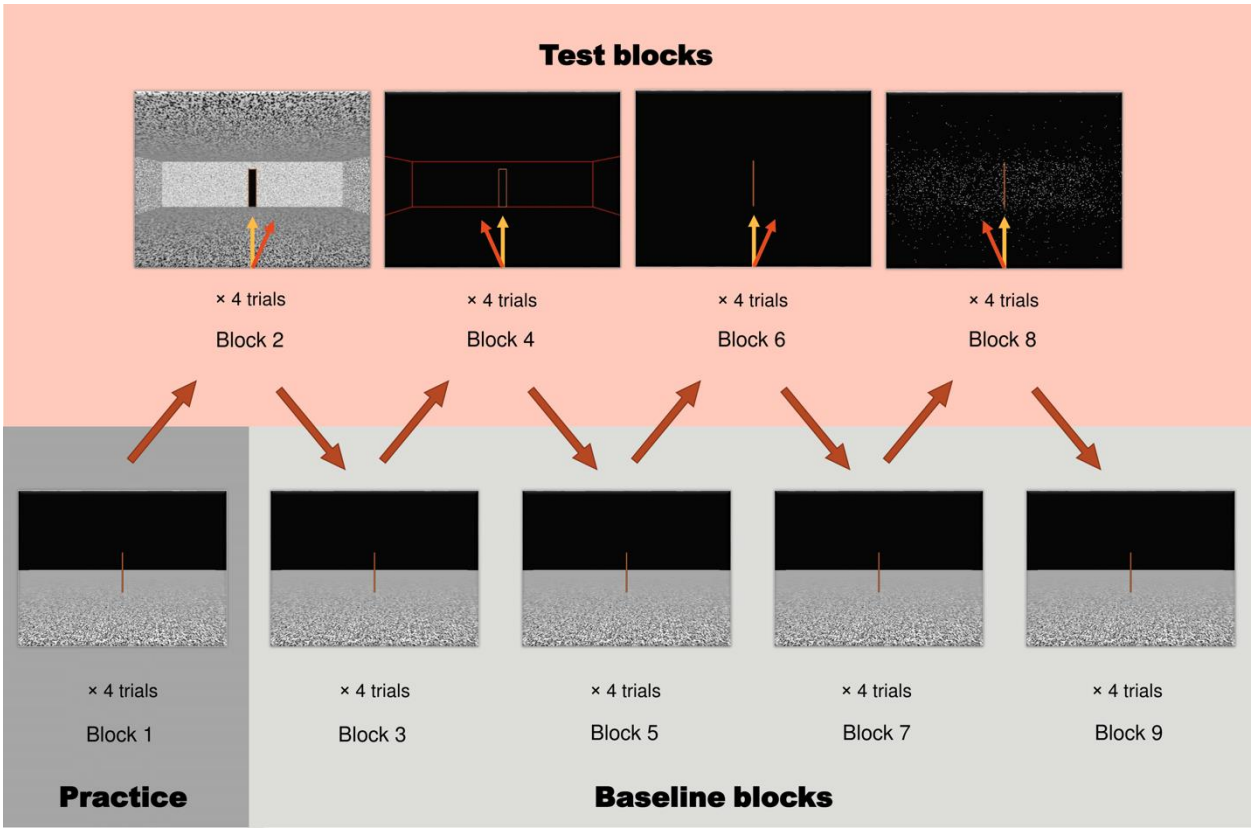

Figure 3.2 *Example of experimental design. The order of the test environments is: room, outlined room, line and dot cloud. Direction of the offset between visual direction (yellow arrow) and physical direction (red arrow) is alternated between test blocks.*

any negative aftereffects that resulted from adaptation in the preceding test block; and (2) to get rid of any aftereffect before the start of the next block. A schematic illustration of the whole procedure was given in **Figure 3.2**.

3.1.1.3.2 Secondary task

To discourage the participant from paying undue attention to their walking behaviour and guessing the real purpose of the study, a secondary task was used as a cover story. Whilst walking to the target, participants could see the colour of the target changing randomly between red, green and yellow every 0.75s. Participants were instructed to attend to the target and press the button on a wireless presenter every time the target turned to a specified colour, e.g. red. Participants were told that this colour responding task was their primary task in this study. In the debriefing session at the end of the experiment, none of the participants reported that they had been aware of the actual purpose of the study. Moreover, none of them indicated being aware of any discrepancy between the visual and actual walking directions. In

addition, the mean response time was 451.42ms (SD = 38.28ms), and no statistical difference was found between the test conditions [$F_{3, 138} = 1.357$, $p = 0.259$, $\eta^2 = 0.029$]. The mean accuracy on the secondary task was 96.51% (SD = 2.04%). These results suggest that our cover story was successful and the participants were paying attention to the secondary task.

3.1.1.3.3 Metronomes and walking speed

In order to help participants keep their walking speed constant across trials, a metronome (80 beats/minute) was played to them via earphones while walking. The participants were told that walking in-time to the metronome was not important but walking at a constant speed across trial was essential. To avoid any confusion resulting from the conflict between the metronome tempo and frequency of colour changing, the rate of the metronome was synchronised with the change of target colour.

3.1.1.4 Procedure

At the beginning of each block, the participants were informed which target colour they should respond to for all the trials within that block. At the beginning of each trial, the virtual environment appeared on the screen with the target in orange. At this point, the participants were asked to orient their body to face the target. When they were ready, the experimenter initiated the trial so that the target started changing colour and the metronome began to play, and the participants were instructed to walk directly to the target. When the participants walked through the target, the trial was finished with the screen turning to blank and the metronome being stopped. Then with the aid of the experimenter, the participants turned around to face the opposite corner of the room.

Prior to the present experiment, each participant took part in a short experiment which involved walking to a target in the physical lab while wearing a pair of prism glasses (see Chapter 5). The reasons for combining the two experiments together were (1) to reduce time demands on the participants and (2) to make the participants feel more confident and comfortable in walking in a VE since they would have obtained experience with wearing the tracking equipment and performing the secondary task.

3.1.1.5 Data analysis

To examine the effects of environmental richness on the overall straightness, repeated-measures ANOVAs were performed on the overall mean target-heading angles. When sphericity assumptions were violated Greenhouse-Geisser corrections were used. In

post hoc tests, Bonferroni corrections were used to correct for the multiple comparison problem.

In addition to overall straightness, we also investigated the time course of cue use. We examined the difference in the change of straightness as a function of distance first and then as a function of both distance and trial. Growth models (see Section 2.4.2.1) were built up with distance or trial added into the model as the level-1 factor and environmental richness (scene) as the level-2 factor. The significance of the factor was evaluated by improvement of the model fit after adding the factor. The parameter estimates in the optimal model (adding factors results in no significant improvement of model fit) describes the difference between conditions in the intercept (i.e., initial straightness at 0.5m or on Trial 1) and slope (i.e., the changing rate of straightness against distance or trial).

3.1.2 Results

3.1.2.1 Overall straightness of walking trajectories in Trial 1

To examine the walking trajectories without the influence of adaptation, we focused on the trajectories in Trial 1. For visual inspection, mean trajectories are plotted in **Figure 3.3a**. These mean trajectories were averaged over the forty-eight participants. Note that the z position is presented as the distance from the target. This is, as we will show, for comparing the data across Experiment 3.1 and 3.2. As can be seen, the straightness of the mean trajectories was different between conditions. As expected, the least straight mean trajectory is in the *Line* condition. The straightness looks similar to predicted by the sole use of egocentric direction. The straightest mean trajectory is in the *Room* condition. The trajectories in the *Cloud* and *Outline* conditions are less straight than in the *Room* condition but straighter than in the *Line* condition.

To verify the observation on the straightness of the trajectories, statistical tests were run on the individual overall mean target-heading angles. The target-heading angles were collapsed across the left- and right-shifted trials with a positive sign indicating the predicted direction. As apparent in **Figure 3.3a**, there is a significant difference between the four conditions [$F_{3, 141} = 18.56$, $p < 0.001$, $\eta^2 = 0.28$]. Corresponding to being the least straight mean trajectory, the overall mean target-heading angle in the *Line* condition was the largest (mean = 9.86°, SD = 2.82°) and significantly larger than in the other conditions [all Bonferroni corrected *p*s < 0.05]. Correspondingly, the *Room* has the smallest overall mean target-heading angle (mean = 5.48°, SD = 2.45°), which is significantly smaller than in the other conditions (all Bonferroni corrected *p*s < 0.01). As shown by the trajectories, there was

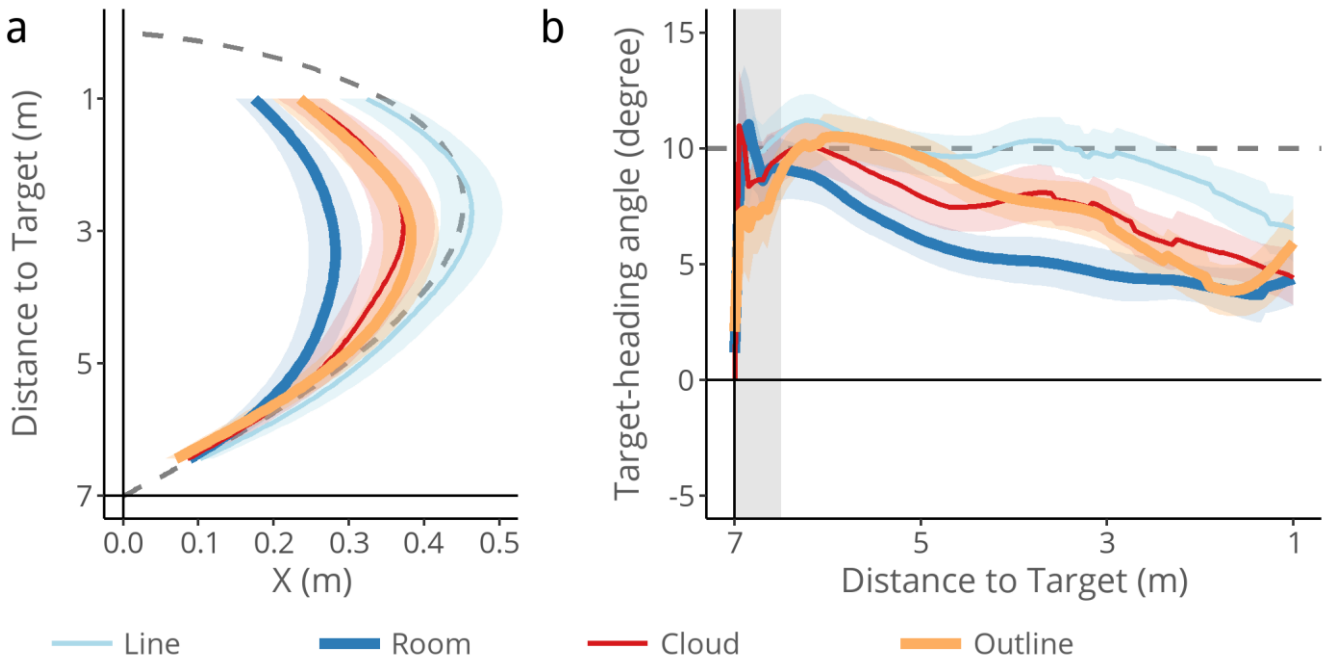

Figure 3.3 (a) *Mean trajectory in Trial 1 averaged across the 48 participants for each condition. Dashed line shows the trajectory that should result if only egocentric direction is used. Shaded areas indicate 95% confidence interval.* ***(b)*** *Mean target-heading angles averaged across the 48 participants as a function of distance in Trial 1.Solid line at 0° indicates that the trajectory is perfectly straight. The straightness decreases up the Y axis. Dashed line at 10° indicates the angular displacement between the visual and physical directions, and corresponds to the predicted trajectory by the sole use of egocentric direction (Dashed line in* ***(a)****. Grey shaded part at the beginning of the distance (0m ~ 0.5m) indicate the data that has been excluded from the final analysis. Shaded ribbons around the average data indicate 95% confidence interval.*

no statistically reliable difference between the *Cloud* and *Outline* conditions (*Cloud*: mean = 7.67°, SD = 3.08°; *Outline*: mean = 7.99°, SD = 2.76°; $p > 0.1$). To test the similarity in the overall mean target-heading angle between the *Cloud* and *Outline* conditions, we calculated a JZS Bayes factor was calculated using default prior [$BF_{01} = 6.18$] (Love et al., 2015; Morey & Rouder, 2015; Rouder, Morey, Speckman, & Province, 2012).

3.1.2.2 Straightness as a function of distance

To reveal differences in the dynamics of the use of cues, the target-heading angle was examined as a function of distance. As shown in **Figure 3.3b**, the target-heading angle reduces over the distance in all conditions, indicating a trend of straightening in the trajectories within in the trial. However, the pattern of straightening looks different. The target-heading angle in

the *Line* condition remained around 10° for the first 4m and then slowly decreased. This pattern suggests that the participants became more reliant on target drift as the cue became more salient when the participants walked closer to the target.

By contrast, the target-heading angle in the *Room* condition decreased directly after the beginning of the trajectory. The decrease was rapid and large for the early 2m (6.5m to 4.5m from the target) and then slowed down for the rest of the trajectory. This decrease replicated the earlier reported results from Warren's group (Bruggeman et al., 2007; Warren et al., 2001). They attributed such a quick decrease at the beginning of a trajectory to the use of optic flow. That is, the observer follows the egocentric direction of the target when making the first step. Once the observer starts moving, optic flow becomes available and its role becomes dominant in the guidance of walking, resulting in a quick decrease in the target-heading angle. However, this hypothesis seems not to hold for the data in the *Cloud* condition. Despite having the richest optic flow, the initial decrease in the *Cloud* condition does not look as quick as in the *Room* condition. In fact, as we will show later, the overall rate of decrease over the distance in the *Cloud* condition was as slow as in the *Line* condition.

The most interesting pattern appears when comparing the data in the *Cloud* and *Outline* conditions. Although the overall straightness was similar between the two conditions, the time course patterns appeared to be markedly different. In contrast to the pattern in the *Cloud* condition, the decrease of mean target-heading angle in the *Outline* condition started later but more rapid. At the early part of the trajectory, the mean target-heading angles look similar between the two conditions. The reduction of mean target-heading angle in the *Cloud* condition starts earlier and more rapid than in the *Outline* condition. However, after ~2m, the mean target-heading angle in the *Outline* condition quickly caught up with the *Cloud* condition. Towards the end of the trial, the mean target-heading angle in the *Outline* condition became as small as in the *Cloud* condition. This tendency can also be clearly seen on the mean trajectories in **Figure 3.3a**, in which the trajectory is more curved in the *Outline* condition from the beginning of the trial, but quickly catches up with the trajectory in the *Cloud* condition at a later point.

To statistically support the above observations, we examined the difference in the pattern of straightening from two aspects: (1) the rate of straightening as reflected by the gradient of target-heading angle against distance (i.e., a linear slope); and (2) the period(s) on the distance where the two conditions become significantly different in terms of straightness. As noted previously, growth modelling was employed for the former, and the in-house time-series analysis for the latter.

To build the growth model, the distance was first added into the model as the level-1 factor. It significantly improved the model fit [$\chi^2(1) = 2403.02$, $p < 0.0001$; see Supplementary materials 8.2.1.2for details], indicating an overall straightening of trajectories as observed. Adding both scene (i.e., *Line, Room, Outline* and *Cloud*) and interaction with distance into the model significantly improved the model fit [scene: $\chi^2(3) = 50.82$, $p < 0.0001$; interaction: $\chi^2(3) = 21.30$, $p < 0.0001$]. This suggests that the four conditions differed not only in the overall magnitude of mean target-heading angle but also in the rate of change against distance (i.e. slope). Evaluation of the model parameter estimates (see Section 2.4.2.1.2) showed that the slope was the flattest in the *Line* condition [estimate slope = -0.28], supporting the observation that the mean target-heading angle reduced slowest in this condition. The *Cloud* condition had a slope slightly steeper than the *Line* condition [estimated slope = -0.75], but the slope was slightly flatter than in the *Room* [estimated slope = -0.90]. The slope in the *Outline* condition was the steepest [estimated slope = -1.46]. Except in the *Line* condition, the slope was significantly negative in all conditions [all Bonferroni *p*s < 0.001], suggesting that target-heading angle decreased significantly over distance except in the *Line* condition. Pairwise comparisons on the slope estimates revealed that the slope in the *Outline* condition was significantly steeper than in the *Line* and *Cloud* conditions [both Bonferroni corrected *p*s < 0.05] (see Supplemental Material 8.2.1.2.5). Together, the statistics here are consistent with the pattern that we observe in **Figure 3.3**.

The trajectories in the *Cloud* and *Outline* conditions had similar overall straightness, but we have shown that they straightened at different rates. Visual inspection further suggests that the straightening started at different time points. To identify the part of the trajectory that the *Cloud* and *Outline* conditions were significantly different, we applied our bespoke permutation-based cluster analysis (see Section 2.4.2.2) on the t-statistics that were calculated by comparing the target-heading angles between the *Outline* and *Cloud* conditions at each point along the trajectory. We found a significant cluster ($p < 0.05$) from 1.33m ~ 2.48m (see **Figure 3.4**). The results further support the observation that the trajectories in the *Cloud* condition straightened earlier than the *Outline* condition, but the latter quickly caught up later in the trajectory.

Why does the trajectory straighten later in the *Outline* condition? In the *Outline* (and *Room*), the target was placed on the front wall. When the participants walked closer to the target, the perspective change in the shape of the front wall would become more obvious; hence the allocentric location cues would become more salient. In other words, the salience of allocentric location cues is inversely proportional to the distance from the target. If the

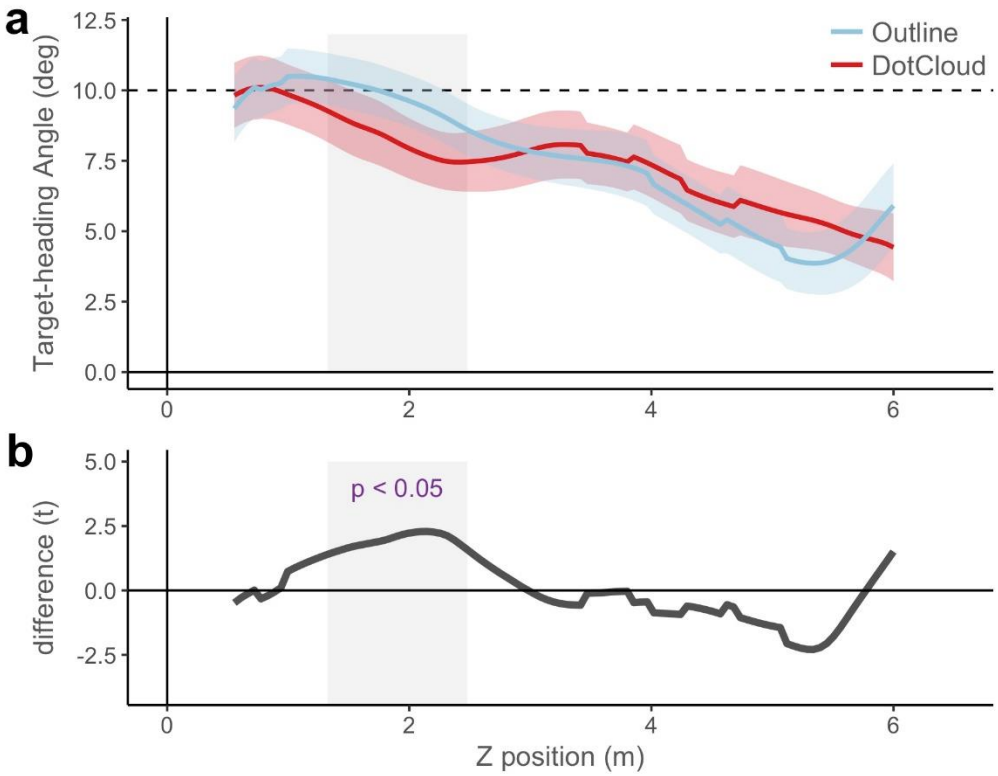

Figure 3.4. (a) *Mean target-heading angles against distance over participants (n = 48) respectively for the Outline and Cloud conditions. Dashed grey line at 10° indicates degree of displacement in the VE. Coloured areas indicate 95% confidence interval. Grey shaded area represents the part on distance where the Cloud condition is significantly straighter than the Outline condition.* ***(b)*** *Difference (t-values) comparing target-heading angle between the Outline and Cloud conditions. Grey area represents the period where t-values are considered (p < 0.05) to be significant as a cluster.*

allocentric location cues contribute to the guidance of walking, one would expect a trajectory that starts to straighten at a later point and faster near the target. This is what we observed on the trajectories in the Outline condition.

Interestingly, there was no such a tendency of late straightening observed in the *Room* condition; in fact, the magnitude of the decrease in the *Room* was smaller than in the *Outline* condition, albeit with better allocentric location cues and optic flow. This might be the case that there was a ceiling effect when the trajectory straightens quickly and hits a plateau.

Taken together, the time course results here showed a pattern that was well captured by the salience of allocentric location cues. At a later point on the trajectory, allocentric location cues become more salient. This corresponds to the late but faster straightening of trajectories in the Outline condition.

3.1.2.3 Straightness as a function of trial

If participants wear prisms for a period of time, adaptation occurs (Redding & Wallace, 1996). A simple example to illustrate this is that, viewing through left-shifting prisms placed in front of your eye and trying to reach the cup that appears to be in front of you, if you make a fast-ballistic movement, your hand will initially end up to the right of the cup. However, over repeated reaches, the error will decrease and finally, you will reach accurately for the cup. Here in our experiment, adaptation is reflected in straightened trajectories (and reduction in target-heading angle) over the test trials. This thus would raise an issue if we examine data that are averaged across the test trials. That is, adaptation rate might vary systematically within a test block depending on the available cues. Such variation could complicate the interpretation of mean walking trajectories that are averaged over the test trials. In other words, the straight mean trajectories that we observed may be due to adaptation to the virtual prisms over the course of several trials, rather than due to the use of cues in the online guidance of walking.

The main purpose of the thesis is investigating the online control of walking, rather than adaptation to prismatic displacement. Therefore, to minimise the possibility that adaptation might take place during the test trials themselves, we deliberately kept the number of trials low (i.e., four in this experiment) and examined the data in the first trial to isolate the influence of adaptation. However, adaptation usually occurs particularly rapidly during the first a few trials (see the data in Bruggeman, Zosh, & Warren, 2007). Therefore, examining the data as a function of trial enables us to see trial-to-trial differences and to obtain a better idea about the extent to which the pattern that we observed on the trajectories in Trial 1 persists across the test trials. For example, the magnitude of straightening is small in the first trial but increases over the subsequent trials as the observer gets better at using the cues.

We examined the early part (5.75m ~ 6.25m from the target) and later part (1.75m ~ 2.25m)[5] as a function of the trial. Because the observer follows the egocentric direction of the target at the onset of a trial, any change in the mean target-heading angle of the early part suggests adaptation that may result from changes in the perceived straight ahead. The

[5] The distances were chosen because the data will be compared to heading judgements in Experiment 2 and the heading judgements were between 7m and 3m (specifically 7~6.25m and 3~2.25m). The choice was based on the assumption that it takes ~1m for participants to process the information and to make step (typical step distance of ~0.35m was used).

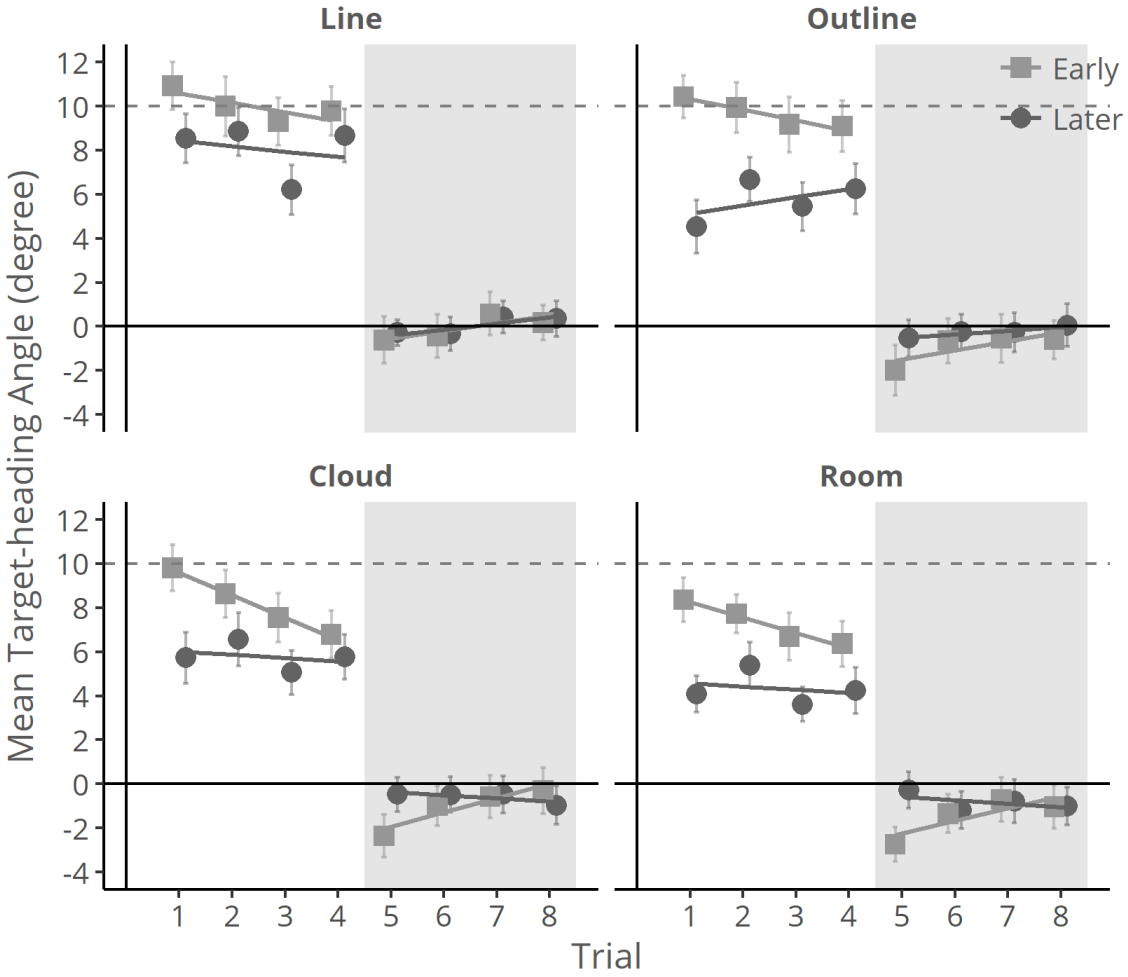

Figure 3.5*. Overall mean target-heading angles as a function of trial for the test blocks (Trial 1 ~ 4) and the subsequent blocks (Trial 5 ~ 8). Shaded region corresponds to the four trials in the test blocks. The overall mean target-heading angles were averaged over the distance (6.5m – 1m to the target) and across trials and participants. Error bars indicate 95% confidence interval.*

difference between the early and later parts indicates the magnitude of straightening that occurred over the course of the trial.

For visual inspection, **Figure 3.5** plots the mean target-heading angles of the early and later parts against trials. The data of the four test trials are shown in the clear areas; whereas the data of the four baseline trials are shown in the shaded areas. As can be seen, the overall pattern of the magnitude of target-heading angles looks general consistent with what we observed on the trajectories in Trial 1. The mean target-heading angle is smaller in the later part than in the early part, indicating a trend of straightening in the trajectories over the course of the trial. The overall magnitude of reduction appears to be the largest in the *Outline* condition, followed by the *Room* condition, and the smallest in the *Line* and *Cloud* conditions, a pattern consistent with the pattern that we observed on the trajectories in Trial 1.

In support of this observation, growth modelling revealed a significant effect of part (early and later) and interaction with scene on the intercept (mean target-heading angle) [respectively $\chi^2(1) = 112.34$, $p < 0.0001$ and $\chi^2(3) = 12.17$, $p < 0.01$] (see Supplementary Materials 8.2.1.3.1).

The mean target-heading angle of the early parts decreased over the test trials at different rates between conditions. The decrease in the *Cloud* condition is the largest, followed by the decrease in the *Room*, and looks the smallest in the *Outline* and *Line* conditions. To verify this, a separate growth model was built on the mean target-heading angles of the early parts (see Supplemental Material 8.2.1.3.2). The model comparisons revealed a significant effect of scene on the slope [$\chi^2(3) = 8.16$, $p = 0.043$]. Evaluation of the model parameters showed a steepest slope in the *Cloud* condition [estimated slope = -1.02] which was marginally steeper than the *Line* condition [estimated difference in slope = 0.59, $z = 0.29$, $p = 0.058$]. The slope in the *Room* [estimated slope = -0.70] conditions were flatter than the *Cloud* condition, but steeper than both *Outline* [estimated slope = -0.48] and *Line* [estimated slope = -0.43] conditions.

The results suggest that there was some adaptation of walking direction to the "virtual prism" during the test trials, and the magnitude of adaptation differed between conditions. The magnitude of adaptation was smaller in the *Line* and *Outline* conditions, the two conditions with the minimum of optic flow. In contrast, in the two conditions with a large amount of optic flow, *Room* and *Cloud*, the magnitude of adaptation was larger. The magnitude of adaptation was the largest in the *Cloud* condition where the amount of optic flow was the richest.

3.1.2.3.1 Aftereffects of adaptation

Back to the cup-reaching example, when you try to reach the cup whilst wearing prisms, you will ultimately reach the cup accurately. If you remove the prisms at this point and try to reach the cup again, you will find your hand end up to the left of the cup, opposite to the deflecting direction of the prisms. This is because the adaptation persists after the removal of the prisms; this is known as a "negative aftereffect". Again, after a few reaches, you will reach the cup accurately, which indicates a full recovery from the negative aftereffect. Similarly, in our experiment, if you adapt to the "virtual prism" during the test trials, after removing the "virtual prism" you will end up heading to the opposite direction of the "virtual prism", resulting in a trajectory veering to that direction and a mean negative target-heading angle.

Immediately after each test block, there were four baseline trials with the "virtual prism" removed. This enables us to assess the aftereffects that resulted from the adaptation to the "virtual prism" in the test trials. As shown in **Figure 3.5**, the magnitude of aftereffects was the smallest *in the Line* condition. The mean target-heading angle of the early part in the first baseline trial (Trial 5) was is -0.61° [SD = 3.69°]. The magnitude of aftereffects was larger in the *Outline* [mean = -1.99°, SD = 3.91°] and the *Cloud* [mean = -2.36°, SD = 3.34°] conditions, and the largest and the *Room* condition [mean = -2.74°, SD = 2.67°]. Except for the *Line* condition, the mean target-heading angle of the early part of Trial 5 was significantly smaller than 0° in all conditions [all one-tailed *p*s < 0.001].

In all conditions, the mean target-heading angles of the early parts increased to be closer to 0° over the baseline trials, as shown in **Figure 3.5**. This suggests a recovery from the aftereffects. On the last trial (Trial 8), the aftereffects were abolished in all conditions [all one-tailed *ps* > 0.05] except the *Room* [mean = -1.04°, t(47) = -2.11, one-tailed $p = 0.02$].

This raises the question of whether the residual aftereffects had any impact on the trajectories in the other conditions. Given the counterbalanced design in this study, the effects of the residual aftereffects would be evenly distributed among the other three conditions in those test blocks following the *Room* condition, resulting in an increase of about ¼° in the average target-heading angles. In addition, the increase would not change the comparison between the *Line*, *Outline* and *Cloud* conditions. Hence, we consider that if there is any residual after-effect, it is very small and it would not change any of the conclusions drawn[6].

3.1.2.4 Walking speed and correlation with target-heading angle

At last, we examined the walking speed and its relationship with the straightness of walking trajectories. As shown in **Figure 3.6a**, the mean walking speed of Trial 1 differed between conditions [$F_{3, 141} = 16.18$, $p < 0.001$, $\eta^2 = 0.032$]. Participants walked fastest in the *Room* condition [M = 0.75m/s, SD = 0.16m/s], and slightly slower in the *Outline* condition [M = 0.74m/s, SD = 0.15m/s]. Participants walked slowest in the *Line* condition [M = 0.68m/s, SD = 0.15m/s], and slightly faster in the *Cloud* condition [M = 0.70m/s, SD = 0.16m/s]. *Post hoc* test revealed that the walking speed in the *Room* and *Outline* conditions

[6] We tried correcting the data using several values as estimates of the residual aftereffects and then corrected the data by subtracting the values. The results were consistent with the analyses on the uncorrected data.

was significantly faster than that in the *Line* and *Cloud* conditions [both Bonferroni *p*s < 0.01]. Thus, the order of walking speed is: *Line* ≈ *Cloud* < *Outline* ≈ *Room*.

As suggested by the model proposed by Warren et al. (2001), the contribution of optic flow depends on the walking speed. Therefore, one might argue that the less straight trajectories in the *Cloud* condition than the *Room* condition could be (to some extent) due to the slower walking speed in the former. If this hypothesis is true, then one would expect to see a negative correlation between walking speed and the magnitude of target-heading angle within both *Cloud* and *Room* conditions. In other words, in these two conditions with rich optic flow, walking faster would lead to more salient optic flow and straighter trajectories. However, as shown in **Figure 3.6b**, the correlation was very weak and did not reach significance in either *Cloud* condition [Pearson's r = -0.081, t(46) = -0.55, p = 0.59] or *Room* condition [Pearson's r = 0.0039, t(46) = 0.026, p = 0.98]. Similarly, there was no significant correlation in the *Line* [Pearson's r = -0.048, t(46) = -0.33, p = 0.74] and *Outline* [Pearson's r = 0.026, t(46) = 0.18, p = 0.86].

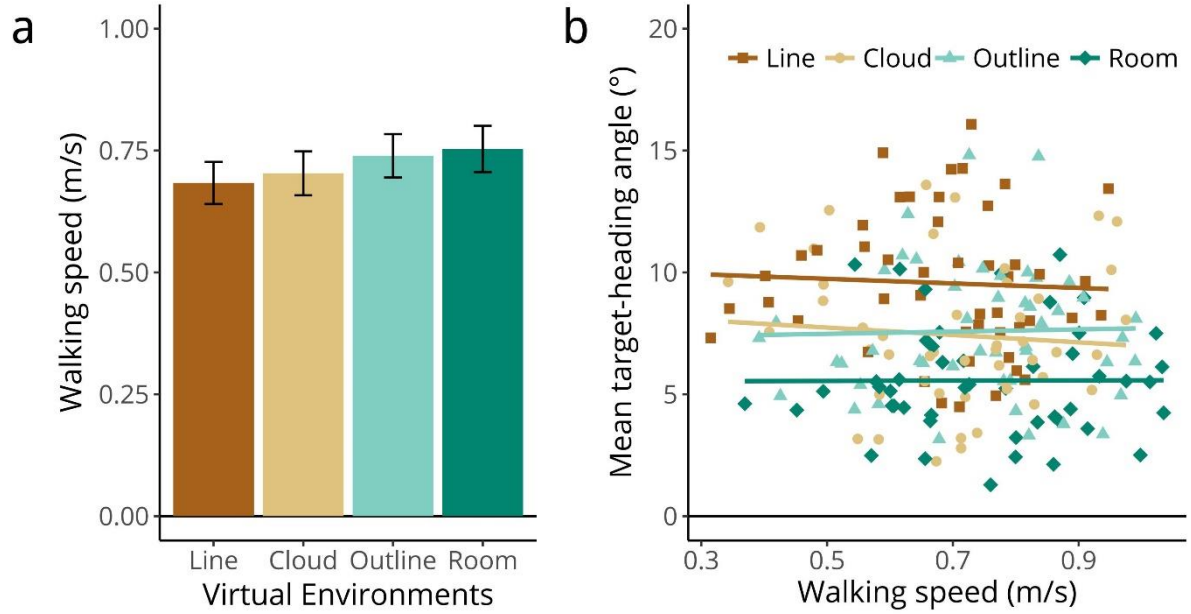

Figure 3.6. (a) *Mean walking speed on Trial 1 in each condition (Line, Cloud, Outline and Room). Error bars correspond to 95% confidence interval.* ***(b)*** *Relationship between walking speed and the magnitude of target-heading angle for each condition.*

3.1.3 Discussion

In Experiment 3.1, we attempted to disassociate the role of optic flow and allocentric location cues. We examined the walking trajectories in four virtual environments that varied

in the richness of cues from three perspectives: overall straightness, the time course of cue use (straightness as a function of distance) and adaptation (straightness as a function of trial). We asked the question whether the pattern of results is better captured by the use of optic flow or allocentric location cues.

3.1.3.1 Does the use of optic flow capture the pattern of results?

If optic flow dominates the control of walking, one would expect to observe the overall straightness of the walking trajectories to be proportional to the richness of optic flow: *Line* < *Outline* < *Room* < *Cloud*. However, the pattern of results is different. Although the *Cloud* condition contains more optic flow than the *Room* condition, the trajectory is significantly more curved. By contrast, the *Outline* condition contains much less optic flow than the *Cloud* condition, but the overall straightness is similar between the two conditions.

In terms of the straightening of trajectory against distance, the pattern is also somewhat unexpected by the use of optic flow. According to Warren et al. (2001), the large increase in the trajectory straightness at the beginning of the path in the *Room* condition is indicative of the dominance of optic flow once it becomes available. Following this logic, we should observe an even larger decrease in the *Cloud* condition; however, the magnitude of the decrease was smaller.

The magnitude of adaptation in the *Cloud* and *Room* conditions that are rich in optic flow appears to be larger than the other conditions. This pattern is compatible with the previously reported observation that optic flow drives adaptation (Bruggeman et al., 2007; Herlihey & Rushton, 2012).

3.1.3.2 Does the use of allocentric location cues capture the pattern of results?

If allocentric location cues dominate the control of walking, one would expect to observe the overall straightness of the walking trajectories to be proportional to the richness of allocentric location cues: *Line* < *Cloud* < *Outline* < *Room*. This hypothesis seems to capture the pattern of results better than the optic flow hypothesis. One thing that is not captured well by the allocentric hypothesis is that the trajectories in the *Outline* and *Cloud* conditions are equally straight. However, the straightening of trajectories in the *Outline* condition is later but more rapid than in the *Cloud* condition. This tendency would be expected as the allocentric location cues would become more salient when the observer is closer to the target (and the front wall). We will investigate the impact of the target distance

in Chapter 4. In the next experiment, we will explore the relationship between walking trajectories and heading judgements.

As we excluded the data at the beginning of the trial (0m ~ 0.5m, about 1 ~ 2 steps) because of the large amount of noise, it is possible that the more rapid straightening up in the *Outline* condition than in the *Cloud* condition might have been driven by artefacts. For example, the target-heading angle in the *Cloud* condition might be high for the first step but rapidly decreased. In the *Outline* condition, however, the target-heading angle might be small initially because the observer did not follow the egocentric direction for the first step. Then the observer started to use the egocentric direction cues so the target-heading angle increased to 10°. This slightly later increase in the target-heading angle might have been responsible for the more rapid straightening in the *Outline* condition. To test this possibility, the data at the beginning of the trial was included in **Figure 3.3b** (grey shaded area). The target-heading angle before 0.5m does appear smaller in the *Outline* condition. However, it should be noted that the data in this range contain a large number of noise due to both slow walking speed at the beginning and smoothing procedure. It should also be noted that, regardless of where the target-heading angle started to decrease, the target-heading angle at the end of the trial in the *Outline* condition was comparable to or even smaller than in the *Cloud* condition. The pattern persisted over the four test trials.

In the following chapters, the target-heading angle data at 0m ~ 0.5m will be included for visual inspection and indicated by dark grey shaded areas in figures for reference.

3.2 Experiment 3.2 Is heading judgement a good predictor of walking trajectories?

A forward translation was simulated through the same four virtual environments. The translation started at four distances from the target (i.e., 7m, 6m, 5m and 3m). Participants were asked to determine the direction of the movement relative to the target. Their heading judgement performance was compared to the walking trajectories in Experiment 3.1. The role of optic flow and allocentric location cues in heading judgement is also examined.

As an aside, we tested a confound that the less straight trajectory in the Cloud condition in Experiment 3.1 was due to the disrupted perception of optic flow by the HMD. If perception optic flow is disrupted by the HMD, one should observe performance to be poor in the *Cloud* condition. Otherwise, the precision should be close to those reported in earlier studies, ~1°-2° (Warren & Hannon, 1988).

If the heading judgement is able to predict the walking trajectories, the precision of heading judgements should follow an order *Line* < *Outline* = *Cloud* < *Room*; and the change in the precision as a function of distance should follow an order *Line* = *Cloud* < *Room* < *Outline*. If the heading judgement relies purely on optic flow, the precision should follow the order *Line* < *Outline* < *Room* < *Cloud* and there should be no change across the distances. If the heading judgement is dominated by allocentric location cues, the precision order should be *Line* < *Cloud* < *Outline* < *Room* and the order of change should be *Line* = *Cloud* < *Room* < *Outline*.

3.2.1 Method

3.2.1.1 Participants

A total of twenty-eight participants were recruited. One participant aborted due to nausea. The demographic statistics of the remaining twenty-seven participants were (mean age = 19.85, SD = 1.51, range: 18 ~ 25, 5 males). All reported normal vision or vision that was corrected to normal vision with contact lenses. None reported impairments of stereo or colour vision. Fourteen participants had completed Experiment 3.1 before taking part in the current study; the remaining participants had no experience with Experiment 3.1.

3.2.1.2 Apparatus

The experiments were written and run in Vizard (Worldviz Inc.) on a laptop (Dell Inc., US). The stimuli were presented on the same head-mounted display (approximately 100° vertical × 95° horizontal, Oculus Rift DK2, Oculus Inc.) that was used in Experiment 3.1. Throughout the experiment, participants were seated and wore the head-mounted display. Their head orientation was tracked by the head-mounted display and updated in the image presented on the HMD. The initial orientation in the VE was calibrated to face the straight-ahead of the participants' body.

3.2.1.3 Stimuli

The stimuli simulated a forward translation from the first-person perspective in the same four virtual scenes (*Line, Outline, Cloud* and *Room*; **Figure 3.1**) from Experiment 3.1. The participant's task was to judge the direction of the simulated movement relative to the target (+: rightwards; -: leftwards). The value of the heading angle was determined using Kesten's adaptive staircase (Kesten, 1958) with an initial value of 5°. The sign of the value was randomised between trials.

The speed of the simulated movement was 0.75m/s, which was determined according to the average walking speed in Experiment 3.1 (0.73m/s). The eye height of the view was adjusted according to each participant's height (*height – 10cm*). This was to match the situation in Experiment 3.1 where the height of the view in the VE was determined by the position of the head rigid body (see Section 2.2).

3.2.1.4 Design and procedure

The experiment was a within-subject design. Each participant viewed the simulated translation in all four virtual scenes. In addition, the four scene conditions were crossed with four distance conditions in which the initial distance to the target was respectively 7m, 6m, 5m, and 3m. The longest 7m corresponds to the overall walking distance in Experiment 3.1. The other three distances were selected on the basis of the intention to observe performances changing over the distances.

The experiment consisted of four blocks, corresponding to the four virtual scenes. Each block consisted of four Kesten's staircases (Kesten, 1958) interleaved with each other. Each staircase corresponded to the four target distance conditions, and contained 25 test trials, yielding 400 test trials in total (25 test trials × 4 distance conditions × 4 scene conditions).

To ensure that the participant was paying attention to the test, each block also contained 15 catch trials that were intermixed with the test trials, yielding a total of 60 catch trials. In these catch trials, the heading angle was set to 10°, and the direction was randomly chosen. For all catch trials, the distance was set to 3.5m, the midpoint of the longest distance. We purposely made the heading judgment task in these catch trials very easy so that an attentive participant should achieve a relatively high accuracy. Indeed, the mean accuracy of all participants who finished the experiment (n = 27) was 98%. Moreover, twenty-four participants achieved an accuracy of at least 98.3%, which means that they got at most one catch trial wrong. The performance on the catch trials suggests that the participants were attentive to the heading-judgment task.

As the participant's head orientation was tracked and updated in the display online, it was necessary to make sure that they all faced the direction of the target at the beginning of each trial. Therefore, we set up a calibration phase before each trial. In the calibration phase, the participant saw a half-transparent blue square and a white fixation across on a black screen. The blue square was placed at the centre of the participant's view and followed the participant's head orientation. The white cross, however, was fixed at the centre of the black

screen, corresponding to the direction of the target. Participants were instructed to move their head so that the centre of the blue patch overlapped with the white cross and to keep them overlapped until the start of the trial. Consequently, at the start of each trial, the participant was facing the direction of the target.

When the trial started, the participants saw their view moving in a virtual scene. The movement lasts 1s at the speed of 0.75m/s. During the 1s of movement, the participants were encouraged to move their head to help distinguish the heading (e.g., by fixating on the target). Once the movement ended, the screen turned blank and the participants were instructed to make the response at this point. Participants were asked to make the response only after the screen turned blank in order to register the response and trigger the next trial. No feedback was given in the test trials.

Before the actual experiment, each participant finished 12 practice trials with feedback. In the practice trials, the virtual scene was the same as the baseline condition in Experiment 3.1 (**Figure 3.1**). Participants experienced 3 trials for each starting distance (7m, 6m, 5m and 3m). Similar to the actual experiment, the starting value of heading angle was 5°, and the value in the following trials was determined using Kesten's staircase. After the practical trials, all participants reported that they were familiar with the procedure and ready for the actual experiment.

The whole experiment was self-paced. Participants could have a break between blocks, but if needed, they could also have a rest within the block by simply not pressing the key. The whole experiment lasted approximately one hour.

3.2.1.5 Data analysis

The response data were fitted using Cumulative Gaussian model (package *glm* in R, version 3.2.4). Thresholds were determined as the distance in stimuli intensity (heading direction) between 25% and 75% accuracy. Any data that were more than 3 standard deviations from the mean were excluded. A total of 2.8% of the data was excluded.

3.2.2 Results

The mean threshold at each distance and in each condition is shown in **Figure 3.7a**. We first examined whether there was no statistical difference between the participants who had taken part in Experiment 3.1 before Experiment 3.2 (Experienced) and those who had not (Novel). There was no significant difference in the pattern of thresholds between the two groups (for more details see Supplementary Materials 8.2.2.1). Therefore, the data from the two groups were combined.

First, we collapsed the thresholds over distances and compared the mean thresholds between conditions. As shown in **Figure 3.7b**, the mean thresholds were significantly different [$F_{1.36,\ 34.09} = 7.566$, $p < 0.01$, $\eta^2 = 0.23$]. The mean thresholds in the *Line* (mean = 1.86°, SD = 1.48°) and *Outline* (mean = 1.65°, SD = 0.54°) conditions were significantly larger than in the *Cloud* (mean = 1.06°, SD = 0.43°) and *Room* (mean = 1.23°, SD = 0.53°) conditions (all one-tailed *p*s < 0.05 except between *Line* and *Room* $p = 0.065$, Bonferroni correction).

Next, we examined the thresholds as a function of distance. As can be seen from **Figure 3.7a**, the thresholds remained relatively constant around 1° throughout distance for both *Cloud* and *Room* conditions. In contrast, the thresholds changed remarkably over the

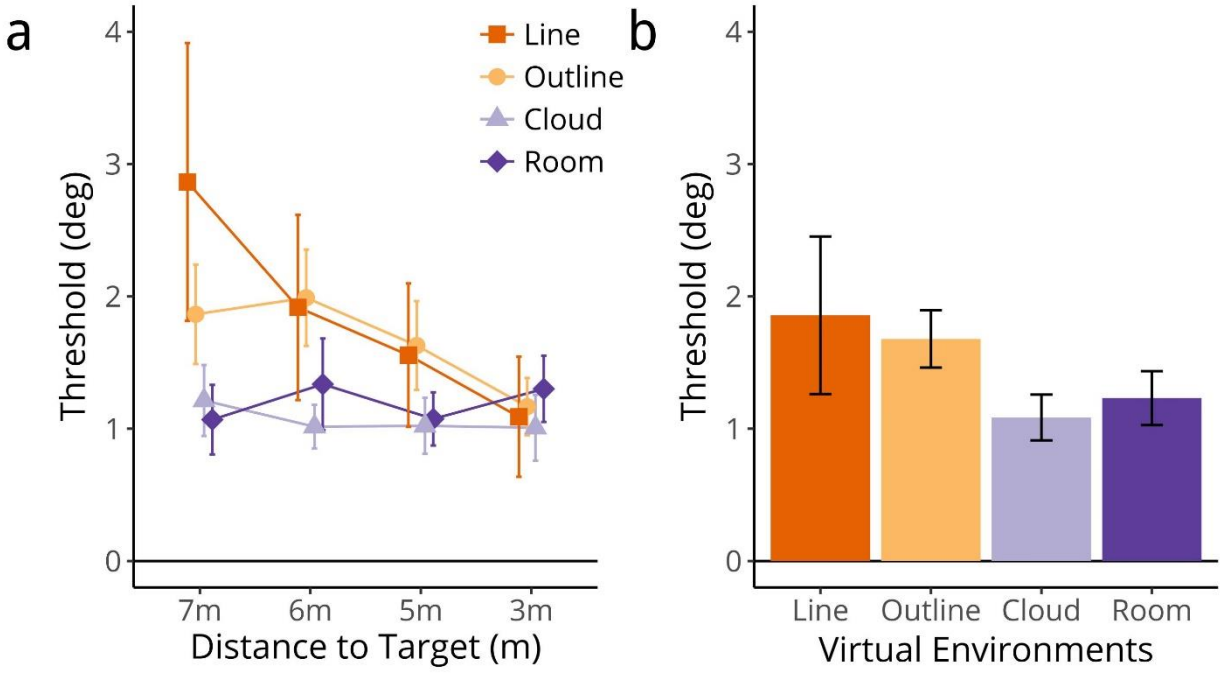

Figure 3.7 (a) *Mean threshold for each virtual environment for each distance (7m, 6m, 5m and 3m). Position of four curves jittered to aid readability. Error bars indicate 95% confidence interval;* ***(b)*** *Mean threshold for each virtual environment. Error bars indicate 95% confidence interval.*

distances in the *Line* and *Outline* conditions. At a far distance from the target (7m), the mean thresholds in the *Line* and *Outline* conditions were respectively 2.48° (SD = 2.12°) and 1.79° (SD = 0.93°). However, near the target (at 3m) the thresholds in the two conditions respectively decreased to 1.08° (SD = 1.15°) and 1.16° (SD = 0.52°), close to the thresholds in the *Cloud* (mean = 1.00°, SD = 0.63°) and *Room* (mean = 1.23°, SD = 0.59°) conditions.

To examine the difference in the gradient of thresholds against distance (slope) between virtual environments, a growth model was built on the individual thresholds with Distance (7m, 6m, 5m, 3m) and Scene (*Line, Outline, Cloud* and *Room*) respectively as the level-1 and level-2 factors. Scene had a significant effect on the slope [$\chi^2(3) = 29.52$, $p < 0.0001$], in support of the observation above that the threshold changed differentially depending on the environment. In particular, tests on the model parameters showed that only the slopes in the *Line* and *Outline* conditions were significantly negative [both *p*s < 0.0001], suggesting that the thresholds decreased significantly when the view moved close to the target. Between the *Line* and *Outline* conditions, the slope was steeper for the former than the latter [$p = 0.083$]. Moreover, the slope in the *Line* was considerably steeper than in the *Cloud* and *Room* conditions [both Bonferroni *p*s < 0.0001]. The slope in the Outline was significantly steeper than in the *Room* condition [Bonferroni $p = 0.026$] and slightly steeper than in the *Cloud* condition [Bonferroni $p = 0.18$]. Together, the results indicate a larger decrease over the distance in the *Line* and *Outline* conditions compared to the *Cloud* and *Room* conditions.

Furthermore, the growth model revealed that the pattern of mean thresholds persists at the far distance (7m) – the thresholds of the *Line* and *Outline* conditions were significantly higher than those of the *Cloud* and *Room* conditions [all Bonferroni *p*s < 0.05]. In contrast, at the close distance (3m), the thresholds became similar between the conditions and there was no significant difference between the conditions [$F_{2.05,\ 49.08} = 0.513$, $p = 0.061$, $\eta^2 = 0.021$].

3.2.3 Discussion

In Experiment 3.2, we asked two questions: (1) whether heading can be perceived accurately from optic flow on the HMD and (2) whether performance on heading judgments can predict walking trajectories. The first question is pertinent to our interpretation of the walking trajectories observed in Experiment 3.1; that is, whether the less straight trajectories observed in the *Cloud* condition were due to disruption of optic flow by the HMD. The second question relates to what the large body of evidence from the heading perception literature tells us about the guidance of walking.

3.2.3.1 Is perception of optic flow disrupted by the HMD?

The question could be answered by the performance of heading judgements in the condition with pure optic flow, the *Cloud* condition. The mean thresholds are around 1° in both conditions, which is close to those reported earlier (Warren & Hannon, 1988). Such a high precision of heading judgements indicates that the perception of optic flow was adequate on the HMD. Therefore, we dismissed the possibility that the less straight trajectories that we observed in the *Cloud* condition in Experiment 3.1 were due to the disruption in the perception of optic flow by viewing the stimuli on the HMD.

3.2.3.2 Can optic flow predict heading judgements?

Before answering the question, I will first evaluate whether the performance of heading judgments was better captured by the hypothesis of optic flow or allocentric location cues. The mean precision of heading judgements across distances followed an order: *Line* = *Outline* < *Cloud* = *Room.* This pattern was captured better by the optic flow hypothesis (*Line* < *Outline* < *Cloud* < *Room*) than by the allocentric hypothesis (*Line* < *Cloud* < *Outline* < *Room*).

The *Line* condition contained target drift. In this condition, the precision of heading judgment increased as the observer got closer to the target. As highlighted in the *General Introduction* (Section 1.3.1) and demonstrated by earlier reported results, the salience of target drift is inversely proportional to the distance from the target. When the observer gets closer to the target, the apparent movement of the target will become more obvious. In this sense, the pattern of heading judgments in the *Line* condition reflects the use of target drift.

The *Outline* condition contained allocentric locational cues in addition to the target drift. However, there appears to be no added influence of allocentric location cues on the heading judgments. The mean precision and the rate of increase in the precision was similar to those in the *Line* condition.

The *Cloud* condition contained the richest optic flow, the mean precision of heading judgment was high independent of the distance to the target. The *Room* condition contained rich optic flow and allocentric location cues, however, like the *Outline* condition, there was no impression of added influence of allocentric locational cues in the heading judgments. Both the average precision and the pattern of precision as a function of distance were similar to those in the *Cloud* condition. The similar average precision might be due to the combined use of optic flow and allocentric location cues in the *Room* condition, because the *Room*

condition contained medium optic flow and allocentric location cues as compared to the *Cloud* condition that contained purely rich optic flow. However, if that is the case, then one would expect to observe some increase in the precision with the distance to target decreases, but the increase was neglectable. The lack of change in the precision, however, might be due to a ceiling effect.

Taken together, the pattern of results cannot be explained by optic flow alone. Target drift may also play an important role. However, the contribution of allocentric location cues remains unclear.

3.2.3.3 Can heading judgements predict walking trajectories?

Next, I turn to the main question of whether the performance on the heading judgment can predict the straightness of walking trajectories. In Experiment 3.1, the overall straightness of walking trajectories follows an order *Line* < *Outline* = *Cloud* < *Room*, which was different from the order of precision of heading judgements in Experiment 3.2. The walking trajectories were significantly straighter in the *Outline* condition than in the *Line* condition, but the precision of heading judgements was similar between the two. The walking trajectories were significantly more curved in the *Cloud* condition than in the *Room* condition, but the precision of heading judgements was also similar between the two.

Taking the change against distance into account, the patterns of results in the two experiments also look different. The difference can be seen by comparing **Figure 3.5** and **Figure 3.7**. It should be noted that, when I examined the magnitude of straightening in the walking trajectories, I had taken into account the time that it might take for the observer to process the information and to make the step by calculating the early part as 5.75 ~ 6.25m from the target and later part as 1.75m ~ 2.25m from the target. The reduction between the early and later parts corresponds to the heading judgements between 7m and 3m (specifically 7m ~ 6.25m and 3m ~ 2.25m). In both *Line* and *Outline* conditions, the precision of heading judgements increased with the distance to target decreased. However, for the walking trajectories, although straightness increased in both conditions, the speed of straightening was significantly higher in the *Outline* than in the *Line* condition. In the *Cloud* and *Room* conditions, the walking trajectories straightened significantly over the distance, but the precision of heading judgements remained constant.

In sum, the precision of heading judgements predicts walking trajectories poorly, both in terms of the average precision and precision as a function of distance.

3.3 General discussion and Summary

In this chapter, our results called into question two important assumptions of the optic flow theory: (1) optic flow controls walking and (2) heading judgements predicts walking trajectories. In both experiments, the richness optic flow and heading judgements were unable to capture the pattern of walking trajectories.

Our results provided evidence for the use of allocentric location cues in the visual guidance of walking. The pattern of walking trajectories was better predicted by the use of allocentric location cues. Furthermore, our results showed a temporal profile of the use of allocentric location cues. When the salience of allocentric location cues increases towards the end of the trajectory, the contribution of the cues becomes more prominent.

In addition, our results suggest that heading judgement may not solely rely on optic flow. When the observer was near the target, the performance in the *Line* condition was comparable to that in the *Room* and *Cloud* conditions, suggesting that target drift may also play an important role in heading judgement.

In the next chapter, we will explore the influence of target location on the walking trajectories.

4 Impact of target location on walking trajectories

In Chapter 3, we provided evidence for the utility of allocentric location cues in the visual guidance of walking. An interesting finding was that the use of cues may depend on the observer's distance from the target. In this chapter, we explore the influence of target location on the straightness of walking trajectories. In two experiments, the walking environment was held constant so that the amount of optic flow and allocentric location cues remained unchanged. However, through manipulating the location of the target, we varied the salience of allocentric location cues. In Experiment 4.1, participants walked in a virtual room. The location of the target was manipulated with respect to the virtual room so that the perspective shape of the room structure was varied, which would lead to varied salient perspective cues. In Experiment 4.2, participants walked on a patterned ground plane towards a target. The initial distance of the target was manipulated so that the strength of target drift and motion parallax was varied. In both experiments, a virtual prism was added to displace the visual direction from the physical direction of the participants. Doing this enabled us to evaluate the impact of the target location from the shape of the resultant walking trajectories.

4.1 Experiment 4.1 Role of perspective cues of symmetry

A potential cue that an observer can use to recover his or her allocentric location during walking is the perspective shape of objects in the environment. As mentioned in Chapter 1 (Section 1.2.1.2), Beusmans (1998) proposed that the perspective shape of objects provides an important source of information about the moving direction. Particularly, the symmetry in the perspective shape could be a powerful cue.

Consider you are walking directly towards a frontoparallel wall. The two sides of the wall will remain at equal distances to your eyes, resulting in a symmetrical expanding motion pattern in the images on your retina (see $\mathbf{t_1}$ in **Figure 4.1a**). If you walk to the right, the distances of the wall at your two sides will become different with the retinal size right part of the wall being larger than the left part. This results in an asymmetrical expanding motion pattern in the retinal image (see $\mathbf{t_2}$ to $\mathbf{t_3}$ in **Figure 4.1a**). Therefore, any change in the symmetry of the retinal image of the wall would signal a change in your walking direction.

In the same vein, if you walk directly to a corner, the retinal image of the two subtending walls will be symmetrical (see $\mathbf{t_1}$ in **Figure 4.1b**), and any change in the symmetry

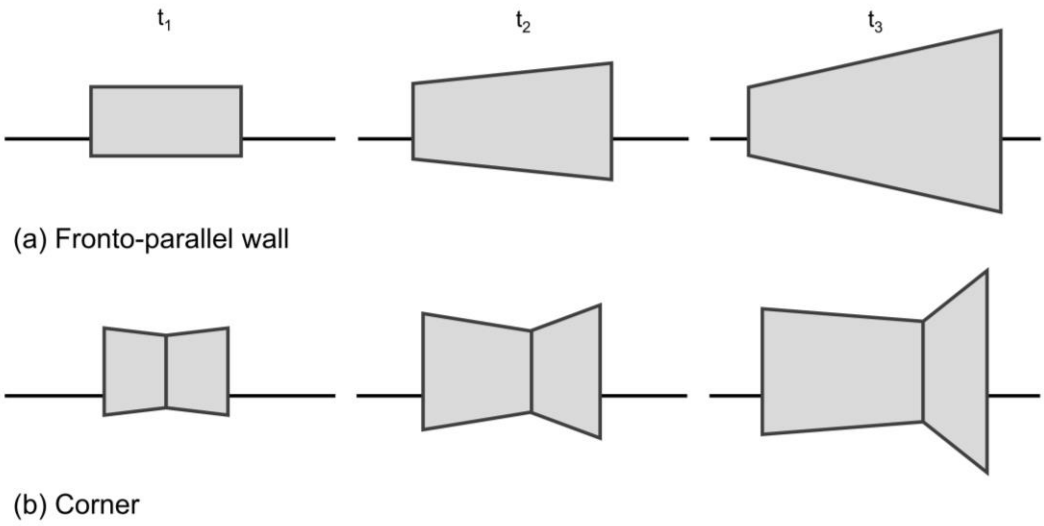

Figure 4.1. *Schematic sample views of an observer's movement towards the right side of a frontoparallel wall* ***(a)*** *and a corner* ***(b)****. In* ***(a)*** *and* ***(b)*** *it can be clearly seen that, from* t_1 *to* t_3*, the movement is to the right of the target object. In both* ***(a)*** *and* ***(b)****, when moving from* t_2 *to* t_3*, the perspective symmetry cues are weaker than when moving from* t_1 *to* t_2*, as the symmetry has been broken.*

of the retinal image of the walls would signal a change in walking direction (see $\mathbf{t_2}$ to $\mathbf{t_3}$ in **Figure 4.1b**).

If you walk at an oblique angle towards a wall or a corner from the beginning, the perspective shape of the walls will look like $\mathbf{t_2}$ in **Figure 4.1a** or **Figure 4.1b**. As the symmetry in the perspective shape of the wall(s) has already been broken, the symmetry cues are weak.

In the three scenarios above, as you walk in the same environment, the amount of optic flow and allocentric location cues remained the same. However, the salience of allocentric location cues or specifically symmetry cues varied with your walking direction. When you walk straight to a fronto-parallel wall or a corner, the symmetry cues are strong. When you walk at an oblique angle to them, the symmetry cues are weak.

To manipulate the salience of the perspective symmetry cues, we changed the location of the target in a virtual room so that participants' walking direction varied with respect to the room. In the Front condition, the target was placed in the middle of the front-parallel wall so that the participants' initial direction at the starting point coincided with the normal to the front-parallel wall ($\alpha = 0°$) (see **Figure 4.2a** for a sample view at the starting point and **Figure 4.2d** for a plane view). In the Corner condition, the target was placed at a corner of the virtual room so that the participants' initial direction bisected the angle of the corner ($\alpha = 45°$) (**Figure 4.2b** and **Figure 4.2e**). In the Oblique condition, a target placed a point between the

positions of the Front and Corner conditions so that the participants' initial direction bisected the directions in the two conditions (**Figure 4.2c** and **Figure 4.2f**). As stressed above, in the Front and Corner conditions, the perspective symmetry cues were stronger than those in the Oblique condition; therefore, it is predicted that the trajectories in these two conditions would be straighter than those in the Oblique condition.

4.1.1 Method

4.1.1.1 Participants

Participants were recruited until, after necessary exclusions, we had a counterbalanced sample for each experiment, twenty-four in total (mean age = 21.42, SD = 2.10, 5 males). In order to obtain these numbers, it was necessary to recruit twenty-eight participants. Reasons for exclusion were technical faults during the experiment such as the motion-tracking server being nonresponsive and a large quantity of data drop-off (n = 4). Full details of exclusions are included in the sections that follow. All participants reported having normal vision or corrected-to-normal vision only by wearing contact lenses. None reported impairment of colour or stereo vision or hearing. Prior to the experiment, participants provided informed written consent in accordance with the requirements of the School of Psychology research ethics committee that approved the research. All were naïve to the actual purposes of the study.

4.1.1.2 Stimuli

A line target (3m in height and 2cm in radius) was created in Vizard with the bottom of the target level with the ground. The line target was positioned in a virtual room with all surfaces painted with a random-noise pattern. This room was the same as the one used in Experiment 3.1. The orientation of the virtual room varied across the three conditions so that the participant was facing one of the three distinct parts of the room: the frontoparallel wall, the corner and a point between the two. The plane view of the three conditions is illustrated in **Figure 4.2**. In the Front condition, the target was placed in the middle of the front wall (see **Figure 4.2d**). In the Corner condition, the target was positioned at a corner of the room (see **Figure 4.2e**). In the Oblique condition, the target was placed at a point between the Front and Corner conditions so that the angle between the walking direction and the normal to the frontoparallel wall is half of that in the Corner condition ($\alpha = 22.5°$) (see **Figure 4.2f** for a plane view and **Figure 4.2c** for a sample of view at the starting point).

The maximum walking distance with optimal motion-tracking coverage was 7m in our lab. Therefore, as in the previous experiment, the initial distance to the target was set to be 7m in the virtual environment. This was fine for the front condition because there was a plenty of space on the two sides of the participant throughout a trial. However, in the Corner

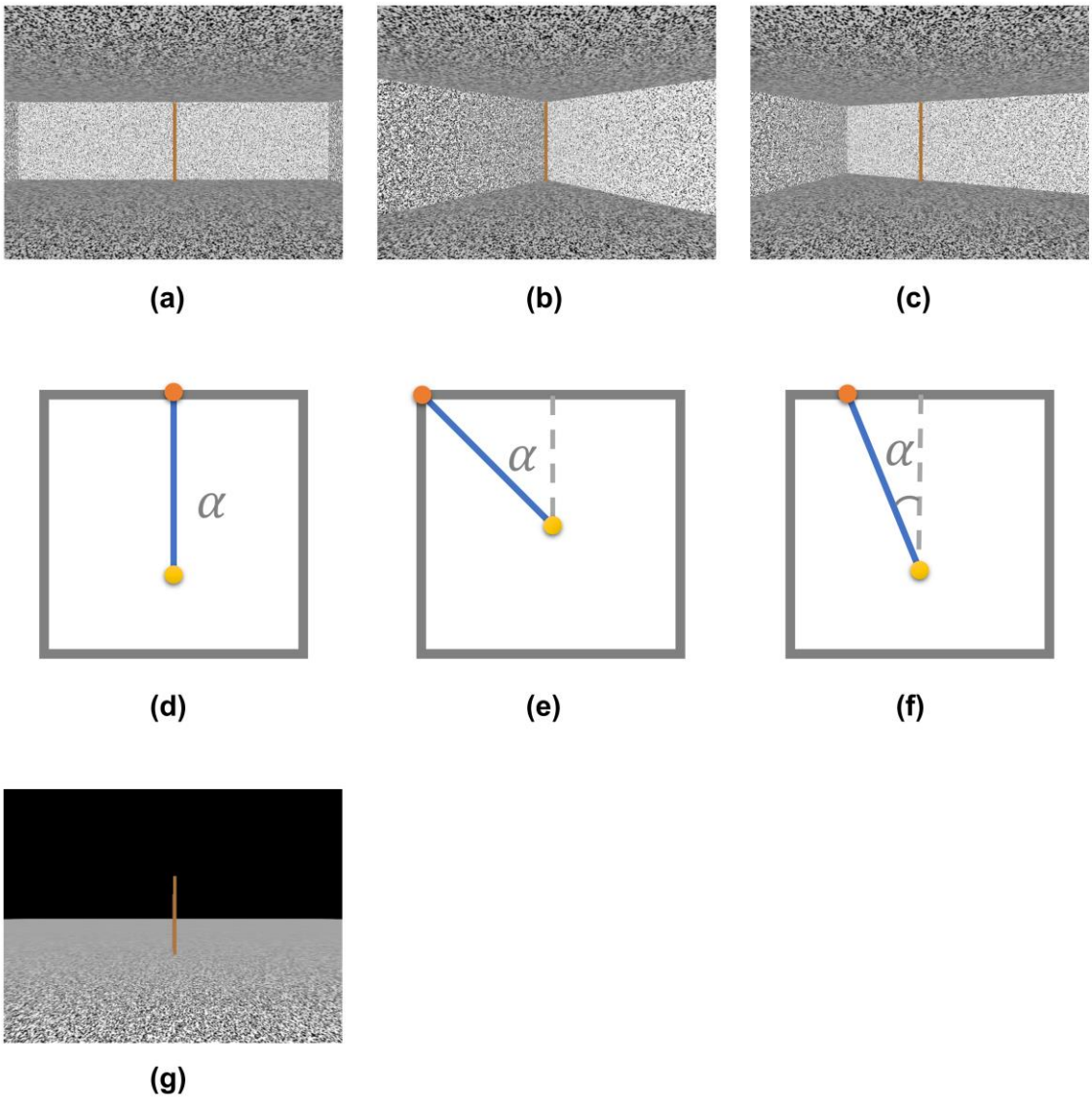

Figure 4.2 (a) – (c) *Sample views of the virtual environments at the starting point.* ***(d) – (f)*** *Plane views of the three conditions.* ***(a)*** *and* ***(d) Front*** *condition, the target was placed in the middle of the front wall. Without displacement, an observer would take a straight path to it with the angle to the normal to the front wall α = 0°.* ***(b)*** *and* ***(e) Corner*** *condition, the target was placed at a corner. Without displacement, the angle between the walking path and the normal to the front wall α = 45°.* ***(c)*** *and* ***(f) Oblique*** *condition, the target was placed at a point between the locations in the Front and Corner conditions. Without displacement, the angle between the walking path and the normal to the front wall α = 22.5°.* ***(g)*** *The environment used in the baseline condition.*

and Oblique condition, because the participant walked in an oblique line to the wall, the space between the participant and the wall reduced while approaching the target. In order to prevent the participant from deliberately walking straight to avoid bumping into the walls, we set the initial target distance to be 8.5m in all conditions. The trial stopped when participants reached 1.5m from the target so that the walking distance was still 7m, under the optimal coverage of the motion-tracking system in the lab.

As Experiment 3.1, a baseline environment was created that included a ground plane with random-noise pattern (see **Figure 4.2g**). The environment is used in the baseline blocks (see Section 4.1.1.3). To match the target distance with the test environment, the line target was also placed at 8.5m from the starting point in the baseline environment. Again, the walking distance was 7m.

4.1.1.3 Experimental design and procedure

There were three test blocks interleaved by four baseline blocks, resulting in seven blocks in total. The three test blocks corresponded to the three conditions. The order of the conditions was counterbalanced across participants. In the baseline blocks, a baseline environment was presented, and there was no offset between visual and physical moving directions so that aftereffect could be assessed and washed out. There were four trials in each block, and hence 44 trials in total. For each participant, the "virtual prism" was right-shifting in half of the blocks and left-shifting in the other half. The order of the "virtual prism" direction and the order of conditions were counterbalanced across participants.

As in Experiment 3.1, participants performed the same colour-responding task to discourage them from paying undue attention to their walking behaviour. To help participants maintain their walking speed, a metronome at 80 beats/min (a beat per 0.75sec) was played while they were walking to the target.

The whole procedure was identical to Experiment 3.1.[7]

[7] Note that there was a short experiment (see Chapter 5) similar to that prior to Experiment 3.1 before the present experiment. The participants were asked to walk to a target in the physical lab while wearing a pair of prism glasses. The purposes for combining the two experiments were (1) to reduce time demands on the participants and (2) to make the participants feel more confident and comfortable in walking in a VE.

4.1.2 Results

4.1.2.1 Straightness of trajectories in Trial 1

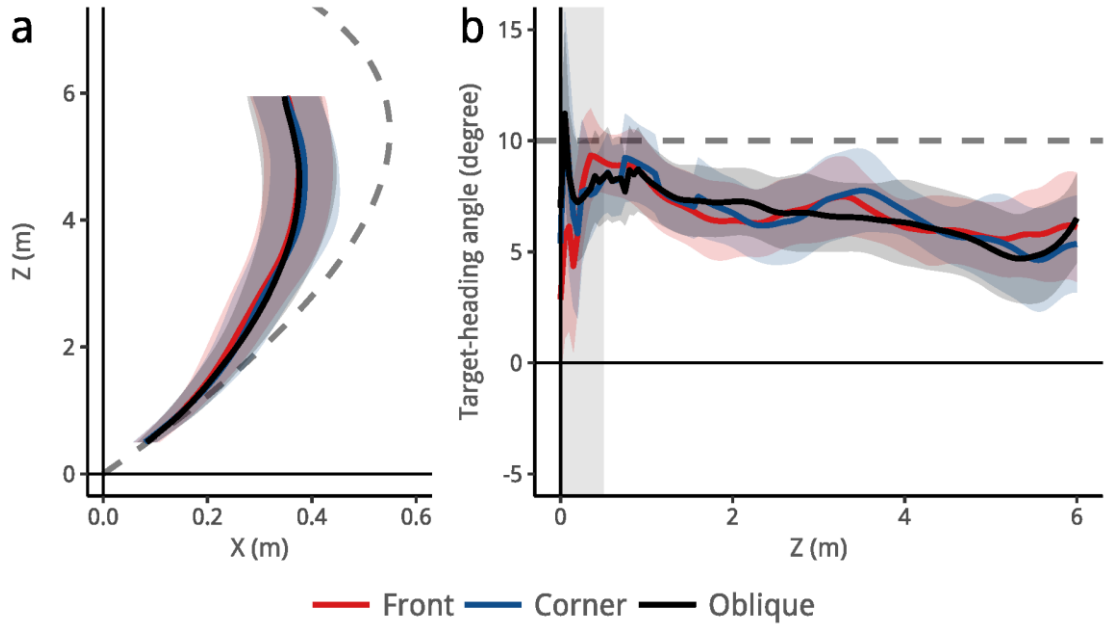

Figure 4.3 ***(a)*** *Mean trajectory in Trial 1 for each condition across 36 participants, Corner (red), Front (blue) and Oblique (black). Dashed line shows the trajectory that should result if only egocentric direction is used. Shaded areas indicate 95% confidence interval.* ***(b)*** *Mean target-heading angle in Trial 1 as a function of distance across 36 participants. Dashed line at 10° indicates the angular displacement between the visual and physical directions, corresponding to the fully curved trajectory indicated by the dashed line in* ***(a)****. Solid line at 0° corresponds to a straight trajectory. Grey shaded area at 0m ~ 0.5m indicates the data that has been excluded from the final analysis. Shaded areas around the target-heading angle data indicate 95% confidence interval.*

We first sought to determine how walking directions affects the overall straightness of mean walking trajectories in Trial 1. The mean trajectories were averaged over the twenty-four participants and plotted in **Figure 4.3a**. According to our hypothesis, the trajectory should be the most curved in the Oblique condition, as the perspective cues are the less rich in this condition. The straightness of trajectory should be comparable between the Front and Corner conditions, as the perspective cues are salient in both conditions. This is not what we observed on the mean trajectories in **Figure 4.3a**. The trajectories look very similar between conditions. Correspondingly, the overall mean target-heading angle was comparable between the Oblique condition (mean = 6.57°, SD = 2.99°), the Front condition (mean 6.72°, SD = 2.96°) and the Corner condition (mean = 6.70°, SD = 2.68°). A repeated-measures ANOVA

based on the individual overall mean target-heading angle did not reveal a significant difference between conditions [$F_{2, 46} = 0.017$, $p = 0.98$, $\eta^2 < 0.01$].

The mean target-heading angles are plotted against distance in **Figure 4.3b**. As reflected by the decrease in the mean target-heading angle, the trajectories in all conditions straightened over distance and no significant differences were found in the rate of straightening [χ^2 (2) = 0.71, $p = 0.70$] (for more details see Supplementary Materials 8.3.1.1). To confirm that there was no significant difference between conditions, we applied our bespoke time-series analysis on the t-statistics along the distance. No significant cluster was found.

4.1.2.2 Mean straightness as a function of trial

The mean target-heading angles of the early (0.5m ~ 1m) and later (5.5m ~ 6m) parts are plotted against the four test trials in **Figure 4.4**. The data in the test trials with "virtual prism" are shown in the clear area. Visual inspection revealed that the pattern of straightening in Trial 1 generally persisted across the trials, as evidenced by the significant reduction of the mean target-heading angle from the early part to the later part [χ^2 (1) = 33.31, $p < 0.0001$] (for more details see Supplementary Materials 8.3.1.2).

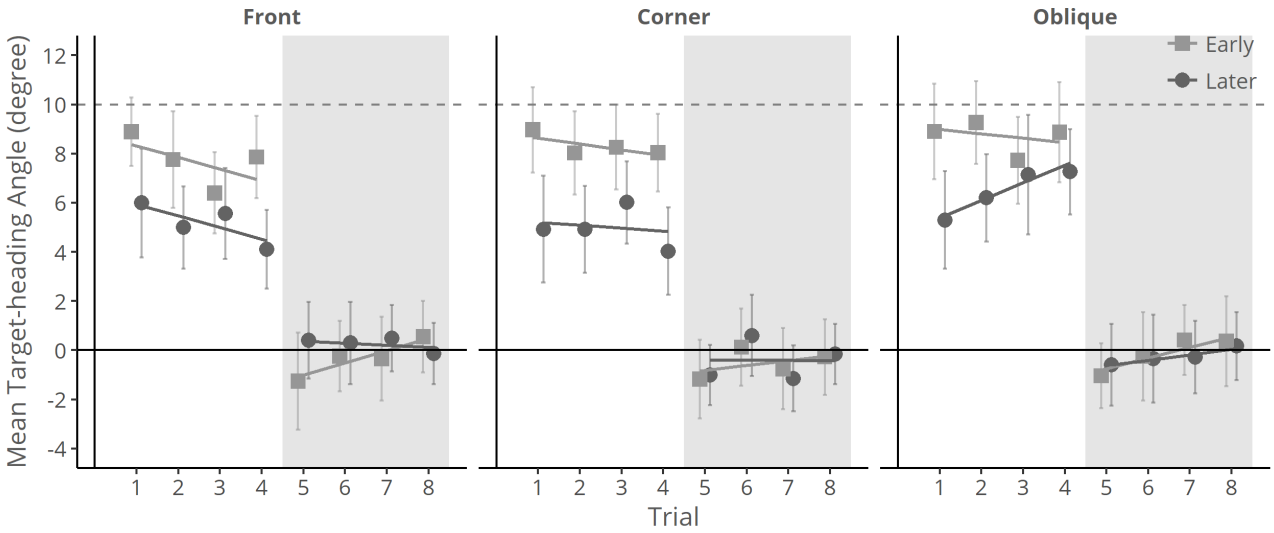

Figure 4.4*. Mean target-heading angle of the early (0.5m ~ 1m) and later (5.5m ~ 6m) parts as a function of trial respectively for each test block (Trial 1 ~ 4) and the subsequent baseline block (Trial 5 ~ 8). The left-hand panel shows the data in the Front condition, the middle panel the Corner condition and the right-hand panel the Oblique condition. Dashed line at 10 ° indicates the angular displacement between the visual and physical orientation. Error bars indicate 95% confidence interval. In the baseline blocks the displacement was removed.*

For the early part, the mean target-heading angle reduced over the test trials at similar rates over the test trials [all *p*s > 0.1]. For the later part, the mean target-heading angle decreased in the Front and Corner conditions as indicated by negative slopes [estimated slope: Front = -0.47; Corner = -0.12,], but increased in the Oblique condition as indicated a positive slope [estimated slope = 0.72]. The increase was significant [z = 2.66, $p < 0.01$], and considerably more positive than in other conditions [to Front: $p < 0.01$; to Corner: $p = 0.068$; both Bonferroni corrected]. These results suggest that, unlike that in the Front and Corner conditions, the reduction between the early and later parts decreased in the Oblique condition.

As shown in the shaded areas in **Figure 4.4**, the early target-heading angles of the first trial in the baseline blocks are all smaller than 0°, indicating some aftereffects in all conditions. The largest magnitude of aftereffects is in the Front condition [mean = -1.26°, SD = 4.68°], followed by the Corner condition [mean = -1.18°, SD = 3.71°]; the least was in the Oblique condition [mean = -1.04°, SD = 3.14°]; but in none of conditions the mean target-heading angle was significantly negative [all *p*s > 0.1]. In all conditions, the overall mean target-heading angles increased to be closer to 0° over trials as reflected by the positive slopes. In the last trial (Trial 4), the early mean target-heading angles in all conditions are around 0°. Together with the data in the test blocks, the pattern suggests that there might be some adaptation in all conditions; however, the magnitude seems small and did not lead to a reliable aftereffect. The similar magnitude of adaptation may be due to the similar richness of optic flow (Bruggeman et al., 2007; Herlihey & Rushton, 2012) or similar amount of target drift (Saunders & Durgin, 2011) between conditions.

4.1.2.3 Walking speed and its relationship with the straightness of trajectories

As shown in **Figure 4.5a**, the mean walking speed of Trial 1 looks similar between the Corner, Front and Oblique conditions. A factorial ANOVA supported this by showing no significant difference in walking speed between the three conditions [$F_{2, 46} = 0.31$, $p = 0.73$, $\eta^2 < 0.01$]. Furthermore, a JZS Bayes factor ANOVA (Love et al., 2015; Morey & Rouder, 2015; Rouder et al., 2012) with default prior scales provided substantial evidence for the null hypothesis that there was no difference in walking speed between the conditions [$B_{01} = 6.75$] (Jeffreys, 1961).

In none of the conditions, was there a substantial correlation between the magnitude of target-heading angle and walking speed [Corner: Pearson's $r = 0.084$; Front: Pearson's $r = -0.064$; Oblique: Pearson's $r = -0.18$; all *p*s > 0.1].

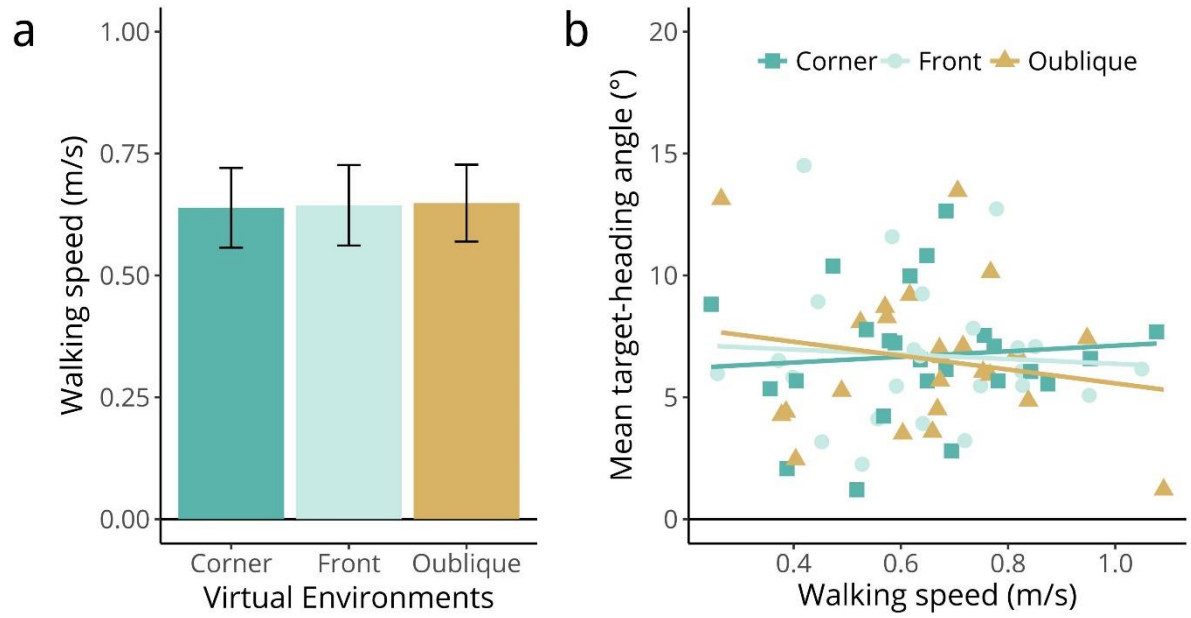

Figure 4.5. (a) *Mean walking speed on Trial 1 in each condition (Corner, Front and Oblique). Error bars correspond to 95% confidence interval.* ***(b)*** *Relationship between walking speed and the magnitude of target-heading angle for each condition.*

4.1.3 Discussion

In this experiment, the richness of perspective cues was manipulated through varying the walking direction of participants within a virtual room. We expected the walking trajectories to be straighter in conditions where the perspective symmetry cues were richer (i.e., the Front and Corner conditions) as compared to the condition where the cues were less (i.e., the Oblique condition). However, we did not find evidence to support our hypothesis. The walking trajectories were similar between conditions in terms of the overall straightness as well as in terms of the pattern of straightening over distance.

An unexpected finding is that the reduction in target-heading angle from the early part to the later part decreased over the trials in the Oblique condition (see **Figure 4.4**), which may suggest a tendency of making less online correction during walking. In Trial 1, the reduction in the mean target-heading angle between the early and later parts in the Oblique condition was comparable to those in the Front and Corner conditions. In the proceeding trials, the magnitude of the reduction remained constant in the Front and Corner conditions but decreased in the Oblique condition. One possibility may concern the decrease in the participants' vigilance as they became familiar with the environment. When walking in an unusual direction like an oblique approach towards a wall, the participants might be more

vigilant at the start (in Trial 1) so that they were more sensitive to signals about any change in their walking direction. In the following trials, when they became more familiar and confident with walking in such a situation, they were more relaxed and thus more vulnerable to the displacement effect of the "virtual prism". Such a change in vigilance would be supported by a difference in walking speed and task performance on the secondary task. However, no significant difference was found between conditions. As the secondary task in our experiment was easy, the lack of difference might be due to a ceiling effect. Varying the difficulty of the secondary task might reveal whether there is an effect of vigilance or attentional load on the use of perspective cues.

In the Oblique condition, the wall on the observer's right-hand side was always closer than that on the left-hand side. This would result in more optic flow on the right side than on the left side. If this unbalanced optic flow affected walking (e.g., the observer walking to equalise the optic flow on the two sides, Duchon & Warren, (2002)), one would expect to see the trajectories being straighter in the right-shifted trials than in the left-shifted trials. However, we did not find a significant difference between conditions to support this hypothesis [$p = 0.54$].

4.2 Experiment 4.2 The impact of target distance

In this experiment, the target was placed at two different distances from the starting point, either near (at 8.5m) or far (at 85m). The target stood on a solid ground plane textured with a random-noise pattern. Coloured disks lay flat on the ground plane with a random arrangement (see **Figure 4.6**).

As in Experiment 4.1, egocentric direction, optic flow and allocentric location cues remained unchanged by the target distance. However, there is a difference in the availability of target drift (i.e., the change of egocentric direction, (Llewellyn, 1971)) and motion parallax (i.e., the distribution of retinal velocities from relative object movement in depth) in the retinal flow field.

As we have shown in Experiment 3.2, when a target is near, target drift is a powerful cue to the accuracy of heading. Typically, the disks closer than and further away than the target would result in a broad range of retinal velocities. When a target is distant, as there were only disks closer than the target, both of these cues are considerably less salient. In this sense, one would expect to see straighter trajectories in the Near condition than the Far condition. In addition, as the salience of cues is inversely proportional to the target distance,

it should increase more rapidly in the Near condition than the Far condition. Thus, one would expect to see trajectories straighten faster in the Near condition than the Far condition.

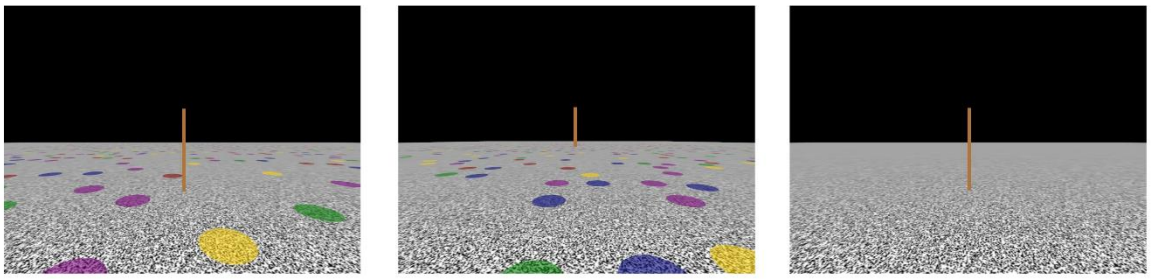

Figure 4.6. *Sample views of the virtual environments at the starting point.* ***(a) Near*** *condition, the target was placed at 8.5m away from the starting point.* ***(b) Far*** *condition, the target was placed at 85m away from the starting point. The radius and height of the target was adjusted accordingly in order to look comparable to that in the Near condition.* ***(c) Baseline*** *condition, the environment used in the baseline blocks.*

4.2.1 Method

4.2.1.1 Participants

The same participants who took part in Experiment 4.1.

4.2.1.2 Stimuli

A ground plane with a horizon at 100m was created and textured with a random-noised pattern. It was covered by randomly distributed round disks (0.5m in radius). The disks were five colours: green, red, blue, yellow and purple. The disks were half-transparent so that the random-noise pattern on the ground was visible through them. The reason we used disks instead of posts is to maintain the perception of relation movement while preventing any occlusion of the target.

In the Near condition, the line target (3m in height and 2cm in radius) was placed at 8.5m from the starting point (**Figure 4.6a**). In the Far condition, the target was placed at 85m from the starting point. The size of the target was enlarged accordingly (~ 15m in height and 20 cm in radius) so that the radius of the two targets appeared the same and the top of them appeared at similar heights (**Figure 4.6b**). A baseline environment that was the same as Experiment 4.1 was also generated for the baseline blocks. In this environment, the target

was also placed at 8.5m from the starting point. Like Experiment 4.1, an invisible trigger to end the trial was placed at 7m from the starting point for all virtual environments.

4.2.2 Results

4.2.2.1 Straightness of trajectories in Trial 1

The mean trajectories of Trial 1 that were twenty-four participants were shown in **Figure 4.7a**. We can see that the trajectories in both conditions are less curved than egocentric

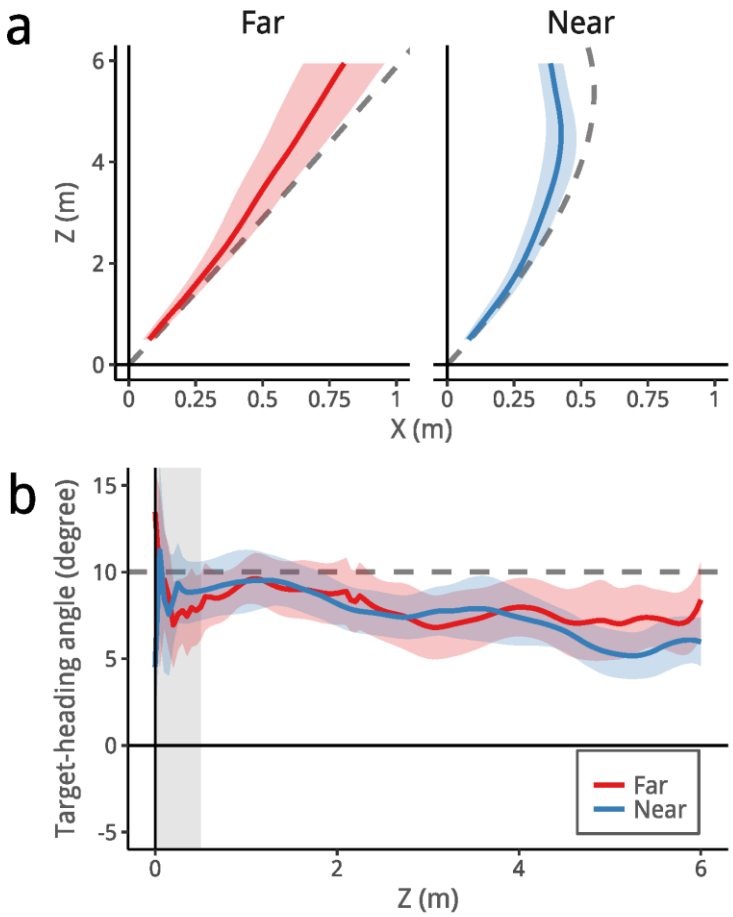

Figure 4.7. ***(a)*** *Mean trajectory in Trial 1 averaged across 24 participants for each condition, Near (blue line in the right-hand panel) and Far (red line in the left-hand panel). Dashed line shows that trajectory that should result if only egocentric direction is used. Shaded areas indicate 95% confidence interval.* ***(b)*** *Mean target-heading angle in Trial 1 as a function of distance across 24 participants. Dashed line at 10° indicates the angular displacement between the visual and physical directions, corresponding to the fully curved trajectory indicated by the dashed line in* ***(a)****. Solid line at 0° corresponds to a straight trajectory. Grey shaded area at 0m ~ 0.5m indicates the data that has been excluded from the final analysis. Shaded areas around the target-heading angle data indicate 95% confidence interval.*

direction prediction (dashed line in **Figure 4.7a)** with the trajectory appears slightly straighter in the Near condition. The overall mean target-heading angles are respectively 7.91° (SD = 3.50°) in the Far condition and 7.50° (SD = 2.16°) in the Near condition. There was no significant difference between the two conditions and the effect size was small [t(23) = 0.40, p = 0.69, r = 0.083].

Figure 4.7b illustrates the mean target-heading angles as a function of distance. For both conditions, the mean target-heading angles significantly decreased over distance [$\chi^2(1)$ = 617.37, $p < 0.0001$], suggesting a trend of straightening in the trajectories. The rate of decrease was different between conditions [$\chi^2(1) = 2.92$, $p = 0.088$], with a marginally more negative slope in the Near condition [estimated difference in slope = -0.38, t = -1.78, p = 0.075]. To further confirm this, we applied our bespoke time series analysis (see Section 2.4.2.2) on the t-values between the two conditions. It revealed that the difference between

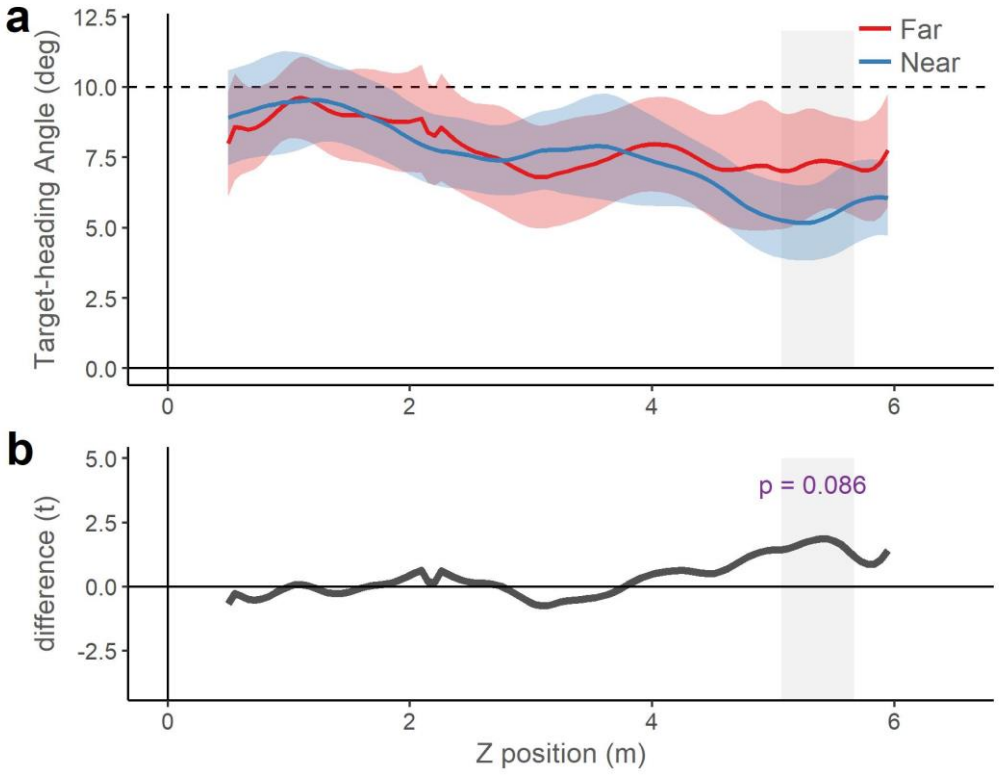

Figure 4.8 (a) *Mean target-heading angles against distance that are averaged over participants (n = 24) respectively for the Far and Near conditions in Trial 1. Dashed grey line at 10° indicates degree of displacement in the VE. Coloured areas indicate 95% confidence interval. Grey shaded area represents the part on distance where the Near condition is significantly straighter than the Far condition.* ***(b)*** *Difference (t-values) comparing target-heading angle between the Far and Near conditions. Grey area represents the period where t-values are considered ($p < 0.05$) to be significant as a cluster.*

the two conditions increased towards the end of a trial. A small cluster was found at the end of the trajectory that approached significance (p = 0.086; see **Figure 4.8**), indicating a trend that the trajectory became straighter in the Near condition than in the Far condition at the end of the trial (see Supplementary Materials 8.3.2.1).

4.2.2.2 Straightness as a function of trial

The mean target-heading angles of early and later parts are plotted as a function of trial in the clear areas in **Figure 4.9**. Consistent with the results above, the mean target-heading angles of the later part were significantly smaller than the early part [$\chi^2(1) = 26.02$, $p < 0.0001$] (see Supplementary Materials 8.3.2.2). This suggests that the pattern that we observed in Trial 1 persisted across the test trials.

Both Near and Far conditions show some decrease in the mean target-heading angle of the early part over the test trials, as indicated by the negative slopes in the two conditions [Far: estimated slope = -0.30; Near: estimated slope = -0.38]; but neither of the slopes was significantly negative [both ps > 0.1]. There was a significant difference in the slope between the early and later parts [$\chi^2(1) = 4.88$, $p = 0.027$] with the early slopes being more negative than the later slopes. However, no effect of target distance was found.

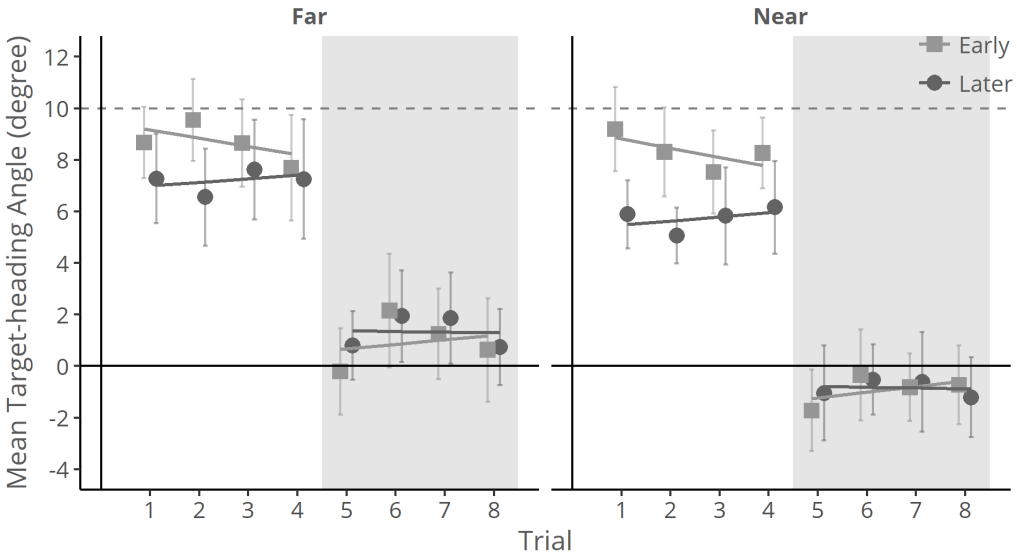

Figure 4.9 *Mean target-heading angle of the early (0.5m ~ 1m) and later (5.5m ~ 6m) parts as a function of trial respectively for each test block (clear areas, Trial 1 ~ 4) and the subsequent baseline block (shaded areas, Trial 5 ~ 8). Left-hand panel shows the data in the Far condition and the right-hand panel the Near condition. Dashed line at 10 ° indicates the angular displacement between the visual and physical orientation. Error bars indicate 95% confidence interval. In the baseline blocks the displacement was removed.*

The mean target-heading angles of the early and later parts in the baseline blocks are plotted against trial in the shaded areas in **Figure 4.9**. In Trial 5, the mean target-heading angle of the early part was significantly smaller than 0° in the Near condition [mean = -1.72°, t(23) = -2.25, p = 0.034], but not in the Far condition [mean = -0.21°, t(23) = -0.26, p = 0.80]. The results suggest that there were reliable aftereffects only in the Near condition. The aftereffects were abolished over the baseline trials as indicated by the mean target-heading angle of the early part becoming closer to 0°. In Trial 8, the mean target-heading angle of the early part was no longer significantly different from 0° [mean = -0.73°, t(21) = -0.98, p = 0.34], suggesting that the aftereffects in the Near condition were washed out in the baseline trials.

4.2.2.3 Walking speed and its relationship with the straightness of trajectories

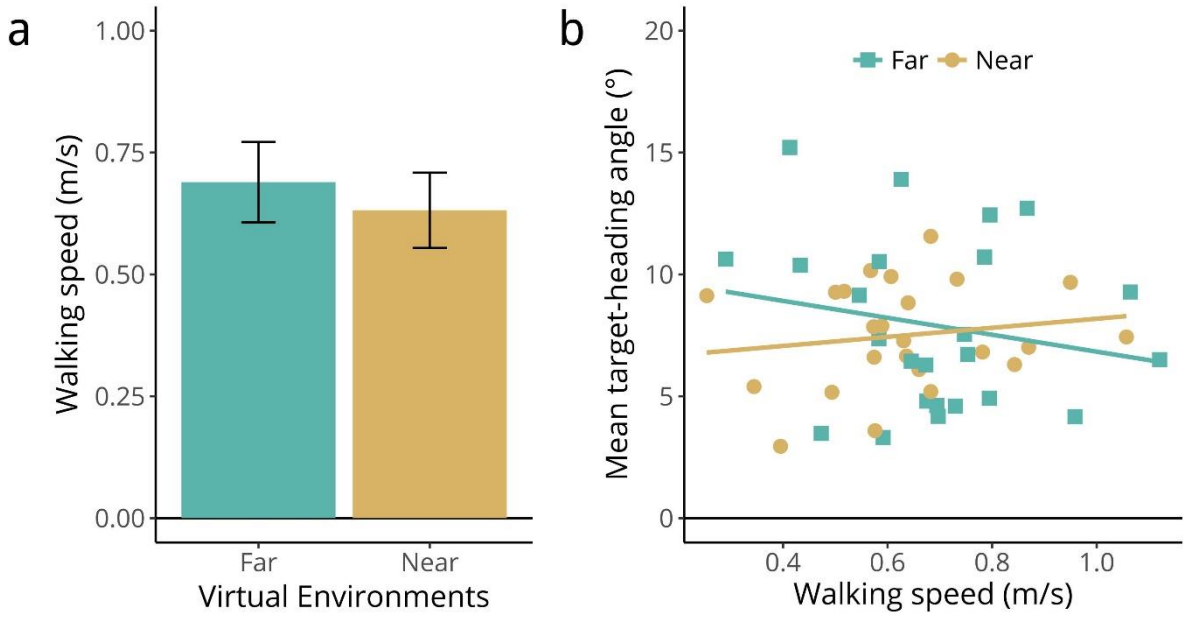

Figure 4.10. (a) *Mean walking speed on Trial 1 in each condition (Near and Far). Error bars correspond to 95% confidence interval.* ***(b)*** *Relationship between walking speed and the magnitude of target-heading angle for each condition.*

As shown in **Figure 4.10a**, the walking speed was faster in the Far condition [M = 0.69m/s, SD = 0.20m/s] than in the Near condition [M = 0.63m/s, SD = 0.18m/s] in Trial 1. The difference was significant [t(23) = 4.58, p < 0.0001].

The relationship between the magnitude of target-heading angle and walking speed is plotted in **Figure 4.10b**. In both Far and Near conditions, there was a weak correlation

between target-heading angle and walking speed [Far: Pearson's r = -0.19; Near: Pearson's r = 0.16]. However, the correlations were not significant [both ps > 0.1].

4.2.3 Discussion

We manipulated the target distance which would result in the varied salience of target drift and motion parallax. We predicted that when the target was near (8.5m), the cues would be more salient and thus the trajectories should be straighter than when the target was far (85m). However, the hypothesis was not supported by the results. There was no significant difference in the trajectories between conditions.

We also hypothesised that the trajectories should straighten up at different rates between the Near and Far conditions if target drift came into play at a closer distance from the target. As the salience of cues would increase more rapidly when the target was near than when it was far, it was expected to see the trajectories straighten faster in the Near condition than in the Far condition. The data showed a trend that was consistent with this hypothesis. First, the rate of straightening was considerably higher in the Near condition than in the Far condition. At the end of the trial, the trajectories in the Near condition were notably straighter than in the Far condition.

Moreover, we found the trend of adaptation appeared to be more reliable in the Near condition than in the Far condition, as evidenced by the significant aftereffects. This could be attributed to the more salient motion parallax or target drift (e.g., Saunders et al., 2011).

One caveat in this experiment is that the role of target drift and motion parallax was not disassociated. Future studies are thus needed to determine the relative contribution of the two cues in the online control of walking and in driving adaptation.

4.3 General discussion and Summary

Through manipulating the target location, we evaluated the impact of the effect on the walking trajectories on the walking trajectories. In two experiments, target location was changed while the environment was kept the same. As such, the amount of optic flow and allocentric location cues remained unchanged but the salience of allocentric location cues varied across conditions. If the allocentric location cues play an important, curvature of walking trajectories should covary with the salience of the allocentric location cues.

In Experiment 4.1, we manipulated the target location in a virtual room which would result in varying salience of perspective symmetry cues. From the overall straightness of walking trajectories in Trial 1, there was no indication of any influence of the manipulation.

However, when breaking down the data as a function of trial and distance respectively, there seems to be some effect of the cue salience. When the perspective symmetry cues were relatively weak, the processing of the cues might be more attentional demanding.

In Experiment 4.2, we manipulated the target distance to be either near or far. The target drift and motion parallax would be more salient when the target was near than when it was far. As expected, the trajectory straightened faster and there was more adaptation in the Near condition than in the Far condition. The results support the role of target drift and motion parallax in the online control of walking and adaptation, but further work is required to distinguish the relative contribution of the two cues.

On the surface, the results in this chapter may seem somewhat inconsistent with the findings in Experiment 3.1. In Experiment 3.1, we observed a compelling pattern of straightness of walking trajectories as a function of the richness of cues. In conditions with rich allocentric location cues (e.g., Room and Outline), the trajectories were considerably straighter or straightened faster. In contrast, in this chapter, we did not observe a clear pattern of trajectory straightness as a function of the salience of allocentric location cues. It should be noted, however, that we only manipulated the salience of allocentric location cues while keeping the amount of allocentric location cues constant. Therefore, as compared to Experiment 3.1, the difference between conditions in this experiment was nuanced. Moreover, only a subset of allocentric location cues was examined in the two experiments of this chapter. It is possible that other types of allocentric location cues remained constantly salient across conditions. Participants might have relied on other allocentric location cues in guiding walking, especially when the salience of cues in question was weak. It is thus not surprising to see small differences in walking trajectory between conditions.

In the next chapter, we will investigate the role of a mental representation of the environment in the visual guidance of walking.

5 Role of prior experience of the environment in the visual guidance of walking

As outlined in Chapter 1, place cells are found in the rat hippocampus that code the instantaneous location of the animal when it is moving in an environment. Each cell fires maximally at a certain place in a given environment so that the animal is able to trace its position in the environment (Muller & Kubie, 1987; O'Keefe, 1976; O'Keefe & Nadel, 1978). It has been shown that when rats are trained in a lit chamber the firing pattern of the place cells remains unaffected after the lights were turned off provided the rat remained in the apparatus (Markus, Barnes, McNaughton, Gladden, & Skaggs, 1994; O'Keefe, 1976; Quirk, Muller, & Kubie, 1990; Save, Nerad, & Poucet, 2000). The results suggest that the representation of the place persists with the removal of visual inputs. In humans, neural responses resembling those of place cells have been found in the hippocampus (Ekstrom et al., 2003). Evidence from functional neuroimaging (e.g., Hartley, Maguire, Spiers, & Burgess, 2003; Iaria, Petrides, Dagher, Pike, & Bohbot, 2003; Maguire et al., 1998) and neuropsychological data (e.g., Spiers, Burgess, Maguire, et al., 2001; Spiers, Burgess, Hartley, Vargha-Khadem, & O'Keefe, 2001) also support the involvement of the hippocampus in accurate navigation.

In the behavioural domain, studies on humans have shown that an internal representation of the external environment can be used in guiding the human's behaviour. For example, early studies on "blind walking" have demonstrated that without visual input, human observers are able to walk to the location of the target that seen previously (Corlett, Patla, & Williams, 1985; Loomis et al., 1993; Loomis, Da Silva, Fujita, & Fukusima, 1992; Rieser, Ashmead, Talor, & Youngquist, 1990; Thomson, 1980, 1983). In these studies, participants were blindfolded and walked to a previously seen target. Despite the absence of visual input, participants were still able to reach the target with considerable accuracy. The results have provided a hint for the role of a mental representation in the visual guidance of walking. However, in these studies, the target was invisible to the walking participants. The role of the internal representation is likely to be different from that in the online control of walking towards a seen target. However, so far rather little is known about the latter.

There is, however, a discrepancy in the results by Harris and Bonas (2002) and from Experiment 3.1 that could provide a hint at the possible contribution of prior knowledge in the online control of walking. In this study, Harris and Bonas (2002) had participants wear

prism glasses and walk along a corridor towards a luminous target. The corridor was either well-lit or in dark. The trajectories in the dark should be more curved but they found that they were similar to those in the well-lit corridor. In Experiment 3.1, the trajectories in the Line condition (in which participants walked towards a visible target in dark) were significantly more curved than those in the Room condition. The conditions were similar between the two studies, but the resultant trajectories were dramatically different. One possibility is that the participants had been well exposed to the lit corridor before walking in dark; therefore, they had been familiar with the layout of the corridor. In contrast, in Experiment 3.1, the virtual environment was entirely novel to the participants. The discrepancy in the results suggests that prior knowledge about the environment contributes to the guidance of walking in the same environment.

In order to explore the potential use of previously gained knowledge, we start with an experiment (Experiment 5.1) in which the participants' experience with the test room was manipulated. Participants were separated into two groups. One group could see the testing room prior to the experiment (Familiar group), and the other could not (Unfamiliar group). The former thus could learn the layout of the test room, whereas the latter could not. Then they walked in the room towards a self-illuminated target with other illumination extinguished. The visual field was displaced by a pair of prism glasses (9°). Any difference in the shape of the walking trajectories between the two groups can be attributed to the difference in their experience with the test room. To preview, we find an effect of familiarity on the walking trajectories.

Building on the findings in Experiment 5.1, we probed the effect of familiarity as a function of the availability of external visual cues in Experiment 5.2. The availability of these cues was systematically manipulated by having the participants walk in either fully or stroboscopically illuminated room. We found that the familiarity effect disappeared in these two conditions. In Experiment 5.3, we further reduced the availability of visual cues in the dark and stroboscopically illuminated room by intermittently illuminated the target. Doing this removed target drift. We found an effect of familiarity in both illumination conditions after removal of target drift. In the last experiment (Experiment 5.4) we investigated the role of peripheral vision and its interaction with the familiarity effect by occluding it in the full illumination condition. Against our prediction, occluding peripheral vision did not reveal an effect of familiarity.

5.1 Experiment 5.1 The role of prior knowledge

Participants were separated into Familiar and Unfamiliar groups and walked towards a luminous target in the dark room while wearing a pair of prism glasses. The prism glasses displaced participants' visual field. If participants walked to keep the target perceptually straight ahead, a curved trajectory with a constant 9° target-heading angle would be produced. If the trajectories were straighter, cues other than egocentric direction would be used. If prior knowledge of the room could be used in the guidance of walking, the trajectories of the Familiar group should be straighter than those of the Unfamiliar group.

5.1.1 Method

5.1.1.1 Participants

Participants were recruited until, after necessary exclusion, we had twelve participants per condition, twenty-four in total. It was necessary to recruit a total of twenty-seven participants to obtain these numbers. Reasons for exclusion were technical faults (i.e., server crashed) during the experiment (n = 2), and not following instructions (n = 1).

The demographic statistics of the twenty-four participants that were included in the analysis were mean age = 20.25, SD = 1.80, range = 18 ~ 25, three males. All participants had self-report normal vision or vision that was corrected to normal with contact lenses. None reported impairment of colour vision or hearing. Participants took part in the experiment for course credit or monetary payment.

All participants provided informed written consent in accordance with the requirements of the School of Psychology research ethics committee that approved the research. None of the participants was aware of the actual purpose of the study or had any previous experience of the test room.

5.1.1.2 Walking environment and equipment

Participants walked through the physical test room (8.3m × 8.3m × 3.4m) (see **Figure 5.1a**). Two black microphone stands were placed in two diagonally opposed corners of the room. Three small LED lights in a bunch (see **Figure 5.1b**) were attached to the microphone stand at a height of 1.5m from the floor. The LEDs were three different colours: red, yellow and green.

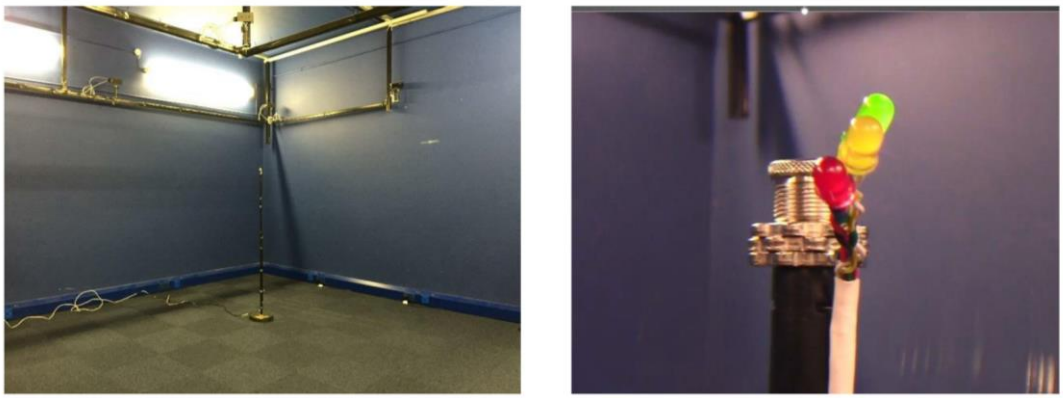

Figure 5.1. (a) *An example view of the test room. A target was placed at a corner. At the target attached three LEDs respectively in colour of red, yellow and green* ***(b)***.

The LEDs on the target were controlled by a custom program written in Vizard (version 5.0, WorldViz, USA) that illuminated the LEDs one at a time at 1Hz. Each LED was turned on for 1 second then the next one was turned on immediately after the previous one was turned off. As there was no blackout interval between two adjacent illuminated LEDs, the participant could see a smooth movement of the target while walking to it. The order in which the LEDs were illuminated was random so that the participant was unable to guess the next illuminated LED.

To rule out the effect of optic flow and/or allocentric cues, during the experiment, the room was pitch black without any illumination except the LEDs on the target.

5.1.1.3 Design and procedure

Participants were required to walk back and forth between the two stands five times, yielding 10 trials in total. In the first 5 trials, they wore a pair of prism glasses that shifted the view either rightwards (+9°) or leftwards (-9°) (see **Figure 2.7**); for the remaining trials, the prism glasses were removed. Half of the participants wore the leftward prism glasses while the other half wore the rightward glasses.

It should be noted that, in the experiments of this chapter, we did not establish an initial baseline session. The reason was that participants may have become familiar with the test room if finishing an initial baseline session before the prism trials, and thus invalidate our investigation of how allocentric maps are formed and used in the visual guidance of walking.

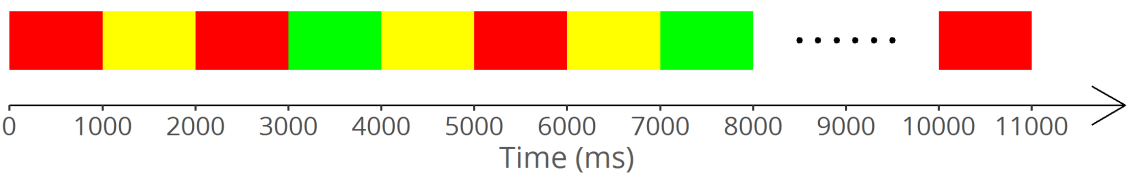

Figure 5.2 *Schematic illustration of how target LEDs were illuminated. Each coloured rectangle represents the duration of the LED and the colour being illuminated. Each LED was illuminated for a whole second. No interval was between any two adjacent illuminations.*

The experimental design was between-subjects. That is, each participant walked in only one condition. It was important that the participants in the Unfamiliar group were not exposed to the test room until the experiment started. They were, therefore, given induction and prepared for the experiment in the corridor outside the test room. Having been set up and ready, they were asked to close their eyes and the experimenter placed the prism glasses in front of their eyes. Still with their eyes closed, participants were led to the test room in dark and were required to keep their eyes closed until the start of the experiment.

Upon arrival, the participants in the Familiar group were led into the test room where they were given induction and prepared for the experiment. During the induction, the experimenter briefly showed the test room and pointed out the location of the targets, but gave no instruction to remember them. Like the participants in the Unfamiliar group, all participants in the Familiar group were required to close their eyes before donning the prism glasses and to keep their eyes closed until the start of the experiment. They were led in a circuitous route to the starting point in the dark room; during this process, they were rotated three times. The reason for this procedure was: (1) to prevent participants from seeing an immediate shift in visual direction that would otherwise be apparent if they put on the prism glasses with their eyes open; (2) to prevent participants from changing their head orientation to compensate for the sudden displacement of the view; (3) to ensure that participants did not know their orientation and position prior to the first trial.

In the dark room, the experimenter used a small torch to locate the starting point on the floor and illuminate a path to it. The light was dim and only covered a small area on the floor so that, even if participants opened their eyes at this point, it was unlikely they would be able to identify their location within the room.

When the participants had reached the starting point, they were turned around (aided by the experimenter) to face the general direction of the target. Then they were instructed to

open their eyes and orient their body to the LED lights on the target. When ready, the participants were instructed to walk towards the target at their normal, self-selected pace.

To ensure that the participants were attending to the target while walking rather than focusing on their walking behaviour and guessing the purpose of the experiment, a colour-responding task similar to that used in previous chapters was given as a cover story. Before the experiment started, a wireless presenter was placed in the participant's dominant hand. The task for the participants was to press the button on the presenter every time they saw the red LED illuminated. In the debriefing session after the experiment ended, none of the participants reported that they were aware of the actual purpose of the study.

When the participants were about 0.5m away from the target, the experimenter stopped the participant and ended the trial by turning off all the LEDs. The participants were asked to close their eyes again and then turned around by the experimenter to face the opposite corner where the target for the next trial stood.

During the experiments, white noise was played to the participants through a pair of earphones. This was to prevent participants using environmental sounds as location cues. The volume of the white noise was checked and adjusted for each participant before the experiment to make sure that the participant could not hear any environmental sound from the test room (e.g., computer, server, etc.).

After Trial 5, the experimenter removed the prism glasses while the participant's eyes were closed. The participant was then turned around to prevent them from seeing any sudden change in the visual direction. Each participant completed 10 trials in total (5 prism trials + 5 after-prism trials). The whole experiment took approximately 30 mins.

5.1.1.4 Data analysis

The walking data were preprocessed and analysed following the identical procedure as in the previous chapters (also see Section 2.4). The overall mean target-heading angles were first examined using standard GLM methods. Then, to investigate the temporal profile of cue use, growth analysis was applied to the mean target-heading angle as a function of distance and as a function of trial respectively.

5.1.2 Results

5.1.2.1 Straightness of mean trajectories

First, we looked at the general effect of experimental manipulation on the overall straightness of trajectories. Instead of the trajectory in Trial 1 as previous experiments, we

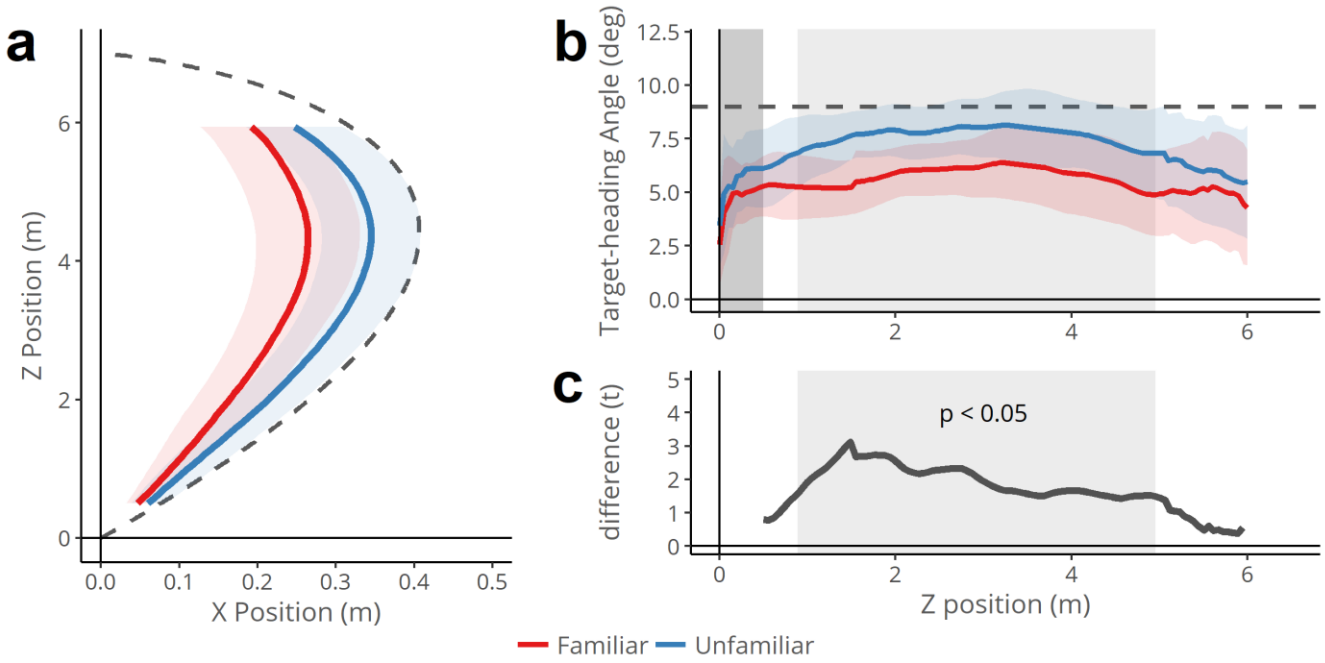

Figure 5.3 (a) *Mean trajectory averaged over the five test trials (1 ~ 5) and the participants (n = 12 per condition) for the familiar group (red) and unfamiliar group (blue) respectively. Dashed line shows the trajectory that should result if egocentric direction was used. Shaded ribbons correspond to 95% confidence interval.* ***(b)*** *Mean target-heading angle against distance averaged over the five test trials (1 ~ 5) and the participants (n = 12 per condition) for the familiar group (red) and unfamiliar group (blue) respectively. Dotted line shows the trajectory that should result if egocentric direction was used. Solid line at 0° corresponds to a straight trajectory. Shaded ribbons correspond to 95% confidence interval. Dark grey shaded area at 0m ~ 0.5m indicates the data that has been excluded from the final analysis. Light grey shaded rectangle indicates significant cluster.* ***(c)*** *Difference (t-values) in the mean target-heading angle as a function of distance. Grey shaded area indicates a cluster with a p-value < 0.5.*

used the mean trajectories that were averaged over the five test trials. This was to increase statistical power. Unlike previous experiments in which a within-subject design was used, in the experiments of this chapter, a between-subject design was used, resulting in a relatively small group size in each condition as compared to previous experiments.

Figure 5.3a illustrates mean walking trajectories that are averaged across the five test trials and over twelve participants. The trajectory predicted by the egocentric direction strategy is plotted (dashed lines) for reference. As evident in the figure, the trajectories are noticeably straighter than the predicted trajectory for both Familiar and Unfamiliar groups [Familiar: mean overall target-heading angle = 5.58°, t(11) = -4.60, $p < 0.001$; Unfamiliar:

mean overall target-heading angle = 7.24°, t(11) = -2.55, p = 0.013]. in the Familiar group than in the Unfamiliar group. The overall mean target-heading angle was 7.24° (SD = 2.38°) in the Unfamiliar group and 5.58° (SD = 2.57°) in the Familiar group. The overall trial difference approached significance with a medium effect size [t(22) = -1.64, one-tailed p = 0.058, r = 0.33].

5.1.2.2 Straightness as a function of distance

Figure 5.3b plots the time course of mean target-heading angles as a function of distance. The graph shows that throughout the trial, the target-heading angle was smaller in the Familiar group than in the Unfamiliar group. A growth model built on the mean target-heading angle with distance as the level-1 predictor confirmed the observation by showing an effect of familiarity on the magnitude of target-heading angle [χ^2 (1) = 6.69, p < 0.01]. The target-heading angle decreased significantly over distance for both groups [χ^2 (1) = 54.58, p < 0.0001], but the rate of change did not differ between groups [χ^2 (1) = 0.26, p = 0.61] (see Supplemental Material 8.4.1.1 for details).

A closer inspection of the time course data reveals that the difference between the two groups is smaller at the beginning and end but larger in the middle of the trajectory. At the beginning, the smaller difference might be caused by the participants not fully orienting to the target. At the end, the reduction of the difference may be due to the use of target drift which is particularly salient close to the target. In the middle of the trajectory, the mean target-heading angle looks considerably larger in the Familiar group than in the Unfamiliar group. To see whether the difference was significant, we applied our bespoke time-series analysis (see Section 2.4.2.2) on the t-values. The analysis revealed a significant cluster from ~1m to ~5m [p = 0.048]. The result is shown in **Figure 5.3c** with the shaded area corresponds to the cluster.

5.1.2.3 Straightness as a function of trial

Next, we broke the data down by trial to see whether a consistent difference was found between the Familiar and Unfamiliar groups. The mean target-heading angle against trial is plotted for each condition in **Figure 5.4**.

Visual inspection revealed a pattern that is consistent with what we observed on the mean trajectories. The mean target-heading angles of the Familiar group was marginally smaller than those of the Unfamiliar group in all trials [$\chi^2(1) = 2.77$, $p = 0.096$]. Over the test trials (see the clear area in **Figure 5.4**), the mean target-heading angle significantly decreased in both groups [$\chi^2(1) = 8.54$, $p < 0.01$]. No difference was found in the rate of decrease between the two groups [$\chi^2(1) = 0.022$, $p = 0.88$] (see Supplementary Materials 8.4.1.2).

The mean target-heading angle in Trial 6 was taken as a measure of aftereffects. As shown in the shaded areas of **Figure 5.4**, the mean target-heading angles of Trial 6 are smaller than 0° for both groups [Familiar: mean = -2.10°, SD = 1.46°; Unfamiliar: mean = -0.83°, SD = 1.86°]. Separate one-sample t-tests revealed that both were significantly smaller than 0° [both one-tailed *p*s < 0.05], indicating a reliable aftereffect following the test trials in both

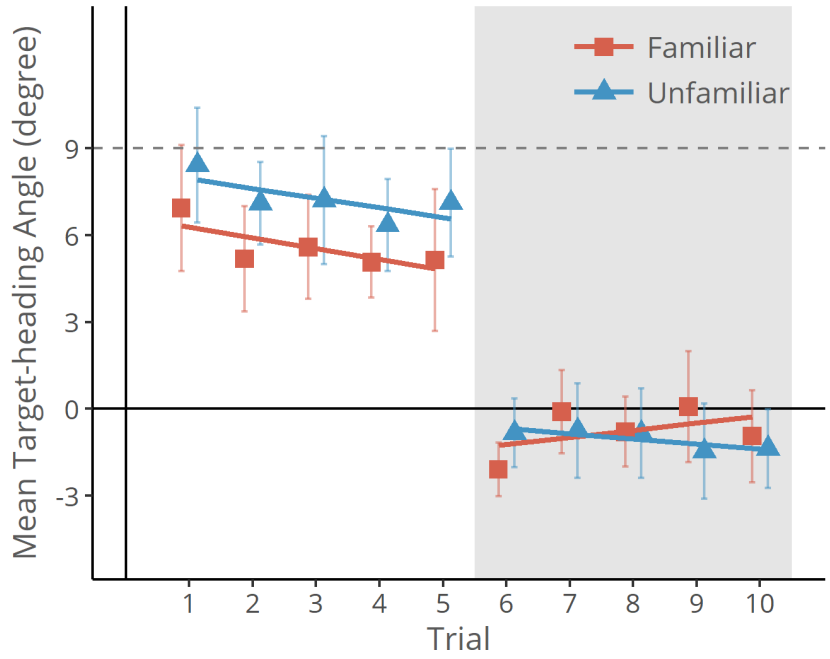

Figure 5.4. *Mean target-heading angle parts as a function of distance for the Familiar and Unfamiliar groups separately. Left-hand panel shows the data in the Continuous condition, and Right-hand panel the data in the Intermittent condition. Clear areas correspond to the test trials (Trial 1 ~ 5) with prism glasses. Shaded areas correspond to the baseline trials (Trial 6 ~ 10) without prism glasses. Dashed lines at 9° correspond to the power of the prism glasses. Error bars indicate 95% confidence interval.*

groups. This is consistent with the decrease of mean target-heading angle in the test trials. The magnitude of aftereffect was marginally larger in the Familiar group than in the Unfamiliar group [t(22) = -1.84, p = 0.079, r = 0.37]. Together, the results here suggest a trend of adaptation over the test trials. As indicated by the magnitude of aftereffects, the degree of adaptation seems to be larger in the Familiar group than the Unfamiliar group.

5.1.2.4 Walking speed and its relationship with the straightness of trajectories

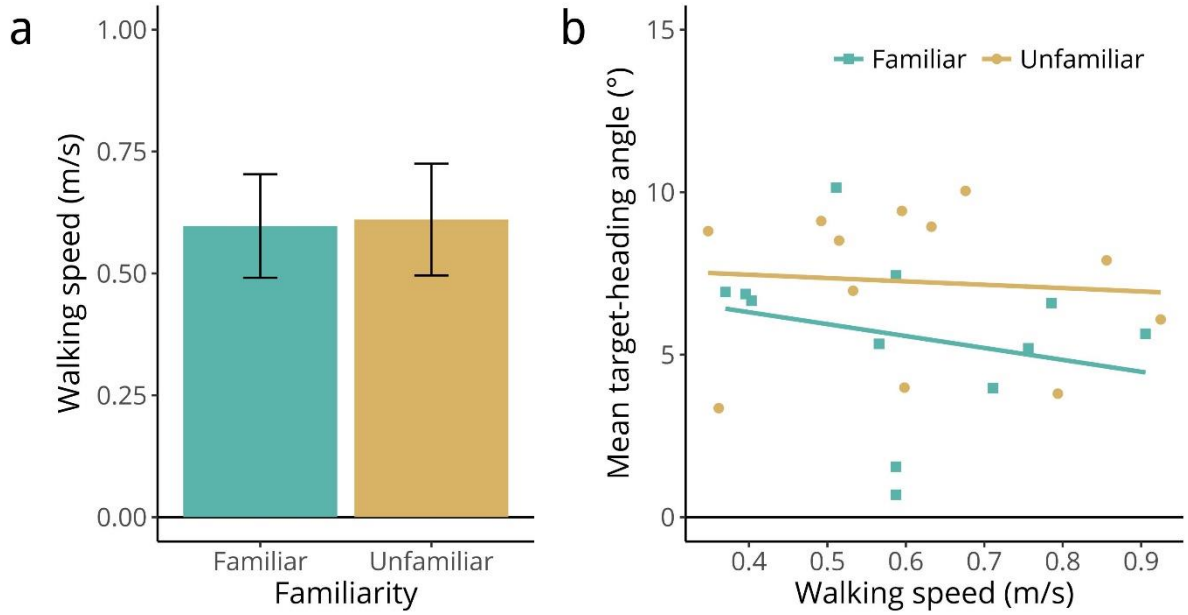

Figure 5.5. (a) *Mean walking speed averaged over five trials and over 12 participants for the Familiar and Unfamiliar groups. Error bars correspond to 95% confidence interval.* ***(b)*** *Relationship between walking speed and the magnitude of target-heading angle for each condition.*

As shown in **Figure 5.5a**, there was no significant difference in walking speed between the Familiar and Unfamiliar groups [t(22) = -0.19, p = 0.85]. There was no significant correlation between the magnitude of target-heading angle and walking speed in either Familiar group [Pearson's r = -0.24, t(10) = -0.78, p = 0.46] or Unfamiliar group [Pearson's r = -0.078, t(10) = -0.25, p = 0.81].

5.1.3 Discussion of Experiment 5.1

When walking towards a continuously visible target in dark, the trajectories of the Familiar group were considerably straighter than those of the Unfamiliar group. The results supported our hypothesis that prior knowledge about the environment has a role in the guidance of walking.

The findings might also explain the discrepancy between the results of Harris and Bonas' (2002) and ours in Experiment 3.1. The participants had seen the corridor in Harris and Bonas' study so they had known about the environment surrounding the target. In Experiment 3.1, the virtual environment was novel to participants so they did not have any knowledge about it in advance.

One may argue that the effect of familiarity may be due to "blind walking" in the Familiar group (Thomson, 1980, 1983). Because participants in this group had seen the environment, and thus knew how far the target was from them when standing at the starting point. They could turn to the direction of the target and then simply walk the remembered distance to the target. If this was true, a straight trajectory would be expected for the Familiar group, which was not what we observed.

In this experiment, the participants walked in an environment with extremely impoverished visual information. It thus raised the question of whether the familiarity effect could be generalised to situations with more visual cues. It may be the case that prior knowledge is only used when the access to visual cues is limited. In Experiment 5.2, we address this question by examining the role of mental representations as a function of the availability of visual cues.

5.2 Experiment 5.2 Role of prior knowledge as a function of availability of visual cues

In Experiment 5.2, we manipulated the availability of visual cues using a temporal method. This was achieved by changing the way the test room was illuminated. In the *Strobe* condition, the test room was intermittently illuminated by six strobe lights at 1Hz. Each flash of the strobes lasted no longer than 10ms. In this condition, optic flow cues were eliminated and some allocentric location cues remained. In the *Lit* condition, the test room was fully illuminated, hence containing rich optic flow and allocentric location cues. If prior knowledge is only used when visual information is limited, one would expect to see similar trajectories between the Familiar and Unfamiliar groups.

5.2.1 Method

5.2.1.1 Participants

We had forty-eight participants (twelve per condition; mean age = 20.44, SD = 4.27, range = 18 ~ 47, eight males). It was necessary to recruit a total of fifty-one participants to obtain these numbers. Reasons for exclusion were technical faults (i.e., the motion-tracking

server crashed) during the experiment (n = 2), and not following instructions (n = 1). Participants were recruited from the same population.

5.2.1.2 Walking environment and equipment

The walking environment and equipment were the same as Experiment 5.1 except that the test room was illuminated by six strobe lights (Equinox Wildzap 1500w analogue disco strobe light) mounted on the ceiling. During each trial, the strobe lights simultaneously flashed at 1Hz and each flash lasted for 10ms, resulting in a series of "snapshots" of the room. Under this condition, optic flow was disrupted. However, some allocentric location cues were available from the brief 'snapshots' of the scene.

In the Lit condition, the test room was fully illuminated by six fluorescent lamps fixed on the edges of the ceiling throughout the experiment. In this condition, both optic flow and allocentric location cues were available.

5.2.1.3 Design and procedure

The procedure was the same as Experiment 5.1. One thing should be noted was that the strobes only flashed during the trials. They were switched off before the trial started and once the trial ended.

As already noted, the participants used in Experiment 5.1 and 5.2 were drawn from the same participant pool. In addition, although the two experiments were carried out separately, the data collection overlapped. As both experiments used a between-subject design we can compare and combine data across Experiment 5.1 and 5.2 for the purposes of analysis. The data from Experiment 5.1 are displayed along with the data of Experiment 5.2 for comparison and will be referred to as *Dark* condition.

5.2.2 Results

5.2.2.1 Straightness of mean trajectories

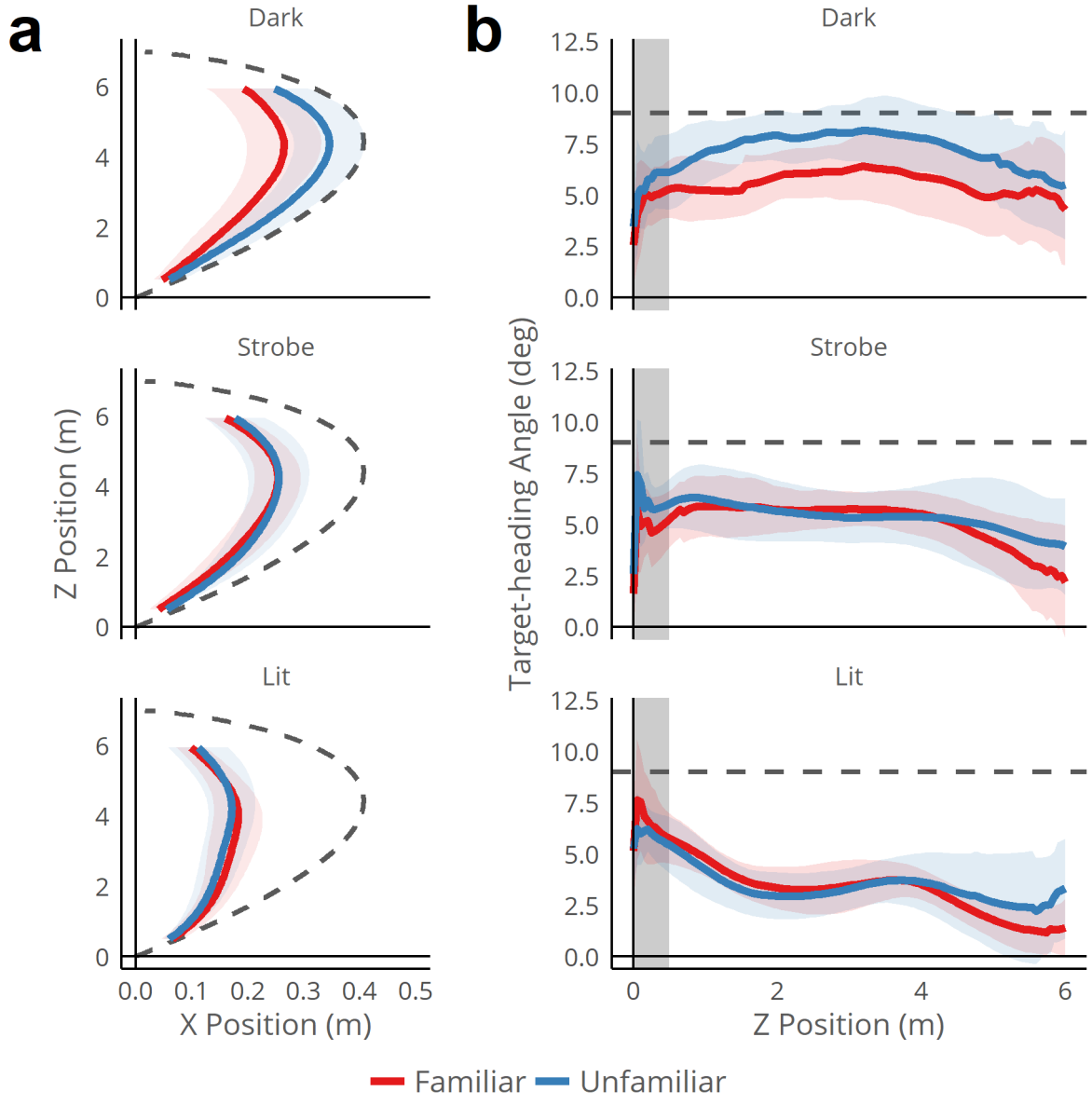

Figure 5.6. (a) *Mean trajectory averaged over the five test trials (1 ~ 5) and the participants (n = 12 per condition) for the familiar group (red) and unfamiliar group (blue) respectively in the dark (upper), strobe (middle) and lit (bottom) conditions. Dashed lines show the trajectories that should result if egocentric direction was used. Shaded ribbons correspond to 95% confidence interval.* ***(b)*** *Mean target-heading angle against distance averaged over the five test trials (1 ~ 5) and the participants (n = 12 per condition) for the familiar group (red) and unfamiliar group (blue) respectively in the dark (upper), strobe (middle) and lit (bottom) conditions. Solid line at 0° corresponds to a straight trajectory. Grey shaded area at 0m ~ 0.5m indicates the data that has been excluded from the final analysis. Dashed lines show the trajectories that should result if egocentric direction was the sole cue used. Shaded ribbons correspond to 95% confidence interval.*

Figure 5.6a illustrates the mean trajectories that were averaged across the five test trials and over the twelve participants in each group. The upper panel shows the data in the Dark condition (from Experiment 5.1), the middle panel the data in the Strobe condition and the lower panel the data in the Lit condition. As expected, the straightness of the mean trajectory increases with the availability of visual cues. Compared to the Dark condition (overall mean target-heading angle = 6.41°, SD = 2.57°), the trajectories are straighter in the Strobe condition (overall mean target-heading angle = 5.18°, SD = 1.84°), and the straightest in the Lit condition (overall mean target-heading angle = 3.24°, SD = 2.56°). Factorial ANOVA confirmed this trend by showing a significant main effect of cue availability [$F_{2, 66}$ = 15.10, $p < 0.0001$, $\eta^2 = 0.30$]. As we have a clear prediction about the direction of the effect, one-tailed t-statistics were used in the *post hoc* tests. The overall mean target-heading angles in the Lit condition was significantly smaller than both the Dark condition [Bonferroni corrected one-tailed $p < 0.0001$] and the Strobe condition [Bonferroni corrected one-tailed $p < 0.01$]. The mean target-heading angle was marginally smaller in the Strobe condition than in the Dark condition [Bonferroni corrected one-tailed $p = 0.059$]. The pattern of results is commensurate with the results of Experiment 3.1 where we have shown that the straightness of a walking trajectory is better predicted by the richness of allocentric location cues.

The trajectories in the Strobe condition were markedly straighter than the trajectory that is predicted by the sole use of egocentric direction (dashed line in **Figure 5.6a**). For both Familiar and Unfamiliar group, the overall mean target-heading angle was significantly smaller than 9° [both *p*s < 0.0001]. The results are in keeping with the findings by Herlihey (2010).

Of particular interest, no main effect of familiarity was found [$F_{1, 66} = 2.22$, $p = 0.14$, $\eta^2 = 0.022$]. As apparent in **Figure 5.6a**, the trajectories are similar between the Familiar and Unfamiliar group in the Strobe and Lit conditions [both *p*s > 0.1; Strobe: Bayes Factor in favour of null hypothesis = 2.55; Lit: Bayes Factor in favour of null hypothesis = 2.60].

5.2.2.2 Straightness as a function of distance

Figure 5.6b shows the mean target-heading angle as a function of distance in each condition. Cue richness has a significant effect on the intercept (target-heading angle at 0.5m) [$\chi^2(2) = 24.89$, $p < 0.0001$]. The effect of cue richness on the slope just fell short of significance [$\chi^2(2) = 3.86$, $p = 0.15$]. Over the whole distance, there was no significant decrease in the Dark condition [estimated slope = -0.13, z = -1.02, $p = 0.31$]. By contrast, there was a significant decrease for both Lit [estimated slope = -0.46, z = -3.59, $p < 0.001$]

and Strobe [estimated slope = -0.42, z = -3.27, $p < 0.01$] conditions. The interaction between familiarity and cue richness has a marginally significant effect on the intercept [$\chi^2(2) = 4.93$, $p = 0.085$]. However, no effect of familiarity or interaction was found on the slope (rate of change in the mean target-heading angle against distance) [both ps > 0.1] (see Supplementary Materials 8.4.2.1).

5.2.2.3 Straightness as a function of trial

Figure 5.7 shows the mean target-heading angles as a function of trial. In clear areas, the data of the five test trials are plotted. The overall pattern looks consistent with what we observed in mean trajectories. Both intercept (magnitude of target-heading angle at 0.5m) and slope (rate of change against trial) varied as a function of the availability of visual cues [respectively $\chi^2(2) = 26.70$, $p < 0.0001$ and $\chi^2(2) = 11.58$, $p < 0.01$].

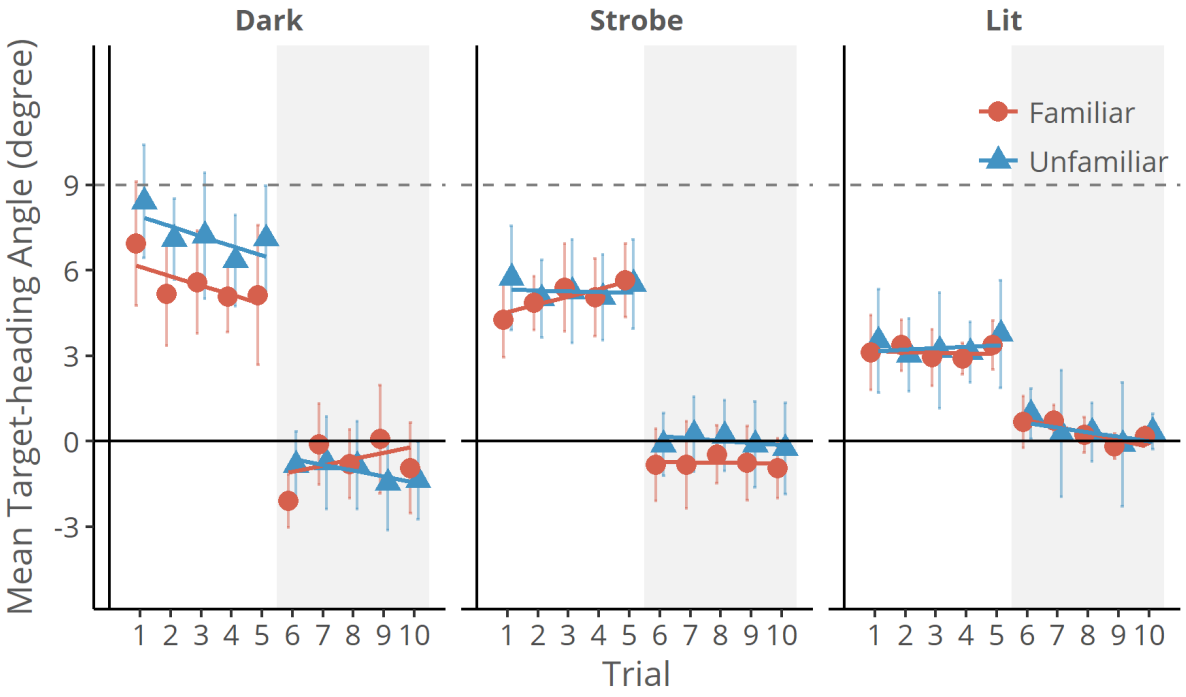

Figure 5.7 *Overall mean target-heading angle as a function of trial averaged over the participants (n=12 per condition). Shaded areas correspond to the test trials with the prism glasses on (Trial 1 ~ 5), and clear areas correspond to the post-prism trials with the prism glasses taken off (Trial 6 ~ 10). Dashed lines at 9° indicate the power of the prism glasses. Error bars represent 95% confidence interval. Left-hand panel shows the data of the Familiar groups respectively under the three Illumination conditions. Right-hand panel shows the data of the Unfamiliar groups respectively under the three Illumination conditions.*

In contrast to the Dark condition, the mean target-heading angles remain relatively constant over the test trials in the Strobe [estimated slope = 0.16, z = 0.14, p = 0.15] and Lit [estimated slope = 0.053, z = 0.49, p = 0.62] conditions. The slopes in the Strobe and Lit conditions were significantly flatter than in the Dark condition [both Bonferroni ps < 0.05]. No effect of familiarity was found on either the overall magnitude of mean target-heading angles [$\chi^2(1) = 1.38$, p = 0.24] or the slope [$\chi^2(1) = 0.43$, p = 0.51] (see Supplementary Materials 8.4.2.2).

We did not find a reliable aftereffect in the Lit and Strobe conditions. The mean target-heading angles of Trial 6 were not significantly smaller than 0° [all one-tailed ps > 0.1], except in the Strobe-Familiar where there was a weak trend [mean = -0.83°, t(11) = -1.43, p = 0.090] (see the shaded areas in **Figure 5.7**).

5.2.2.4 Walking speed and its relationship with the straightness of trajectories

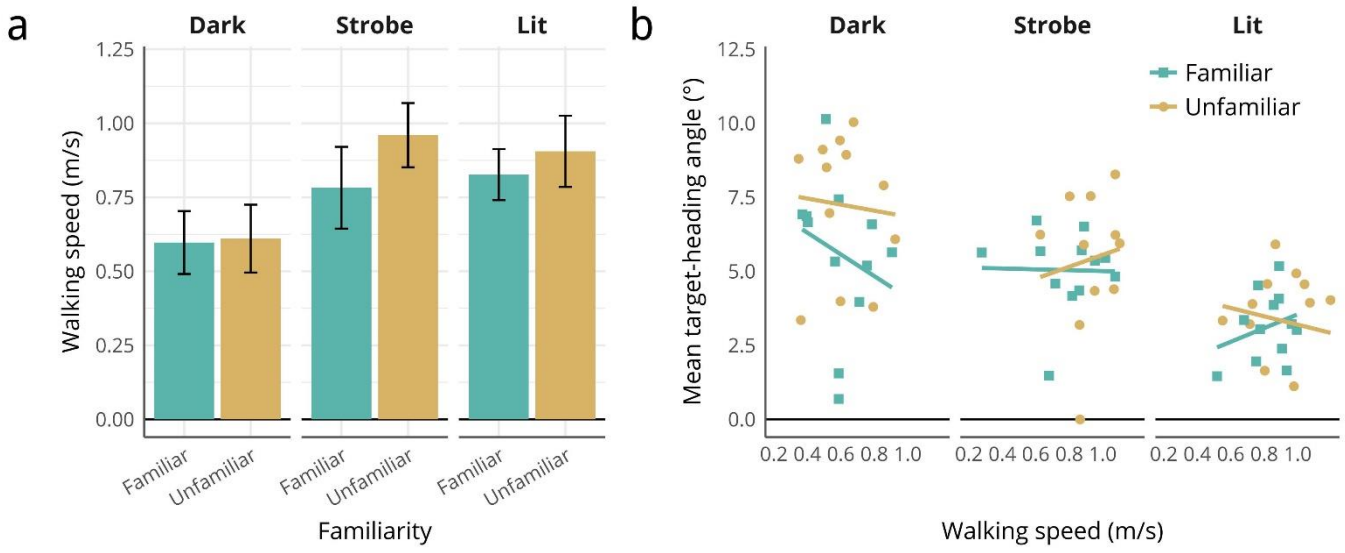

Figure 5.8. (a) *Mean walking speed averaged over the five test trials and over 12 participants in each group (Familiar and Unfamiliar) for the three conditions: Dark, Strobe and Lit. Error bars correspond to 95% confidence interval.* ***(b)*** *Relationships between target-heading angle and walking speed respectively for the Familiar and Unfamiliar groups in each condition (Dark, Strobe and Lit).*

Mean walking speed is plotted as a function of familiarity respectively for the Dark, Strobe and Lit conditions in **Figure 5.8a**. The speed was significantly different between these conditions [$F_{2, 66} = 17.61$, $p < 0.0001$, $\eta^2 = 0.32$]. *Post hoc* tests using Bonferroni correction for multiple comparison problems revealed that the mean speeds in the Strobe and Lit conditions were significantly higher than in the Dark condition [both Bonferroni ps <

0.0001], but there was no significant difference between the Strobe and Lit conditions [Bonferroni $p > 0.1$].

There was also a main effect of familiarity [$F_{1, 66} = 4.57$, $p = 0.036$, $\eta^2 = 0.042$]. Interestingly, the walking speed in the Unfamiliar group [mean = 0.83m/s, SD = 0.23m/s] was faster than in the Familiar group [mean = 0.74m/s, SD = 0.20m/s]. No significant interaction was found between familiarity and visual richness [$F_{2, 66} = 1.29$, $p = 0.28$, $\eta^2 = 0.024$].

The relationships between the magnitude of target-heading angle and walking speed are depicted for each condition in **Figure 5.8b**. There was no significant correlation in either Familiar group or Unfamiliar group for any condition [all *p*s > 0.1].

5.2.3 Discussion of Experiment 5.2

In this experiment, the familiarity effect was evaluated as a function of the availability of visual cues. When visual cues were available in the environment, there was no detectable familiarity effect. The results support our hypothesis that prior knowledge may play a role in the guidance of walking by compensating for a limited access to other visual cues. The difference between the cue availability conditions also strengthened our previous findings of the use of allocentric location cues.

5.2.3.1 Evidence of the use of allocentric location cues

The results reinforced our findings in Experiment 3.1 where we have shown that the trajectories are better predicted by the richness of allocentric location cues. Here, the availability of visual cues was varied by a temporal manipulation. As a result, the amount of optic flow was in an order Dark = Strobe < Lit, whereas the amount of allocentric location cues was in an order Dark < Strobe < Lit. The straightness of trajectories that we observed in this experiment followed an order Dark < Strobe < Lit. As in Experiment 3.1, the pattern of trajectories was better predicted by the order of allocentric location cues.

The results also replicated and extended recent findings by Herlihey (2010) in a medium-sized indoor environment. As already described in Chapter 1, Herlihey (2010) asked participants to close their eye when moving and open their eye when stopped for each step. By doing this, optic flow was eliminated but allocentric location cues were maintained. The trajectories were noticeably straighter than would be expected if only egocentric direction cues were used, and similar to those in the condition with full access to optic flow. Here we observed a similar pattern. The Strobe condition contained allocentric location cues but no

optic flow. The trajectories in this condition were considerably straighter than that predicted by egocentric direction alone.

In the Lit condition, the trajectories were the straightest. In this condition, the participants had access to rich cues in a wide visual field including both central and peripheral vision. It is possible that allocentric location cues may come from peripheral vision, which gives the observer a strong sense of where they are in space. We will explore this possibility in Experiment 5.4. Before that, we will look at the role of target drift.

5.2.3.2 Potential use of target drift

When the target is continuously visible, the change of direction of target results in a movement of the target relative to the observer, or target drift. The observer can use this cue to guide walking by cancelling the drift of the target. As mentioned in Chapter 1 (Section 1.3.1), researchers have shown mathematically that when an observer walks to cancel the drift, the trajectory will straighten out (Rushton, 2004; Rushton, Wen, & Allison, 2002). The trajectories of the Unfamiliar group in the Dark condition might suggest a tendency of the use of target drift. In this condition, there were no other available cues and the participants did not have any prior experience with the room, the trajectories were still significantly straighter than that predicted by egocentric direction (see **Figure 5.3** and Section 5.1.2.1).

The potential use of target drift also gives rise to the question: if we further reduce the availability of visual cues in the environment by removing target drift, given that the role of familiarity may depend on the cue availability, can we observe a larger effect of familiarity?

In Experiment 5.3, we will explore the role of target drift and its interaction with the familiarity effect. We will remove the target drift to see whether that would make the trajectories more curved and whether that would increase the reliance on prior knowledge.

5.3 Experiment 5.3 Target drift and the familiarity effect

In this experiment, we evaluated whether removing target drift would reveal a larger effect of familiarity. We removed the drift cues in the Dark and Strobe conditions[8] by illuminating the target in an intermittent way (see **Figure 5.9**). If target drift plays a role, the trajectories would be more curved after removal of it. In addition, if removing target drift

[8] Theoretically target drift should also be removed in the Lit condition for a more complete comparison. However, it is practically impossible to set up an intermittent target in a real full-lit room because the post is always seen.

strengthened the tendency to switch to reliance on prior knowledge, the difference in the trajectories between the Familiar and Unfamiliar groups should be larger after removal of target drift.

5.3.1 Method

Sixty participants were recruited from the same population in order to have forty-eight participants (twelve per condition) in total (mean age = 19.98, SD = 2.15, range = 18 ~ 26, one male). Reasons for exclusion were technical faults (i.e., the motion-tracking server crashed) during the experiment (n = 12).

Participants walked in the same test room either in dark or illuminated by strobes. The LEDs on the target was illuminated intermittently. That is, each LED was illuminated only for 50ms and then extinguished for 950ms before the next one was turned on. The result was that participants saw a series of very brief 'snapshots' of the target. The relatively long blackout intervals between the 'snapshots' disrupted the apparent movement of the target so

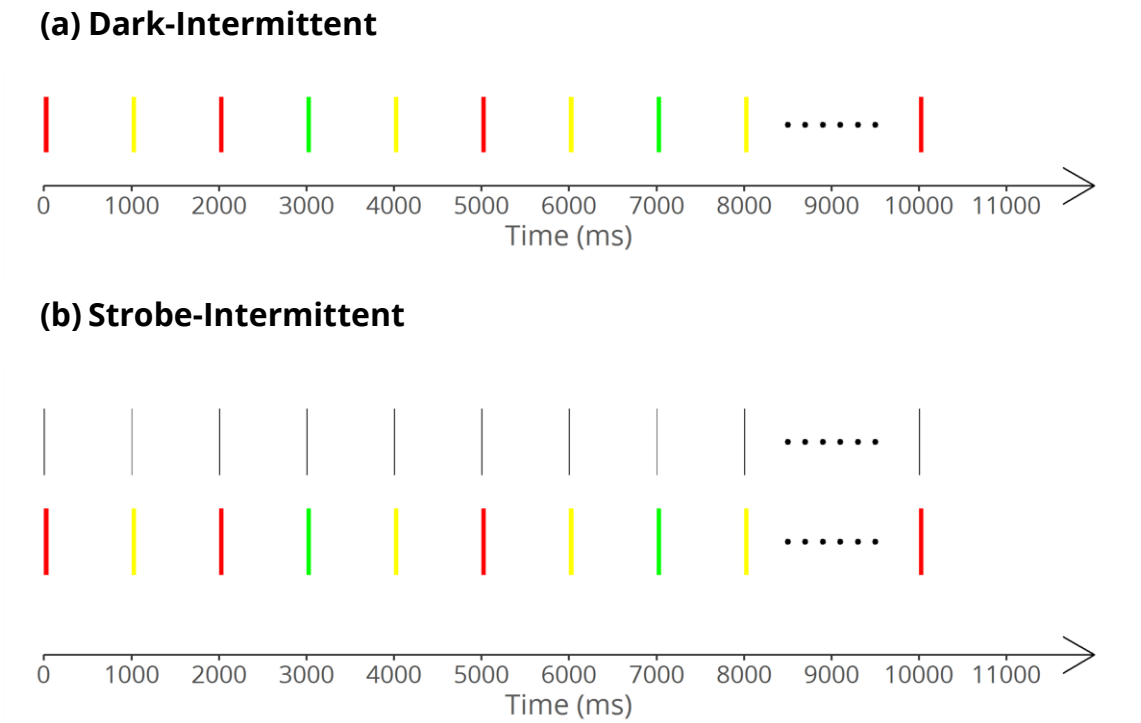

Figure 5.9. *Schematic illustration of the Intermittent illumination of LEDs on the target for* ***(a)*** *the Dark condition and* ***(b)*** *the Strobe condition. Each coloured rectangle represents the duration of the LED in corresponding colour being illuminated. Black vertical lines in* ***(b)*** *represent flashes of the strobes. The illumination of each LED spanned only 50ms. The interval between any two adjacent illuminations was 950ms. The flash of the strobes and the illumination of the LED started at the same time.*

that target drift was removed. As in previous experiments, the order in which the LEDs were illuminated was random so that the participant was unable to guess the next illuminated LED. In the Strobe condition, the illumination of the LEDs was synchronised with the flashes of the strobes (see **Figure 5.9b** for illustration).

5.3.2 Results

5.3.2.1 Straightness of mean trajectories

In **Figure 5.10a,** the mean trajectories that were averaged over the five test trials are illustrated. By comparing the trajectories in the right column (Intermittent condition) to those in the left column (Continuous condition), it is evident that removing target drift produced more curved trajectories. Factorial ANOVA revealed a significant main effect of target drift [$F_{1, 88} = 6.53$, $p = 0.012$, $\eta^2 = 0.056$].

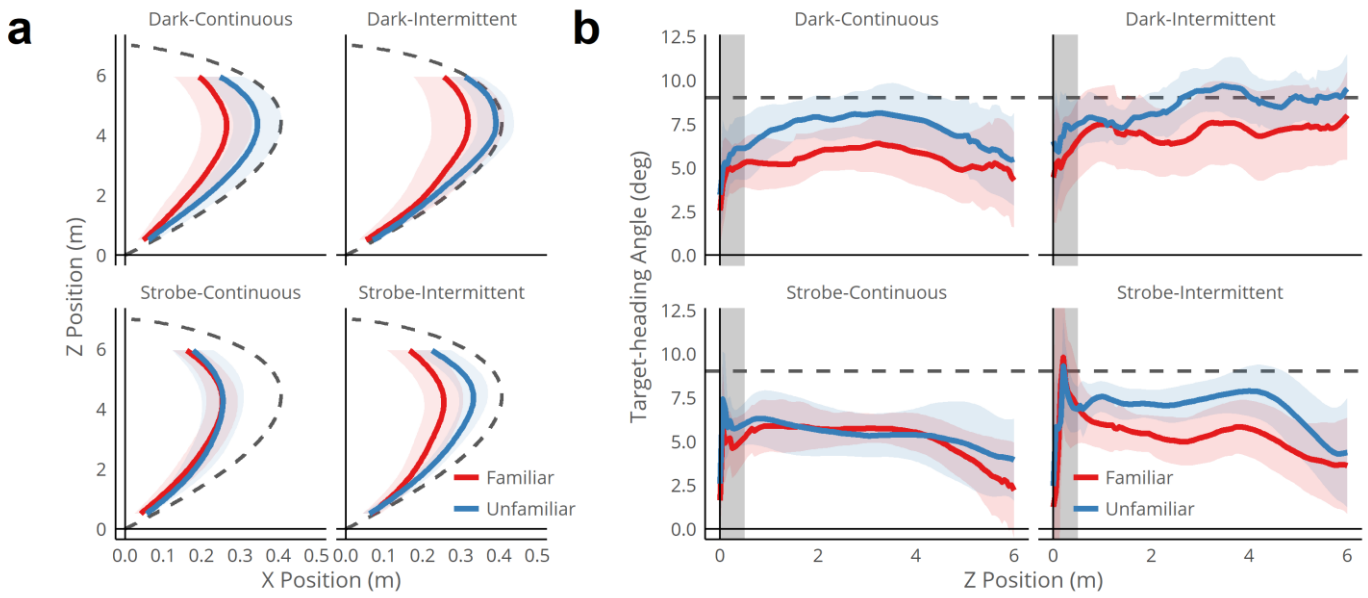

Figure 5.10. (a) *Mean trajectory averaged over the five test trials (1 ~ 5) and the participants (n = 12 per condition) for the Familiar group (red) and Unfamiliar group (blue) respectively in each condition. Dashed lines show the trajectories that should result if egocentric direction was used. Shaded areas correspond to 95% confidence interval.* ***(b)*** *Mean target-heading angle against distance averaged over the five test trials (1 ~ 5) and the participants (n = 12 per condition) for the Familiar group (red) and Unfamiliar group (blue) respectively in each condition. Dashed lines show the trajectories that should results if egocentric direction was used. Solid line at 0° corresponds to a straight trajectory. Grey shaded area at 0m ~ 0.5m indicates the data that has been excluded from the final analysis. Shaded areas correspond to 95% confidence interval.*

The trajectories were still more curved in the Dark condition than in the Strobe condition, as evident by the main effect of cue availability [$F_{1, 88} = 11.42$, $p < 0.01$, $\eta^2 = 0.098$]. The effect of cue availability was not affected by the presence of target drift [$F_{1, 88} = 0.46$, $p = 0.50$, $\eta^2 < 0.01$].

The question of particular interest is whether the familiarity effect remained after removal of target drift. Generally, the trajectories are still straighter in the Familiar group than in the Unfamiliar group [$F_{1, 88} = 7.93$, $p < 0.01$, $\eta^2 = 0.068$]. Although there was no significant interaction between familiarity and target drift [$F_{1, 88} = 0.47$, $p = 0.49$, $\eta^2 < 0.01$], it can be clearly seen from **Figure 5.10a** that the degree of familiarity effect looks somewhat different after removal of target drift. In the Dark condition, the trajectories were still more curved in the Unfamiliar group (mean = 8.64°, SD = 1.63°) than the Familiar group (mean = 7.12°, SD = 3.31°). Because Levene's test showed that the variances of the Familiar and Unfamiliar groups were unequal [$F_{1, 22} = 4.67$, $p = 0.042$], Welch's t-test was used to correct for the unequal variances. Although the difference did not reach significance [Welch's $t(16.07) = 1.43$, $p = 0.17$], there was a medium effect size [$r = 0.34$] which indicates a substantial effect.

The most interesting pattern appears in the Strobe condition. In the presence of target drift, there was no effect of familiarity. After removal of target drift, however, the trajectories of the Unfamiliar group became significantly more curved than those of the Familiar group [$t(22) = 2.19$, $p = 0.040$, $r = 0.42$]. The results are consistent with the hypothesis that removing target drift reduced a critical amount of visual information which makes the observer more reliant on prior knowledge.

5.3.2.2 Straightness as a function of distance

Figure 5.10b illustrates the mean target-heading angle as a function of distance. The upper panel shows the data from the Strobe condition in Experiment 5.2 for reference, and the lower panel the data from the present experiment.

As clearly shown in the lower panel of **Figure 5.10b**, the pattern of target-heading angle as a function of distance looks very different between the Familiar and Unfamiliar groups. For the Familiar group, the target-heading angle decreased gradually in a similar way to those in Experiment 5.2 (see the upper panel of **Figure 5.10b**). By contrast, for the Unfamiliar group, the target-heading angle remains around 9° (the deflecting power of the

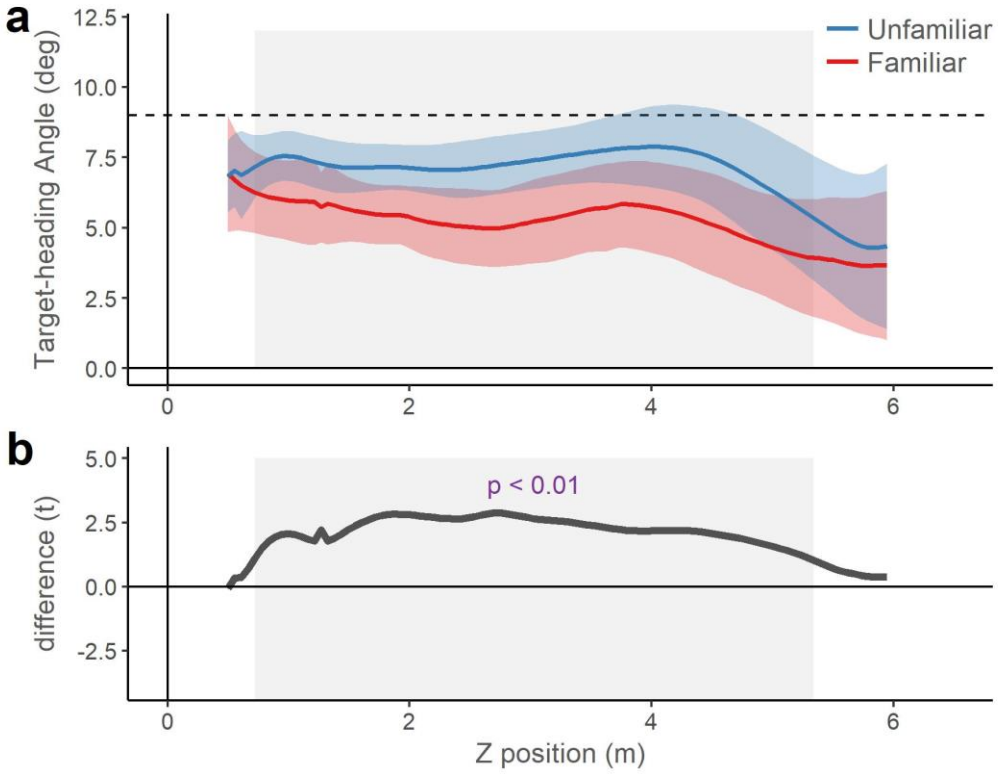

Figure 5.11. (a) *Mean target-heading angles against distance over participants (n = 12) respectively for the Familiar and Unfamiliar groups. Dashed grey line at 9° indicates degree of displacement in the VE. Coloured areas indicate 95% confidence interval. Grey shaded area represents the part on distance where the Familiar group is significantly straighter than the Unfamiliar group.* ***(b)*** *Difference (t-values) comparing target-heading angle between the Familiar and Unfamiliar groups. Grey area represents the period where t-values are considered (p < 0.05) to be significant as a cluster.*

prism glasses) until ~3.5m. Then the target-heading angle decreased very quickly. Near the end of the trajectory, the target-heading angle is comparable between the Unfamiliar and Familiar group. Although the growth modelling did not reveal a difference in the linear rate

of change between the two group [χ^2 (1) = 0.23, p = 0.63] (see Supplemental Material 8.4.3.1), our in-house time series analysis found a significant cluster covering almost the whole distance except the last ~1m (see **Figure 5.11**). The large decrease at the end of the trajectory in the Unfamiliar group might reflect increase salience of allocentric location cues and target displacement.

5.3.2.3 Straightness as a function of trial

The overall mean target-heading angles are plotted against trials in **Figure 5.12**. The pattern of the overall magnitude of mean target-heading angles is generally consistent with the pattern of mean walking trajectories. There was a significant effect of target drift [χ^2(1) = 6.34, p = 0.012], cue availability [χ^2(1) = 11.86, p < 0.0001] and familiarity [χ^2(1) = 6.68, p <

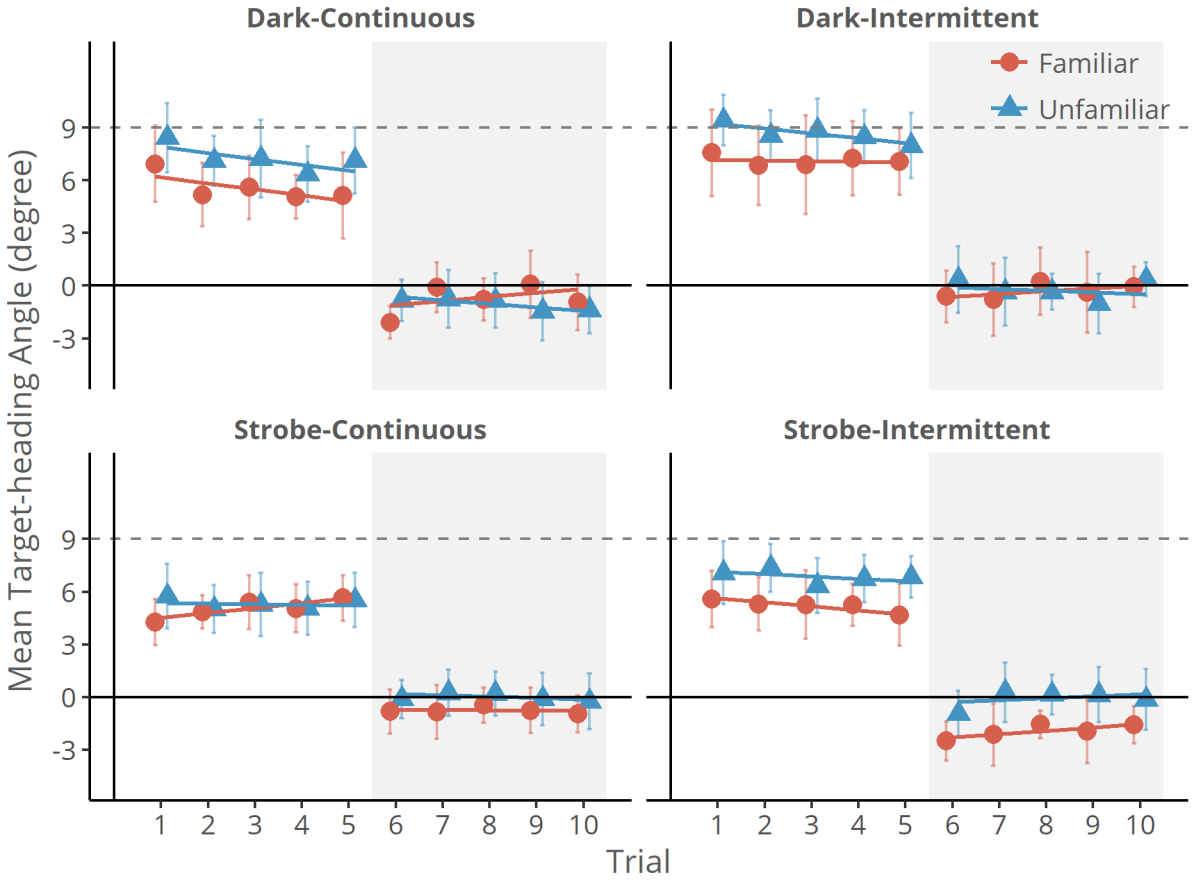

Figure 5.12. *Mean target-heading angle as a function of trial for each combination of conditions (Continuous-Familiar, Continuous-Unfamiliar, Intermittent-Familiar and Intermittent-Unfamiliar). Clear areas (Trial 1 ~ 5) correspond to the test trials with prism glasses. Shaded areas correspond to the baseline trials after the prism glasses were removed. Dashed lines at 9° indicate the power of the prism glasses. Error bars correspond to 95% confidence interval.*

0.01] on the magnitude of mean target-heading angle across the test trials (see Supplementary Materials 8.4.3.2 for details).

There was a general trend of decrease in the mean target-heading angle over the test trials [$\chi^2(1) = 6.21$, $p = 0.013$]. As shown in **Figure 5.12**, the rate of decrease looks similar between the Familiar and Unfamiliar groups [$\chi^2(1) = 0.90$, $p = 0.34$], but faster in the Continuous condition than in the Intermittent condition [$\chi^2(1) = 3.42$, $p = 0.065$]. The difference between the Continuous and Intermittent conditions was also affected by the cue availability [$\chi^2(1) = 4.45$, $p = 0.035$]. One-sample tests on parameters revealed that only in the Dark-Continuous condition, the mean target-heading angle significantly decreased over the test trials [estimated slope = -0.34, z = -2.98, $p < 0.01$].

The shaded areas in **Figure 5.12** show the data in the baseline trials after removal of prism glasses. The aftereffects look more evident in the Familiar group than in the Unfamiliar group [$F_{1, 88} = 7.12$, $p < 0.01$, $\eta^2 = 0.067$]. In the Dark condition, the aftereffects look more evident in the Continuous condition than the Intermittent condition; whereas the Strobe condition shows an opposite pattern. The significant interaction between target drift and cue availability confirmed this observation [$F_{1, 88} = 9.38$, $p < 0.01$, $\eta^2 = 0.089$]. Across the conditions, there was a reliable aftereffect for the Familiar group in all conditions [all one-tailed ps < 0.05 except in Dark-Intermittent one-tailed $p = 0.093$]. For the Unfamiliar group, aftereffects were significant in the Dark-Continuous and Strobe-Intermittent [both one-tailed ps < 0.05] but not in the Dark-Intermittent and Strobe-Continuous conditions [both ps > 0.1].

5.3.2.4 Walking speed and its relationship with the straightness of trajectories

In **Figure 5.13a**, the mean speeds were plotted as a function of familiarity for both Continuous and Intermittent conditions. The mean speed was slower in the Intermittent condition [mean = 0.63m/s, SD = 0.23m/s] than in the Continuous condition [mean = 0.74m/s, SD = 0.23m/s; $F_{1,88} = 8.59$, $p < 0.01$, $\eta^2 = 0.052$], and slower in the Dark condition [mean = 0.54m/s, SD = 0.18m/s] than in the Strobe condition [mean = 0.83m/s, SD = 0.20m/s; $F_{1,88} = 59.79$, $p < 0.0001$, $\eta^2 = 0.37$].

Marginally significant interactions were observed between familiarity and cue richness [$F_{1, 88} = 3.09$, $p = 0.082$, $\eta^2 = 0.019$] and between familiarity and target drift [$F_{1, 88} = 3.07$, $p = 0.083$, $\eta^2 = 0.019$]. No three-way interaction was observed. As shown in **Figure 5.13a**, the interactions seem to be driven by the faster speed of the Unfamiliar group [mean = 0.96m/s, SD = 0.17m/s] than the Familiar group [mean = 0.78m/s, SD = 0.22m/s; t(22) = -2.23, $p = 0.037$]. From the scatter plot in the left-lower panel of **Figure 5.13b**, it seems that the

slower mean speed was driven by an extreme value. However, robust t-test based on 20% trimmed mean (Mair & Wilcox, 2017; Yuen, 1974) still revealed a significant difference between the Familiar and Unfamiliar groups [t(12.92) = 2.18, p = 0.048].

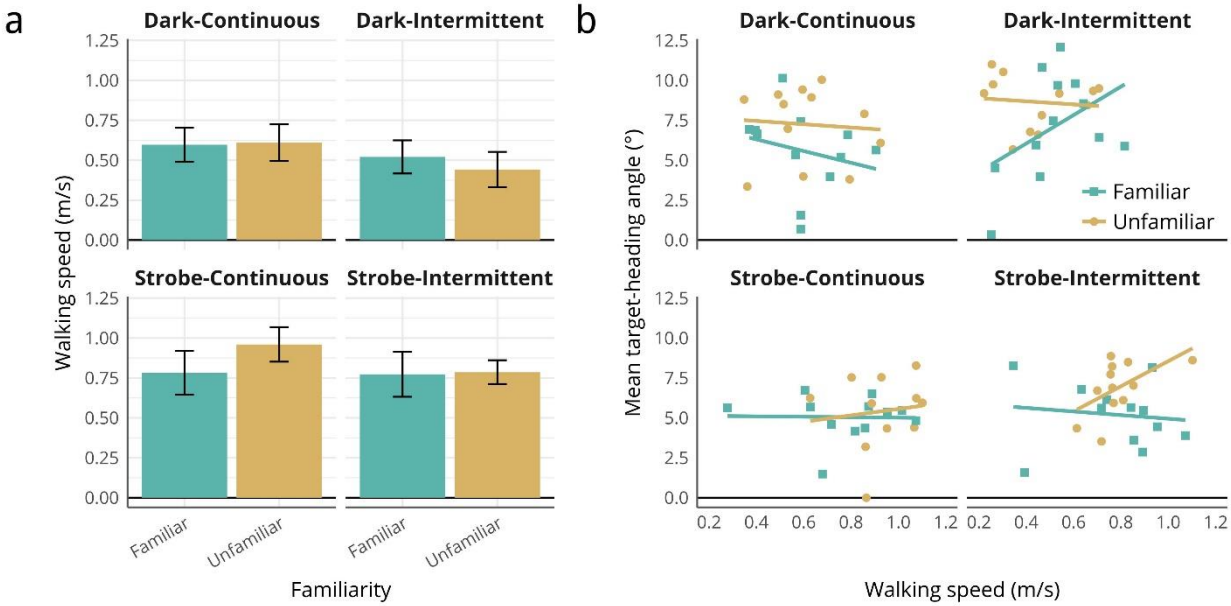

Figure 5.13. (a) *Mean walking speed averaged over the five test trials and over 12 participants in each group (Familiar and Unfamiliar) respectively for richness (Dark and Strobe) and target drift (Continuous and Intermittent) conditions. Error bars correspond to 95% confidence interval.* ***(b)*** *Relationships between target-heading angle and walking speed respectively for the Familiar and Unfamiliar groups respectively for richness (Dark and Strobe) and target drift (Continuous and Intermittent) conditions.*

There was no significant correlation between the magnitude of target-heading angle and walking speed for all conditions [all ps > 0.1] except a strong and marginally significant correlation for the Unfamiliar group in the Strobe-Intermittent condition [Pearson's r = 0.56, t(10) = 2.07, p = 0.065]. The correlation was positive, suggesting that the faster the participant walked, the less straight the trajectory was.

5.3.3 Discussion of Experiment 5.3

In this experiment, we removed target drift in the Dark and Strobe conditions. The trajectories became more curved, supporting the role of target drift in the guidance of walking. More interestingly, the impact on the familiarity effect differed between the conditions. In the Dark condition, there was still an effect of familiarity, suggesting the effect of familiarity is robust when visual cues are restricted. In the Strobe condition, no effect of

familiarity was observed in the absence of target drift; however, after removal of it, a clear effect of familiarity emerged. The results provide further support for the hypothesis that prior knowledge plays a role in situations with limited cues. Furthermore, the pattern of results suggests that, rather than being combined with the use of other cues in a standard linear way. Prior knowledge appears to come into play in an "either-or" fashion. It is used when it is needed.

As already mentioned, peripheral vision might be critical for the use of allocentric location cues. In Experiment 5.4, we will investigate this possibility by imposing a restriction on the visual field of the participants.

5.4 Experiment 5.4 Influence of restricted FoV

You may have experienced difficulties in crossing the road wearing a raincoat with hood up occluding your peripheral vision. To cross the road safely, you either swing your head to try to see the whole environment before crossing or have to pull your hood down irrespective of the weather. Indeed, participants wearing night vision goggles (FoV = 30°) took a longer time to find a target object and made more errors when navigating a life-size walking maze, as compared to those who did not wear night vision goggles (Gauthier et al., 2006). Another study compared navigation performance when the horizontal FoV was limited to either 40° or 90°. Participants were asked to finish a set of spatial memory tests including sketching a map of the environment and judging the spatial relationships (i.e., relative direction and distance) between objects after actively exploring a maze-like environment. It turned out that participants with the wide FoV drew better maps in terms of layout, scale and geometry than those with the narrow FoV but there was no effect of FoV size on the direction and distance judgements. The results suggest that FoV restriction in this range (40° ~ 90°) has an impact on the spatial representation of the layout of the environment but not on the memory of the locations of objects in the environment (Guterman et al., 2009). However, as the study did not include a control group without any FoV restriction, it may be possible that the participants with the wide FoV (90°) had some degraded spatial representation if compared to controls with a normal FoV.

Fortenbaugh, Hicks, Hao and Turano (2007) examined the memory of the locations of target objects as a function of FoV sizes from 0° to 40° in healthy participants. The participants were asked to learn the locations of target statues in a virtual environment. The memory of the locations was tested by placing the target back to its original place. The placement errors increased as the FoV size decreased, suggesting that when the FoV is

further limited to below 40°, there is an impact of FoV restriction on the memory of object locations in the environment. The study was later replicated in patients with peripheral visual field loss (PFL) with FoV ranging from 5° to 30° (Fortenbaugh, Hicks, & Turano, 2008). The patients showed a similar pattern of results to those healthy participants with FoV restriction on normal vision in the previous study (Fortenbaugh et al., 2007).

In addition to the formation of a spatial representation, Turano and colleagues suggest that restriction on FoV may also have an impact on updating the spatial relationships in the representation when the observer is walking in the environment (Turano et al., 2005). Using virtual reality techniques, they found that when walking towards a remembered but invisible goal, patients with peripheral visual field loss (PFL) (and hence smaller FoV ranging from 11° to 173°[9]) showed larger deviations in their walking paths than those with normal vision did. A potential explanation is that with a narrow visual field, it was difficult for PFL patients to keep the goal and other landmark objects or reference positions in the visual field simultaneously and therefore their ability to update the locations in the spatial representation was compromised.

In a more recent study by Herlihey (2010), reduced visual calibration of perceived straight ahead was observed when the participants' FoV was restricted by placing a pair of goggles (~ 80°) on top of the prism glasses. Given the earlier findings as outlined above, the slower calibration might be due to the impact of FoV restriction on establishing and/or updating a spatial representation of the walking environment. If so, restricting FoV to ~80° is sufficient to produce an effect on a walking trajectory.

In this experiment, we investigated the role of FoV on the formation and use of spatial representation in guiding walking. We restricted the participants' FoV by using a pair of goggles (~ 75°) similar to those used in Herlihey's (2010). If the restriction has an impact on the use of a previously formed spatial representation of the room, we would expect to see more curved trajectories in the Unfamiliar groups than in the Familiar group. If the restricted FoV has an impact on the online formation of a spatial representation while walking, the trajectories should straighten up slower in the Unfamiliar group wearing goggles than in the Unfamiliar group without goggles. If the restriction has a general effect on the guidance of walking, the trajectories should be more curved for participants who wore prisms than for those who did not.

[9] It should be noted that the FoV provided by the HMD used in this study was about 96° (total horizontal by adding FoV of each eye) × 38° (vertical).

5.4.1 Method

Twenty-seven participants were recruited from the same population in order to have twenty-four participants (twelve per condition) in total (mean age = 20.33, SD = 4.29, range = 18 ~ 40, three males). Reasons for exclusion were technical faults during the experiment (n = 3).

(a) **(b)**

Figure 5.14. *Illustration of the equipment worn by participants in the two conditions.* ***(a)*** *The "Goggles" condition, the participants wore prism glasses walking in the fully illuminated room.* ***(b)*** *The "NoGoggles" condition, the participants wore a pair of goggles on top of the prism glasses. The FoV was restricted to 73° horizontally.*

Participants walked in the same room under full illumination wearing a pair of prisms. A pair of field restricting goggles were placed on top of the prism glasses (see **Figure 5.14**). The goggles restricted the FoV to 73° (horizontally). To examine the role of FoV, we compared the data from Experiment 5.2 (the *NoGoggles* condition) with the data from the present experiment (the *Goggles* condition). In the NoGoggles condition, as the participants wore only the prism glasses, the FoV should be the same as wearing normal optic spectacles (~ 110°).

5.4.2 Results

5.4.2.1 Straightness of mean trajectories

The mean trajectories are plotted in **Figure 5.15a**. The upper panel shows the data from the Lit condition in Experiment 5.2 (the NoGoggles condition) for reference, and the lower panel shows the data from the present experiment (the Goggles condition). From the

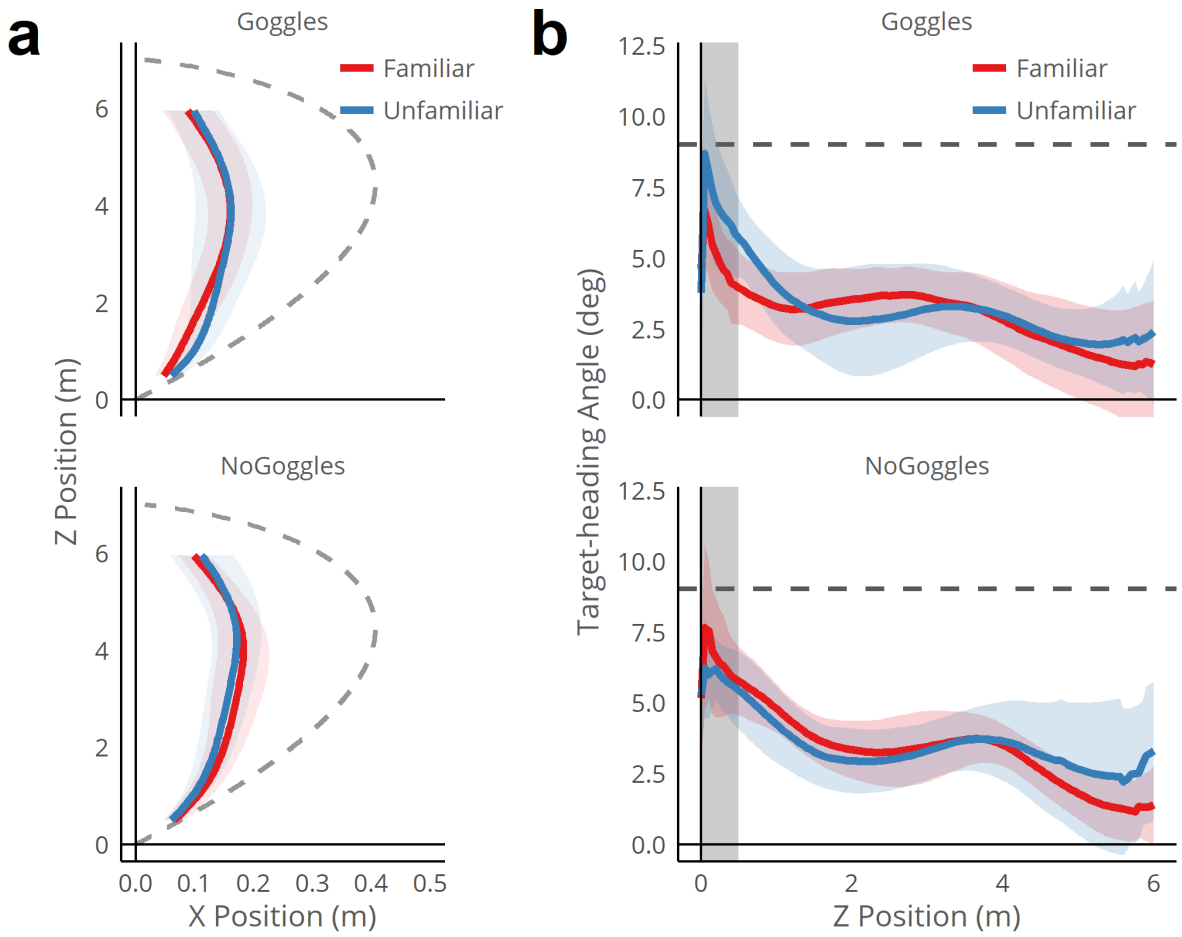

Figure 5.15. (a) *Mean trajectory averaged over the five test trials (1 ~ 5) and the participants (n = 12 per condition) for the familiar group (red) and unfamiliar group (blue) respectively. Dashed line shows the trajectory that should result if egocentric direction was used. Shaded ribbons correspond to 95% confidence interval.* ***(b)*** *Mean target-heading angle against distance averaged over the five test trials (1 ~ 5) and the participants (n = 12 per condition) for the familiar group (red) and unfamiliar group (blue) respectively Dotted line shows the trajectory that should result if egocentric direction was used. Solid line at 0° corresponds to a straight trajectory. Grey shaded area at 0m ~ 0.5m indicates the data that has been excluded from the final analysis. Shaded ribbons correspond to 95% confidence interval.*

trajectories, it can be seen that restricting the FoV by goggles did not influence the walking trajectories or the effect of familiarity. The shape of the walking trajectories is very similar between conditions. A factorial ANOVA on the individual overall mean target-heading angles did not find any significant effect of FoV restriction [$F_{1, 44} = 0.47$, $p = 0.50$, $\eta^2 = 0.010$], familiarity [$F_{1, 44} = 0.11$, $p = 0.74$, $\eta^2 < 0.01$], or interaction [$F_{1, 44} = 0.0022$, $p = 0.96$, $\eta^2 < 0.01$].

5.4.2.2 Mean straightness as a function of distance

Visual inspection on the mean target-heading angle as a function of distance reveals some interesting patterns (see **Figure 5.15b**). In the NoGoggles condition (the Lit condition in Experiment 5.2), the target-heading angle decreased quickly after the beginning of the trial and then plateaued, consistent with the pattern reported elsewhere (Bruggeman et al., 2007; Warren et al., 2001). By contrast, in the Goggles condition, the target-heading angle remained constant for a few metres before it quickly dropped. Based on the patterns, we applied our in-house time-series analysis on the t-values between the two conditions and expected to find a significant cluster near the end of trial where the target-heading angles in the Goggles condition look smaller for the Familiar group than for the Unfamiliar group; however, the analysis did not reveal a significant cluster (see Supplementary Materials 8.4.4.1 for details).

5.4.2.3 Straightness as a function of trial

The mean target-heading angles were plotted against trials in **Figure 5.16**. In the Goggles condition, there was no effect of familiarity in terms of magnitude of mean target-heading angle [$\chi^2(1) = 0.079$, $p = 0.78$] or the rate of change over the test trials [$\chi^2(1) = 1.90$,

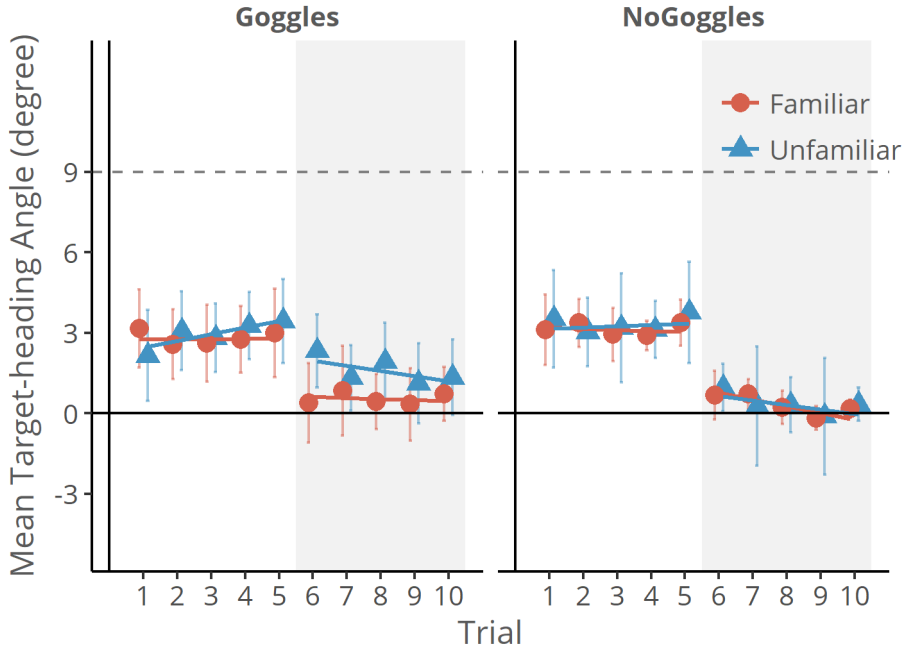

Figure 5.16. *Mean target-heading angle as a function of trial for each combination of conditions (Goggles-Familiar, Goggles-Unfamiliar, NoGoggles-Familiar and NoGoggles-Unfamiliar). Clear areas (Trial 1 ~ 5) correspond to data in the test trials. Shaded areas (Trial 6 ~ 10) correspond to data in the baseline trials. Dashed line at 9° indicate the power of the prism glasses. Error bars correspond to 95% confidence interval.*

p = 0.17]. Across the experiments, there was no significant effect of restricting FoV on the magnitude of mean target-heading angle [$\chi^2(1) = 0.30$, $p = 0.58$] or the rate of change [$\chi^2(1) = 1.24$, $p = 0.26$] (see Supplementary Materials 8.4.4.2 for details).

There was no indication of aftereffects. None of the conditions has a mean target-heading angle smaller than 0° in Trial 6 (see the shaded areas in **Figure 5.16**). Interestingly, the mean target-heading angle of Trial 6 was significant larger than 0° for the Unfamiliar group in both NoGoggles [mean = 0.97°, t(11) = 2.38, $p = 0.036$] and Goggles [mean = 2.33°, t(11) = 3.79, $p < 0.01$], which is in the opposite direction to that predicted for negative aftereffects. The reason behind this pattern is unclear.

5.4.2.4 Walking speed and its relationship with the straightness of trajectories

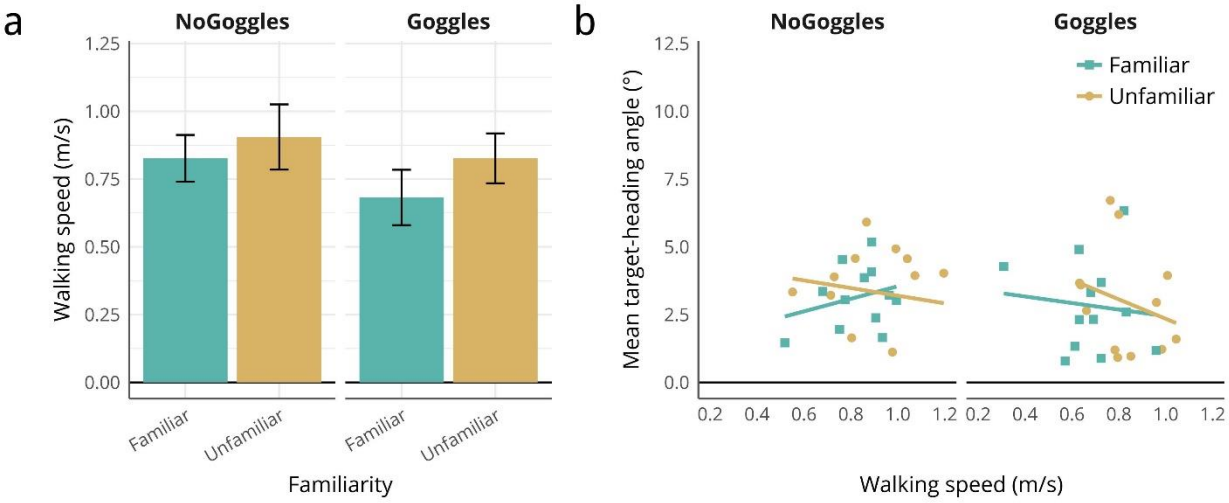

Figure 5.17. (a) *Mean walking speed averaged over the five test trials and over 12 participants in each group (Familiar and Unfamiliar) respectively for FoV (NoGoggles and Goggles) conditions. Error bars correspond to 95% confidence interval.* ***(b)*** *Relationships between target-heading angle and walking speed respectively for the Familiar and Unfamiliar groups respectively for FoV (NoGoggles and Goggles) conditions.*

We also compared the walking speed in each condition to see whether restricting FoV would slow down walking speed (**Figure 5.17a**). As expected, participants wearing goggles walked more slowly than those who did not wear goggles [$F_{1, 44} = 5.92$, $p = 0.019$, $\eta^2 = 0.11$]. Interestingly, the Unfamiliar participants walked faster than the Familiar participants [$F_{1, 44} = 5.92$, $p = 0.019$, $\eta^2 = 0.10$]. No interaction was found significant. In the Goggles condition, no significant correlation was observed for either the Familiar group [Pearson's $r = -0.11$, $p = 0.73$] or the Unfamiliar group [Pearson's $r = -0.26$, $p = 0.41$] (see **Figure 5.17b**).

5.4.3 Discussion of Experiment 5.4

In this experiment, we restricted the participants' FoV to ~75° using goggles. Based on earlier findings on the relationship between FoV size and spatial representation, we predicted that limiting the FoV would result in an effect of familiarity in the participants who wore goggles, and different straightening rates across trials in the Unfamiliar participants depending on whether they wore goggles or not. However, we found that the trajectories were similar between the Familiar and Unfamiliar groups in the Goggles condition and there was no effect of goggles on the straightening rate for the Unfamiliar participants. Overall, there was no difference in the straightness of trajectory between the participants who wore goggles and those who did not.

A possible reason for the lack of effect of FoV restriction is that the restricted FoV was not sufficiently narrow. In comparison to the restriction in our experiment (~75°), FoV was restricted to a narrower degree (e.g., 40°) in those studies in which an effect on spatial representation was observed. In our experiment, the Unfamiliar-Goggles participants might still have sufficient visual information to generate a spatial representation at the onset of the first trial such that the difference to the other groups (i.e., Familiar-Goggles and Unfamiliar-NoGoggles) disappeared quickly.

Another possibility is that all groups had other potential visual cues to use so that it is not necessary to rely on a spatial representation to guide walking. For example, as the target was placed in front of a corner, the alignment between the target and corner could be a powerful cue for the guidance of walking. Wearing goggles should have no impact on the use of this cue, and participants might have used this cue to compensate for the restricted FoV.

Alternatively, the goggles may provide a frame of reference indicating the viewer's true egocentric direction (e.g., Wilkie & Wann, 2003). This would reduce the perceived displacement induced by the prism and in turn decrease the potential difference between the Familiar and Unfamiliar groups. The use of reference frame provided by the goggles should also lead to a straighter trajectory in the Goggles condition than the NoGoggles condition, which was not what we observed. However, this could be a reflection of a ceiling effect.

The fact that restricting the FoV slowed down the participants' walking speed may hint at a possibility that the participants were paying more attention to their walking and/or available visual cues in the environment, which could to some extent compensate for the limited visual field. However, it is not clear why unfamiliar participants walked faster than familiar participants. It may due to sampling noise.

5.5 General discussion and summary

Across Experiment 5.1 – 5.4, we compared the walking trajectories of participants who were familiar with the test room to those who were not. Using environments with restricted visual cues, we uncovered robust evidence for a role of prior experience with the environment in the guidance of walking. Furthermore, we found that the information from prior experience is not linearly added to other cues. Rather, it is used when it is needed.

5.5.1 What information in prior knowledge is important?

In our experiment, the participants in the Familiar group were led into the test room before the experiment started. During the preparation, they could see the room. This enabled them to incidentally learn the spatial layout of the room. A question thus arises: what information acquired in advance is important for the guidance of walking? For example, is it important to learn the global shape of the room or just the area surrounding the target? Is it necessary to have the detailed knowledge or an abstract of the room structure would be sufficient? To answer these questions, one could manipulate the amount of information that the participants could get before the experiment. For instance, one could occlude the parts of the room that contain critical geometrical information (e.g., corner) during the preparation, so that the participants would not be able to learn all the information about the geometry of the room. Alternatively, instead of leading the participants into the lab before the experiment, one could show them a stereoscopic video, a normal 2-D video, photographs (taken from various viewpoints or from a single direction) or an abstract ground plane of the test room before the experiment. Then the straightness of walking trajectories could be evaluated as a function of the richness of details in the participants' knowledge.

It should be noted that the participants in the Familiar group had some physical interaction with the test room prior to the experiment. They entered the lab, walked to the rest area, and saw the room during the process. Therefore, it gives rise the question whether it is necessary to actively experience the environment. To test this, one could have participants sitting in a wheelchair and push them into the test room. Any difference in their walking trajectories compared to those who have actively walked in the room would show the contribution of active interaction in the formation of a mental representation.

5.5.2 Building a mental representation on-the-fly?

In these Strobe and Lit conditions, the participants in the Unfamiliar group could see the room after the experiment started. Did they develop a mental representation whilst

walking? If so, how quick could the process be? These questions are particularly interesting for situations like the Strobe condition where the participants only could see discrete snapshots of the room. However, our results are unable to answer these questions.

In the next chapter, we probe a related question: whether a mental representation of the configuration of a landmark array could be formed while walking and contribute to the guidance of walking.

6 Development of a mental representation of landmark configuration during walking

The results from Chapter 5 are consistent with people using previously formed mental representations of the environment to guide walking to a visible target, especially when the amount of immediately available visual information is limited. The test environment in Chapter 5 was a medium-size square room so there were numerous cues, including geometric cues and landmarks, which could be used to form the mental representation of the environment.

While Chapter 3 focused on geometric cues in navigating to a seen target, an earlier study has shown particularly interesting results suggesting that prior experience of a scene containing landmarks can also contribute to the control of locomotion (Andersen & Enriquez, 2006). In this study, participants were asked to control a simulated forward movement through an array of landmarks. The simulated movement was perturbed by a forcing function and the participants' task was to maintain a straight path of the movement. The layout of landmarks was either the same in every trial or changed between. Participants were found to be more sensitive to the perturbation and more accurate in controlling the path when the layout of landmarks remained constant. The authors argue that repeated exposure to the landmarks enabled participants to form an "allocentric" mental representation, which aided their performance on the task. This conclusion overlaps with our own. We decided to investigate whether their finding would replicate with an active walking task.

For this experiment, based on the description provided by Anderson and Enriquez (2006), we created a virtual world populated with post "landmarks". Instead of steering a simulated movement under lateral perturbation, our participants walked through the landmarks towards a target while wearing prism glasses.

Similar to Andersen et al.'s study, in the *Changed* condition, the post landmarks were randomly repositioned each trial. As in previous experiments, our participants walked back and forth throughout the experiment. This setup enabled us to include two different conditions in which the landmark layout remained the same. The first "same" condition was that the position of the posts always appeared the same relative to the participants' viewpoint, called the *Egocentrically-Same* condition. Because the walking direction alternated between trials, setting up this condition required the whole virtual environment to be flipped around after each trial (for schematic illustration see the middle row of **Figure 6.1**). The second

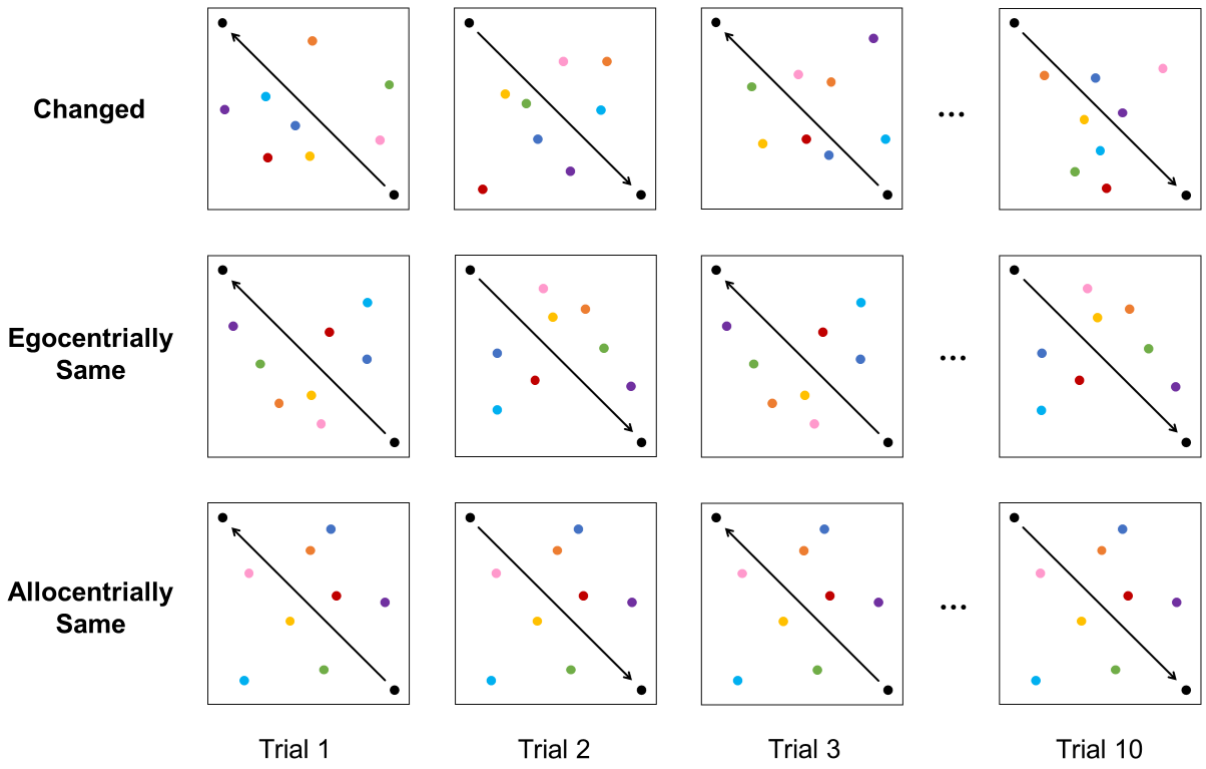

Figure 6.1. *Diagram of the arrangement of landmarks (not drawn to scale) for the three layout conditions. The top row shows the 'Changed' condition, in which the layout of the posts was randomly changed every trial. The middle row shows the 'Egocentrically-Same" condition, in which the layout of the posts remained the same for all the trials in the block irrelative to the participants' walking direction. The bottom row shows the 'Allocentrically-Same' condition, in which the layout of the posts was flipped around every trial so that the layout appeared the same to the participants regardless of their walking direction. Colour dots indicate the positions of the coloured posts. Black dots correspond to the starting point and target position. Black arrow indicates the walking direction.*

"same" condition, the layout of the landmarks remained the same with respect to the physical world and independent of the participants' viewpoint, called the *Allocentrically-Same* condition (see the bottom row of **Figure 6.1**).

In addition to the two "same" conditions, there are another two important modifications that we made to our stimuli based on Andersen et al.'s study (2006). First, in Andersen et al.'s study the landmarks were identical vertical bars, but in our experiment, the landmarks were identifiable posts that were individuated by colour. The motivation was to make the layout easier to recognise, especially when participants viewed the layout from different viewpoints in the Allocentrically-Same condition. The second modification was that, instead of a ground plane defined by randomly distributed dots, we used a ground with a

solid surface. This was to make the virtual environment appear more natural and to create a stronger sense of immersion.

If a mental representation of the layout was developed while walking and at the same time used in the guidance of walking, we would expect the averaged trajectories to be straighter and straighten more rapidly over the trials in the two "same" conditions – Egocentrically-Same and Allocentrically-Same. Any difference in the straightness of walking trajectories between the Egocentrically-Same and Allocentrically-Same conditions would inform about the nature of the mental representation. If the mental representation was in an egocentric frame of reference, then one would expect the trajectories to be straighter in the Egocentrically-Same condition. If the mental representation was in an allocentric frame of reference, as suggested by Andersen et al. (2006), then one would expect the trajectories to be straighter in the Allocentrically-Same condition (partly because the flipping of the environment would impair the performance in the Egocentrically-Same condition). If the egocentric and allocentric mental representations exist in parallel, the trajectory straightness and rate of straightening should be similar between the Egocentrically-Same and Allocentrically-Same conditions.

6.1 Method

6.1.1 Participants

A counterbalanced sample of participants was obtained (n = 24, mean age = 20.08, SD = 2.99, range: 18 ~ 31; 2 males) after necessary exclusions. In order to obtain these numbers, it was necessary to recruit thirty-one participants. Data from seven participants were removed from further analysis due to technical faults (e.g., large amount of signal drop-outs or computer crash). All participants reported having normal vision or corrected-to-normal vision only by wearing contact lenses. None reported impairment of colour or stereo vision or hearing. Prior to the experiment, the participants provided informed written consent in accordance with the requirements of the School of Psychology research ethics committee. All participants were naïve to the actual purposes of the study.

6.1.2 Stimuli

We used a similar design as in previous experiments. The test blocks with virtual prism were interleaved with the baseline blocks without the virtual prism. In the baseline blocks, the environment was the same as that used in the previous experiments: a ground

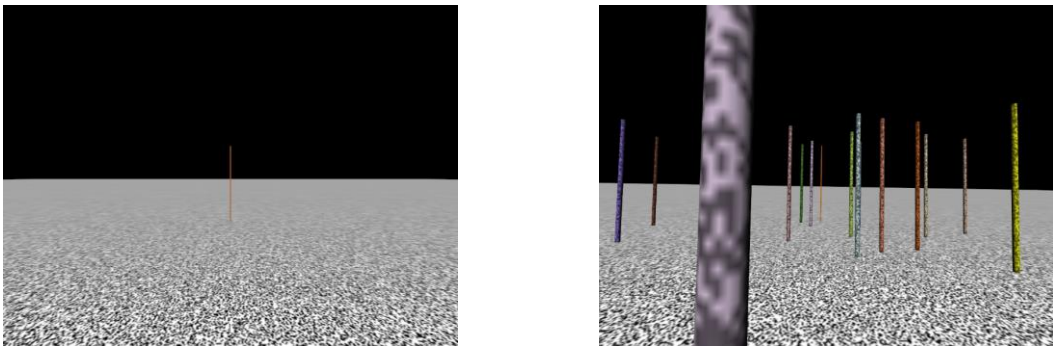

(a) **(b)**

Figure 6.2. *Sample views of the virtual environments at the starting point:* ***(a)*** *the baseline environment, and* ***(b)*** *the test environment with an array of coloured posts added to the baseline environment.*

plane painted with random-noise pattern and a line target (height = 3m and radius = 2cm) was placed at 8.5m from the starting point.

The test environment was generated by supplementing the baseline environment. An array of 20 posts (height = 3m and radius = 5cm) were randomly distributed on the ground plane within a range of 12m × 12m. There were at least 10 posts in the field of view of the observer standing at the starting point. All posts were painted a random-noise pattern. Each post was identifiable by its colour (for an example view of the test environment see **Figure 6.2**). In order to prevent any post from occluding the target at the outset of the trial when the participants stood at the starting point, no post was placed on the line between the starting point and the target. However, there was no visible "corridor" formed by the posts.

6.1.3 Design

The experiment consisted of three conditions. For all conditions, the posts were randomly distributed in Trial 1. In the Changed condition, the layout of the posts was changed every trial by repositioning the posts. In the Allocentrically-Same condition, the position of the posts was fixed with respect to the physical test room and layout of the posts remained the constant (as specified in Trial 1). Participants walked back and forth through the posts. To illustrate, consider **Figure 6.1**, in Trial 1 the participant would see the purple post on the right and the green post on the left. In Trial 2, the walking direction reversed and the participant would see the purple post on the left and the green post on the right. In this condition, the layout of the virtual scene remained constant relative to the physical world.

In the Egocentrically-Same condition, the position of the posts always appeared the same to the participants. In other words, the participants always walked in the same direction throughout the posts regardless of their walking direction in the physical room. Again, see **Figure 6.1**, in Trial 1 the pink post was on the left of the observer and the blue one on the right. In Trial 2, the observer turned around and walked in the opposition direction (in the physical room), the pink post still appeared on the left and the blue on the right. Therefore, in this condition, the virtual scene rotated 180 degrees with respect to the physical world between each trial.

Each participant completed 7 blocks. The even-numbered blocks (i.e., Block 2, 4 and 6) were test blocks in which the participants experienced the three conditions (i.e., "Changed", "Egocentrically Same" and "Allocentrically Same"). Each test block contained 10 trials. In the test blocks, the visual direction was displaced to the right (10°) or left (-10°) from the physical direction. The orders of the displacement direction and conditions were counterbalanced across participants.

The odd-numbered blocks (i.e., Block 1, 3, 5 and 7) were baseline blocks in which the baseline environment was displayed and the offset between the visual and physical direction was removed. In the baseline blocks, there were 6 trials. The first baseline block was used as a practice so that the participants could familiarise themselves with walking in a virtual environment and the experimental procedure. All participants reported being ready for the actual experiment after the first block. The other baseline blocks were used for examining and removing any aftereffects due to adaptation to the displacement in the preceding test block.

Like previous experiments, the same secondary task was used to discourage the participants from paying undue attention to their walking behaviour. The participants were asked to attend to the target and press the button on a remote control every time the target turned to a specified colour, e.g. red. Participants were told that this colour responding task was their primary task in this study. In the debriefing session at the end of the experiment, none of the participants reported that they had been aware of the actual purpose of the study. Moreover, none of them indicated being aware of any discrepancy between the visual and actual walking directions.

As in earlier experiments, to help participants keep their walking speed constant across trials, a metronome (80 beats/minute) was played to them via earphones during each trial. The participants were told that walking in-time to the metronome was not important but walking at a constant speed across trial was essential. The rate of the metronome was

synchronised with the change of target colour so that every time the target changed its colour, participants would hear a beat of the metronome. This was to avoid any confusion resulting from the conflict between the metronome tempo and frequency of colour changing.

6.1.4 Procedure

The procedure was identical to the previous experiments. Participants were told not to adjust their walking direction if they were going to collide with any post, and were encouraged to walk through the post if it was on their way. The posts were virtual and did not exist in the physical room.

6.2 Results

6.2.1 Straightness of mean walking trajectories

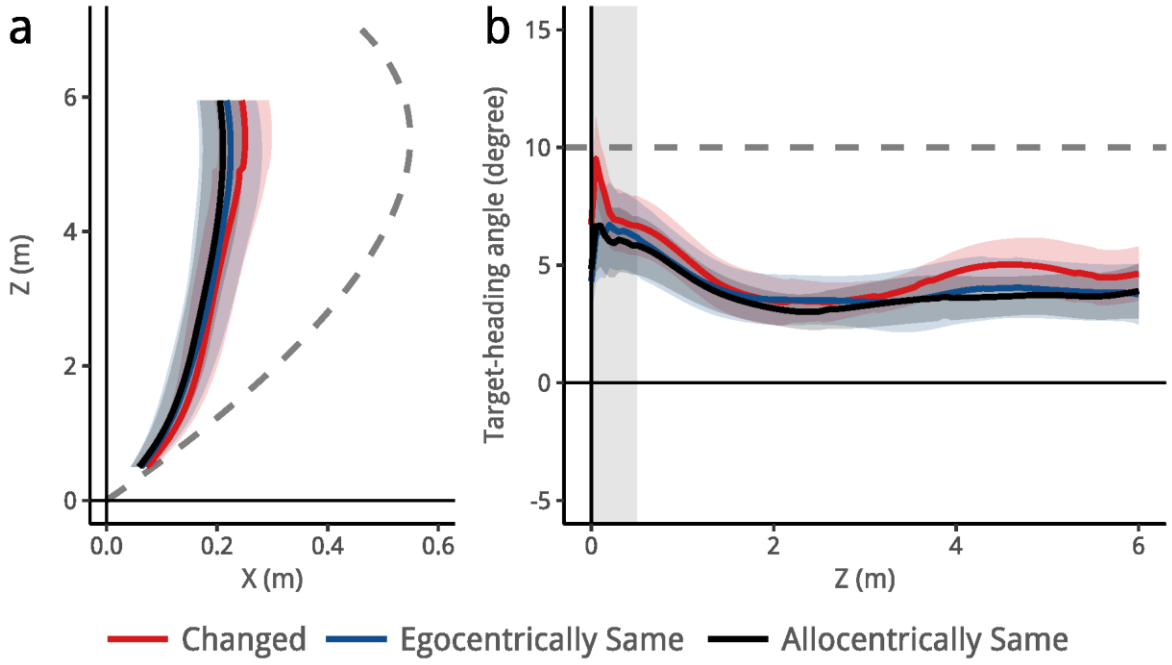

Figure 6.3. (a) *Mean trajectory averaged over the nine test trials (Trial 2 ~ 10) for each condition across 24 participants. Dashed line shows the trajectory that should result if only egocentric direction is used. Shaded areas indicate 95% confidence interval.* ***(b)*** *Mean target-heading angle as a function of distance averaged across the nine test trials (Trial 2 ~ 10) and 24 participants. Dashed line at 10° indicates the angular displacement between the visual and physical orientations. Solid line at 0° corresponds to a straight trajectory. Grey shaded area at 0m ~ 0.5m indicates the data that has been excluded from the final analysis. Shaded areas around the target-heading angle data indicate 95% confidence interval.*

The mean trajectories are plotted in **Figure 6.3a**. They were averaged over Trial 2 ~ 10 and the twenty-four participants. Note that we did not examine the trajectories in Trial 1 as in previous experiments. The reason was that the environment in Trial 1 was always novel to participants and the effect of layout manipulation would be maximally detectable on the mean trajectories over the subsequent trials. Therefore,we excluded the trajectories of Trial 1 to increase the sensitivity of our analysis.

The mean trajectory in the Changed condition is the most curved, where the overall mean target-heading angle is 4.46° (SD = 2.04°). The mean trajectory in the Egocentrically-Same condition is slightly straighter, where the overall mean target-heading angle is 3.98° (SD = 2.28°). The mean trajectory in the Allocentrically-Same condition is the straightest and has an overall mean target-heading angle of 3.77° (SD = 1.50°). However, the difference between the conditions is small and did not reach statistical significance [$F_{2, 46} = 0.83$, $p = 0.44$, $\eta^2 = 0.022$].

As shown in **Figure 6.3b**, the pattern of mean target-heading angle as a function of distance is similar between conditions: the mean target-heading angle decreased rapidly in the early part of the trajectory and then plateaued. Growth modelling did not reveal a significant difference in the rate of change against the distance between conditions [$\chi^2(2) = 1.06$, $p = 0.59$] (see Supplementary Material 8.5.1 for details). Furthermore, our bespoke time-series analysis did not find any significant cluster on the difference between conditions. Taken together, the statistics support the observation that the manipulation of the landmark configuration does not influence the pattern of straightening of trajectories within a trial.

6.2.2 Mean target-heading angles as a function of trial

The potentially more important results are the rate of change over the test trials. **Figure 6.4** plots the mean target-heading angle of the early (0.5m ~ 1m) and later (5.5m ~ 6m) parts as a function of trial for each condition. Clear areas show the mean target-heading angles of the test trials (Trial 1 ~ 10) where a "virtual prism" was implemented. As shown in the clear areas, the pattern of both early and later parts as a function of trial looks very similar between conditions. The mean target-heading angle of the later part was significantly smaller than that of the early part [$\chi^2(1) = 32.02$, $p < 0.0001$], and decreased significantly slower than that of the early part [$\chi^2(1) = 10.85$, $p < 0.01$] (for more details about the analysis see Supplementary Material 8.5.2). Overall, the mean target-heading angle of the early part significantly decreased over the trials [estimated slope = -0.18, t =-4.22, $p < 0.0001$]. No effect of landmark configuration was found on the rate of change against trial [$\chi^2(2) = 2.65$, p

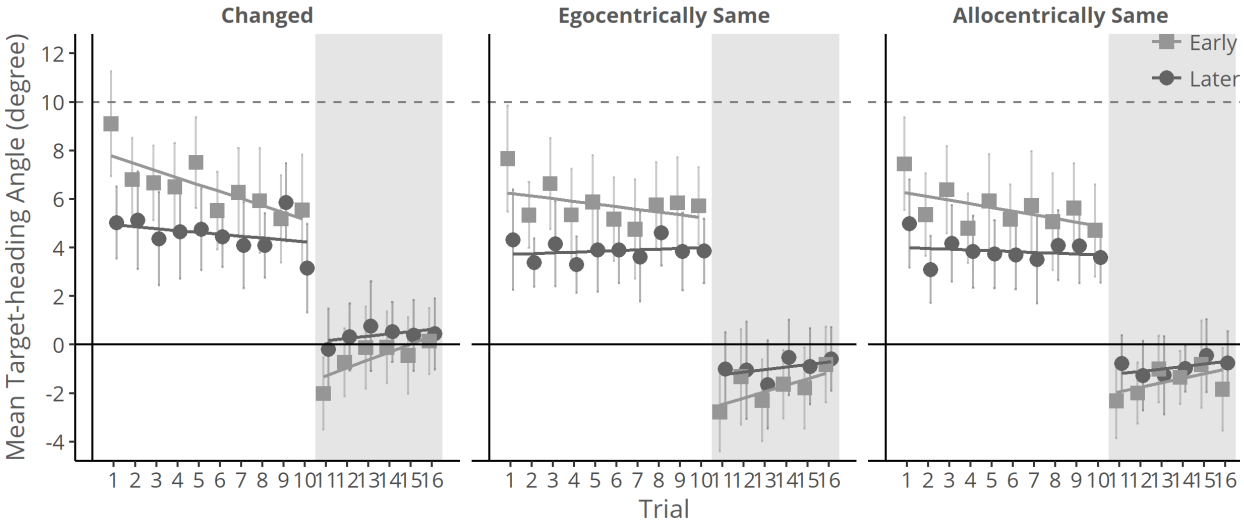

Figure 6.4. *Mean target-heading angle as a function of trial respectively for the early part (0.5m ~ 1m) and later part (5.5m ~ 6m) and for each condition (Changed, Egocentrically-Same and Allocentrically-Same). Clear areas correspond to the test trials (Trial 1 ~ 10) with "virtual prism". Shaded areas correspond to the baseline trials (Trial 11 ~ 16) without "virtual prisms". Dashed line at 10° indicates the degree of deflection of the "virtual prism". Error bars indicate 95% confidence interval. The central panel, left-hand panel, and right-hand panel.*

= 0.27], or was there any effect of interaction between landmark configuration and part on the magnitude of mean target-heading angle [$\chi^2(2) = 0.05$, $p = 0.98$] or rate of change [$\chi^2(2) = 0.73$, $p = 0.69$].

Each test block was immediately followed by a baseline block in which the displacement was removed. The shaded areas in **Figure 6.4** illustrate the mean target-heading angles of the early part (0.5m ~ 1m) and later part (5.5m ~ 6m) against trial for each condition in these baseline blocks (Trial 11 ~ 16). A negative target-heading angle indicates that the trajectory curves to the opposite of the direction of the virtual prism. Here in the first trial of the baseline blocks (Trial 11), the mean target-heading angles of the early parts in three conditions were respectively -2.02° [SD = 3.45°] in the Changed condition, -2.77° [SD = 3.86°] in the Egocentrically-Same condition and -2.32° [SD = 3.65°] in the Allocentrically-Same condition. The mean target-heading angles were all significantly smaller than 0° [all one-tailed *p*s < 0.01], indicating the occurrence of aftereffects in all conditions. There was, however, no statistical difference in the magnitude of aftereffects between the three conditions [$F_{2, 44} = 0.087$, $p = 0.92$, $\eta^2 = 0.004$]. These results are consistent with the results above that the decrease in the mean target-heading angle of the early part was comparable between conditions.

The mean target-heading angles of the early part increased significantly to be closer to 0° in all conditions, indicating an abolishment of the aftereffects over the baseline trials. In Trial 16, the mean target-heading angle of the early part was not statistically different from 0° [both *p*s > 0.1] except in the Allocentrically-Same condition [mean = -1.84°, t(22) = -2.25, *p* = 0.035]. These results suggest that some residual aftereffects left after the baseline block after the Allocentrically-Same condition. Because we had a fully counterbalanced design, the impact of the residual aftereffects increased the target-heading angle data in the Changed and Egocentrically-Same conditions by approximately 1/3° and does not change the pattern of results.

6.2.3 Walking speed and its relationship with the straightness of trajectories

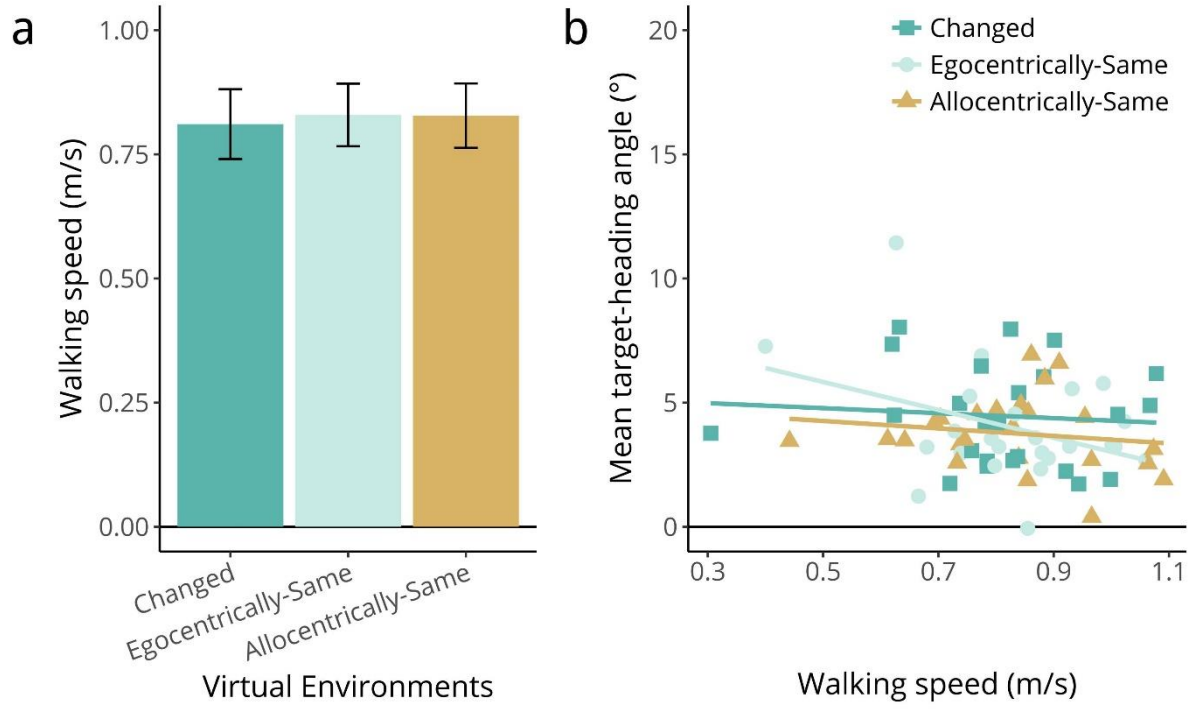

Figure 6.5. (a) *Mean walking speed averaged over nine trials (Trial 2 ~ Trial 10) for each condition (Changed, Egocentrically-Same and Allocentrically-Same) across 24 participants. Error bars correspond to 95% confidence interval.* ***(b)*** *Relationship between walking speed and the magnitude of target-heading angle for each condition.*

The mean walking speeds averaged over the nine trials from Trial 2 to Trial 10 are plotted in **Figure 6.5a**. As shown in the figure, there was no significant difference between the conditions [$F_{2, 46} = 2.17$, $p = 0.13$, $\eta^2 < 0.01$]. A JZS Bayes factor ANOVA with default prior scales provided weak evidence for the null hypothesis that there was no difference in walking

speed between the three conditions [B_{01} = 1.70] (Jeffreys, 1961; Love et al., 2015; Morey & Rouder, 2015; Rouder et al., 2012).

Figure 6.5b plots the relationship between the magnitude of target-heading angle and walking speed. In both Changed and Allocentrically-Same conditions, the correlation between target-heading angle and walking speed was weak and not significant [Changed: Pearson's r = -0.082; Allocentrically-Same: Pearson's r = -0.15; both ps > 0.1]. In the Egocentrically-Same condition, however, there was a moderate but not significant negative correlation between target-heading angle and walking speed [Pearson's r = -0.37, t(22) = -1.85, p = 0.078].

6.3 Discussion

Andersen et al.'s (2006) findings suggest that an allocentric representation of the scene is used for control of locomotion. In this chapter, we sought to replicate their results in active walking. We hypothesised that (1) the walking trajectories should be more curved and (2) the rate of straightening should be slower when the layout of landmarks was changed than when the layout remained the same. Following on from this, if the mental representation is egocentric, then we should observe the straightest trajectories and most rapid straightening rate in the Egocentrically-Same condition. If the mental representation is allocentric, the straightest trajectories and fastest straightening rate are expected in the Allocentrically-Same condition. A co-existence of both representations predicts similar straightness and straightening rate in these two "same" conditions.

Against our hypotheses, however, manipulating the layout of the landmarks did not have any detectable effect on the walking trajectories or the rate of straightening. The walking trajectories were similar regardless of whether the layout was changed or not. In all conditions, the trajectories straightened up significantly over the test trials at similar rates.

The results are inconsistent with Andersen et al.'s (2006). There are several methodological differences that could explain the discrepancy in the results. First, the landmarks were identical in their study whereas identifiable in our study. We used the identifiable landmarks so that when participants walked back and forth they knew that they were walking in the same environment (in the Allocentrically-Same condition). We also thought that making them identifiable could facilitate the development of a mental representation of the layout. However, the opposite could also be true. Without identifiable landmarks, the viewer may tend to rely on the overall layout rather than noticing individual landmarks. Therefore, participants in Andersen et al.'s study might more likely to form a

mental representation of the landmark layout, whereas our participants might less likely to do so for being more reliant on individual landmarks.

Second, there is an important methodological difference between our study and Andersen et al.'s study concerning the type of perturbation that was introduced in the experiment. In Andersen et al.'s study, simulated forward movement was perturbed by a lateral force. In the present study, however, the participants' visual direction was displaced from their physical direction by the virtual prism, resulting in a conflict between visual information and information from other non-visual senses. To build an allocentric map of the environment, it is required to integrate information from multiple sensory modalities (Hafting et al., 2005; Jacobs et al., 2013; O'Keefe & Nadel, 1978; O'Mara, 2017; Yoder & Taube, 2014). Therefore, the conflicting information between sensory inputs that was induced by the virtual prism might have inhibited the development of an allocentric representation in our participants. In order to allow participants to form an allocentric representation, it would be more appropriate to set up a learning session in which participants walked through the landmarks without a virtual prism. After the learning session, the virtual prism could be added while participants continue to walk in the same environment. The trajectories after the learning session may reveal a similar effect of mental representations as Andersen et al. (2006) did.

Third, our participants might be using a view-based strategy when walking towards the target. Studies have demonstrated that bees or ants return to a feeding site by matching the retinal image as closely as possible to the image they had learned previously (Cartwright & Collett, 1983; Graham & Collett, 2002; Lent, Graham, & Collett, 2010; Wehner & Räber, 1979). It has also been suggested that humans navigate on the basis of an internal representation that links actions with their sensory consequences; for example, snapshots of the target and surrounding scene (Franz, Schölkopf, Mallot, & Bülthoff, 1998; Gillner & Mallot, 1998; Mallot & Gillner, 2000). Based on this idea, Glennerster and colleagues proposed a view-based model for human navigation (Gootjes-Dreesbach, Pickup, Fitzgibbon, & Glennerster, 2017; Pickup, Fitzgibbon, Gilson, & Glennerster, 2011). According to this model, our participants might have remembered a series of snapshots of view along with their way to the target in Trial 1. In the subsequent trials, they tried to walk to simply match their retinal image with the remembered snapshots. If this hypothesis is true, then it would predict the trajectories to be the most curved in the Egocentrically-Same condition, because the participants would try to replicate the sequence of images that they learned on Trial 1. By contrast, the trajectories would be the straightest in the Changed condition, because the

changing layout would prevent the participants to use the strategy based on the sequence of the image that they previously saw. However, as shown in **Figure 6.4**, this is not what we observed in our data.

6.4 Summary

In this chapter, we were unable to replicate Andersen et al.'s study (2006). It should be noted that there are several methodological differences that could be responsible. First, the landmarks in our experiment were posts that could be identified by colour. This might make the participants tend to be more reliant on individual landmarks rather than on the overall layout of the landmarks. Second, the displacement between the visual and physical directions imposed by the virtual prism might impede the integration of information from a range of senses which in turn inhibited the development of a mental representation. Last, our participants might be using a view-based strategy to guide themselves to the target. Using such a strategy would result in replicating the curved trajectory in Trial 1. Although we did not find evidence for the development and utilisation of a mental representation while walking, our results can be regarded as informative for future research.

7 General discussion

7.1 Summary

To date, research has focused on the roles of optic flow and/or egocentric direction in visually-guided walking. The aim of this thesis was to examine the possible role of allocentric location cues when walking to a seen target. We manipulated the availability of allocentric location cues and evaluated the impact on walking. To achieve this aim we employed a standard paradigm. An offset was introduced (by prisms or VR) between seen direction and movement direction so that if you executed a movement towards the seen direction of an object you would actually move on a path slightly offset from the direction of the object. The shape of walking trajectories under the offset provides a measure to access the relative contribution of cues. In order to assess the time course of cue use, time series analyses including growth modelling and an in-house cluster-based permutation test were used. The details about the methodology and analyses were provided in Chapter 2.

We began by questioning two important assumptions of the optic flow theory that (1) richness of optic flow and (2) heading judgements can predict walking trajectories (Chapter 3). In the first experiment (Experiment 3.1), we systematically varied the amount of allocentric location information and optic flow in four virtual environments. The straightness of walking trajectories in the environment would follow different orders as predicted by the two hypotheses. It turns out that the allocentric location hypothesis captures the pattern of trajectories better than the optic flow hypothesis. The trajectories in the condition with the richest optic flow were similar to those in the condition with minimal optic flow but a large amount of allocentric location cues.

In the second experiment (Experiment 3.2), we examined the performance on a heading judgement task in the same environments and then compared it to the walking trajectories obtained in the first experiment. The pattern of heading judgements was better captured by the optic flow hypothesis, but only at a further distance from the target. When closer to the target, the performance of heading judgements became similar between conditions. Overall, the pattern of heading judgements is unable to predict the pattern of the walking trajectories that we observed in the same environments.

In Chapter 4, we assessed the influence of target location on the walking trajectories. In Experiment 4.1, we manipulated the target location within a virtual room so that the salience of perspective symmetry cues varied. We did not find any indication of the effect from the trajectories in the first trial. In Experiment 4.2, we placed the target either near or far

from the starting point. The target drift and motion parallax were more salient when it was near than when it was far. The trajectories straightened faster within a trial when the target was near. This would be expected as the relative salience of target drift and motion parallax would be inversely proportional to the distance from the target.

In Chapter 5, we took a further step by probing the use of prior experience with the environment. We manipulated the familiarity the observers had with the environment by preparing them inside the test room or outside the room. For the observers who were prepared inside the room, knowledge about the room could be acquired in advance; whereas for those who were prepared outside the room, they did not have any prior experience with the room. With the amount of external visual cues held constant, the difference between the two groups could be attributed to whether they had seen the environment or not.

In the first experiment (Experiment 5.1), we uncovered a role for prior experience in the guidance of walking. Walking in darkness towards a self-illuminated target, trajectories of the Familiar group were markedly straighter than those of the Unfamiliar group. In the second experiment (Experiment 5.2), we investigated how prior experience and visual cues combine. We manipulated the amount of visual cues by illuminating the same test room either by strobes of by normal fluorescent lights. It turned out that the combination of prior experience and visual cues is non-linear.

To explore the interaction between prior experience and visual cues, in the subsequent two experiments, we reduced the richness of visual cues respectively by removing target drift in the dark and strobe-illuminated room (Experiment 5.3) and removing peripheral cues in the fully lit room (Experiment 5.4). In Experiment 5.3, we showed that, after removal of target drift, the trajectories became significantly more curved and an effect of familiarity emerged in the strobe-illuminated room. In Experiment 5.4, however, we did not observe any effect of restricting FoV on the walking trajectories or the familiarity effect.

Taking the results from Chapter 5 together, we provided evidence for the role of prior knowledge in the visual guidance of walking. Leading on from these findings, we attempted to replicate an earlier study by Andersen et al. (2006) to further probe the question of whether an allocentric representation could be formed across trials based on the configuration of an array of landmarks. The layout of the landmarks was set up in three arrangements: randomly changed from trial to trial, constant with respect to the observer's view (egocentrically) and constant with respect to the physical world (allocentrically). Based on the findings by Andersen et al. (2006), we predicted that the trajectories should be straighter in the two constant conditions and the straightest in the allocentric one. However, we were unable to

replicate Andersen et al.'s (2006) results in active walking. The most likely origin of the discrepancy may be the perturbation paradigm that we used in the walking experiment. It is possible that the offset between the visual and physical movement directions impeded the development of a mental representation.

In summary, the most important finding that emerged from this thesis is that we have identified an important role of a new type of cues – *allocentric location cues* – in the visual guidance of walking. Furthermore, previously required knowledge about the environment can be used in the guidance of walking when it is needed.

7.2 Implications

Our results provide several important implications for researchers who work on optic flow and are interested in the visually guided walking as well as researchers who work in the field of spatial learning and navigation.

As pointed out at the beginning of the thesis, a large body of work on visually guided walking has rested on two assumptions: (1) that the richness of optic flow predicts walking trajectories; and (2) that heading judgements tap the same processes as the online control of walking (and the latter could be inferred from the performance on the former). Our results challenged both assumptions. It is, therefore, necessary to reconsider these assumptions.

Our results pointed to a previously unrecognised role of allocentric location cues in the visual guidance of walking. As stressed throughout the thesis, the human walking literature has focused on optic flow and egocentric direction. So far, very few studies have considered other visual cues in the online control of walking towards a visible target (see Herlihey 2010).

Further, we uncovered a role for prior knowledge of the environment in the guidance of walking. This finding goes considerably beyond the earlier work on "blind walking" (Thomson, 1980, 1983) that showed an observer is able to walk open-loop to an object in the previously seen environment. Our finding suggests that, like animals, humans might develop some forms of internal representation of the spatial structure of the environment, which may inspire a new line of research in the field of visually guided walking.

7.2.1 Cue combination in the guidance of walking

The extensive literature on perceptual cue combination has demonstrated that humans are capable of integrating information from multiple sources of cues to estimate environmental properties in a statistically optimal fashion, namely the maximum-likelihood

(MLE) rule. According to the MLE rule, the final estimate of the property is the weighted average of estimates from each individual cue (Ernst & Banks, 2002; Hillis, Ernst, Banks, & Landy, 2002; Landy, Maloney, Johnston, & Young, 1995). More recently, cue integration consistent with the MLE rule has also been suggested in the domain of spatial navigation (e.g., Chen, McNamara, Kelly, & Wolbers, 2017) and reorientation (e.g., Xu, Regier, & Newcombe, 2017).

How does the brain assign weight to each individual cue? It has been suggested that the weight of the individual estimates is determined by variance as well as the discrepancy between them (Ernst & Banks, 2002; Landy et al., 1995). When the discrepancy between cues is small, the weight of the estimate is inversely proportional to its variance. In other words, the less noisy and more reliable the stimulus is, the more contribution it makes to the final estimate. When the discrepancy is large, however, the brain may discount the discrepant cues and rely on other stronger cues (Landy et al. 1995). Hillis and colleagues (2002) found that when the cues were from the same modality, e.g. vision, information from single cues was lost and the observer relies on the combination of the cues, whereas when the cues were from different modalities, single-cue information was used in case of large discrepancies between cues.

For the guidance of walking, there are several visual cues that an observer could use, e.g., egocentric direction, optic flow and allocentric location cues. As these cues are subject to noise, it would be beneficial for an observer to use multiple cues in combination in guiding their walking, and in cases of large discrepancies, to discount cues.

Warren et al. (2001) have proposed a simple model that combines the egocentric direction and optic flow cues in a linear way (see the beginning of Chapter 3). According to this model, the egocentric direction of the target is used when the environment is visually impoverished and optic flow becomes increasingly important as the visual richness of the environment increases. In this thesis, the evidence is provided for the role of allocentric location cues and mental representations in the guidance of walking. Therefore, the contribution of these cues should be taken into consideration. Moreover, the straightness of trajectories varied as a function of walking distance. For example, in the *Line* condition of Experiment 3.1, the trajectory straightened up when the observer got closer to the target. As the target drift cue becomes more salient as the distance from the target decreases, the straightening suggests that target drift might come into play at a later point of the trial. Therefore, the weighting of cues in the guidance of walking may be a dynamic process (Landy et al., 1995).

One thing should be noted is that prisms (or 'virtual prisms') were used in this thesis. The use of prisms introduced a discrepancy between egocentric direction and other cues (i.e., optic flow and allocentric location cues). This is what we need in order to distinguish the contribution of optic flow and allocentric location cues. However, the use of prisms may also bring some confounds according to cue combination models. For example, the brain could discount egocentric direction and rely on other cues, or probably the other way around. If so, one would expect either very much straight trajectories or fully curved trajectories in the conditions with optic flow and allocentric location cues. However, the trajectories had an intermediate curvature, suggesting that the cues were combined in our experiments.

In addition to visual cues, body-based cues such as proprioceptive and vestibular cues could also provide important information for the guidance. Again, wearing prisms displaces the visual direction from the physical movement direction. Therefore, there was also a discrepancy between the shifted visual cues (i.e., egocentric direction cues) and the body-based cues. According to Ernst and Banks (2002), when visual stimuli are noisy, cues from other sensory modalities may become dominant. Would this be the case in those visually impoverished conditions (e.g., the *Line* condition in Chapter 3 and the *Dark* conditions in Chapter 5) that the participants relied on body-based cues rather than visual cues? If so, one would expect a straighter trajectory in these conditions; however, the observed trajectories were as curved as the sole use of egocentric direction predicts. The reason may be that, although the environment was poor in visual richness, the target was clearly visible. Therefore, as compared to body-based cues, the egocentric direction cues may have less variance and hence could be assigned more weight in combination.

7.3 Limitations

There are two caveats that should be noted. The first caveat is that we introduced a secondary task in all experiments. The main purpose of the task was to prevent the participants from paying undue attention to their walking and making an adjustment that they normally do not do. The secondary task also prompted the participants to fixate their gaze on the target throughout the trial. When fixating the target, the signals from eye muscles (and/or neck muscles) might have provided extraretinal information about the observer's walking direction. For example, when walking in a straight line to a target, it is expected that the eyes and head are facing straight forward. If deviating from the straight line, the eyes (and neck) would turn in order to keep the gaze on the target. The turning of eyes and neck would signal the drift in walking direction or the curvature in the walking path. The more curved the

walking path is, the stronger the signal will be. Therefore, such extraretinal signals may play a role in the guidance of walking, especially in cases where reliance on visual cues (i.e., egocentric direction) predicts a curved path, making the trajectory less curved than predicted by the use of visual cues only. As noted in the preceding section, the trajectories in those visually impoverished conditions were generally as curved as predicted by egocentric direction, we would expect the contribution of extraretinal signals from eye and neck to be small.

Another issue about fixating the target is that it would yield fewer eye movements. That is, the eye would focus on the area where the target stood in the scene and make less scanning of the environment. In real-world navigation, people rarely walk with their gaze fixating on their goal. Instead, they would look around (e.g., enjoying the view or searching for a place) or gaze at something that attracts their attention (e.g., an interesting storefront or someone dressed unusually). Thus, it is possible that people may be more reliant on spatial representation in natural walking than in our laboratory setting. For example, they could use other landmark objects to infer the location of their target or they could update their orientation relative to the target based on the structure of the scene. If there were more scanning in our experiments, the contribution of allocentric location cues might have been larger. To test this, it might be to use a task that does not artificially make the observer fixate the target, e.g., an auditory task while walking.

The second caveat concerns the standard perturbation paradigm that we use in all our walking experiments, which is to insert an offset between the seen direction and actual movement direction. As we have discussed in Chapter 6, the offset might result in conflicts between information from different sensory inputs. The conflicts might impede the integration of the information from multiple sensory modalities which is thought to be important for building a mental representation of the environment. One solution is to set up a learning phase where participants can experience the environment without offset. Then the offset could be added so that the relative use of cues could be assessed from the walking trajectories. However, it would be interesting to investigate the question of how exactly the offset would affect the representation development. The answers would shed light on how information from different senses integration to form a coherent representation of the external world.

7.4 Future directions

This thesis raised more questions than it could answer. Here we introduced the concept of allocentric location cues. This is a broad concept and encompasses all kinds of visual cues that can inform about the observer's current position and orientation with respect to the environment. We have provided some ideas about what these cues might be (e.g., perspective change in the shape of an object), but the question of what exactly these cues are and how they are used remains open.

Another related question is how these cues are combined (with each other and with other types of cues). As highlighted in the previous section, few studies have been done on cue combination in the guidance of walking. Within the visual domain, an earlier model included a linear combination of weighted cues (see Warren & Fajen, 2004). In this thesis, however, our results suggest that the relationships between cues might be more complicated and nonlinear. Between the visual cues and cues from other modalities (i.e., proprioceptive and vestibular signals), it remains an interesting question whether and how the use of prisms (or 'virtual prisms') would affect the combination between the cues. Therefore, future studies could develop new models that accommodate the use of allocentric location cues and complicated cue interactions within the visual domain as well as between vision and other senses.

The most interesting finding in this thesis is that prior experience can contribute to the online control of walking. What was learned? What information is necessary for the guidance of walking? How is the information used? It will be an exciting path to follow.

7.5 Overall conclusions

Allocentric location cues have an important role in the visual guidance of walking. Most importantly, when access to visual cues is limited, prior knowledge of the walking environment contributes to the online control of walking.

8 Supplementary Materials

8.1 Chapter 2 – Supplementary materials

8.1.1 The smoothing problem

For each trial, the frequency of the walking sway was specified by using Fourier transformation. Then this sway frequency is to be used in a filter so that the signal with a frequency higher than the sway (including the sway itself) will be filtered out from the data.

As shown in **Figure 8.1a**, an ideal filter (lowpass) would be a filter with a clear cut at the cut-off frequency. That is, for the signal with a frequency lower than the cut-off frequency, the amplitude response will be 1, which means that the signal is fully maintained in the data. In contrast, for the signal with a frequency higher than the cut-off frequency, the amplitude response will be 0, which means that the signal is fully removed from the data.

A filter that has been used in Warren et al. (2001) and other studies is the Butterworth filter. One of the biggest advantages of the Butterworth filter is its flat response. However, instead of having a clear cut as the ideal filter, the Butterworth filter has a relatively slow rolling off (**Figure 8.1a**). The passband corresponds to the signal that will be maintained and the stopband to the signal that will be removed. Between the passband and stopband is the transition. The narrower the transition width is, the closer the Butterworth filter to the ideal filter. The transition width can be set up via the order of the Butterworth filter. The higher the order is, the narrower the transition width. However, in Warren et al.'s study (2001), the authors used a

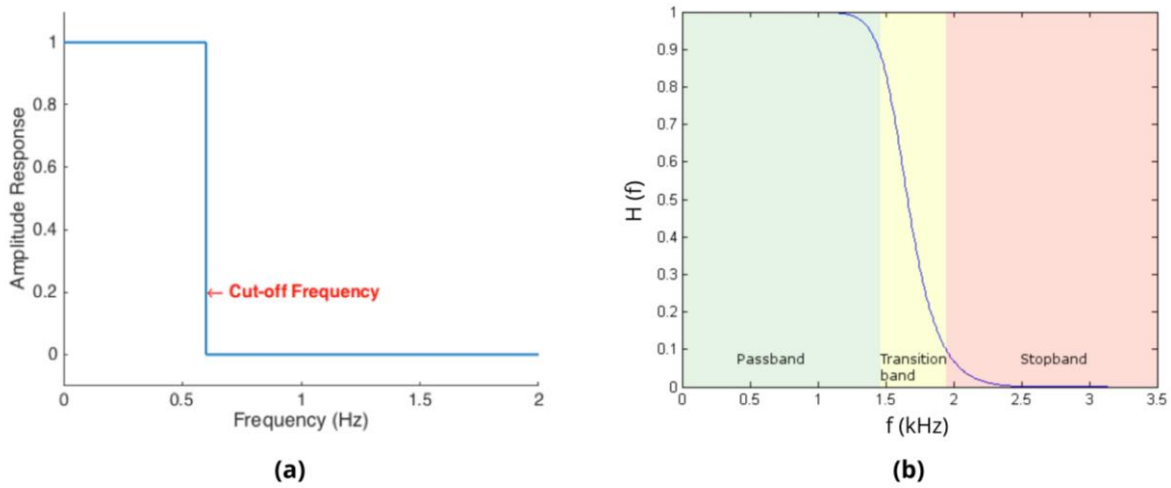

Figure 8.1. (a) *Illustration of an ideal filter.* ***(b)*** *Illustration of a Butterworth filter.*

Butterworth filter with an order of two, which yields a slow transition (see **Figure 8.2a**). This means that the signals at frequencies around the cut-off frequency were mostly maintained. It is unclear why they chose this particular number for the order of the Butterworth filter, as they didn't specify the reason in their paper.

Another important property of the Butterworth filter regards the cut-off frequency of normal walking. The cut-off frequency for Butterworth filter refers to the frequency where the amplitude response is $1/\sqrt{2} \approx 0.707$, or -3dB (see **Figure 8.2a**). As can be seen from **Figure 8.1a**, a large part of the signal at the cut-off frequency will be maintained. Therefore, if the sway frequency is used as the cut-off, there will still be much oscillation left in the data (as shown by the red lines in **Figure 8.3**). As a result, the target-heading angle data that is calculated from the filtered trajectory data will still contain a lot of oscillation.

Alternatively, a Butterworth filter can be generated for each individual trial. In this filter, the stopband is set to be the sway frequency so that at this frequency the signal will be greatly reduced (see **Figure 8.2b**). In this way, the oscillation caused by the walking sway could be mostly removed (see the yellow lines in **Figure 8.3**).

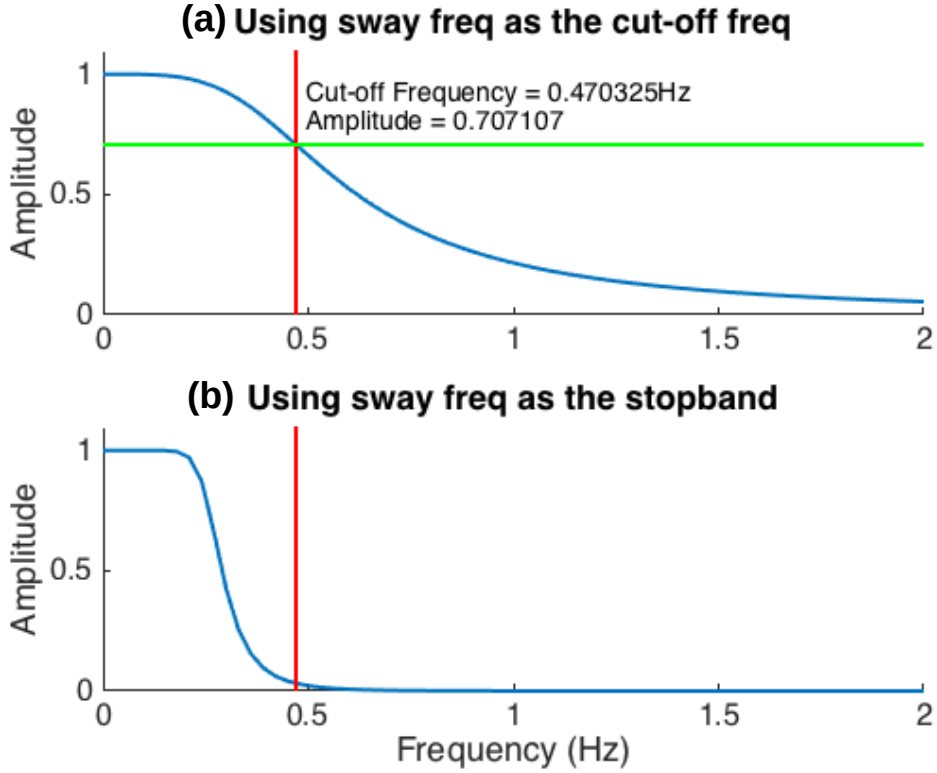

Figure 8.2 *Frequency response of Butterworth filters. (a): the response of using the sway frequency as the cut-off. (b): the response of using the sway frequency as the stopband*

However, to use this method, a value for the passband is also needed, which is the frequency from which the amplitude response starts to reduce (see **Figure 8.2**). Due to the nature of the Butterworth filter, there is no clear "cut-off", and there is a transition from the passband to the stopband. The closer the passband to the stopband, the quicker the response changes over the transition, but probably with some cost.

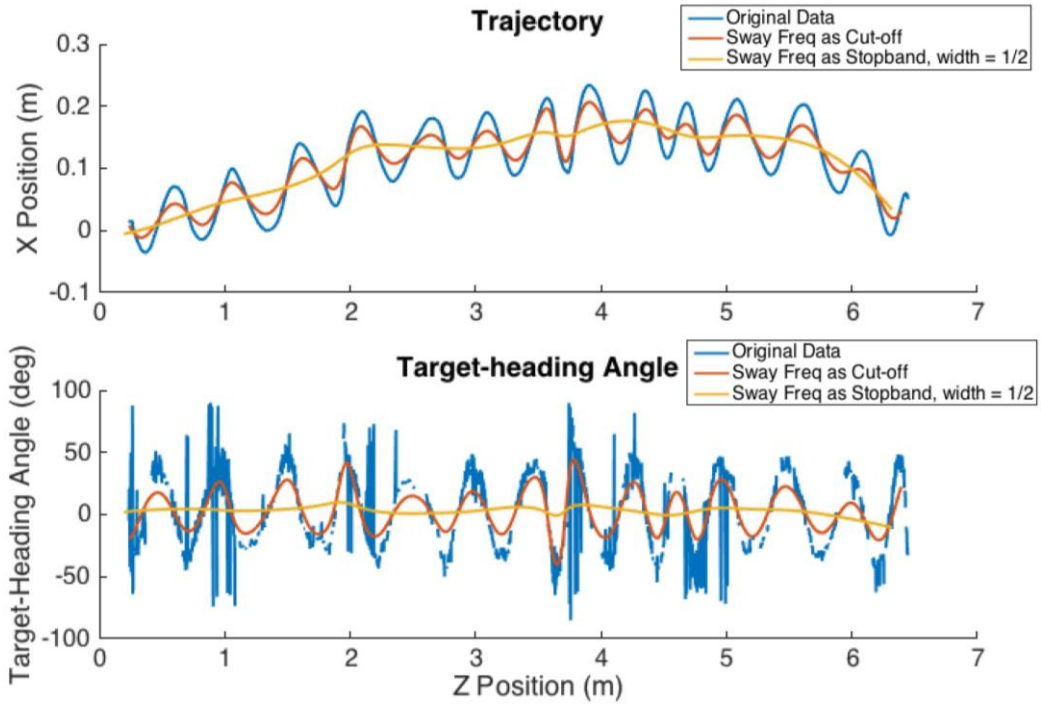

Figure 8.3 *Example data illustrating the effects of the Butterworth filters.*

8.1.2 Choosing the filter

Although the FIR filter has a benefit that the filtered data converge with the original data at two ends, the Butterworth filter was chosen instead of the FIR filter. The main reason is that the FIR filter contains some ripples that may distort the shape of the walking trajectory (see **Figure 8.4**). It can be seen from **Figure 8.4** that there are ripples before and after the transition band. Those ripples after the stopband are not problematic as the corresponding amplitude responses are small, around 0. It is the ripple that before the passband that is much more worrying. As will be discussed later in this section, the frequencies before the passband are related to the curvature of the trajectory itself. The amplitude response before the passband is larger than 1. This will magnify the signals at these frequencies and thus result in a more curved trajectory than the original one.

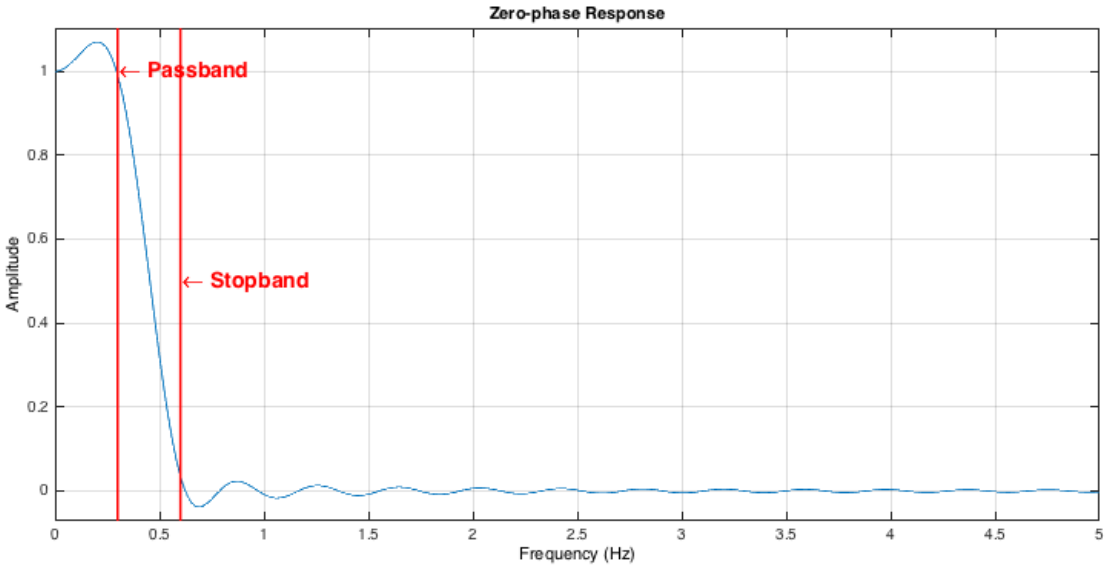

Figure 8.4 *An example of frequency response of FIR. Red lines indicate the passband and stopband respectively.*

The second reason to choose the Butterworth filter instead of the FIR filter is that when the transition band is narrower than a certain value – not a small value sometimes, the filter requires a sample data longer than the original data for calculation, which is difficult to fulfil.

8.1.3 The definition of the passband and stopband

When the filter is confirmed, the next thing to do is to define the passband and stopband. Before going to the details about how to find these two values, I'll first describe the frequency constitution of the data.

8.1.3.1 Frequencies in the data

Figure 8.5a gives an example of the frequency response of the data in a single trial. The larger the amplitude response (indicated by y-axis) is, the more important role that the corresponding frequency (indicated by x-axis) plays in the signal. From the figure, we can see that there are two frequencies that play an important role in the data. The first one is a very low frequency, close to zero, but the corresponding amplitude response is high (indicated by the green line in **Figure 8.5a**). This frequency is related to the curvature of the walking trajectory. This is of main interest to us and we want to keep it in the data. The second frequency is usually between 0.5Hz to 1Hz

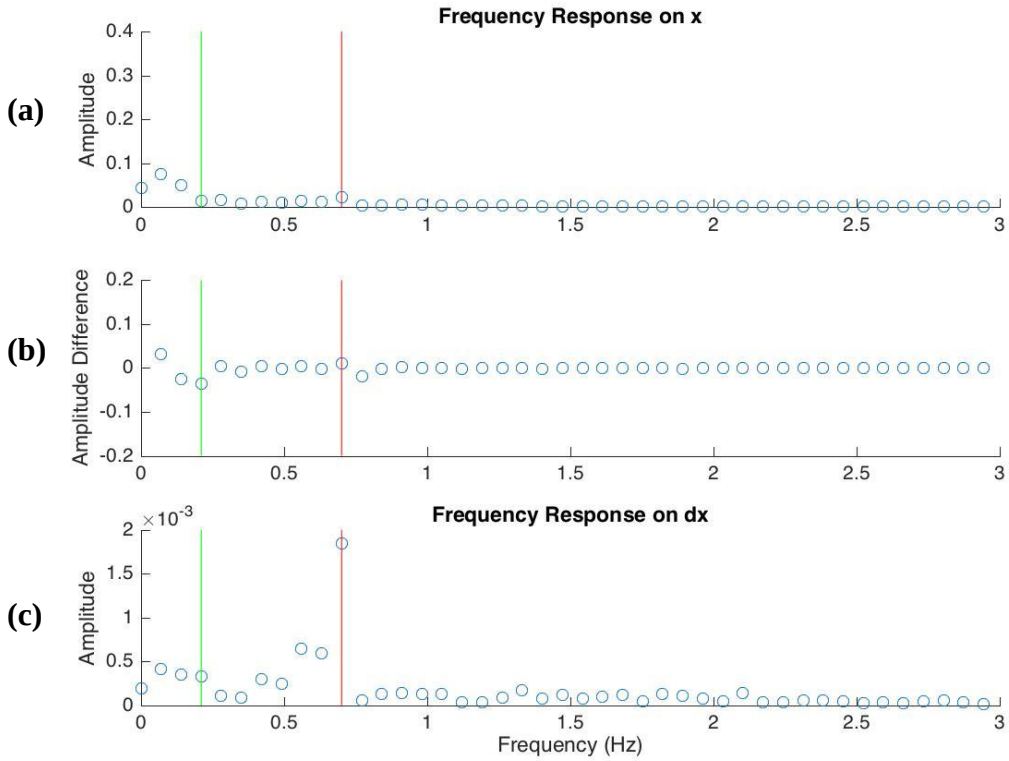

Figure 8.5 *(a) Frequency response of Fourier transformation on the x position data. (b) Difference of the amplitude response. (c) Frequency response of Fourier transformation on the differential x position data. Red lines indicate the stopband defined by the sway frequency. Green lines indicate the passband defined by the end of the curvature frequencies.*

(indicated by the red line). This frequency is related to the walking sway oscillation, and this is what we want to remove from the data.

8.1.3.2 Passband and stopband

To remove the frequencies that are related to the walking sway, the stopband is defined as the sway frequency (as indicated by red lines in **Figure 8.5a**). To quickly locate the stopband, Fourier transformation was calculated on the differential x data (see **Figure 8.5c**). Doing this can help reduce the amplitude responses of the curvature frequencies and facilitate the localization of the sway frequency. As shown in **Figure 8.5**, the frequency of dx that shows the largest amplitude response corresponds to the sway frequency[10].

[10] In most case, yes, but not always. In some cases, it does not correspond to the sway frequency (defined as the frequency corresponding to the largest amplitude response after the curvature frequency 'hill'), but usually one point before or after the sway frequency (note that

It can also be observed from **Figure 8.5** that there is more than one frequency that relates to the curvature of the walking trajectory. These frequencies are clustered together and form a 'hill'. The frequency corresponding to the peak of the 'hill' is the main frequency of the curvature. As the curvature of the trajectory is what we are most interested in, we want to keep all the frequencies that are related to the curvature. Therefore, the passband is defined as the frequency at the left foot of the 'hill' (as indicated by green lines in **Figure 8.5**).

To locate the left foot of the 'hill' as the passband, a Matlab protocol was used to search for the point of which the decreasing trend of the amplitude response stopped[11]. It starts from the lowest point on the differential amplitude response against frequency (see **Figure 8.5b**). If the point did not correspond to the stopping point of the 'hill' on **Figure 5a** (usually one or two points before or after), the adjustment would be made until the stopping point is located.

The result of the filter can be seen in **Figure 8.6**.

they are discrete). In such a case, however, it is easy to locate the sway frequency by using the frequency response of x data and its differential frequency response in combination with the frequency response of dx.

[11] From **Figure 8.5** it can be seen that after the point the difference between any two adjacent points becomes considerably smaller, and oscillating around zero.

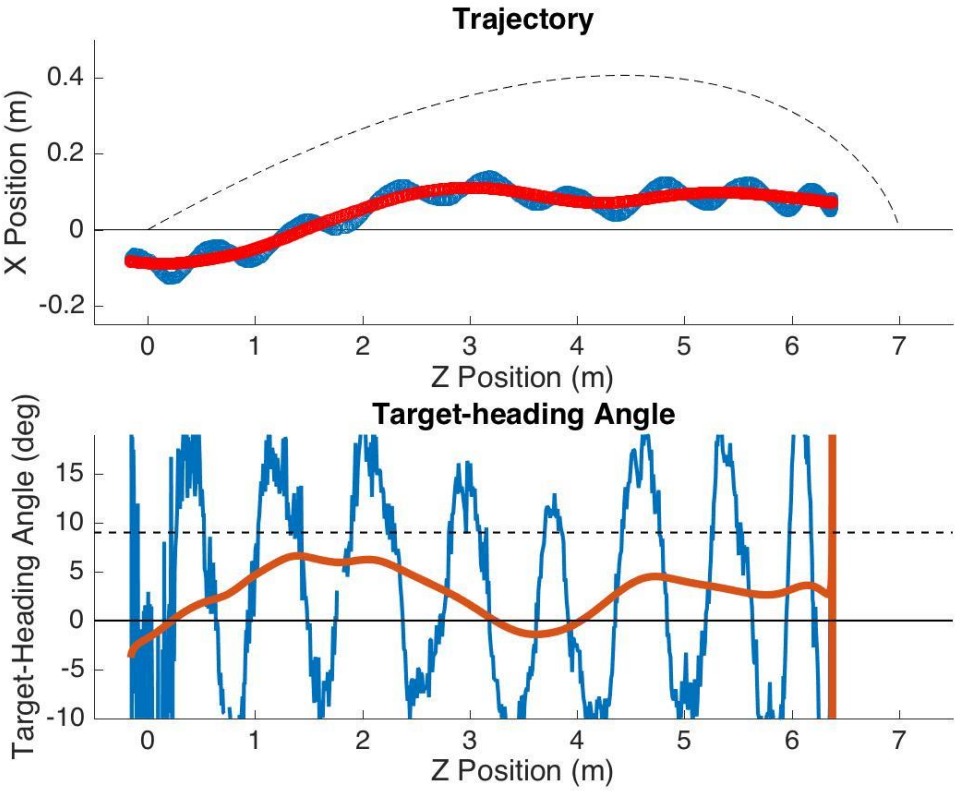

Figure 8.6 *Example of filtered data. The upper panel shows the trajectory data. Blue line corresponds to the original data. Red line corresponds to the filtered data. Dashed line indicates the prediction of the sole use of egocentric direction. The lower panel shows the target-heading angle data. Blue line represents the target-heading angle calculated on the original trajectory data. Red line represents the target-heading angle calculated on the filtered trajectory data. Dashed line indicates the power of the prisms.*

8.2 Chapter 3 - Supplementary Materials

8.2.1 Experiment 3.1

8.2.1.1 Comparing optic flow between the Cloud and Room conditions

In Experiment 3.1, we assumed that the *Cloud* condition contained richer optic flow but less allocentric location cues than the *Room* condition does. Based on this assumption, we hypothesised that trajectories should have been straighter in the *Cloud* condition if optic flow plays a dominant role in the guidance of walking. Deviation from the hypothesis was considered as evidence for the role of allocentric location cues in the guidance of walking. In this section, we provide analysis to support the assumption that there is richer optic flow in the *Cloud* condition than in the *Room* condition.

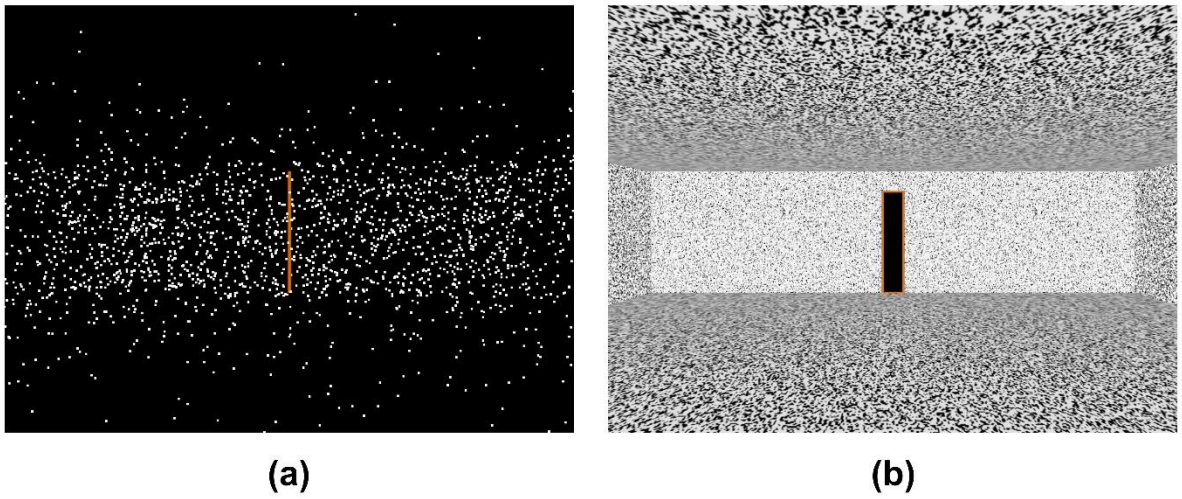

Figure 8.7. *Sample views of the Cloud condition* ***(a)*** *and the Room condition* ***(b)****.*

In the *Cloud* condition, an observer walked through a dense 3-dimensional (3D) random field of dots (**Figure 8.7a**); and in the *Room* condition, the same observer walked through a room with smooth textured surfaces (**Figure 8.7b**). We argue that optic flow was richer in the *Cloud* condition than in the *Room* condition because (1) heading is easier recovered from the flow field in the *Cloud* condition and (2) the *Cloud* condition contained motion parallax cues whereas the *Room* condition did not.

8.2.1.1.1 Heading is more easily recovered from flow field in the Cloud condition

Optic flow is a radial pattern in the retinal image when the observer moves forward along a straight line. Vectors in the pattern radiate from a static point, or focus of expansion (FoE). When the observer's gaze direction is fixed relative to the direction of movement, the retinal location of the FoE corresponds with the direction of the movement. In this case, the

FoE can be used to recover the direction of self-motion or heading (Gibosn 1950, 1979). In this sense, the more easily the FoE can be located in the flow field, the more readily the heading can be recovered by optic flow.

What kind of flow field has a FoE that is more easily located? A classic optic flow field is formed by vectors pointing outwards from the static FoE. The magnitude of the vectors varies as a function of distance from the FoE (or eccentricity), forming a velocity gradient with a 'bottom' at the location of FoE. it would be natural to think that the larger the velocity gradient is (with more large vectors in the vicinity of FoE), the more easily the FoE can be located (see **Figure 8.8** for illustration).

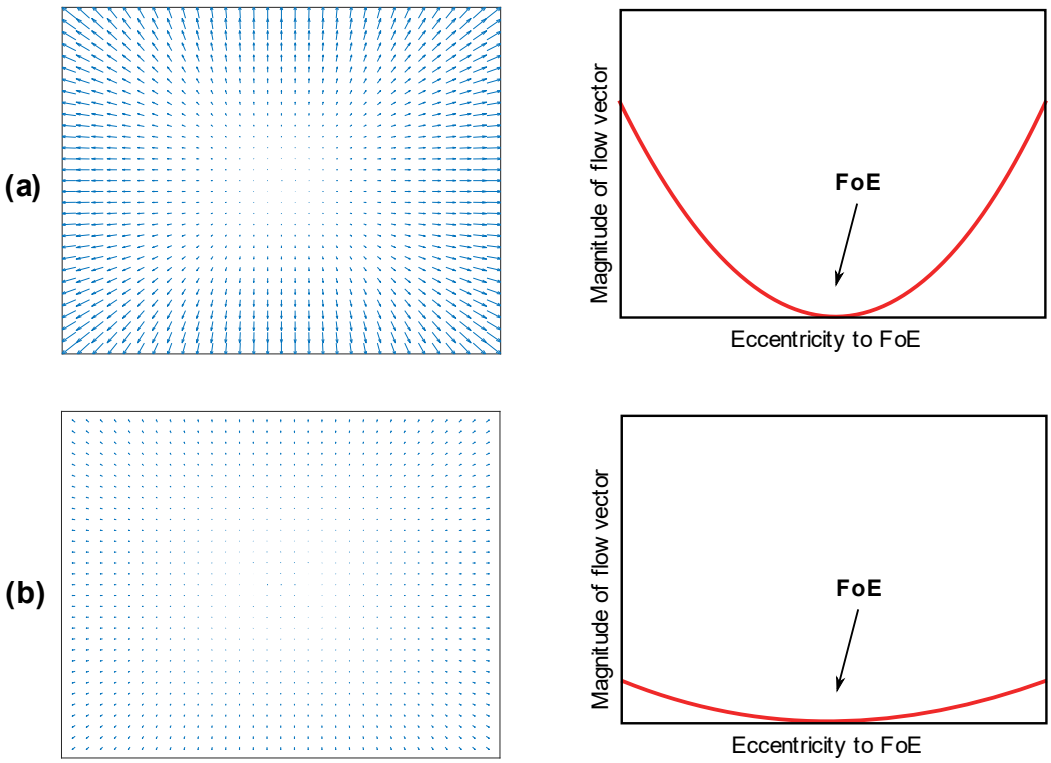

Figure 8.8. *Optic flow patterns with two different gradients. In the pattern* ***(a)*** *the gradient of the flow field is larger than the gradient field in the pattern* ***(b)****. By comparing the two patterns one can see that the FoE in* ***(a)*** *is more discernible than in* ***(b)****.*

What kind of structure of the scene can generate a flow field with large velocity gradient at a given walking speed? To calculate the flow vector, consider a point *P* in a 3D space, it has an instantaneous position in the Cartesian coordinate system [*x*, *y*, *z*] that is fixed with respect to the eye. Its position [x_p, y_p] on the retina that is projected from the 3D position (see **Figure 8.9** for illustration) can be conveniently estimated as

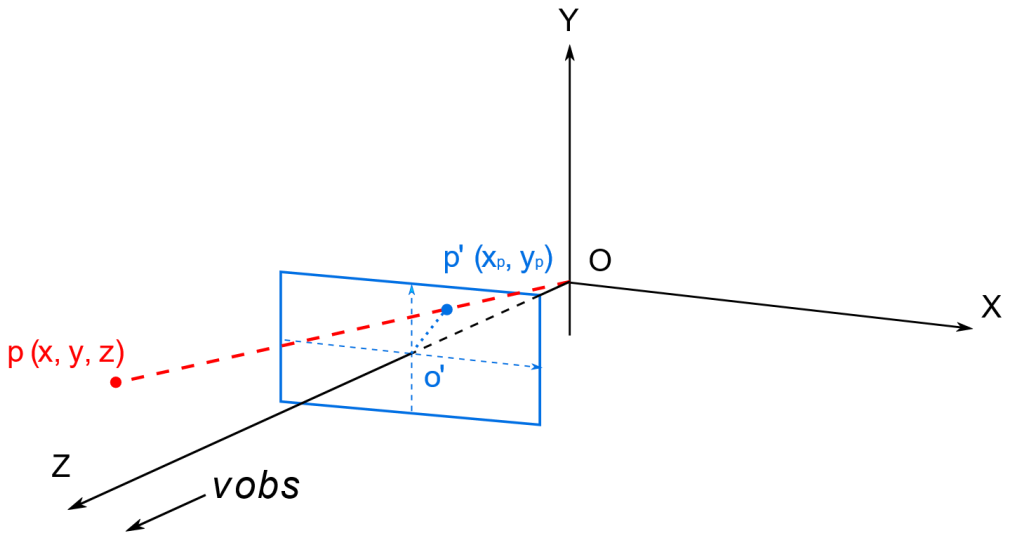

Figure 8.9. *An external coordinate system OXYZ fixed with an observer's eye. The observer moves along the z-axis at the velocity v_{obs}, and the gaze is fixed with the direction of movement. The blue frame represents the observer's retina. A point P has a location in the external coordinate system $[x, y, z]$ and a retinal location $[x_p, y_p]$. The dotted line connecting the retinal image of P' and O' indicates the eccentricity of P' from the target.*

$$x_p = \frac{x}{z}, \qquad y_p = \frac{y}{z}, \tag{8.5}$$

and the eccentricity from the FoE, or E_p is

$$E_p = \sqrt{x_p^2 + y_p^2} \tag{8.2}$$

It follows that

$$E_p = \sqrt{\frac{x^2}{z^2} + \frac{y^2}{z^2}}. \tag{8.3}$$

If the observer moves forward at a velocity of v_{obs}, then the velocity V_p at which P moves away from the FoE on the retina will be:

$$V_p = \frac{dE_p}{dt}, \tag{8.4}$$

and the elements in space move relatively to the observer's eyes at

$$v_{obs} = -\frac{dz}{dt}. \tag{8.5}$$

Substituting from (8.1) and (8.3) to (8.4) we obtain

$$V_p = \frac{\sqrt{x_p^2 + y_p^2}}{z} v_{obs} \quad (8.6)$$

From (8.6) we can see that the velocity at which a point moves on the retina depends on both its distance in depth to the eye (z) and its eccentricity form the FoE. For points at the same distance from the eye, the closer they are to the edges of the visual field, the faster they appear to move outward. In the same vein, at a given retinal position, the closer the point is to the eye, the faster it appears to move outward.

In the *Cloud* condition, the dots filled up the whole 3D space and thus cover a wide range in depth. They can generate large velocity vectors across the visual field. Even for those points that appear close to the centre of the visual field (i.e., small x_p and y_p), they can also be very close to the observer's eyes and yield large velocity vectors. Therefore, the velocity gradient should be large in the *Cloud* condition.

In the *Room* condition, however, the visual elements have a very restricted distribution. They were fixed to the surfaces of the room and thus cannot be very close to the observer's eye. Especially for those elements with small eccentricity, they were fixed to the front wall and hence also the furthest from the observer. Therefore, they cannot generate large flow vectors. As a result, the gradient in the *Room* condition should smaller than in the *Cloud* condition.

To illustrate the difference in the flow pattern between the *Cloud* and *Room* conditions, we calculated the flow vectors for the *Cloud* and *Room* conditions when the observer was at 6m from the target at the velocity of 1m/s (see **Figure 8.10**). For the *Cloud* condition, the image positions and vectors were calculated on the positions of the dots in the visual field. For the *Room* condition, the same number of elements were sampled randomly from the surfaces of the room. Based on the positions of the elements in the 3D space, the retinal locations and velocity vectors were calculated according to Equation (8.6). In support of our speculation, the FoE appears to be more discernible in the *Cloud* condition (**Figure 8.10a upper**) than in the *Room* condition (**Figure 8.10b upper**). In the *Room* condition, although the vectors in the *Room* condition appear large on the floor, ceiling and side walls, they are further from the FoE. For the vectors on the front wall, although they are close to the FoE, they are small in magnitude. In the *Cloud* condition, the vectors can still be large when close to the FoE. To better visualise the structure of retinal flow field, a heat map of the magnitude of velocity vectors was plotted as a function of retinal location respectively for the *Cloud* and *Room* conditions. The heat maps confirmed what we observed on the vector fields.

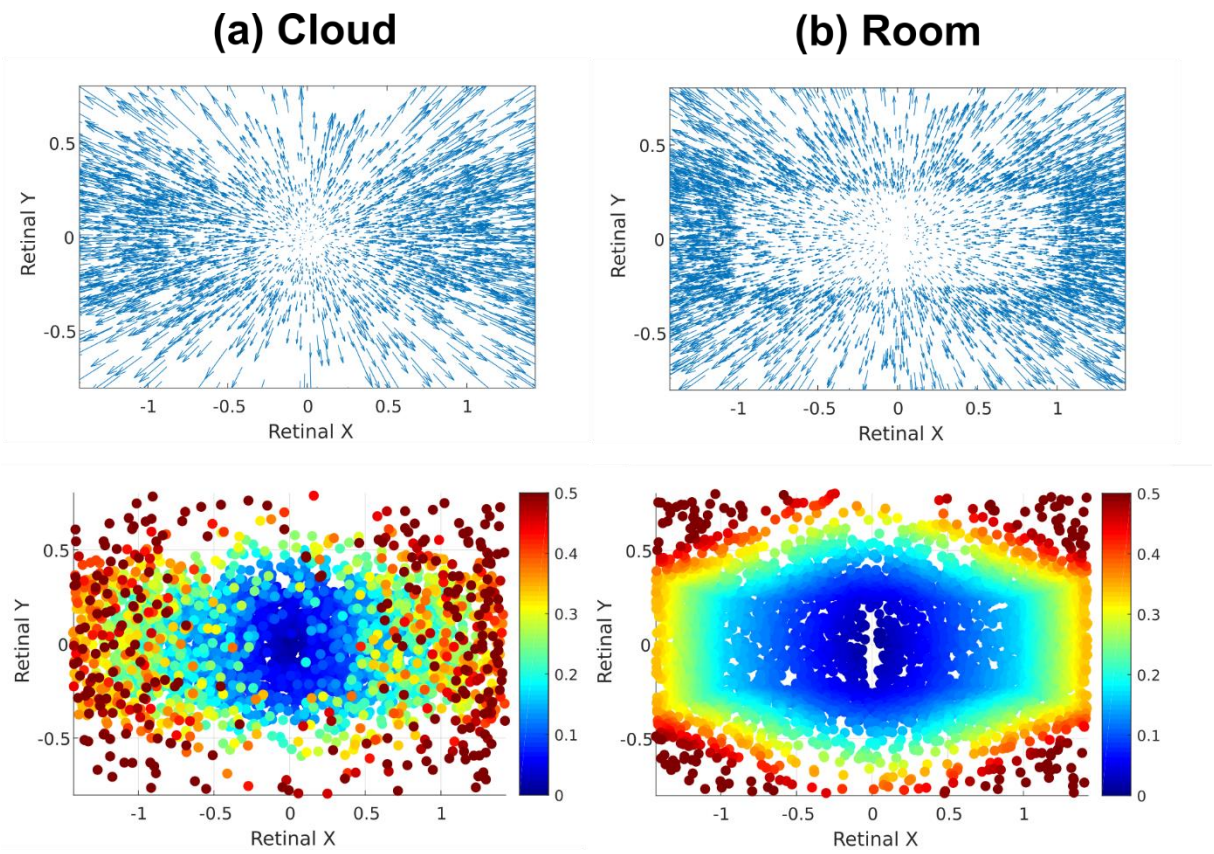

Figure 8.10. *Comparing the structure of retinal flow field between the Cloud and Room conditions.* ***(a) Upper****: the vector field in the Cloud condition.* ***Lower****: the heat map of the magnitude of velocity vectors in the Cloud condition as a function of retinal location.* ***(b) Upper****: the vector field in the Room condition.* ***Lower****: the heatmap of the magnitude of velocity vectors in the Room condition as a function of retinal location.*

The *Cloud* heat map has a smaller 'bottom' (blue area in **Figure 8.10a lower**) than the *Room* condition does (blue area **Figure 8.10b lower**). In other words, in the *Room* condition a relatively wide area around the FoE is consist of vectors in small magnitude, whereas in the *Cloud* condition only a small area around the FoE is consist of small vectors. There are even some large vectors near the FoE (light blue dots around the centre of the visual field). Therefore, the FoE is more well-defined in the *Cloud* condition and thus the heading is more easily recovered from optic flow in the *Cloud* condition.

8.2.1.1.2 Cloud has more motion parallax cues than the Room does.

In the preceding section, we considered the case when there was only a simple translational movement with the observer's gaze directed to the direction of the movement. Here we consider a more complicated case when there is a rotational component in addition to the translational component in the retinal flow field, due to eye rotation or head movement.

In this case, FoE can be recovered using motion parallax (Longuet-Higgins & Prazdny, 1980). To illustrate this, consider two points $[x_{p1}, y_{p1}]$ and $[x_{p2}, y_{p2}]$ appear close to each other on the retina but differ in depth position z_1 and z_2. Their images on the retina will have the same rotational velocities V_{R1} and V_{R2} but different translation velocities V_{T1} and V_{T2}. According to Equation (1.6),

$$V_{T1} = \frac{\sqrt{x_{p1}^2 + y_{p1}^2}}{z_1} v_{obs},\ V_{T2} = \frac{\sqrt{x_{p2}^2 + y_{p2}^2}}{z_2} v_{obs}. \tag{1.7}$$

As the images of the two points are very close to each other, the positions of the two points on the retina can be seen as

$$x_{p1} \approx x_{p2},\ \ y_{p1} \approx y_{p2}. \tag{1.8}$$

Therefore, the directions of the velocity vectors of the two points $(\frac{x_{p1}}{y_{p1}}, \frac{x_{p2}}{y_{p2}})$ are almost the same, and thus the relative velocity between the two points will also be in the same direction and points to the FoE. The velocities of the two points will follow the ratio

$$\frac{V_{T1}}{V_{T2}} \approx \frac{z_2}{z_1}. \tag{1.8}$$

That is, the larger the distance between the two points in depth, the larger the relative velocity between them will be, and the easier the FoE can be located when there is a rotational component in the retinal field. In other words, for the FoE to be easy to locate, the retinal field should contain many pairs of points that are close on the retina but distant in depth.

Such a pair of dots can be easily found in the *Cloud* condition. As the dots filled up the whole volume of the space, the chance was high that the dots appeared close on the retina but were distant from each other in depth. there are many pairs of dots that are close in retinal location but differ in depth distance. In the *Room* condition, however, the existence of such a pair was rare. As the visual elements are fixed to the surfaces, dots that appear close to each other in retinal location will also be close in depth. Take the right wall for example, if we take two dots that appear close to each other, they are also close in depth. In this sense, the motion parallax cues are available in the *Cloud* condition but not in the *Room* condition. Thus, it should be easier to locate the FoE from the retinal field with a rotation component.

Together, the *Cloud* condition contains richer optic flow then the *Room* condition does in that (1) the flow field has a clearer FoE and (2) there are more motion parallax cues.

8.2.1.2 Target-heading angle as a function of distance on Trial 1

8.2.1.2.1 Building up the growth model

The procedure of model building followed the procedure that was outlined in Chapter 2 (Section 2.4.2.1.3). First, a taxonomy of models was fitted on the target-heading angles. Each model in the taxonomy extends the previous one by including a predictor. By comparing the fit of the two adjacent models, the significance of the predictor could be determined.

To build a growth model, we started with a baseline model (`baseline`) with only a constant value or intercept that corresponds to the mean target-heading angle across the distance (2m – 6m from target). In the second model (`distRI`), distance was added as the level-1 predictor. Then in the third model (`distRS`), linear random effects were included to allow the slope (rate of change in target-heading angle against distance) to vary across participants around the population average slope. Scene (*Line*, *Outline*, *Cloud* and *Room*) and interaction term (`Scene × distance`) were then sequentially added into the fourth (`scne.int`) and fifth (`scne.slp`) models as the level-2 predictor (see the code below). The two predictors respectively quantify the effect of cue richness on the early target-heading angle at 6m from the target and the rate of change in the target-heading angle across distance.

```
# Setting up a baseline model that includes random intercepts
baseline   <- lme(target-heading_angle ~ 1, random = ~ 1|SubjectNo/Scene, data = o
ffset_trial1, method = "ML", na.action = na.exclude, control = list(opt="optim"))

# Adding "distance" as the level-1 fixed effect
distRI     <- update(baseline,  .~. + distance)
# Introducing random slopes
distRS     <- update(distRI,    random = ~ distance|SubjectNo/Scene)

# Adding Scene as the level-2 fixed effect
# Effects of Scene on the intercept
scne.int   <- update(distRS,    .~. + Scene)
# Effects of Scene on the slope
scne.slp   <- update(scne.int,  .~. + Scene : distance)
```

8.2.1.2.2 Comparing the models

Then we made a decision about the significance of each predictor. This was done using the likelihood-ratio test that compares -2LL (minus 2 times the log-likelihood, or `L.Ratio` in the output table below) between the models before and after including the predictor. The R code and output for the model comparisons is listed below.

As shown in the output table, all the subsequent models in the taxonomy have a significantly fit improvement relative to the previous model. This suggests that all the predictors that were included have an effect. For example, the model `scne.slp` is significantly better than the model `scne.int` ($p < 0.0001$). Because the `scne.slp` has the interaction term (`Scene × distance`) added in, the result suggests that the four conditions differed in the rate of change of target-heading angle.

```
# Code
anova(baseline, distRI, distRS, scne.int, scne.slp)

# Output
##          Model df      AIC      BIC    logLik   Test  L.Ratio p-value
## baseline     1  4 64680.64 64710.77 -32336.32
## distRI       2  5 62279.63 62317.28 -31134.81 1 vs 2 2403.015  <.0001
## distRS       3  9 55185.27 55253.05 -27583.63 2 vs 3 7102.359  <.0001
## scne.int     4 12 55140.45 55230.82 -27558.22 3 vs 4   50.820  <.0001
## scne.slp     5 15 55125.15 55238.11 -27547.57 4 vs 5   21.298   1e-04
```

8.2.1.2.3 Single parameter tests in the model scne.slp

As all the predictors added into the model have an effect, it is necessary to evaluate the estimated values of the parameters in the final model `scne.slp`. These estimates describe how target-heading angle and its change differed between conditions. For hypothesis tests for each parameter, *t*-values and associated *p*-values were computed. The R code and output are shown below.

```
# Code
summary(scne.slp, corr = FALSE)

# Output
## Fixed effects: target-heading_angle ~ distance + Scene + distance:Scene
##                            Value Std.Error    DF   t-value p-value
## (Intercept)             9.142117 0.5077571 13583 18.004902  0.0000
## distance               -0.746785 0.1786752 13583 -4.179569  0.0000
## SceneLine               1.283495 0.7178930   141  1.787864  0.0759
## SceneOutline            1.726041 0.7178723   141  2.404384  0.0175
## SceneRoom              -1.906724 0.7178697   141 -2.656086  0.0088
## distance:SceneLine      0.466518 0.2516177 13583  1.854076  0.0637
## distance:SceneOutline  -0.717978 0.2516140 13583 -2.853491  0.0043
## distance:SceneRoom     -0.152893 0.2516062 13583 -0.607667  0.5434
```

In the output above, the column named *`Value`* shows the estimated value of the parameter. The columns named *`t-value`* and *`p-value`* show the result of the statistical test on the parameter. As the *Cloud* condition was chosen as the reference, the *`Intercept`* and *`distance`* in the output above respectively corresponds to the magnitude of the target-heading angle at the beginning of the distance (6m from the target) and the rate of change in

the *Cloud* condition. For the *Cloud* condition, the statistical results on the `Intercept` and `distance` indicate that both values are significantly different from 0 [both *p*s < 0.0001].

The third to the fifth row of the output correspond to the difference in the magnitude of the target-heading angle at 6m from target between the *Cloud* condition and other conditions. The sixth to the eighth row of the output correspond to the difference in the rate of change or slope between the *Cloud* and other conditions.

Note that the different results here only show estimated slopes in the *Cloud* condition and comparisons between the *Cloud* condition and other conditions. Therefore, in order to obtain more information about other conditions, we used *multcomp* package (Hothorn et al., 2008) to run one-sample t-tests on the estimated slopes of conditions and pairwise comparisons on the slopes. The R code and outputs are shown below.

8.2.1.2.4 Estimation of slope parameters

As shown in the output below, the `Estimate` column shows the estimated slope (or rate of change in target-heading angle) for each condition. The larger the absolute value of the number is, the steeper the slope and thus the faster the target-heading angle changes. The negative signs mean that the target-heading angle decreases in all conditions. Here we can see that the *Outline* condition has the most rapid decrease in target-heading angle.

To test whether the estimated slope is different from 0, *z*-values and *p*-values are computed and shown in the list. Here we can see that, except the *Line* condition, all conditions have a slope significantly different from 0.

```
# Code
contrast.matrix <- rbind(
  "Slope: Cloud - 0  "            = c(0, 1, 0, 0, 0, 0, 0, 0),
  "Slope: Line - 0   "            = c(0, 1, 0, 0, 0, 1, 0, 0),
  "Slope: Outline - 0"            = c(0, 1, 0, 0, 0, 0, 1, 0),
  "Slope: Room - 0   "            = c(0, 1, 0, 0, 0, 0, 0, 1)
)
comps <- glht(scne.slp, contrast.matrix)
summary(comps, test = adjusted("bonferroni"))

# Output
##   Simultaneous Tests for General Linear Hypotheses
##
## Fit: lme.formula(fixed = target-heading_angle ~ distance + Scene + distance:Sce
ne,
##     data = offset_trial1, random = ~distance | SubjectNo/Scene,
##     method = "ML", na.action = na.exclude, control = list(opt = "optim"))
##
## Linear Hypotheses:
##                          Estimate Std. Error z value Pr(>|z|)
```

```
## Slope: Cloud - 0   == 0  -0.7468     0.1786  -4.181 0.000116 ***
## Slope: Line - 0    == 0  -0.2803     0.1786  -1.569 0.466598
## Slope: Outline - 0 == 0  -1.4648     0.1786  -8.200 8.88e-16 ***
## Slope: Room - 0    == 0  -0.8997     0.1786  -5.037 1.89e-06 ***
## ---
## Signif. codes:  0 '***' 0.001 '**' 0.01 '*' 0.05 '.' 0.1 ' ' 1
## (Adjusted p values reported -- bonferroni method)
```

8.2.1.2.5 Pairwise comparison on the slopes between the conditions

For pairwise comparisons on the slopes between the environments, another contrast matrix was used (see the R code below). In the output list, the `Estimate` column shows the difference in slope between the conditions, and the associated *z*- and *p*-values. Here we can see that the slope was significantly steeper in the *Outline* condition than in the *Line* and *Cloud* conditions [both Bonferroni *p*s < 0.05].

```
# Code
contrast.matrix <- rbind(
  "Slope: Line - Cloud   "           = c(0, 0, 0, 0, 0,  1,  0, 0),
  "Slope: Outline - Cloud"           = c(0, 0, 0, 0, 0,  0,  1, 0),
  "Slope: Room - Cloud   "           = c(0, 0, 0, 0, 0,  0,  0, 1),
  "Slope: Outline - Line "           = c(0, 0, 0, 0, 0, -1,  1, 0),
  "Slope: Room - Line    "           = c(0, 0, 0, 0, 0, -1,  0, 1),
  "Slope: Room - Outline "           = c(0, 0, 0, 0, 0,  0, -1, 1)
)
comps <- glht(scne.slp, contrast.matrix)
summary(comps, test = adjusted("bonferroni"))

# Output
##   Simultaneous Tests for General Linear Hypotheses
##
## Fit: lme.formula(fixed = target-heading_angle ~ distance + Scene + distance:Sce
ne,
##     data = offset_trial1, random = ~distance | SubjectNo/Scene,
##     method = "ML", na.action = na.exclude, control = list(opt = "optim"))
##
## Linear Hypotheses:
##                              Estimate Std. Error z value Pr(>|z|)
## Slope: Line - Cloud    == 0   0.4665     0.2515   1.855   0.3819
## Slope: Outline - Cloud == 0  -0.7180     0.2515  -2.854   0.0259 *
## Slope: Room - Cloud    == 0  -0.1529     0.2515  -0.608   1.0000
## Slope: Outline - Line  == 0  -1.1845     0.2515  -4.709 1.49e-05 ***
## Slope: Room - Line     == 0  -0.6194     0.2515  -2.463   0.0828 .
## Slope: Room - Outline  == 0   0.5651     0.2515   2.247   0.1480
## ---
## Signif. codes:  0 '***' 0.001 '**' 0.01 '*' 0.05 '.' 0.1 ' ' 1
## (Adjusted p values reported -- bonferroni method)
```

8.2.1.3 Mean target-heading angles of the early and late parts as a function of trial

8.2.1.3.1 Building the growth model

A taxonomy of models was fitted on the mean target-heading angles that were averaged over the early (5.75m ~ 6.25m from target) and late (1.75m ~ 2.25m from target) parts. Predictors Trial (1 ~ 4) and associated random effects, Part (early and late), Scene (*Line*, *Outline*, *Cloud* and *Room*) and interaction terms were sequentially added into the models. The R code is listed below.

```
# Setting up a baseline model that includes only random intercepts
baseline        <- lme(target-heading_angle ~ 1, random = ~1|SubjectNo/Scene/Part,
 data = offset.end.long, method = "ML", na.action = na.exclude, control = list(opt
 = "optim"))

# Adding Trial as the level-1 fixed effect
TrialRI           <- update(baseline, .~. + Trial)
# Introducing random slopes
TrialRS           <- update(TrialRI,  random = ~ Trial|SubjectNo/Scene/Part)
# Modelling a first-order autoregressive covariance structure
TrialAR           <- update(TrialRS, correlation = corAR1())

# Effects of Part on the intercept
PartRI        <- update(TrialAR,    .~. + Part)
# Effects of Part on the slope
PartRS        <- update(PartRI,     .~. + Part : Trial)

# Effects of Scene on the intercept
sceneRI       <- update(PartRS,     .~. + Scene)
# Effects of Scene on the slope
sceneRS       <- update(sceneRI,    .~. + Scene : Trial)

# Effects of interaction on the intercept
ScenePartI    <- update(sceneRS,    .~. + Scene : Part)
# Effects of interaction on the slope
ScenePartS    <- update(ScenePartI, .~. + Scene : Part : Trial)
```

On the basis of model `baseline`, model `TrialRI` added level-1 predictor Trial (1 ~ 4). Model `TrialRS` added random effects to allow individual slopes to vary around the population average slope. Model `TrialAR` took autocorrelation into account. Model `PartRI` added the level-2 predictor Part (early and late) to examine the difference between the early and late parts in the magnitude of a mean target-heading angle. Model `PartRS` added the interaction term (Part × Trial) for the difference between the early and late parts in slope (or rate of change). Model `sceneRI` added the level-2 predictor Scene (*Line*, *Outline*, *Cloud* and *Room*) for effects of cue richness on the magnitude of mean target-heading angles of the two parts. Model `sceneRS` added the interaction term (Scene × Trial) for effects of cue richness on the slopes (or rates of change) over trials. Model `ScenePartI` added the interaction term

(Scene × Part) for any differential effects of cue richness on the mean target-heading angles depending on the early or late part. Model `ScenePartS` added the three-way interaction (Scene × Part × Trial) for differential effects of cue richness depending on the early or late part on the slopes (or rates of change).

The R code and output for model comparisons are listed below.

```
# Code
anova(baseline, TrialRI, TrialRS, TrialAR, PartRI, PartRS, sceneRI, sceneRS, Scene
PartI, ScenePartS)

# Output
##            Model df      AIC      BIC    logLik     Test  L.Ratio p-value
## baseline     1    5 8190.645 8217.327 -4090.323
## TrialRI      2    6 8163.500 8195.517 -4075.750   1 vs 2  29.1457  <.0001
## TrialRS      3   12 8159.339 8223.374 -4067.669   2 vs 3  16.1610  0.0129
## TrialAR      4   13 8157.267 8226.638 -4065.633   3 vs 4   4.0720  0.0436
## PartRI       5   14 8046.927 8121.635 -4009.463   4 vs 5 112.3401  <.0001
## PartRS       6   15 8024.319 8104.363 -3997.160   5 vs 6  24.6076  <.0001
## sceneRI      7   18 7995.196 8091.249 -3979.598   6 vs 7  35.1230  <.0001
## sceneRS      8   21 7990.996 8103.058 -3974.498   7 vs 8  10.2001  0.0169
## ScenePartI   9   24 7984.829 8112.900 -3968.415   8 vs 9  12.1667  0.0068
## ScenePartS  10   27 7985.279 8129.359 -3965.639  9 vs 10   5.5504  0.1357
```

8.2.1.3.2 Building models on the early part mean target-heading angles

Then, to look at the target-heading angles at the early part of the trajectory (6m from target), we built a growth model separately on the mean target-heading angles of the early part (averaged over 5.75m ~ 6.25m). The R code is listed below.

```
# Code
baseline      <- lme(target-heading_angle ~ 1, random = ~1|SubjectNo/Scene, data =
 offset.end.long[end == "early"], method = "ML", na.action = na.exclude, control =
 list(opt = "optim"))

TrialRI       <- update(baseline, .~. + Trial)
TrialRS       <- update(TrialRI,  random = ~ Trial|SubjectNo/Scene)
TrialAR       <- update(TrialRS, correlation = corAR1())

sceneRI       <- update(TrialAR,  .~. + Scene)
sceneRS       <- update(sceneRI,  .~. + Scene : Trial)

anova(baseline, TrialRI, TrialRS, TrialAR, sceneRI, sceneRS)

# Output
##           Model df      AIC      BIC    logLik   Test  L.Ratio p-value
## baseline      1  4 4021.058 4039.628 -2006.529
## TrialRI       2  5 3960.439 3983.652 -1975.220 1 vs 2 62.61862  <.0001
## TrialRS       3  9 3966.334 4008.116 -1974.167 2 vs 3  2.10577  0.7163
## TrialAR       4 10 3968.333 4014.758 -1974.166 3 vs 4  0.00107  0.9739
## sceneRI       5 13 3952.597 4012.949 -1963.299 4 vs 5 21.73552  0.0001
## sceneRS       6 16 3950.435 4024.715 -1959.217 5 vs 6  8.16209  0.0428
```

Model `baseline` is the simple model containing only an intercept. Model `TrialRI` added the level-1 predictor Trial (1 ~ 4). Model `TrialRS` added random effects and Model `TrialAR` took into account autocorrelation. Model `sceneRI` added the level-2 predictor Scene (*Line*, *Outline*, *Cloud* and *Room*) for effects of cue richness on the magnitude of mean target-heading angles. Model `sceneRS` added the interaction term Scene × Trial for effects of cue richness on the slopes (or rates of change) in the mean target-heading angle over trials.

As shown in the output, adding Scene × Trial significantly improved the fit of model `sceneRS` [p = 0.043], suggesting that the slopes of the early part differed significantly between conditions. Next, we evaluated the estimated slopes in each condition.

8.2.1.3.3 Slope of the early parts against trials

The R code and output for evaluation of estimated slopes is shown below.

```
# Code
contrast.matrix <- rbind(
  "Cloud"      = c(0, 1, 0, 0, 0, 0, 0, 0),
  "Line"       = c(0, 1, 0, 0, 0, 1, 0, 0),
  "Outline"    = c(0, 1, 0, 0, 0, 0, 1, 0),
  "Room"       = c(0, 1, 0, 0, 0, 0, 0, 1)
)
postHocs <-glht(sceneRS, contrast.matrix) #, linfct = mcp(ExpNo = "Tukey"))
summary(postHocs, test = adjusted("none"))

# Output
##   Simultaneous Tests for General Linear Hypotheses
##
## Fit: lme.formula(fixed = target-heading_angle ~ trial_ct + Scene + trial_ct:Sce
ne,
##     data = offset.end.long[end == "early"], random = ~trial_ct |
##         SubjectNo/Scene, correlation = corAR1(), method = "ML",
##     na.action = na.exclude, control = list(opt = "optim"))
##
## Linear Hypotheses:
##              Estimate Std. Error z value Pr(>|z|)
## Cloud == 0    -1.0154     0.1608  -6.313 2.74e-10 ***
## Line == 0     -0.4298     0.1618  -2.657  0.00789 **
## Outline == 0  -0.4777     0.1608  -2.970  0.00298 **
## Room == 0     -0.7018     0.1608  -4.363 1.28e-05 ***
## ---
## Signif. codes:  0 '***' 0.001 '**' 0.01 '*' 0.05 '.' 0.1 ' ' 1
## (Adjusted p values reported -- none method)
```

The column `Estimate` shows the estimated slope for each condition. Here we can see that the slope was the steepest in the *Cloud* condition [estimated slope = -1.02], followed by the slope in the *Room* condition [estimated slope = -0.70]. The slopes in the *Outline* and *Line* conditions are similarly flat. The associated z- and p-values indicate that the slopes in all conditions are smaller than 0, suggesting a trend of decreasing.

8.2.1.3.4 Compare slope of the early parts between conditions

We then compared the estimated slopes between conditions. The R code and output is shown below.

```
# Code
contrast.matrix <- rbind(
  "Line - Cloud"       = c(0, 0, 0, 0, 0, 1, 0, 0),
  "Outline - Cloud"    = c(0, 0, 0, 0, 0, 0, 1, 0),
  "Room - Cloud"       = c(0, 0, 0, 0, 0, 0, 0, 1),
  "Outline - Line"     = c(0, 0, 0, 0, 0, -1, 1, 0),
  "Room - Line"        = c(0, 0, 0, 0, 0, -1, 0, 1),
  "Room - Outline"     = c(0, 0, 0, 0, 0, 0, -1, 1)
)
postHocs <-glht(sceneRS, contrast.matrix)
summary(postHocs, test = adjusted("bonferroni"))

# Output
##   Simultaneous Tests for General Linear Hypotheses
##
## Fit: lme.formula(fixed = target-heading_angle ~ trial_ct + Scene + trial_ct:Sce
ne,
##     data = offset.end.long[end == "early"], random = ~trial_ct |
##         SubjectNo/Scene, correlation = corAR1(), method = "ML",
##     na.action = na.exclude, control = list(opt = "optim"))
##
## Linear Hypotheses:
##                       Estimate Std. Error z value Pr(>|z|)
## Line - Cloud == 0      0.58559    0.22644   2.586   0.0582 .
## Outline - Cloud == 0   0.53768    0.22577   2.382   0.1034
## Room - Cloud == 0      0.31353    0.22577   1.389   0.9895
## Outline - Line == 0   -0.04791    0.22644  -0.212   1.0000
## Room - Line == 0      -0.27205    0.22644  -1.201   1.0000
## Room - Outline == 0   -0.22414    0.22577  -0.993   1.0000
## ---
## Signif. codes:  0 '***' 0.001 '**' 0.01 '*' 0.05 '.' 0.1 ' ' 1
## (Adjusted p values reported -- bonferroni method)
```

The column `Estimate` shows the estimated difference in slope between the two conditions. The associated *z*- and *p*-values test the hypothesis of whether the difference is different from 0. Here we can see that the difference in the estimated slopes between the *Line* and *Cloud* conditions is 0.59, which is marginally different from 0 [$z = 2.59$, Bonferroni $p = 0.058$]. The difference in the other comparisons did not survive the threshold.

8.2.2 Experiment 3.2

8.2.2.1 Building up the growth model

In Experiment 3.2, we had two groups. The Experienced group did Experiment 3.1 (walking) before Experiment 1 (heading judgements), whereas the Novel group only did Experiment 2 and did not do Experiment 1. We compared the thresholds between the two

groups to investigate whether having taken part in the walking experiment would have any effect on the performance on the heading judgment experiments.

To build a growth model, we started with a baseline model (`baseline`) with only the intercept. Distance (7m, 6m, 4m and 3m from target) was first added into the model (`distRI`) as the level-1 predictor, followed by the random effect on the slope (which allows the slope varies between participants) in model `distRS`. Scene, group and relevant interaction terms were then sequentially added into the model as the level-2 predictor (`scn.int`, `scn.slp`, `grp.int`, `grp.slp`, `scn.grp.int` and `scn.grp.slp`). The R code is listed below with tested effects stated in the comments.

```
# Setting up a baseline model that includes only random intercepts
baseline       <- lme(threshold ~ 1, random = ~1|SubjectNo/Scene, data = threshs,
method = "ML", na.action = na.exclude, control = list(opt="optim"))

# Adding in distance as the level-1 fixed effect
distRI         <- update(baseline,     .~. + distance)
# Introducing random slopes
distRS         <- update(distRI,      random = ~ distance|SubjectNo/Scene)

# Effects of Scene on the intercept
scn.int        <- update(distRS,       .~. + Scene)
# Effects of Scene on the slope
scn.slp        <- update(scn.int,      .~. + Scene : distance)

# Effects of Group on the intercept
grp.int        <- update(scn.slp,      .~. + Group)
# Effects of Group on the slope
grp.slp        <- update(grp.int,      .~. + Group : distance)

# Effects of Scene × Group interaction on the intercept
scn.grp.int    <- update(grp.slp,      .~. + Scene : Group)
# Effects of Scene × Group interaction on the slope
scn.grp.slp    <- update(scn.grp.int,  .~. + Scene : Group : distance)
```

8.2.2.1.1 Model comparisons

Then we compared the fit of the models to test the effects of the predictors that were added sequentially into the models. The R code and output is listed below.

```
# Code
anova(baseline, distRI, distRS, scn.int, scn.slp, grp.int, grp.slp)

# Output
##             Model df      AIC      BIC    logLik    Test   L.Ratio p-value
## baseline        1  4 1223.726 1239.887 -607.8629
## distRI          2  5 1193.992 1214.194 -591.9962  1 vs 2  31.73337  <.0001
## distRS          3  9 1112.829 1149.192 -547.4147  2 vs 3  89.16297  <.0001
## scn.int         4 12 1112.260 1160.743 -544.1301  3 vs 4   6.56914  0.0870
## scn.slp         5 15 1088.743 1149.347 -529.3717  4 vs 5  29.51682  <.0001
```

```
## grp.int         6 16 1090.727 1155.371 -529.3633  5 vs 6   0.01673  0.8971
## grp.slp         7 17 1091.991 1160.675 -528.9954  6 vs 7   0.73596  0.3910
## scn.grp.int     8 20 1097.465 1178.270 -528.7323  7 vs 8   0.52612  0.9131
## scn.grp.slp     9 23 1100.466 1193.392 -527.2332  8 vs 9   2.99819  0.3919
```

From the output, we can see that group does not have an effect on the intercept [$\chi^2(1) = 0.017$, $p = 0.90$] or on the slope [$\chi^2(1) = 0.74$, $p = 0.39$]. Moreover, there was no significant interaction between *group* and *scene* [both *p*s > 0.1]. The results suggest that there was no substantial difference between the two groups in the pattern of results. For parsimony, we collapsed the data from the two groups by excluding the predictor *group* and associated interactions from the model. In other words, we chose the model `scn.slp` as the final model for parameter estimate evaluation.

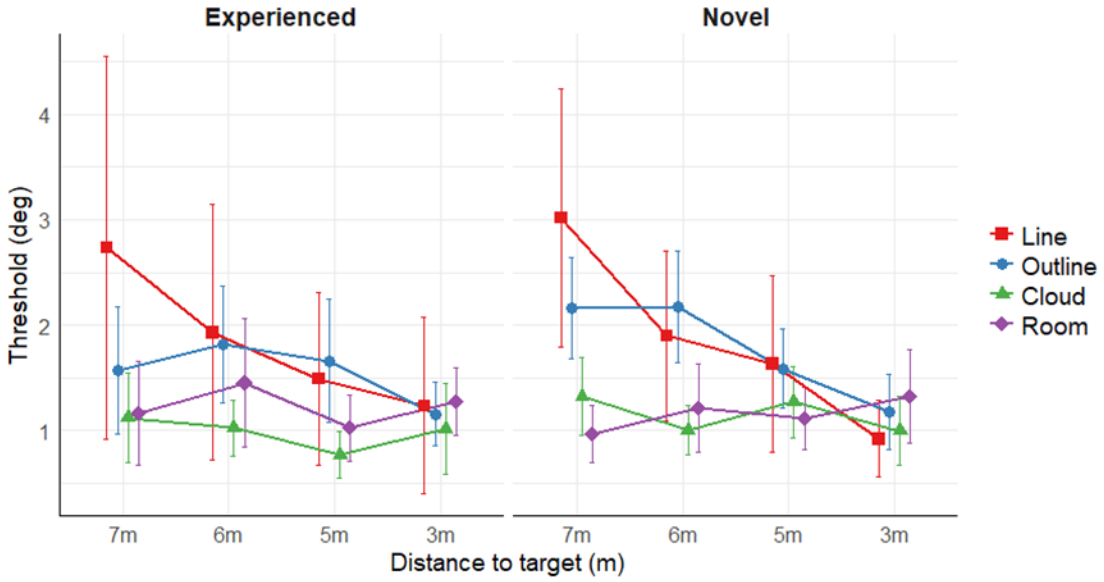

Figure 8.11. *Thresholds as a function of distance for both Experienced and Novel groups*

8.2.2.1.2 Parameter estimates for the model scn.slp.

To assess whether the slope parameters estimated in the model `scn.slp`, a contrast matrix was created for simultaneous one-sample tests using *multcomp* package (Hothorn, Bretz, and Westfall 2008). The R code and output are shown below.

```
# Code
contrast.matrix <- rbind(
        "Slope: Line    - 0"        = c(0, 1, 0, 0, 0, 0, 0, 0),
        "Slope: Outline - 0"        = c(0, 1, 0, 0, 0, 1, 0, 0),
        "Slope: Cloud   - 0"        = c(0, 1, 0, 0, 0, 0, 1, 0),
        "Slope: Room    - 0"        = c(0, 1, 0, 0, 0, 0, 0, 1)
)
comps <- glht(scn.slp, contrast.matrix)
summary(comps, test = adjusted("bonferroni"))
```

```
# Output
##   Simultaneous Tests for General Linear Hypotheses
##
## Fit: lme.formula(fixed = threshold ~ distance + Scene + distance:Scene,
##     data = threshs, random = ~distance | SubjectNo/Scene, method = "ML",
##     na.action = na.exclude, control = list(opt = "optim"))
##
## Linear Hypotheses:
##                          Estimate Std. Error z value Pr(>|z|)
## Slope: Line    - 0 == 0 -0.41454    0.06169  -6.720 7.25e-11 ***
## Slope: Outline - 0 == 0 -0.21442    0.06097  -3.517  0.00174 **
## Slope: Cloud   - 0 == 0 -0.03880    0.06135  -0.633  1.00000
## Slope: Room    - 0 == 0  0.01678    0.06153   0.273  1.00000
## ---
## Signif. codes:  0 '***' 0.001 '**' 0.01 '*' 0.05 '.' 0.1 ' ' 1
## (Adjusted p values reported -- bonferroni method)
```

The column `Estimate` shows the estimated slope for each condition. Here we can see that the slope was the steepest in the *Line* [estimated slope = -0.41] and *Outline* [estimated slope = -0.21] conditions. In contrast, the slopes are relatively flat in the *Cloud* [estimated slope = -0.039] and *Room* conditions [estimated slope = 0.017]. The associated *z*- and *p*-values indicate that only in the *Line* and *Outline* conditions the slopes were significantly different from 0 [both Bonferroni *p*s < 0.001].

For pairwise comparisons on the slopes between the conditions, another contrast matrix was used. The R code and output are shown below.

```
# Code
contrast.matrix <- rbind(
        "Outline - Line   "     = c(0, 0, 0, 0, 0,  1,  0, 0),
        "Cloud   - Line   "     = c(0, 0, 0, 0, 0,  0,  1, 0),
        "Room    - Line   "     = c(0, 0, 0, 0, 0,  0,  0, 1),
        "Cloud   - Outline"     = c(0, 0, 0, 0, 0, -1,  1, 0),
        "Room    - Outline"     = c(0, 0, 0, 0, 0, -1,  0, 1),
        "Room    - Cloud  "     = c(0, 0, 0, 0, 0,  0, -1, 1)
)
comps <- glht(scn.slp, contrast.matrix)
summary(comps, test = adjusted("bonferroni"))

# Output
## Simultaneous Tests for General Linear Hypotheses
##
## Fit: lme.formula(fixed = threshold ~ distance + Scene + distance:Scene,
##     data = threshs, random = ~distance | SubjectNo/Scene, method = "ML",
##     na.action = na.exclude, control = list(opt = "optim"))
##
## Linear Hypotheses:
##                          Estimate Std. Error z value Pr(>|z|)
## Outline - Line    == 0  0.20012    0.08129   2.462   0.0829 .
## Cloud   - Line    == 0  0.37574    0.08157   4.606 2.46e-05 ***
## Room    - Line    == 0  0.43133    0.08172   5.278 7.83e-07 ***
## Cloud   - Outline == 0  0.17562    0.08104   2.167   0.1813
## Room    - Outline == 0  0.23121    0.08113   2.850   0.0262 *
## Room    - Cloud   == 0  0.05559    0.08150   0.682   1.0000
```

```
## ---
## Signif. codes:  0 '***' 0.001 '**' 0.01 '*' 0.05 '.' 0.1 ' ' 1
## (Adjusted p values reported -- bonferroni method)
```

The column `Estimate` shows the estimated difference in slope between any two conditions. The associated *z*- and *p*-values test the hypothesis of whether the difference is different from 0. Here we can see that the slope in the *Line* condition is significantly steeper than in the *Cloud* and *Room* conditions [both Bonferroni *p*s < 0.0001]. The slope in the *Outline* condition is significantly steeper than in the *Room* condition [Bonferroni $p < 0.05$]. There is also a marginal difference between the *Line* and *Outline* conditions [Bonferroni $p = 0.083$].

8.2.2.2 Head orientation

We recorded the head orientation (yaw, pitch and roll) for investigating whether the participants strategically rotated their head in order to facilitate the use of some cues. Here, therefore, the difference in the yaw between the beginning and end of a trial is of the primary interest. The yaw data in the right-shifting trials were flipped around so as to combine with the data from the left-shifting trials. Positive yaw differences indicate that the head was turning to the same direction of the simulated movement, and negative yaw differences the opposite. The data were illustrated in ***Figure 8.12***.

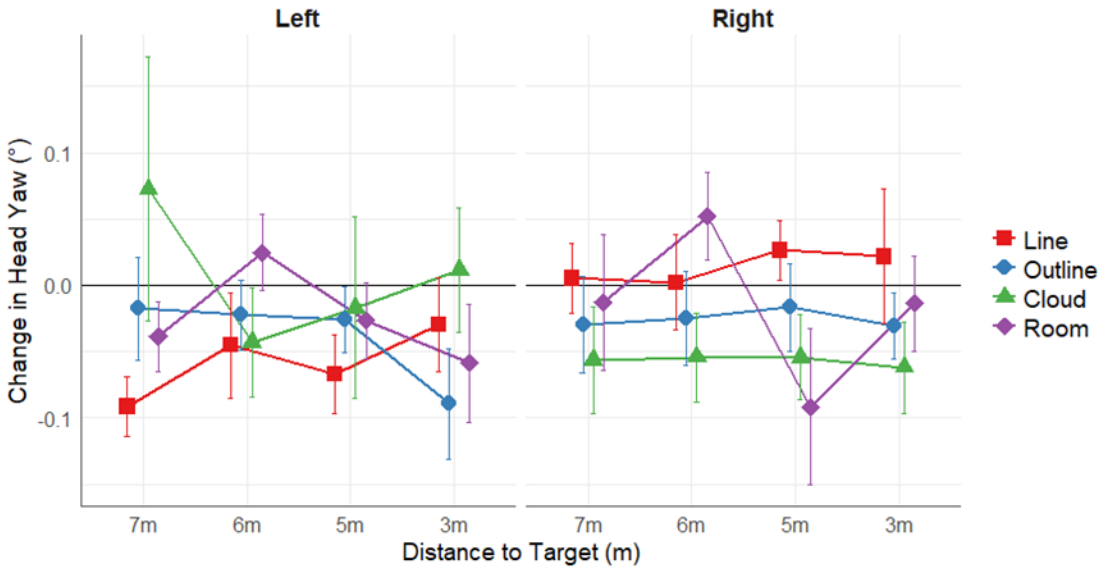

Figure 8.12 *The change of head yaw respectively for the left-shifting (left-handed panel) and right-shifting (right-handed panel) trials. Error bars indicate 95% confidence intervals.*

8.2.2.2.1 Build a growth model

We examined the yaw data as a function of distance from the target (7m, 6m, 4m and 3m), the direction of the simulated movement (right- and leftwards) and cue richness (*Line*, *Outline*, *Cloud* and *Room*). A taxonomy of models was fitted on the yaw data with predictors added in sequentially. On the basis of model `baseline`, model `dst.int` included the level-1 predictor *distance*. Model `dst.slp` included random effects to allow the slopes of the yaw data against distance to vary among participants. Model `scn.int` and `scn.slp` respectively included the level-2 predictor *Scene* and interaction term *Scene* × *distance* so that the effect of cue richness on the magnitude of yaw and slope can be tested. Model `drt.int` and `drt.slp` respectively included the level-2 predictor *Direction* and interaction term *Distance* × *distance* to test the effect of simulation direction on the magnitude of yaw and slope. Model `scn.drt.int` and `scn.drt.slp` respectively included the interaction term *Scene* × *Direction* and *Scene* × *Direction* × *distance* to test the effect of *Scene* × *Direction* interaction on the magnitude of yaw and slope. The R code and output are listed below.

```
# Code
baseline    <- lme(abs_meandYaw ~ 1, random = ~ 1|SubjectNo/Scene/Direction, data
= yaw_diff_means, method = "ML", na.action = na.exclude, control = list(opt="optim
"))

dst.int     <- update(baseline,    .~. + distance)
dst.slp     <- update(dst.int,     random = ~ distance|SubjectNo/Scene/Direction)

scn.int     <- update(dst.slp,     .~. + Scene)
scn.slp     <- update(scn.int,     .~. + Scene : distance)

drt.int     <- update(scn.slp,     .~. + Direction)
drt.slp     <- update(drt.int,     .~. + Direction : distance)

scn.drt.int <- update(drt.slp,     .~. + Scene : Direction)
scn.drt.slp <- update(scn.drt.int, .~. + Scene : Direction : distance)

anova(baseline, dst.int, dst.slp, scn.int, scn.slp, drt.int, drt.slp, scn.
drt.int, scn.drt.slp)

# Output
##             Model df       AIC       BIC   logLik   Test  L.Ratio p-value
## baseline        1  5 -278.9667 -255.2054 144.4834
## dst.int         2  6 -277.6862 -249.1725 144.8431 1 vs 2 0.719435  0.3963
## dst.slp         3 12 -265.6867 -208.6595 144.8434 2 vs 3 0.000564  1.0000
## scn.int         4 15 -259.8828 -188.5988 144.9414 3 vs 4 0.196089  0.9782
## scn.slp         5 18 -257.0048 -171.4639 146.5024 4 vs 5 3.121961  0.3732
## drt.int         6 19 -255.1623 -164.8691 146.5811 5 vs 6 0.157504  0.6915
## drt.slp         7 20 -253.4774 -158.4320 146.7387 6 vs 7 0.315097  0.5746
## scn.drt.int     8 23 -253.5568 -144.2546 149.7784 7 vs 8 6.079459  0.1078
## scn.drt.slp     9 26 -248.7469 -125.1879 150.3735 8 vs 9 1.190102  0.7554
```

As shown in the output, none of the predictors significantly improves the model fit. The results suggest that there was no effect of distance to target, simulation direction or cue richness on the rotation of the head during simulation. It seems that the participants did not rotate their head significantly to help judge the heading of the simulated movement.

8.3 Chapter 4 - Supplementary Materials

8.3.1 Experiment 4.1

8.3.1.1 Target-heading angle as a function of distance

8.3.1.1.1 Building up the growth model

To examine the effect of the target position in the room (*Scene*) on the rate of change in the target-heading angle as a function of distance, *distance* (0.5m ~ 6m from starting point) and *Scene* were respectively added into the model as the level-1 and level-2 predictors. On the basis of model `baseline`, model `distRI` included *distance* and model `distRS` included random slopes. Model `scne.int` included *Scene* and model `scne.slp` included *Scene* × *distance*, respectively for testing the effect of target position on the magnitude of the target-heading angle at 0.5m and slope of target-heading angle against distance. The R code is shown below.

```
# Setting up a baseline model that includes only random intercepts
baseline   <- lme(target-heading_angle ~ 1, random = ~ 1|SubjectNo/Scene, data = o
ffset_trial1, method = "ML", na.action = na.exclude, control = list(opt="optim"))

# Adding distance as the level-1 fixed effect
distRI     <- update(baseline,  .~. + distance)
# Introducing random slopes
distRS     <- update(distRI,    random = ~ distance|SubjectNo/Scene)

# Adding Scene (position of the target in the room) as the level-2 fixed  effect
# Effects of Scene on the intercept
scne.int   <- update(distRS,    .~. + Scene)
# Effects of Scene on the slope
scne.slp   <- update(scne.int,  .~. + Scene : distance)
```

8.3.1.1.2 Model comparisons

Then the models were compared to determine the significance of the predictors. The R code and output are listed below.

```
# Code
anova(baseline, distRI, distRS, scne.int, scne.slp)

# Output
##          Model df      AIC      BIC    logLik   Test   L.Ratio p-value
## baseline     1  4 36648.58 36676.10 -18320.29
```

```
## distRI       2  5 35997.84 36032.23 -17993.92 1 vs 2  652.7450  <.0001
## distRS       3  9 34377.73 34439.63 -17179.86 2 vs 3 1628.1127  <.0001
## scne.int     4 11 34381.69 34457.35 -17179.84 3 vs 4    0.0387  0.9809
## scne.slp     5 13 34384.98 34474.40 -17179.49 4 vs 5    0.7055  0.7028
```

As shown in the output, adding *distance* into the model significantly improved the model fit [$\chi^2(1) = 652.75$, $p < 0.0001$], suggesting that there was an overall trend of decreasing in the magnitude of target-heading angle over the distance. However, adding the interaction term *Scene* × *distance* did not make any significant improvement on the model fit [$\chi^2(2) = 0.71$, $p = 0.70$], suggesting that the decreasing rate did not differ between conditions.

8.3.1.2 Mean target-heading angles of the early and later parts as a function of test trial

8.3.1.2.1 Building the growth model

A taxonomy of models was fitted on the mean target-heading angles that were averaged over the early (0.5m ~ 1m) and late (5.5m ~ 6m) parts. On the basis of model `baseline`, model `TrialRI` included the level-1 predictor *Trial*. Model `TrialRS` included the associated random effects and model `TrialAR` took autocorrelation into account. Model `PartRI` and model `PartRS` included the level-2 predictor *Part* (early and late) and interaction with *Trial*. Model `sceneRI` and model `sceneRS` included the level-2 predictor *Scene* (*Corner*, *Front* and *Oblique*) and interaction with *Trial*. Model `ScenePartI` and model `ScenePartS` included the interaction between the two level-2 predictors *Part* and *Scene* as well as their interaction with *Trial*.

```
# Setting up a baseline model that includes only random intercepts
baseline      <- lme(target-heading_angle ~ 1, random = ~ 1|SubjectNo/Scene/Part,
data = offset.end.long, method = "ML", na.action = na.exclude, control = list(opt
= "optim"))

# Adding Trial as the level-1 fixed effect
TrialRI       <- update(baseline, .~. + Trial)
# Introducing random slopes
TrialRS       <- update(TrialRI,  random = ~ Trial|SubjectNo/Scene/Part)
# Modelling a first-order autoregressive covariance structure
TrialAR       <- update(TrialRS, correlation = corAR1())

# Effects of Part on the intercept
PartRI        <- update(TrialAR,    .~. + Part)
# Effects of Part on the slope
PartRS        <- update(PartRI,     .~. + Part : Trial)

# Effects of Scene on the intercept
sceneRI       <- update(PartRS,     .~. + Scene)
# Effects of Scene on the intercept
sceneRS       <- update(sceneRI,    .~. + Scene : Trial)
```

```
# Effects of interaction on the intercept
ScenePartI    <- update(sceneRS,    .~. + Scene : Part)
# Effects of interaction on the intercept
ScenePartS    <- update(ScenePartI, .~. + Scene : Part : Trial)
```

8.3.1.2.2 Comparing the models

Then we compared the fit of the models for testing the significance of the predictors. The R code and output are listed below.

```
# Code
anova(baseline, TrialRI, TrialRS, TrialAR, PartRI, PartRS, sceneRI, sceneRS, Scene
PartI, ScenePartS)

# Output
##          Model df      AIC      BIC    logLik     Test   L.Ratio p-value
## baseline     1  5 3125.434 3147.197 -1557.717
## TrialRI      2  6 3125.872 3151.988 -1556.936   1 vs 2   1.56259  0.2113
## TrialRS      3 12 3129.625 3181.857 -1552.812   2 vs 3   8.24667  0.2206
## TrialAR      4 13 3126.131 3182.716 -1550.066   3 vs 4   5.49376  0.0191
## PartRI       5 14 3094.817 3155.753 -1533.408   4 vs 5  33.31465  <.0001
## PartRS       6 15 3094.421 3159.710 -1532.210   5 vs 6   2.39592  0.1217
## sceneRI      7 17 3096.994 3170.989 -1531.497   6 vs 7   1.42634  0.4901
## sceneRS      8 19 3093.218 3175.918 -1527.609   7 vs 8   7.77675  0.0205
## ScenePartI   9 21 3095.317 3186.722 -1526.659   8 vs 9   1.90067  0.3866
## ScenePartS  10 23 3095.799 3195.909 -1524.899  9 vs 10   3.51799  0.1722
```

From the output we can see that including *Part* into the model significantly increased the fit [$\chi^2(1) = 33.31$, $p < 0.0001$] of model `PartRI`, suggesting that the mean target-heading angle of the early and late parts differed significantly. Adding the interaction term *Scene* and *Trial* significantly improved the model fit [$\chi^2(2) = 7.78$, $p = 0.021$] of model `sceneRS`, suggesting that the overall rate of change of both early and late parts differed significantly between conditions. Next, we compared the rate of change between conditions respectively for the early and late parts by evaluating estimated slopes in model `ScenePartS`.

8.3.1.2.3 Estimation slope parameters for the early part

The R code and output for evaluating slope estimates of the early parts are shown below. In the output list, the column `Estimate` shows the estimated slope for each condition. Here we can see that the slope was the steepest in the *Front* condition [estimated slope = -0.48]. The associated *z*- and *p*-values indicate that the slope in the *Front* condition is marginally different from 0 [$z = -1.76$, $p = 0.078$].

```
# Code
contrast.matrix <- rbind(
  "Corner - 0"   = c(0, 1, 0, 0, 0, 0, 0, 0, 0, 0, 0, 0),
  "Front  - 0"   = c(0, 1, 0, 0, 0, 0, 1, 0, 0, 0, 0, 0),
  "Oblique - 0"  = c(0, 1, 0, 0, 0, 0, 0, 1, 0, 0, 0, 0)
```

```
)
postHocs <-glht(ScenePartS, contrast.matrix)
summary(postHocs, test = adjusted("none"))

# Output
##   Simultaneous Tests for General Linear Hypotheses
##
## Fit: lme.formula(fixed = target-heading_angle ~ Trial + Part + Scene + Trial:Pa
rt +
##     Trial:Scene + Part:Scene + Trial:Part:Scene, data = offset.end.long,
##     random = ~Trial | SubjectNo/Scene/Part, correlation = corAR1(),
##     method = "ML", na.action = na.exclude, control = list(opt = "optim"))
##
## Linear Hypotheses:
##                   Estimate Std. Error z value Pr(>|z|)
## Corner - 0 == 0   -0.2393     0.2701  -0.886    0.376
## Front  - 0 == 0   -0.4759     0.2701  -1.762    0.078 .
## Oblique - 0 == 0  -0.1823     0.2707  -0.674    0.501
## ---
## Signif. codes:  0 '***' 0.001 '**' 0.01 '*' 0.05 '.' 0.1 ' ' 1
## (Adjusted p values reported -- none method)
```

8.3.1.2.4 Pairwise comparison on the slope parameters for the early part

The R code and output for comparing the slope estimates of the early parts between conditions are shown below. In the output list, the column `Estimate` shows the difference between the estimated slopes. The columns *z*-value and *p*-value can be used for hypothesis tests of whether the difference between the two conditions is different from 0. Here we can see that there was no difference in the estimated slopes for the early parts between conditions.

```
# Code
contrast.matrix <- rbind(
  "Front  - Corner"    = c(0, 0, 0, 0, 0, 0,  1, 0, 0, 0, 0, 0),
  "Oblique - Corner"   = c(0, 0, 0, 0, 0, 0,  0, 1, 0, 0, 0, 0),
  "Oblique - Front"    = c(0, 0, 0, 0, 0, 0, -1, 1, 0, 0, 0, 0)
)
postHocs <-glht(ScenePartS, contrast.matrix)
summary(postHocs, test = adjusted("bonferroni"))

# Output
##   Simultaneous Tests for General Linear Hypotheses
##
## Fit: lme.formula(fixed = target-heading_angle ~ Trial + Part + Scene + Trial:Pa
rt +
##     Trial:Scene + Part:Scene + Trial:Part:Scene, data = offset.end.long,
##     random = ~Trial | SubjectNo/Scene/Part, correlation = corAR1(),
##     method = "ML", na.action = na.exclude, control = list(opt = "optim"))
##
## Linear Hypotheses:
##                       Estimate Std. Error z value Pr(>|z|)
## Front  - Corner == 0  -0.23665    0.36654  -0.646        1
## Oblique - Corner == 0  0.05695    0.36698   0.155        1
## Oblique - Front == 0   0.29360    0.36698   0.800        1
## (Adjusted p values reported -- bonferroni method)
```

8.3.1.2.5 Estimation of slope parameters for the later part

The R code and output for evaluating slope estimates of the late parts are shown below. In the output list, the column `Estimate` shows the estimated slope for each condition. The *z*- and *p*-values can be used for hypothesis tests of whether the estimated slope in the corresponding condition is different from 0.

```
# Code
contrast.matrix <- rbind(
  "Corner - 0"    = c(0, 1, 0, 0, 0, 1, 0, 0, 0, 0, 0, 0),
  "Front  - 0"    = c(0, 1, 0, 0, 0, 1, 1, 0, 0, 0, 1, 0),
  "Oblique - 0"   = c(0, 1, 0, 0, 0, 1, 0, 1, 0, 0, 0, 1)
)
postHocs <-glht(ScenePartS, contrast.matrix)
summary(postHocs, test = adjusted("none"))

# Output
##   Simultaneous Tests for General Linear Hypotheses
##
## Fit: lme.formula(fixed = target-heading_angle ~ Trial + Part + Scene + Trial:Pa
rt +
##     Trial:Scene + Part:Scene + Trial:Part:Scene, data = offset.end.long,
##     random = ~Trial | SubjectNo/Scene/Part, correlation = corAR1(),
##     method = "ML", na.action = na.exclude, control = list(opt = "optim"))
##
## Linear Hypotheses:
##                    Estimate Std. Error z value Pr(>|z|)
## Corner - 0 == 0   -0.1147     0.2701  -0.425  0.67108
## Front  - 0 == 0   -0.4697     0.2701  -1.739  0.08201 .
## Oblique - 0 == 0   0.7210     0.2707   2.664  0.00773 **
## ---
## Signif. codes:  0 '***' 0.001 '**' 0.01 '*' 0.05 '.' 0.1 ' ' 1
## (Adjusted p values reported -- none method)
```

8.3.1.2.6 Pairwise comparison on the slope parameters for the later part

The R code and output for comparing the slope estimates of the late parts between conditions are shown below. In the output list, the column `Estimate` shows the difference in the estimated slopes between the two conditions in the corresponding comparison. The columns *z*-value and *p*-value can be used for hypothesis tests of whether the difference between the two conditions is different from 0.

```
# Code
contrast.matrix <- rbind(
  "Front  - Corner"    = c(0, 0, 0, 0, 0, 0, 1, 0, 0, 0, 1, 0),
  "Oblique - Corner"   = c(0, 0, 0, 0, 0, 0, 0, 1, 0, 0, 0, 1),
  "Oblique - Front"    = c(0, 0, 0, 0, 0, 0, -1, 1, 0, 0, -1, 1)
)
postHocs <-glht(ScenePartS, contrast.matrix) #, linfct = mcp(ExpNo = "Tukey"))
summary(postHocs, test = adjusted("bonferroni"))
```

```
# Output
##   Simultaneous Tests for General Linear Hypotheses
##
## Fit: lme.formula(fixed = target-heading_angle ~ Trial + Part + Scene + Trial:Pa
rt +
##     Trial:Scene + Part:Scene + Trial:Part:Scene, data = offset.end.long,
##     random = ~Trial | SubjectNo/Scene/Part, correlation = corAR1(),
##     method = "ML", na.action = na.exclude, control = list(opt = "optim"))
##
## Linear Hypotheses:
##                         Estimate Std. Error z value Pr(>|z|)
## Front  - Corner == 0   -0.3550     0.3665  -0.969  0.99837
## Oblique - Corner == 0   0.8356     0.3670   2.277  0.06835 .
## Oblique - Front == 0    1.1906     0.3670   3.244  0.00353 **
## ---
## Signif. codes:  0 '***' 0.001 '**' 0.01 '*' 0.05 '.' 0.1 ' ' 1
## (Adjusted p values reported -- bonferroni method)
```

8.3.2 Experiment 4.2

8.3.2.1 Target-heading angle as a function of distance

8.3.2.1.1 Building up the growth model

To examine the effect of target distance (*Scene*) on the rate of change in the target-heading angle as a function of distance, *distance* (0.5m ~ 6m from starting point) and *Scene* (Near and Far) were respectively added into the model as the level-1 and level-2 predictors. On the basis of model `baseline`, model `distRI` included *distance* and model `distRS` included random slopes. Model `scne.int` included *Scene* and model `scne.slp` included *Scene* × *distance*, respectively for testing the effect of target distance on the magnitude of the target-heading angle at 0.5m and slope of target-heading angle against distance. The R code is shown below.

```
# Setting up a baseline model that includes only random intercepts
baseline   <- lme(target-heading_angle ~ 1, random = ~ 1|SubjectNo/Scene, data = o
ffset_trial1, method = "ML", na.action = na.exclude, control = list(opt="optim"))

# Adding "distance" as the level-1 fixed effect
distRI     <- update(baseline,  .~. + distance)
# Introducing random slopes
distRS     <- update(distRI,    random = ~ distance|SubjectNo/Scene)

# Adding Scene (landmark layout) as the level-2 fixed effect
# Effects of Scene on the intercept
scne.int   <- update(distRS,    .~. + Scene)
# Effects of Scene on the slope
scne.slp   <- update(scne.int,  .~. + Scene : distance)
```

8.3.2.1.2 Comparing the models

Then we made a decision about the significance of each predictor. This was done using the likelihood-ratio test that compares -2LL (minus 2 times the log-likelihood) between the models before and after including the predictor. The R code and output for the model comparisons are listed below. In the output list, the first column shows the name of the model. The column `logLik` shows the magnitude of log-likelihood of the model. The column `L.Ratio` shows the -2LL between the current model and the previous model before the predictor was added in. The *p*-values can be used to determine whether the improvement of model fit is significant. Here we can see that model `scne.slp` is marginally better than model `scne.int` [$\chi^2(1) = 2.92$, $p = 0.088$], suggesting that target distance has an effect on the rate of change in the target-heading angle against distance.

```
# Code
anova(baseline, distRI, distRS, scne.int, scne.slp)

# Output
##          Model df      AIC      BIC    logLik   Test   L.Ratio p-value
## baseline     1  4 23459.12 23485.03 -11725.56
## distRI       2  5 22843.75 22876.13 -11416.88 1 vs 2  617.3696  <.0001
## distRS       3  9 21605.55 21663.83 -10793.78 2 vs 3 1246.2008  <.0001
## scne.int     4 10 21607.25 21672.01 -10793.62 3 vs 4    0.3040  0.5814
## scne.slp     5 11 21606.33 21677.56 -10792.17 4 vs 5    2.9178  0.0876
```

8.3.2.1.3 Parameters in the model scne.slp

To see how the two conditions (Near and Far) differed in the rate of change in target-heading angle over distance (0.5m ~ 6m), we examined the model parameters estimated. The R code to show the parameter estimates and the output is listed below. In the output list, the column `Value` shows the estimated values of the model parameters. The column `t-value` and `p-value` can be used for hypothesis tests of whether the corresponding estimated parameter is different from 0. As the Far condition was the reference condition, the rows `Intercept` and `distance` show the estimated intercept (target-heading angle at 0.5m) and slope (rate of change) in the Far condition. The row `Near` and `distance:Near` respectively show the difference in the estimated intercept and slope between the Near and Far condition. Here we can see that the slope of the Far condition is significantly different from 0 [estimated slope = -0.41, t = -2.53, $p = 0.011$], and there is a marginal difference in slope between the Near and Far conditions [estimated difference = -0.38, t = -1.78, $p = 0.075$].

```
# Code
summary(scne.slp, corr = FALSE)
```

```
# Output
## Fixed effects: target-heading_angle ~ distance + Scene + distance:Scene
##                         Value   Std.Error    DF    t-value   p-value
## (Intercept)         8.993957   0.7267292  4747  12.375941    0.0000
## distance           -0.407102   0.1606113  4747  -2.534703    0.0113
## Near                0.640817   1.0252988    23   0.625005    0.5381
## distance:Near      -0.377906   0.2123493  4747  -1.779644    0.0752
```

8.3.2.2 Mean target-heading angles of the early and later parts as a function of test trial

8.3.2.2.1 Building the growth model

A taxonomy of models was fitted on the mean target-heading angles that were averaged over the early (0.5m ~ 1m) and late (5.5m ~ 6m) parts. On the basis of model `baseline`, model `TrialRI` included the level-1 predictor *Trial*. Model `TrialRS` included the associated random effects and model `TrialAR` took autocorrelation into account. Model `PartRI` and model `PartRS` included the level-2 predictor *Part* (early and late) and interaction with *Trial*. Model `sceneRI` and model `sceneRS` included the level-2 predictor *Scene* (Near and Far) and interaction with *Trial*. Model `ScenePartI` and model `ScenePartS` included the interaction between the two level-2 predictors *Part* and *Scene* as well as their interaction with *Trial*.

```
# Setting up a baseline model that includes only random intercepts
baseline      <- lme(target-heading_angle ~ 1, random = ~1|SubjectNo/Scene/Part, d
ata = offset.end.long, method = "ML", na.action = na.exclude, control = list(opt =
 "optim"))

# Adding Trial as the level-1 fixed effect
TrialRI       <- update(baseline, .~. + Trial)
# Introducing random slopes
TrialRS       <- update(TrialRI,  random = ~ Trial|SubjectNo/Scene/Part)
# Modelling a first-order autoregressive covariance structure
TrialAR       <- update(TrialRS, correlation = corAR1())

# Effects of Part on the intercept
PartRI        <- update(TrialAR,    .~. + Part)
# Effects of Part on the slope
PartRS        <- update(PartRI,     .~. + Part : Trial)

# Effects of Scene on the intercept
sceneRI       <- update(PartRS,     .~. + Scene)
# Effects of Scene on the intercept
sceneRS       <- update(sceneRI,    .~. + Scene : Trial)

# Effects of interaction on the intercept
ScenePartI    <- update(sceneRS,    .~. + Scene : Part)
# Effects of interaction on the intercept
ScenePartS    <- update(ScenePartI, .~. + Scene : Part : Trial)
```

8.3.2.2.2 Comparing the models

Then we compared the fit of the models for testing the significance of the predictors. The R code and output are listed below. In the output list, the first column shows the name of the model. The column `logLik` shows the magnitude of log-likelihood of the model. The column `L.Ratio` shows the -2LL between the current model and the previous model before the predictor was added in. The *p*-values can be used to determine whether the improvement of model fit is significant. Here we can see that model `PartRI` and `PartRS` are significantly better than the previous one, suggesting an effect of *Part* (early and late) on the intercept (magnitude of the target-heading angle at 0.5m) and slope (rate of change as a function of distance).

```
# Code
anova(baseline0, baseline, TrialRI, TrialRS, TrialAR, PartRI, PartRS, sceneRI, sce
neRS, ScenePartI, ScenePartS)

# Output
##            Model df      AIC      BIC    logLik     Test  L.Ratio p-value
## baseline     1    5 2068.398 2088.099 -1029.199
## TrialRI      2    6 2069.967 2093.608 -1028.984   1 vs 2  0.43133  0.5113
## TrialRS      3   12 2078.055 2125.337 -1027.027   2 vs 3  3.91250  0.6885
## TrialAR      4   13 2074.856 2126.078 -1024.428   3 vs 4  5.19890  0.0226
## PartRI       5   14 2050.827 2105.990 -1011.414   4 vs 5 26.02851  <.0001
## PartRS       6   15 2047.944 2107.046 -1008.972   5 vs 6  4.88363  0.0271
## sceneRI      7   16 2048.156 2111.198 -1008.078   6 vs 7  1.78786  0.1812
## sceneRS      8   17 2050.141 2117.124 -1008.071   7 vs 8  0.01470  0.9035
## ScenePartI   9   18 2050.296 2121.219 -1007.148   8 vs 9  1.84507  0.1744
## ScenePartS  10   19 2052.290 2127.153 -1007.145  9 vs 10  0.00586  0.9390
```

8.3.2.2.3 Separate one-sample tests on the slope parameters

The slopes of the early part in the two conditions were assessed by evaluating the estimated slope parameters in the model `ScenePartS`. The R code and output are shown below. In the output list, the column `Estimate` shows the estimated slope of the early part for each condition. The *z*- and *p*-values can be used for hypothesis tests of whether the estimated slope in the corresponding condition is different from 0.

```
# Code
contrast.matrix <- rbind(
  "Far - 0"   = c(0, 1, 0, 0, 0, 0, 0, 0),
  "Near  - 0" = c(0, 1, 0, 0, 0, 1, 0, 0)
)
postHocs <-glht(ScenePartS, contrast.matrix)
summary(postHocs, test = adjusted("none"))

# Output
##   Simultaneous Tests for General Linear Hypotheses
##
## Fit: lme.formula(fixed = meanErr ~ Trial + Part + Scene + Trial:Part +
```

```
##     Trial:Scene + Part:Scene + Trial:Part:Scene, data = offset.end.long,
##     random = ~Trial | SubjectNo/Scene/Part, correlation = corAR1(),
##     method = "ML", na.action = na.exclude, control = list(opt = "optim"))
##
## Linear Hypotheses:
##                Estimate Std. Error z value Pr(>|z|)
## Far - 0 == 0    -0.2953     0.2686  -1.100    0.272
## Near  - 0 == 0  -0.3782     0.2648  -1.428    0.153
## (Adjusted p values reported -- none method)
```

8.4 Chapter 5 - Supplementary Materials

8.4.1 Experiment 5.1

8.4.1.1 Mean target-heading angle as a function of distance

8.4.1.1.1 Building the growth model

A taxonomy of models was fitted on the mean target-heading angles averaged over Trial 1 ~ 5 as a function of distance (0.5m ~ 6m). On the basis of model `baseline`, model `dstRI` included the level-1 predictor *distance* and model included random slopes. Model `fmlMI` included the level-2 predictor *Familiarity* and model `fmlMS` included the interaction term *Familiarity* × *distance*. The former tests the effect of *Familiarity* on the magnitude of the mean target-heading angle at 0.5m (intercept) and the latter tests the effect of *Familiarity* on the slope of target-heading angle as a function of distance.

```
# Setting up a baseline model that includes only random intercepts
baseline      <- lme(target-heading-angle ~ 1, random = ~ 1 | SubjectNo, data = of
fset.mean, method = "ML", na.action = na.exclude, control = list(opt = "optim"))

# Adding distance as the level-1 fixed effect
dstRI       <- update(baseline, .~. + distance )
dstRS       <- update(dstRI, random = ~ distance |SubjectNo)

# Effects of Familiarity on the intercept
fmlMI     <- update(dstRS,     .~. + Familiarity)
# Effects of Familiarity on the slope
fmlMS     <- update(fmlMI,     .~. + Familiarity : distance)
```

8.4.1.1.2 Comparing the models

Then we compared the fit of the models for testing the significance of the predictors. The R code and output are listed below. In the output list, the first column shows the name of the model. The column `logLik` shows the magnitude of log-likelihood of the model. The larger the number is, the better the model fit. The column `L.Ratio` shows the -2LL between the current model and the previous model before the predictor was added in, which is used here as an index of improvement of model fit. The *p*-values can be used to determine whether

the improvement of model fit is significant. Here we can see that adding *distance* (model `dstRI`) and *Familiarity* (model `fmlMI`) improves the model fit. However, adding the interaction term *Familiarity* × *distance* did not improve the model fit, suggesting no difference in slope between the Familiar and Unfamiliar groups.

```
# Code
anova(baseline, dstRI, dstRS, fmlMI, fmlMS)

# Output
##          Model df      AIC      BIC    logLik   Test  L.Ratio p-value
## baseline     1  3 8541.162 8558.511 -4267.581
## dstRI        2  4 8488.586 8511.719 -4240.293 1 vs 2  54.5751  <.0001
## dstRS        3  6 7521.895 7556.594 -3754.948 2 vs 3 970.6915  <.0001
## fmlMI        4  7 7517.201 7557.683 -3751.600 3 vs 4   6.6941  0.0097
## fmlMS        5  8 7518.937 7565.203 -3751.469 4 vs 5   0.2636  0.6076
```

8.4.1.2 Mean target-heading angle as a function of test trial

8.4.1.2.1 Building the growth model

A taxonomy of models was fitted on the mean target-heading angles as a function of trial. On the basis of model `baseline`, model `TrialRI` included the level-1 predictor *Trial*[12]. Model `fml.int` included the level-2 predictor *Familiarity* and model `fml.slp` included the interaction term *Familiarity* × *Trial*. The former tests the effect of *Familiarity* on the magnitude of mean target-heading angle in Trial 1 and the latter tests the effect of *Familiarity* on the slope of target-heading angle as a function of trial.

```
# Setting up a baseline model that includes only random intercepts
baseline      <- lme(target-heading_angle ~ 1, random = ~ 1 | SubjectNo, data = of
fset.err.long, method = "ML", na.action = na.omit)

# Adding Trial as the level-1 fixed effect
TrialRI       <- update(baseline,  .~. + Trial)
# Effects of Familiarity on the intercept
fml.int       <- update(TrialRI, .~. + Familiarity)
# Effects of Familiarity on the slope
fml.slp       <- update(fml.int,  .~. + Familiarity : Trial)
```

8.4.1.2.2 Comparing the models

Then we compared the fit of the models for testing the significance of the predictors. The R code and output are listed below. In the output list, the first column shows the name of the model. The column `logLik` shows the magnitude of log-likelihood of the model. The

[12] Because adding random slopes did not improve the model fit, for parsimony, we excluded random slopes from the growth model.

column `L.Ratio` shows the -2LL between the current model and the previous model before the predictor was added in. The *p*-values can be used to determine whether the improvement of model fit is significant. Here we can see that adding *Trial* (model `TrialRI`) and *Familiarity* (model `fml.int`) improves the model fit.

```
# Code
anova(baseline, TrialRI, fml.int, fml.slp)

# Output
##           Model df      AIC      BIC    logLik   Test  L.Ratio p-value
## baseline      1  3 553.9547 562.3171 -273.9773
## TrialRI       2  4 547.4112 558.5612 -269.7056 1 vs 2  8.54342  0.0035
## fml.int       3  5 546.6419 560.5794 -268.3210 2 vs 3  2.76930  0.0961
## fml.slp       4  6 548.6197 565.3446 -268.3098 3 vs 4  0.02227  0.8814
```

8.4.2 Experiment 5.2

8.4.2.1 Mean target-heading angle as a function of distance

8.4.2.1.1 Building the model

A taxonomy of models was fitted on the mean target-heading angles as a function of walking distance (0.5m ~ 6m). On the basis of model `baseline`, model `dstRI` included the level-1 predictor *distance* and model `dstRS` introduced random slopes. Model `fml.int` included the level-2 predictor *Familiarity* and model `fml.slp` included the interaction term *Familiarity* × *distance*. Model `cue.int` included the level-2 predictor *Cue* (Dark, Strobe and Lit) and model `cue.slp` included its interaction with *distance*. Model `fml.cue.int` included the *Familiarity* × *distance* interaction and model `fml.cue.slp` included the three-way interaction *Familiarity* × *Cue* × *distance* for testing the differential effect of familiarity on the slope depending on cue availability.

```
baseline     <- lme(headingErr ~ 1, random = ~1|SubjectNo, data = offset.long, met
hod = "ML", na.action = na.exclude, control = list(opt = "optim"))

# Adding distance as the level-1 fixed effect
dstRI        <- update(baseline,    .~. + distance)
dstRS        <- update(dstRI, random = ~ distance|SubjectNo)

# Effect of Familiarity on the intercept
fml.int      <- update(dstRS,       .~. + Familiarity)
# Effect of Familiarity on the Slope
fml.slp      <- update(fml.int,     .~. + Familiarity : distance)

# Effect of cue availability on the intercept
cue.int      <- update(fml.slp,     .~. + Cue)
# Effect of cue availability on the Slope
cue.slp      <- update(cue.int,     .~. + Cue : distance)

# Interaction on the intercept
fml.cue.int  <- update(cue.slp,     .~. + Familiarity : Cue)
```

```r
# Interaction on the slope
fml.cue.slp  <- update(fml.cue.int, .~. + Familiarity : Cue : distance)
```

8.4.2.1.2 Compare the models

The R code and output for model comparisons are listed below. In the output list, the first column shows the name of the model. The column `logLik` shows the magnitude of log-likelihood of the model. The column `L.Ratio` shows the -2LL between the current model and the previous model before the predictor was added in. The *p*-values can be used to determine whether the improvement of model fit is significant.

```r
# Code
anova(baseline, dstRI, dstRS, fml.int, fml.slp, cue.int, cue.slp, fml.cue.int, fml
.cue.slp)

# Output
##             Model df      AIC      BIC    logLik   Test  L.Ratio p-value
## baseline        1  3 176143.1 176168.5 -88068.53
## dstRI           2  4 174798.8 174832.7 -87395.37 1 vs 2 1346.311  <.0001
## dstRS           3  6 169718.5 169769.5 -84853.27 2 vs 3 5084.212  <.0001
## fml.int         4  7 169719.6 169779.1 -84852.82 3 vs 4    0.902  0.3423
## fml.slp         5  8 169720.9 169788.8 -84852.46 4 vs 5    0.716  0.3976
## cue.int         6 10 169700.0 169784.9 -84840.01 5 vs 6   24.890  <.0001
## cue.slp         7 12 169700.2 169802.0 -84838.09 6 vs 7    3.857  0.1454
## fml.cue.int     8 14 169699.2 169818.1 -84835.62 7 vs 8    4.927  0.0851
## fml.cue.slp     9 16 169701.6 169837.4 -84834.78 8 vs 9    1.676  0.4326
```

8.4.2.1.3 Parameter estimates in the model fml.cue.int

The R code and output for showing the estimated parameters in the final model `fml.cue.int` is shown below. In the output above, the column named *`Value`* shows the estimated value of the parameter. The columns named *`t-value`* and *`p-value`* show the result of the hypothesis test on the parameter. If the *p*-value reaches the threshold ($\alpha = 0.05$), it is suggested that the parameter estimate is different from 0. Here the Dark-Familiar condition is the reference condition, therefore the rows `Intercept` and `distance` show the estimates of the intercept and slope in the Dark-Familiar condition. The rows below show the estimates of the difference in the intercept and slope between the Dark-Familiar condition and other conditions.

```r
# Code
summary(fml.cue.int, corr = FALSE)

# Output
## Fixed effects: headingErr ~ distance + Familiarity + Cue + distance:Familiarity
 +      distance:Cue + Familiarity:Cue
##                                    Value Std.Error    DF   t-value   p-value
## (Intercept)                     5.985018 0.5517343 35857 10.847645    0.0000
```

```
## distance                        -0.195048 0.1483862 35857 -1.314464    0.1887
## Unfamiliar                       1.626211 0.7466591    66  2.177984    0.0330
## Lit                             -1.204657 0.7636395    66 -1.577521    0.1195
## Strobe                           0.481590 0.7636432    66  0.630648    0.5304
## distance: Unfamiliar             0.129219 0.1483846 35857  0.870840    0.3838
## distance:Lit                    -0.335111 0.1817343 35857 -1.843964    0.0652
## distance:Strobe                 -0.285451 0.1817330 35857 -1.570718    0.1163
## Unfamiliar:Lit                  -2.142856 1.0061833    66 -2.129687    0.0369
## Unfamiliar:Strobe               -1.784672 1.0061851    66 -1.773701    0.0807
```

8.4.2.1.4 Estimation of slope parameters

Here we examined the estimated average slope between the Familiar and Unfamiliar groups for each cue condition (Dark, Strobe and Lit). This was also done by creating a contrast matrix using *multcomp* package (Hothorn et al., 2008). The R code and output are shown below. In the output list, the column `Estimate` shows the estimated slope of each condition. The *z*- and *p*-values are the results of hypothesis tests of whether the estimated slope in the corresponding condition is different from 0. Here we can see that except the Dark condition, both Strobe and Lit conditions have a significant negative slope.

```
# Code
contrast.matrix <- rbind(
  "Dark"              = c(0, 1, 0, 0, 0, 0.5, 0, 0, 0, 0),
  "Strobe"            = c(0, 1, 0, 0, 0, 0.5, 0, 1, 0, 0),
  "Lit"               = c(0, 1, 0, 0, 0, 0.5, 1, 0, 0, 0)
)
postHocs <-glht(fml.cue.int, contrast.matrix)
summary(postHocs, test = adjusted("none"))

# Output
##   Simultaneous Tests for General Linear Hypotheses
##
## Fit: lme.formula(fixed = headingErr ~ distance + Familiarity + Cue +
##     distance:Familiarity + distance:Cue + Familiarity:Cue, data = offset.long,
##     random = ~distance | SubjectNo, method = "ML", na.action = na.exclude,
##     control = list(opt = "optim"))
##
## Linear Hypotheses:
##             Estimate Std. Error z value Pr(>|z|)
## Dark == 0    -0.1304     0.1285  -1.015 0.310018
## Strobe == 0  -0.4159     0.1285  -3.237 0.001209 **
## Lit == 0     -0.4656     0.1285  -3.623 0.000291 ***
## ---
## Signif. codes:  0 '***' 0.001 '**' 0.01 '*' 0.05 '.' 0.1 ' ' 1
## (Adjusted p values reported -- none method)
```

8.4.2.2 Mean target-heading angle as a function of test trials

8.4.2.2.1 Building the model

A taxonomy of models was fitted on the mean target-heading angles as a function of trial (1 ~ 5). On the basis of model `baseline`, model `trialM` included the level-1 predictor *Trial*. Model `trialMS` introduced random slopes and model `trialMAR` took autocorrelation into account. Model `fml.int` included the level-2 predictor *Familiarity* and model `fml.slp` included the interaction term *Familiarity* × *Trial*. Model `cue.int` included the level-2 predictor *Cue* (Dark, Strobe and Lit) and model `cue.slp` included its interaction with *Trial*. The former tests the difference in the intercept or magnitude of the target-heading angle between Dark, Strobe and Lit condition; and the latter tests the difference in slope between the three conditions. Model `fml.cue.int` included the *Familiarity* × *Trial* interaction and model `fml.cue.slp` included the three-way interaction *Familiarity* × *Cue* × *Trial* for testing the differential effect of familiarity on the slope depending on cue availability.

```
baseline      <- lme(target-heading_angle ~ 1, random = ~ 1 | SubjectNo, data = of
fset.err.long,  method = "ML", na.action = na.omit)

trialM        <- update(baseline, .~. + Trial)
trialMS       <- update(trialM,   random = ~ Trial|SubjectNo, control = list(opt =
 "optim", maxIter = 500))
trialMAR      <- update(trialMS,  correlation = corAR1())

# Effect of Familiarity on the intercept
fml.int       <- update(trialMAR,     .~. + Familiarity)
# Effect of Familiarity on the Slope
fml.slp       <- update(fml.int,      .~. + Familiarity : Trial)

# Effect of cue availability on the intercept
cue.int       <- update(fml.slp,      .~. + Cue)
# Effect of cue availability on the Slope
cue.slp       <- update(cue.int,      .~. + Cue : Trial)

# Interaction on the intercept
fml.cue.int   <- update(cue.slp,      .~. + Familiarity : Cue)
# Interaction on the slope
fml.cue.slp   <- update(fml.cue.int,  .~. + Familiarity : Cue : Trial)
```

8.4.2.2.2 Compare the models

The R code and output for model comparisons are listed below. In the output list, the first column shows the name of the model. The column `logLik` shows the magnitude of log-likelihood of the model. The column `L.Ratio` shows the -2LL between the current model and the previous model before the predictor was added in. The *p*-values can be used to determine whether the improvement of model fit is significant. Here we can see that both model

`cue.int` and model `cue.slp` are significantly better than the previous one, suggesting that both magnitude of target-heading angle in Trial 1 and rate of change in target-heading angle across trials varied as a function of cue availability.

```
# Code
anova(baseline, trialM, trialMS, trialMAR, fml.int, fml.slp, cue.int, cue.slp, fml
.cue.int, fml.cue.slp)

# Output
##          Model df      AIC      BIC    logLik    Test   L.Ratio p-value
## baseline     1  3 1562.290 1573.948 -778.1451
## trialM       2  4 1563.202 1578.746 -777.6010  1 vs 2    1.0882  0.2969
## trialMS      3  6 1567.142 1590.459 -777.5713  2 vs 3    0.0594  0.9707
## trialMAR     4  7 1539.852 1567.054 -762.9258  3 vs 4   29.2909  <.0001
## fml.int      5  8 1540.467 1571.556 -762.2338  4 vs 5    1.3840  0.2394
## fml.slp      6  9 1542.039 1577.014 -762.0194  5 vs 6    0.4286  0.5126
## cue.int      7 11 1519.339 1562.086 -748.6696  6 vs 7   26.6997  <.0001
## cue.slp      8 13 1511.761 1562.281 -742.8806  7 vs 8   11.5779  0.0031
## fml.cue.int  9 15 1513.469 1571.761 -741.7348  8 vs 9    2.2916  0.3180
## fml.cue.slp 10 17 1515.257 1581.321 -740.6285 9 vs 10    2.2125  0.3308
```

8.4.2.2.3 Estimation of slope parameters

Here we examined the estimated average slope between the Familiar and Unfamiliar groups for each cue condition (Dark, Strobe and Lit) by evaluating the parameter estimates in model `cue.slp`. The R code and output are shown below. In the output list, the column `Estimate` shows the estimated slope of each condition. The *z*- and *p*-values are the results of hypothesis tests of whether the estimated slope in the corresponding condition is different from 0. Here we can see that target-heading angle only decreased significantly in the Dark condition.

```
# Code
contrast.matrix <- rbind(
  "Dark"   = c(0, 1, 0, 0, 0, 0, 0, 0),
  "Strobe" = c(0, 1, 0, 0, 0, 0, 0, 1),
  "Lit"    = c(0, 1, 0, 0, 0, 0, 1, 0)
)
postHocs <-glht(cue.slp, contrast.matrix)
summary(postHocs, test = adjusted("none"))

# Output
##   Simultaneous Tests for General Linear Hypotheses
##
## Fit: lme.formula(fixed = meanErr ~ Trial + Familiarity + Cue + Trial:Familiarit
y +
##     Trial:Cue, data = offset.err.long, random = ~Trial | SubjectNo,
##     correlation = corAR1(), method = "ML", na.action = na.omit,
##     control = list(opt = "optim", maxIter = 500))
##
## Linear Hypotheses:
##             Estimate Std. Error z value Pr(>|z|)
## Dark == 0   -0.29607    0.10950  -2.704  0.00686 **
```

```
## Strobe == 0  0.15793    0.10950   1.442  0.14924
## Lit == 0     0.05331    0.10950   0.487  0.62639
## ---
## Signif. codes:  0 '***' 0.001 '**' 0.01 '*' 0.05 '.' 0.1 ' ' 1
## (Adjusted p values reported -- none method)
```

8.4.2.2.4 Pairwise comparison on the slope estimates between the conditions

Then we created another contrast matrix and ran on the parameter estimates in model `cue.slp` for pairwise comparison on the average slopes between the Dark, Strobe and Lit conditions. The R code and output are shown below. In the output list, the column `Estimate` shows the estimated difference in slope between the two conditions in the comparison. The *z*- and *p*-values are the results of hypothesis tests of whether the estimated difference is different from 0.

```
# Code
contrast.matrix <- rbind(
  "Strobe - Dark"   = c(0, 0, 0, 0, 0, 0, 0, 1),
  "Lit - Dark"      = c(0, 0, 0, 0, 0, 0, 1, 0),
  "Strobe - Lit"    = c(0, 0, 0, 0, 0, 0, -1, 1)
)
postHocs <-glht(cue.slp, contrast.matrix)
summary(postHocs, test = adjusted("bonferroni"))

# Output
##   Simultaneous Tests for General Linear Hypotheses
##
## Fit: lme.formula(fixed = meanErr ~ Trial + Familiarity + Cue + Trial:Familiarit
y +
##     Trial:Cue, data = offset.err.long, random = ~Trial | SubjectNo,
##     correlation = corAR1(), method = "ML", na.action = na.omit,
##     control = list(opt = "optim", maxIter = 500))
##
## Linear Hypotheses:
##                     Estimate Std. Error z value Pr(>|z|)
## Strobe - Dark == 0   0.4540     0.1341   3.385  0.00213 **
## Lit - Dark == 0      0.3494     0.1341   2.605  0.02756 *
## Strobe - Lit == 0    0.1046     0.1341   0.780  1.00000
## ---
## Signif. codes:  0 '***' 0.001 '**' 0.01 '*' 0.05 '.' 0.1 ' ' 1
## (Adjusted p values reported -- bonferroni method)
```

8.4.3 Experiment 5.3

8.4.3.1 Mean target-heading angle as a function of distance

8.4.3.1.1 Building the growth model

A taxonomy of models was fitted on the mean target-heading angles averaged over Trial 1 ~ 5 as a function of distance (0.5m ~ 6m) in the *Strobe* condition. On the basis of

model `baseline`, model `dstRI` included the level-1 predictor *distance* and model `dstRS` included random effects. Model `fmlMI` included the level-2 predictor *Familiarity* and model `fmlMS` included the interaction term *Familiarity* × *distance*. The former tests the effect of *Familiarity* on the magnitude of the mean target-heading angle at 0.5m and the latter tests the effect of *Familiarity* on the slope of target-heading angle as a function of distance. Model `dspMI` included the level-2 predictor *Drift* (Continuous and Intermittent) and model `dspMS` included the interaction term *Drift* × *distance*. The former tests the effect of target drift on the magnitude of the target-heading angle at 0.5m and the latter tests the effect of target drift on the rate of change in target-heading angle against distance. Model `intMI` and model `intMS` included the interaction *Familiarity* × *Drift* and *Familiarity* × *Drift* × *distance*, testing the effects of the interaction on the magnitude of the target-heading angle at 0.5m (intercept) and rate of change (slope) respectively.

```
# Setting up a baseline model that includes only random intercepts
baseline    <- lme(target-heading_angle ~ 1, random = ~1|SubjectNo, data = offset.
mean, method = "ML", na.action = na.exclude, control = list(opt = "optim"))

# Adding distance as the level-1 fixed effect
dstRI       <- update(baseline,  .~. + distance)
dstRS       <- update(dstRI,     random = ~ distance |SubjectNo)

# Effect of Familiarity on the intercept
fmlMI       <- update(dstRS,     .~. + Familiarity)
# Effect of Familiarity on the Slope
fmlMS       <- update(fmlMI,     .~. + Familiarity : distance)

# Effect of Drift on the intercept
dspMI       <- update(fmlMS,     .~. + Drift)
# Effect of Drift on the slope
dspMS       <- update(dspMI,     .~. + Drift : distance)

# Interaction on the intercept
intMI       <- update(dspMS,     .~. + Familiarity : Drift)
# Interaction on the slope
intMS       <- update(intMI,     .~. + Familiarity : Drift : distance)
```

8.4.3.1.2 Comparing the models

We compared the models for effects of predictors. The R code and output for model comparisons are listed below. In the output list, the first column shows the name of the model. The column `logLik` shows the magnitude of log-likelihood of the model. The column `L.Ratio` shows the -2LL between the current model and the previous model before the predictor was added in. The *p*-values can be used to determine whether the improvement of model fit is significant.

```
# Code
anova(baseline, dstRI, dstRS, fmlMI, fmlMS, dspMI, dspMS, intMI, intMS)

# Output
##          Model df      AIC      BIC    logLik   Test   L.Ratio p-value
## baseline     1  3 19513.69 19533.12 -9753.846
## dstRI        2  4 18904.63 18930.53 -9448.314 1 vs 2  611.0636  <.0001
## dstRS        3  6 16281.73 16320.59 -8134.866 2 vs 3 2626.8960  <.0001
## fmlMI        4  7 16280.68 16326.01 -8133.338 3 vs 4    3.0551  0.0805
## fmlMS        5  8 16282.45 16334.26 -8133.223 4 vs 5    0.2307  0.6310
## dspMI        6  9 16282.04 16340.33 -8132.020 5 vs 6    2.4067  0.1208
## dspMS        7 10 16283.97 16348.73 -8131.983 6 vs 7    0.0733  0.7866
## intMI        8 11 16282.91 16354.15 -8130.457 7 vs 8    3.0520  0.0806
## intMS        9 12 16284.86 16362.57 -8130.428 8 vs 9    0.0583  0.8092
```

8.4.3.2 Mean target-heading angle as a function of trial

8.4.3.2.1 Building the model

A taxonomy of models was fitted on the mean target-heading angles as a function of trial (1 ~ 5). On the basis of model `baseline`, model `trialM` included the level-1 predictor *Trial*. Model `trialMS` introduced random slopes and model `trialMAR` took autocorrelation into account. Model `fml.int` included the level-2 predictor *Familiarity* (Familiar and Unfamiliar) and model `fml.slp` included the interaction term *Familiarity* × *Trial*. Model `drf.int` included the level-2 predictor *Drift* (Continuous and Intermittent) for effects of target drift on the magnitude of target-heading angle in Trial 1 (intercept) and model `drf.slp` included the interaction term *Drift* × *Trial* for effects of target drift on the rate of change in target-heading angle across trials (slope). Model `cue.int` included the level-2 predictor *Cue* (Dark and Strobe) and model `cue.slp` included its interaction with *Trial*. The rest of the models included interaction terms one by one for effects of interactions between level-2 predictors on the magnitude of target-heading angle or the rate of change (if *Trial* was involved in the interaction term).

```
baseline       <- lme(target-heading_angle ~ 1, random = ~ 1 | SubjectNo, data = o
ffset.err.long,  method = "ML", na.action = na.omit)

trialM         <- update(baseline, .~. + Trial)
trialMS        <- update(trialM,   random = ~ Trial|SubjectNo, control = list(opt
= "optim", maxIter = 500))
trialMAR       <- update(trialMS,  correlation = corAR1())

# Effect of Familiarity on the intercept
fml.int        <- update(trialMAR,      .~. + Familiarity)
# Effect of Familiarity on the Slope
fml.slp        <- update(fml.int,       .~. + Familiarity : Trial)

# Effect of target Drift on the intercept
```

```
drf.int        <- update(fml.slp,       .~. + Drift)
# Effect of target Drift on the slope
drf.slp        <- update(drf.int,       .~. + Drift : Trial)

# Effect of Cue availability on the intercept
cue.int        <- update(drf.slp,       .~. + Cue)
# Effect of Cue availability on the Slope
cue.slp        <- update(cue.int,       .~. + Cue : Trial)

# Interactions
fml.drf.int    <- update(cue.slp,       .~. + Familiarity : Drift)
fml.drf.slp    <- update(fml.drf.int,   .~. + Familiarity : Drift : Trial)

fml.cue.int    <- update(fml.drf.slp,   .~. + Familiarity : Cue)
fml.cue.slp    <- update(fml.cue.int,   .~. + Familiarity : Cue : Trial)

drf.cue.int    <- update(fml.cue.slp,   .~. + Drift : Cue)
drf.cue.slp    <- update(drf.cue.int,   .~. + Drift : Cue : Trial)

final.int      <- update(drf.cue.slp ,  .~. + Familiarity : Cue : Drift)
final.slp      <- update(final.int,     .~. + Familiarity : Cue : Drift : Trial)
```

8.4.3.2.2 Compare the models

The R code and output for model comparisons are listed below. In the output list, the first column shows the name of the model. The column `logLik` shows the magnitude of log-likelihood of the model. The column `L.Ratio` shows the -2LL between the current model and the previous model before the predictor was added in. The *p*-values can be used to determine whether the improvement of model fit is significant.

Here we can see that model `trialM` is significantly improved by including *Trial*, suggesting that there was a general linear trend of change in the magnitude of target-heading angle over the test trials.

More importantly, model `fml.int`, model `drf.int`, model `cue.int` and model `drf.cue.slp` are significantly improved in the model fit (highlighted in the output list), suggesting a significant effect of the predictor that was added into the model. These results respectively suggest an effect of familiarity, target drift and cue availability on the magnitude of target-heading angle in Trial 1.

In addition, model `cue.slp` shows a marginally improved fit, suggesting that cue availability may have an effect on the slope of target-heading angle against trial. That is, the magnitude of target-heading angle changed at different rates between the Dark and Strobe conditions.

```
# Code
anova(baseline, trialM, trialMS, trialMAR, fml.int, fml.slp, drf.int, drf.slp, cue
```

```
.int, cue.slp, fml.drf.int, fml.drf.slp, fml.cue.int, fml.cue.slp, drf.cue.int, dr
f.cue.slp , final.int, final.slp)

# Output
##             Model df      AIC      BIC    logLik     Test   L.Ratio    p-value
## baseline        1  3 2125.245 2137.747 -1059.622
## trialM          2  4 2121.033 2137.704 -1056.517   1 vs 2  6.211562     0.0127
## trialMS         3  6 2123.326 2148.331 -1055.663   2 vs 3  1.707657     0.4258
## trialMAR        4  7 2107.229 2136.401 -1046.614   3 vs 4 18.096840     <.0001
## fml.int         5  8 2102.553 2135.893 -1043.276   4 vs 5  6.676372     0.0098
## fml.slp         6  9 2103.651 2141.158 -1042.825   5 vs 6  0.901993     0.3422
## drf.int         7 10 2099.311 2140.986 -1039.656   6 vs 7  6.339350     0.0118
## drf.slp         8 11 2101.093 2146.936 -1039.546   7 vs 8  0.218447     0.6402
## cue.int         9 12 2091.228 2141.238 -1033.614   8 vs 9 11.864733     0.0006
## cue.slp        10 13 2089.811 2143.989 -1031.906  9 vs 10  3.416514     0.0645
## fml.drf.int    11 14 2091.294 2149.640 -1031.647 10 vs 11  0.517028     0.4721
## fml.drf.slp    12 15 2093.175 2155.687 -1031.587 11 vs 12  0.119884     0.7292
## fml.cue.int    13 16 2094.611 2161.291 -1031.305 12 vs 13  0.563721     0.4528
## fml.cue.slp    14 17 2096.609 2167.456 -1031.304 13 vs 14  0.002124     0.9632
## drf.cue.int    15 18 2098.280 2173.295 -1031.140 14 vs 15  0.328756     0.5664
## drf.cue.slp    16 19 2095.834 2175.017 -1028.917 15 vs 16  4.446028     0.0350
## final.int      17 20 2097.221 2180.571 -1028.611 16 vs 17  0.612907     0.4337
## final.slp      18 21 2097.206 2184.724 -1027.603 17 vs 18  2.015353     0.1557
```

8.4.3.2.3 Estimation of slope parameters

As the model comparisons revealed an effect of interaction between target drift and cue availability on slope and the effect does not depend on familiarity, we then examined the estimated averaged slope between Familiar and Unfamiliar groups in each *Cue* × *Drift* condition by evaluating the parameter estimates in model `drf.cue.slp`. The R code and output are shown below. In the output list, the column `Estimate` shows the estimated slope of each condition. The *z*- and *p*-values are the results of hypothesis tests of whether the estimated slope in the corresponding condition is different from 0. Here we can see that target-heading angle only decreased significantly in the Dark-Continuous condition.

```
# Code
contrast.matrix <- rbind(
  "Dark: Continuous"    = c(0, 1, 0, 0, 0, 0.5, 0, 0, 0, 0, 0, 0, 0, 0),
  "Dark: Intermittent"  = c(0, 1, 0, 0, 0, 0.5, 1, 0, 0, 0, 0, 0.5, 0, 0),
  "Strob: Continuous"   = c(0, 1, 0, 0, 0, 0.5, 0, 1, 0, 0, 0, 0, 0.5, 0),
  "Strob: Intermittent" = c(0, 1, 0, 0, 0, 0.5, 1, 1, 0, 0, 0, 0.5, 0.5, 1)
)
postHocs <-glht(drt.cue.slp, contrast.matrix)
summary(postHocs, test = adjusted("none"))

# Output
##   Simultaneous Tests for General Linear Hypotheses
##
## Fit: lme.formula(fixed = meanErr ~ Trial + Familiarity + Drift + Cue +
##     Trial:Familiarity + Trial:Drift + Trial:Cue + Familiarity:Drift +
##     Familiarity:Cue + Drift:Cue + Trial:Familiarity:Drift + Trial:Familiarity:C
```

```
ue +
##     Trial:Drift:Cue, data = offset.err.long, random = ~Trial |
##     SubjectNo, correlation = corAR1(), method = "ML", na.action = na.omit,
##     control = list(opt = "optim", maxIter = 500))
##
## Linear Hypotheses:
##                            Estimate Std. Error z value Pr(>|z|)
## Dark: Continuous == 0     -0.3396     0.1141  -2.976  0.00292 **
## Dark: Intermittent == 0   -0.1515     0.1141  -1.328  0.18418
## Strob: Continuous == 0     0.1213     0.1141   1.063  0.28761
## Strob: Intermittent == 0  -0.1778     0.1148  -1.548  0.12152
## ---
## Signif. codes:  0 '***' 0.001 '**' 0.01 '*' 0.05 '.' 0.1 ' ' 1
## (Adjusted p values reported -- none method)
```

8.4.4 Experiment 5.4

8.4.4.1 Mean target-heading angle as a function of distance

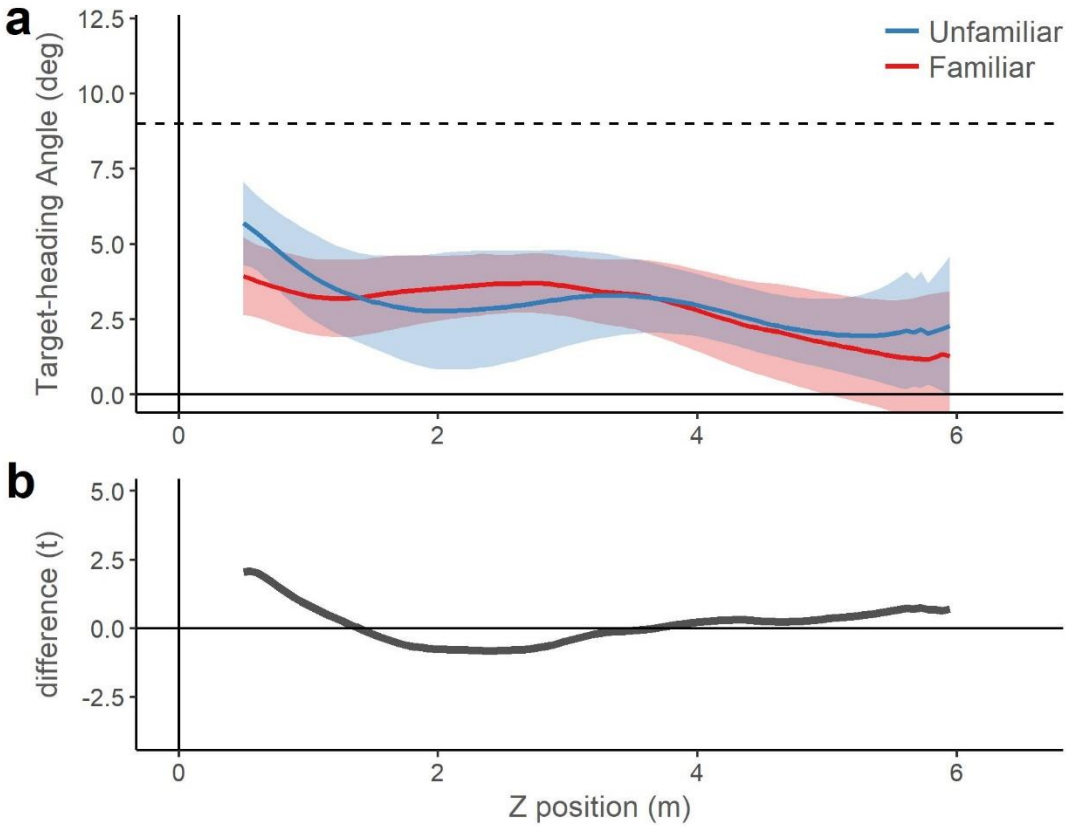

Figure 8.13. (a) *Mean target-heading angle against distance averaged over the five prism trials (1 ~ 5) and the participants (n = 12 per condition) for the familiar group (red) and unfamiliar group (blue) respectively. Dotted line at 9° indicates the power of the prism glasses. Shaded ribbons correspond to 95% confidence interval. Grey shaded rectangle indicates significant cluster.* ***(b)*** *Differences (t-values) in the mean target-heading angle as a function of distance.*

In **Figure 8.13a**, the mean target-heading angle in the Familiar group looks smaller than that in the Unfamiliar group. To confirm whether there was an effect, we applied our bespoke time series analysis on the t-values that were computed by comparing the data between the Familiar and Unfamiliar group (see **Figure 8.13b**). No significant cluster was found.

8.4.4.2 Mean target-heading angle as a function of test trials

8.4.4.2.1 Building the model

A taxonomy of models was fitted on the mean target-heading angles as a function of trial (1 ~ 5). On the basis of model `baseline`, model `trialM` included the level-1 predictor *Trial*. Model `trialMS` introduced random slopes and model `trialMAR` took autocorrelation into account. Model `fml.int` included the level-2 predictor *Familiarity* (Familiar and Unfamiliar) and model `fml.slp` included the interaction term *Familiarity* × *Trial*. Model `fov.int` included the level-2 predictor *FoV* (NoGoggles and Goggles) and model `fov.slp` included the interaction term *FoV* × *Trial*. The former tests the effect of restriction of FoV by goggles on the magnitude of target-heading angle in Trial 1 (intercept) and the latter tests the effect on the rate of change in target-heading angle across trials (slope). Model `fml.fov.int` and model `fml.fov.slp` respectively included the interaction between the level-2 predictors *Familiarity* × *FoV* and the three-way interaction term *Familiarity* × *FoV* × *Trial* to test the effect of the interaction on the intercept and slope of target-heading angle. The R code and output are listed below.

```
baseline      <- lme(target-heading_angle ~ 1, random = ~ 1 | SubjectNo, data = of
fset.err.long,  method = "ML", na.action = na.omit)

trialM        <- update(baseline,    .~. + Trial)
trialMS       <- update(trialM,      random = ~ Trial|SubjectNo, control = list(op
t = "optim", maxIter = 500))
trialMAR      <- update(trialMS,     correlation = corAR1())

# Effect of Familiarity on the intercept
fml.int       <- update(trialMAR,    .~. + Familiarity)
# Effect of Familiarity on the Slope
fml.slp       <- update(fml.int,     .~. + Familiarity : Trial)

# Effect of Restriction on FoV on the intercept
fov.int       <- update(fml.slp,     .~. + FoV)
# Effect of Restriction on FoV on the Slope
fov.slp       <- update(fov.int,     .~. + FoV : Trial)

# Interaction on the intercept
fml.fov.int   <- update(fov.slp,     .~. + Familiarity : FoV)
# Interaction on the slope
fml.fov.slp   <- update(fml.fov.int, .~. + Familiarity : FoV : Trial)
```

8.4.4.2.2 Compare the models

Then we compared the models. The R code and output for model comparisons are listed below. In the output list, the first column shows the name of the model. The column `logLik` shows the magnitude of log-likelihood of the model. The larger the `logLik` is, the

better the model fit. The column `L.Ratio` shows the -2LL between the current model and the previous model before the predictor was added in, an index for improvement of model fit. The *p*-values can be used to determine whether the improvement of model fit is significant. From the output list, we can see that adding the predictors did not improve the model fit, which suggests that there was no effect of these predictors.

```
# Code
anova(baseline, trialM, trialMS, trialMAR, fml.int, fml.slp, fov.int, fov.slp, fml
.fov.int, fml.fov.slp)

# Output
##             Model df      AIC      BIC    logLik    Test  L.Ratio p-value
## baseline        1    3 960.4497 970.8791 -477.2249
## trialM          2    4 961.0730 974.9788 -476.5365  1 vs 2  1.37675  0.2407
## trialMS         3    6 965.0785 985.9373 -476.5393  2 vs 3  0.00553  0.9972
## trialMAR        4    7 883.0683 907.4035 -434.5341  3 vs 4 84.01022  <.0001
## fml.int         5    8 884.7319 912.5436 -434.3660  4 vs 5  0.33637  0.5619
## fml.slp         6    9 884.4733 915.7615 -433.2366  5 vs 6  2.25863  0.1329
## fov.int         7   10 886.1746 920.9392 -433.0873  6 vs 7  0.29872  0.5847
## fov.slp         8   11 886.9315 925.1726 -432.4657  7 vs 8  1.24309  0.2649
## fml.fov.int     9   12 888.9047 930.6223 -432.4523  8 vs 9  0.02678  0.8700
## fml.fov.slp    10   13 890.4683 935.6624 -432.2342 9 vs 10  0.43636  0.5089
```

8.5 Chapter 6 - Supplementary Materials

8.5.1 Target-heading angle as a function of distance

8.5.1.1 Building up the growth model

A taxonomy of models was fitted on the mean target-heading angles averaged over Trial 2 ~ Trial 10 as a function of walking distance (0.5m ~ 6m). On the basis of model `baseline`, model `dstRI` included the level-1 predictor *distance* and model `dstRS` introduced random slopes. Model `scne.int` included the level-2 predictor *Scene* (Changed, Egocentrically-Same and Allocentrically-Same) and model `scne.slp` included the interaction term *Scene* × *distance*. The former tests the effect of *Scene* on the magnitude of the target-heading angle at 0.5m (intercept) and the latter tests the effect of *Scene* on the rate of change in target-heading angle over the distance (slope).

```
# Setting up a baseline model that includes only random intercepts
baseline   <- lme(target-heading_angle ~ 1, random = ~ 1|SubjectNo/Scene, data = o
ffset_mean, method = "ML", na.action = na.exclude, control = list(opt="optim"))

# Adding "distance" as the level-1 fixed effect
distRI     <- update(baseline,  .~. + distance)
# Introducing random slopes
distRS     <- update(distRI,    random = ~ distance|SubjectNo/Scene)

# Adding Scene (landmark layout) as the level-2 fixed effect
```

```
# Effects of Scene on the intercept
scne.int   <- update(distRS,    .~. + Scene)
# Effects of Scene on the slope
scne.slp   <- update(scne.int,  .~. + Scene : distance)
```

8.5.1.2 Comparing the models

The models were compared to see whether adding the predictor would improve the fit. The R code and output are listed below. In the output list, the first column shows the name of the model. The column `logLik` shows the magnitude of log-likelihood of the model. The larger the `logLik` is, the better the model fit. The column `L.Ratio` shows the -2LL between the current model and the previous model before the predictor was added in, an index for improvement of model fit. The *p*-values can be used to determine whether the improvement of model fit is significant. From the output list, we can see that adding *distance* and random slopes significantly improved the model fit (model `distRI` and `distRS`). The results suggest that the target-heading angle decreased over distance and the rate of decrease varied significantly between individual participants. However, adding *Scene* did not bring any significant improvement in model fit (model `scne.int` and `scne.slp`), suggesting no effect of landmark configuration on the intercept or slope of the target-heading angle.

```
# Code
anova(baseline, distRI, distRS, scne.int, scne.slp)

# Output
##          Model df      AIC      BIC    logLik   Test   L.Ratio p-value
## baseline     1  4 28344.99 28372.51 -14168.49
## distRI       2  5 28205.30 28239.71 -14097.65 1 vs 2  141.6826  <.0001
## distRS       3  9 26980.23 27042.16 -13481.11 2 vs 3 1233.0779  <.0001
## scne.int     4 11 26982.41 27058.11 -13480.20 3 vs 4    1.8154  0.4034
## scne.slp     5 13 26985.35 27074.81 -13479.67 4 vs 5    1.0618  0.5881
```

8.5.2 Mean target-heading angles of the early and later parts as a function of test trial

8.5.2.1 Building the growth model

A taxonomy of models was fitted on the mean target-heading angles averaged over walking distance 0.5m ~ 1m (early) and 5.5m ~ 6m (late) as a function of trial (Trial 1 ~ Trial 10). On the basis of model `baseline`, model `TrialRI` included the level-1 predictor *Trial*. Model `TrialRS` introduced random slopes and model `TrialAR` took autocorrelation into account. Model `PartRI` included the level-2 predictor *Part* (early and late) to test the difference between the early and late parts in the magnitude of target-heading angle in Trial 1

(intercept). Model `PartRS` included the interaction term *Part* × *Trial* to test the difference between the early and late parts in the rate of change in target-heading angle over trials (slope). Model `sceneRI` included the level-2 predictor *Scene* (Changed, Egocentrically-Same and Allocentrically-Same) and model `sceneRS` included the interaction term *Scene* × *Trial*. Model `ScenePartI` included the interaction between the two level-2 predictors *Part* × *Scene* and model `ScenePartS` included the interaction term between the level-1 and level-2 predictors *Part* × *Scene* × *Trial*. The R code is listed below.

```
# Setting up a baseline model that includes only random intercepts
baseline          <- lme(target-heading_angle ~ 1, random = ~1|SubjectNo/Scene/Par
t, data = offset.end.long, method = "ML", na.action = na.exclude, control = list(o
pt = "optim"))

# Adding Trial as the level-1 fixed effect
TrialRI           <- update(baseline,   .~. + Trial)
# Introducing random slopes
TrialRS           <- update(TrialRI,    random = ~ Trial|SubjectNo/Scene/Part)
# Modelling a first-order autoregressive covariance structure
TrialAR           <- update(TrialRS,    correlation = corAR1())

# Effects of Part on the intercept
PartRI            <- update(TrialAR,    .~. + Part)
# Effects of Part on the slope
PartRS            <- update(PartRI,     .~. + Part : Trial)

# Effects of Scene on the intercept
sceneRI           <- update(PartRS,     .~. + Scene)
# Effects of Scene on the intercept
sceneRS           <- update(sceneRI,    .~. + Scene : Trial)

# Effects of interaction on the intercept
ScenePartI        <- update(sceneRS,    .~. + Scene : Part)
# Effects of interaction on the intercept
ScenePartS        <- update(ScenePartI, .~. + Scene : Part : Trial)
```

8.5.2.2 Comparing the models

Then we compared the models to examine the effect of predictors. The R code and output are listed below. In the output list, the first column shows the name of the model. The column `logLik` shows the magnitude of log-likelihood of the model. The larger the `logLik` is, the better the model fit. The column `L.Ratio` shows the -2LL between the current model and the previous model before the predictor was added in, an index for improvement of model fit. The *p*-values can be used to determine whether the improvement of model fit is significant. From the output list, we can see that adding *Trial* and random slopes significantly improved the model fit (model `distRI` and `distRS`). The results suggest that the target-heading angle decreased over the trials and the rate of decrease varied significantly between

individual participants. Importantly, adding *Part* (model `PartRI`) and *Part* × *Trial* (model `PartRS`) significantly improved the model fit (highlighted in the output list). These results suggest that the early and late parts not only differed in the magnitude of target-heading angle in Trial 1 (intercept) but also differed in the rate of change (slope).

```
# Code
anova(baseline, TrialRI, TrialRS, TrialAR, PartRI, PartRS, sceneRI, sceneRS, Scene
PartI, ScenePartS)

# Output
##            Model df      AIC      BIC    logLik     Test  L.Ratio p-value
## baseline       1    5 7595.723 7622.050 -3792.861
## TrialRI        2    6 7580.512 7612.105 -3784.256   1 vs 2  17.2103  <.0001
## TrialRS        3   12 7570.063 7633.248 -3773.031   2 vs 3  22.4497  0.0010
## TrialAR        4   13 7530.636 7599.087 -3752.318   3 vs 4  41.4264  <.0001
## PartRI         5   14 7500.616 7574.332 -3736.308   4 vs 5  32.0204  <.0001
## PartRS         6   15 7491.766 7570.747 -3730.883   5 vs 6  10.8502  0.0010
## sceneRI        7   17 7494.870 7584.382 -3730.435   6 vs 7   0.8957  0.6390
## sceneRS        8   19 7496.216 7596.259 -3729.108   7 vs 8   2.6545  0.2652
## ScenePartI     9   21 7500.165 7610.739 -3729.082   8 vs 9   0.0507  0.9750
## ScenePartS    10   23 7503.437 7624.542 -3728.718  9 vs 10   0.7279  0.6949
```

8.5.2.3 Parameter estimates in the model PartRS

In order to obtain the estimated value for the average slopes of the early part, we evaluated the parameter estimates of the fixed effects in the model `PartRS`. The R code and output are shown below. The column `Value` shows the estimated values of the parameters. As the early part was chosen as the reference level, the row `Intercept` and `Trial` respectively show the estimates of the intercept and slope of the mean target-heading angle of the early part. The row `Late` shows the estimate of the difference in intercept between the late and early parts, and the row `Trial:Late` shows the difference in slope. Here we can see that the estimated slope of the early part is -0.18, significantly smaller than 0 [t = -4.22, $p < 0.0001$].

```
# Code
summary(PartRS, corr = FALSE)

# Output
## Fixed effects: target-heading_angle ~ Trial + Part + Trial:Part
##
##                    Value Std.Error   DF   t-value p-value
## (Intercept)     6.774432 0.4154415 1284 16.306586   0e+00
## Trial          -0.183676 0.0435513 1284 -4.217468   0e+00
## Late           -2.556713 0.3477093   71 -7.353020   0e+00
## Trial:Late      0.157519 0.0467514 1284  3.369296   8e-04
```

9 Reference

Aggleton, J. P., Poirier, G. L., Aggleton, H. S., Vann, S. D., & Pearce, J. M. (2009). Lesions of the fornix and anterior thalamic nuclei dissociate different aspects of hippocampal-dependent spatial learning: implications for the neural basis of scene learning. *Behavioral Neuroscience*, *123*(3), 504–519. https://doi.org/10.1037/a0015404

Aguirre, G. K., Detre, J. A., Alsop, D. C., & D'Esposito, M. (1996). The parahippocampus subserves topographical learning in man. *Cerebral Cortex*, *6*(6), 823–829. https://doi.org/10.1093/cercor/6.6.823

Allman, J., Miezin, F., & McGuinness, E. (1985). Direction- and velocity-specific responses from beyond the classical receptive field in the middle temporal visual area (MT). *Perception*, *14*(2), 105–126. https://doi.org/10.1068/p140105

Andersen, G. J., & Enriquez, A. (2006). Use of landmarks and allocentric reference frames for the control of locomotion. *Visual Cognition*, *13*(1), 119–128. https://doi.org/10.1080/13506280500405675

Andersen, R. A. (2011). Inferior Parietal Lobule Function in Spatial Perception and Visuomotor Integration. In *Comprehensive Physiology*. https://doi.org/10.1002/cphy.cp010512

Andersen, R. A., Bracewell, R. M., Barash, S., Gnadt, J. W., & Fogassi, L. (1990). Eye position effects on visual, memory, and saccade-related activity in areas LIP and 7a of macaque. *The Journal of Neuroscience : The Official Journal of the Society for Neuroscience*, *10*(4), 1176–96. Retrieved from http://www.ncbi.nlm.nih.gov/pubmed/2329374

Andersen, R. A., Essick, G. K., & Siegel, R. M. (1985). Encoding of spatial location by posterior parietal neurons. *Science*, *230*(4724), 456 LP-458. Retrieved from http://science.sciencemag.org/content/230/4724/456.abstract

Andersen, R. A., Shenoy, K. V, Crowell, J. A., & Bradley, D. C. (1999). Neural mechanisms for self-motion perception in area MST. *International Review of Neurobiology*, *44*, 219–233.

Andersen, R. a, & Zipser, D. (1988). The role of the posterior parietal cortex in coordinate transformations for visual-motor integration. *Canadian Journal of Physiology and Pharmacology*, *66*(4), 488–501. https://doi.org/10.1139/y88-078

Ashby, F. G. (2011). *Statistical analysis of fMRI data*. MIT press.

Auger, S. D., Zeidman, P., & Maguire, E. A. (2017). Efficacy of navigation may be influenced by retrosplenial cortex-mediated learning of landmark stability.

Neuropsychologia, *104*(April), 102–112. https://doi.org/10.1016/j.neuropsychologia.2017.08.012

Banks, M. S., Ehrlich, S. M., Backus, B. T., & Crowell, J. A. (1996). Estimating heading during real and simulated eye movements. *Vision Research*, *36*(3), 431–443. https://doi.org/10.1016/0042-6989(95)00122-0

Barry, C., Hayman, R., Burgess, N., & Jeffery, K. J. (2007). Experience-dependent rescaling of entorhinal grids. *Nature Neuroscience*, *10*(6), 682–684. https://doi.org/10.1038/nn1905

Beusmans, J. M. H. (1998). Perceived object shape affects the perceived direction of self-movement. *Perception*, *27*(1992), 1079–1085. https://doi.org/10.1068/P271079

Bingman, V. P., Erichsen, J. T., Anderson, J. D., Good, M. A., & Pearce, J. M. (2006). Spared feature-structure discrimination but diminished salience of environmental geometry in hippocampal-lesioned homing pigeons (Columba livia). *Behavioral Neuroscience*, *120*(4), 835–841. https://doi.org/10.1037/0735-7044.120.4.835

Bisiach, E., Perani, D., Vallar, G., & Berti, A. (1986). Unilateral neglect: Personal and extra-personal. *Neuropsychologia*, *24*(6), 759–767. https://doi.org/10.1016/0028-3932(86)90075-8

Blair, H. T., Cho, J., & Sharp, P. E. (1998). Role of the lateral mammillary nucleus in the rat head direction circuit: A combined single unit recording and lesion study. *Neuron*, *21*(6), 1387–1397. https://doi.org/10.1016/S0896-6273(00)80657-1

Blair, H. T., & Sharp, P. E. (1995). Anticipatory head direction signals in anterior thalamus: evidence for a thalamocortical circuit that integrates angular head motion to compute head direction. *The Journal of Neuroscience*, *15*(9), 6260–6270.

Bradley, D. C., Maxwell, M., Andersen, R. A., Banks, M. S., & Shenoy, K. V. (1996). Mechanisms of heading perception in primate visual cortex. *Science*, *273*(5281), 1544–1547. https://doi.org/10.1126/science.273.5281.1544

Bridgeman, B. (1972). Visual receptive fields sensitive to absolute and relative motion during tracking. *Science*, *178*(4065), 1106–1108. https://doi.org/10.1126/science.178.4065.1106

Britten, K. H., & van Wezel, R. J. (1998). Electrical microstimulation of cortical area MST biases heading perception in monkeys. *Nature Neuroscience*, *1*(1), 59–63. https://doi.org/10.1038/259

Brotchie, P. R., Andersen, R. A., Snyder, L. H., & Goodman, S. J. (1995). Head position signals used by parietal neurons to encode locations of visual stimuli. *Nature*.

https://doi.org/10.1038/375232a0

Bruggeman, H., Zosh, W., & Warren, W. H. (2007). Optic Flow Drives Human Visuo-Locomotor Adaptation. *Current Biology*, *17*(23), 2035–2040. https://doi.org/10.1016/j.cub.2007.10.059

Burgess, N. (2008). Spatial cognition and the brain. *Annals of the New York Academy of Sciences*, *1124*, 77–97. https://doi.org/10.1196/annals.1440.002

Calvert, E. S. (1950). Visual aids for landing in bad visibility with particular reference to the transition from instrument to visual flight. *Transactions of the Illuminating Engineering Society*, *15*(6_IEStrans), 183–219.

Calvert, E. S. (1954). Visual Judgments in Motion. *Journal of Navigation*, *7*(3), 233. https://doi.org/10.1017/S0373463300020907

Cardin, V., Hemsworth, L., & Smith, A. T. (2012). Adaptation to heading direction dissociates the roles of human MST and V6 in the processing of optic flow. *Journal of Neurophysiology*, *108*(3), 794–801. https://doi.org/10.1152/jn.00002.2012

Cardin, V., & Smith, A. T. (2010). Sensitivity of human visual and vestibular cortical regions to egomotion-compatible visual stimulation. *Cerebral Cortex*, *20*(8), 1964–1973. https://doi.org/10.1093/cercor/bhp268

Carmack, J. (2013). Latency Mitigation Strategies. Retrieved from http://www.altdevblogaday.com/2013/02/22/latency-mitigation-strategies/

Cartwright, B. A., & Collett, T. S. (1983). Landmark learning in bees. *Journal of Comparative Physiology*, *151*(4), 521–543.

Chen, X., McNamara, T. P., Kelly, J. W., & Wolbers, T. (2017). Cue combination in human spatial navigation. *Cognitive Psychology*, *95*, 105–144. https://doi.org/10.1016/j.cogpsych.2017.04.003

Cheng, K. (1986). A purely geometric module in the rat's spatial representation. *Cognition*, *23*(2), 149–178. https://doi.org/10.1016/0010-0277(86)90041-7

Chokron, S. (2003). Right parietal lesions, unilateral spatial neglect, and the egocentric frame of reference. *NeuroImage*, *20*(SUPPL. 1), 75–81. https://doi.org/10.1016/j.neuroimage.2003.09.002

Clark, B. J., Harris, M. J., & Taube, J. S. (2012). Control of anterodorsal thalamic head direction cells by environmental boundaries: Comparison with conflicting distal landmarks. *Hippocampus*, *22*(2), 172–187. https://doi.org/10.1002/hipo.20880

Corlett, J. T., Patla, A. E., & Williams, J. G. (1985). Locomotor estimation of distance after visual scanning by children and adults. *Perception*, *14*(3), 257–263.

https://doi.org/10.1068/p140257

Crowell, J. A., & Banks, M. S. (1993). Perceiving heading with different retinal regions and types of optic flow. *Perception & Psychophysics*, *53*(3), 325–37. https://doi.org/10.3758/BF03205187

Cutting, J. E. (1986). *Perception with an eye for motion* (Vol. 29). Mit Press Cambridge, MA.

Cutting, J. E., Springer, K., Braren, P. a, & Johnson, S. H. (1992). Wayfinding on foot from information in retinal, not optical, flow. *Journal of Experimental Psychology. General*, *121*(1), 41–72. https://doi.org/10.1037/0096-3445.121.2.129

Cutting, J. E., Vishton, P. M., Flückiger, M., Baumberger, B., & Gerndt, J. D. (1997). Heading and path information from retinal flow in naturalistic environments. *Perception & Psychophysics*, *59*(3), 426–441. https://doi.org/10.3758/BF03211909

Darling, W. G., Pizzimenti, M. A., & Rizzo, M. (2003). Unilateral posterior parietal lobe lesions affect representation of visual space. *Vision Research*, *43*(15), 1675–1688. https://doi.org/10.1016/S0042-6989(03)00179-2

Doeller, C. F., Barry, C., & Burgess, N. (2010). Evidence for grid cells in a human memory network. *Nature*, *463*(7281), 657–661. https://doi.org/10.1038/nature08704

Duchon, A. P., & William H Warren, J. (2002). A Visual Equalization Strategy for Locomotor Control: Of Honeybees, Robots, and Humans. *Psychological Science*, *13*(3), 272–278. https://doi.org/10.1111/1467-9280.00450

Dudchenko, P. A. (2007). Does shape matter? Theoretical comment on Jones, Pearce, Davies, Good, and McGregor (2007). *Behavioral Neuroscience*, *121*(6), 1442–1446. https://doi.org/10.1037/0735-7044.121.6.1442

Duffy, C. J. (2000). Optic flow analysis for self-movement perception. *International Review of Neurobiology*, *44*, 199.

Duffy, C. J., & Wurtz, R. H. (1991). Sensitivity of MST neurons to optic flow stimuli. I. A continuum of response selectivity to large-field stimuli. *Journal of Neurophysiology*, *65*(6), 1329–45. Retrieved from http://www.ncbi.nlm.nih.gov/pubmed/1875243

Duffy, C. J., & Wurtz, R. H. (1995). Response of monkey MST neurons to optic flow stimuli with shifted centers of motion. *Journal of Neuroscience*, *15*(7 Pt 2), 5192–5208.

Duffy, C. J., & Wurtz, R. H. (1997). Medial superior temporal area neurons respond to speed patterns in optic flow. *The Journal of Neuroscience : The Official Journal of the Society for Neuroscience*, *17*(8), 2839–2851.

Duhamel, J.-R. R., Bremmer, F., Ben Hamed, S., & Graf, W. (1997). Spatial invariance of visual receptive fields in parietal cortex neurons. *Nature*, *389*(6653), 845–8.

https://doi.org/10.1038/39865

Dukelow, S. P., DeSouza, J. F. X., Culham, J. C., van den Berg, A. V, Menon, R. S., & Vilis, T. (2001). Distinguishing subregions of the human MT+ complex using visual fields and pursuit eye movements. *Journal of Neurophysiology*, *86*(4), 1991–2000.

Dupont, P., De Bruyn, B., Vandenberghe, R., Rosier, A.-M., Michiels, J., Marchal, G., … Orban, G. A. (1997). The kinetic occipital region in human visual cortex. *Cerebral Cortex (New York, NY: 1991)*, *7*(3), 283–292.

Ekstrom, A. D., Kahana, M. J., Caplan, J. B., Fields, T. A., Isham, E. A., Newman, E. L., & Fried, I. (2003). Cellular networks underlying human spatial navigation., *425*(6954), 184–188. https://doi.org/10.1038/nature01964

Epstein, R. A., & Vass, L. K. (2014). Neural systems for landmark-based wayfinding in humans. *Philosophical Transactions of the Royal Society of London. Series B, Biological Sciences*, *369*(1635), 20120533. https://doi.org/10.1098/rstb.2012.0533

Erickson, R. G., & Thier, P. (1991). A neuronal correlate of spatial stability during periods of self-induced visual motion. *Experimental Brain Research*, *86*(3), 608–616. https://doi.org/10.1007/BF00230534

Ernst, M. O., & Banks, M. S. (2002). Humans integrate visual and haptic information in a statistically optimal fashion. *Nature*, *415*(6870), 429–433. https://doi.org/10.1038/415429a

Fajen, B. R., & Warren, J. (2000). Go with the flow. *Trends in Cognitive Sciences*, *4*(10), 369–370. https://doi.org/10.1016/S1364-6613(00)01532-1

Ferber, S., & Karnath, H. O. (1999). Parietal and occipital lobe contributions to perception of straight ahead orientation. *Journal of Neurology, Neurosurgery, and Psychiatry*, *67*(5), 572–8. https://doi.org/10.1136/jnnp.67.5.572

Fortenbaugh, F. C., Hicks, J. C., Hao, L., & Turano, K. A. (2007). Losing sight of the bigger picture: Peripheral field loss compresses representations of space. *Vision Research*, *47*(19), 2506–2520. https://doi.org/10.1016/j.visres.2007.06.012

Fortenbaugh, F. C., Hicks, J. C., & Turano, K. A. (2008). The effect of peripheral visual field loss on representations of space: Evidence for distortion and adaptation. *Investigative Ophthalmology and Visual Science*, *49*(6), 2765–2772. https://doi.org/10.1167/iovs.07-1021

Franz, M. O., Schölkopf, B., Mallot, H. A., & Bülthoff, H. H. (1998). Where did I take that snapshot? Scene-based homing by image matching. *Biological Cybernetics*, *79*(3), 191–202.

Freeman, T. C. A., Banks, M. S., & Crowell, J. (2000). Extraretinal and retinal amplitude and phase errors during Filehne illusion and path perception. *Perception & Psychophysics*, *62*(5), 900–9. https://doi.org/10.3758/BF03212076

Freeman, T. C. A., Champion, R. A., Sumnall, J. H., & Snowden, R. J. (2009). Do we have direct access to retinal image motion during smooth pursuit eye movements? *Journal of Vision*, *9*, 33.1-11. https://doi.org/10.1167/9.1.33.Introduction

Friston, K. J., Ashburner, J., Kiebel, S. J., Nichols, T. E., & Penny, W. D. (Eds.). (2007). *Statistical Parametric Mapping: The Analysis of Functional Brain Images*. Academic Press. Retrieved from http://store.elsevier.com/product.jsp?isbn=9780123725608

Frost, B. J., & Nakayama, K. (1983). Single visual neurons code opposing motion independent of direction. *Science (New York, N.Y.)*, *220*(4598), 744–5. https://doi.org/10.1126/science.6836313

Fyhn, M., Molden, S., Witter, M. P., Moser, E. I., & Moser, M. B. (2004). Spatial representation in the entorhinal cortex. *Science*, *305*(5688), 1258–1264. https://doi.org/10.1126/science.1099901

Galati, G., Lobel, E., Vallar, G., Berthoz, A., Pizzamiglio, L., & Bihan, D. Le. (2000). The neural basis of egocentric and allocentric coding of space in humans: a functional magnetic resonance study. *Experimental Brain Research*, *133*(2), 156–164. https://doi.org/10.1007/s002210000375

Galletti, C., Battaglini, P. P., & Fattori, P. (1993). Parietal neurons encoding spatial locations in craniotopic coordinates. *Experimental Brain Research*, *96*(2), 221–229.

Gallistel, C. R. (1990). *The organization of learning*. MIT press Cambridge, MA.

Gauthier, M., Parush, A., Macuda, T., Tang, D., Craig, G., & Jennings, S. (2006). Spatial navigation using night vision goggles (Vol. 6224, p. 62240G–6224–13). Retrieved from http://dx.doi.org/10.1117/12.663454

Gibson, J. J. (1950). *The perception of the visual world*. Houghton Mifflin.

Gibson, J. J. (1958). Visually controlled locomotion and visual orientation in animals. *British Journal of Psychology*, *49*(3), 182–194. https://doi.org/10.1111/j.2044-8295.1958.tb00656.x

Gibson, J. J. (1979). The Ecological Approach to Visual Perception. *Houghton Mifflin-Boston*.

Gillner, S., & Mallot, H. A. (1998). Navigation and Acquisition of Spatial Knowledge in a Virtual Maze. *Journal of Cognitive Neuroscience*, *10*(4), 445–463. https://doi.org/10.1162/089892998562861

Golob, E. J., Stackman, R. W., Wong, A. C., & Taube, J. S. (2001). On the behavioral significance of head direction cells: Neural and behavioral dynamics during spatial memory tasks. *Behavioral Neuroscience*. https://doi.org/10.1037//0735-7044.115.2.285

Gootjes-Dreesbach, L., Pickup, L. C., Fitzgibbon, A. W., & Glennerster, A. (2017). Comparison of view-based and reconstruction-based models of human navigational strategy. *Journal of Vision*, *17*(9), 11. https://doi.org/10.1167/17.9.11.doi

Gouteux, S., Thinus-Blanc, C., & Vauclair, J. (2001). Rhesus monkeys use geometric and nongeometric information during a reorientation task. *Journal of Experimental Psychology: General*, *130*(3), 505–519. https://doi.org/10.1037/0096-3445.130.3.505

Graham, P., & Collett, T. S. (2002). View-based navigation in insects: how wood ants (Formica rufa L.) look at and are guided by extended landmarks. *Journal of Experimental Biology*, *205*(16), 2499–2509.

Grieves, R. M., & Jeffery, K. J. (2017). The representation of space in the brain. *Behavioural Processes*, *135*, 113–131. https://doi.org/10.1016/j.beproc.2016.12.012

Guterman, P. S. (2009). *When Sight Closes in: The Effects of Field of View on Wayfinding and Spatial Representation*. York University.

Guterman, P. S., Allison, R. S., Jennings, S., Craig, G., Parush, A., Gauthier, M., & Macuda, T. (2009). The outer limits: How limiting the field of view impacts navigation and spatial memory. *Journal of Vision*, *9*(8), 1137. Retrieved from http://dx.doi.org/10.1167/9.8.1137

Guterman, P. S., Allison, R. S., & Rushton, S. K. (2007). The visual control of walking: Do we go with the (optic) flow? *Journal of Vision*, *7*(9), 1017.

Hafting, T., Fyhn, M., Molden, S., Moser, M., & Moser, E. I. (2005). Microstructure of a spatial map in the entorhinal cortex. *Nature*, *436*(7052), 801–806. https://doi.org/10.1038/nature03721

Hahn, S., Andersen, G. J., & Saidpour, A. (2003). Static scene analysis for the perception of heading. *Psychological Science*, *14*(6), 543–548. https://doi.org/10.1046/j.0956-7976.2003.psci_1463.x

Harris, J. M. (2001). The future of flow? *Trends in Cognitive Sciences*, *5*(1), 7–8.

Harris, J. M., & Bonas, W. (2002). Optic flow and scene structure do not always contribute to the control of human walking. *Vision Research*, *42*(13), 1619–1626. https://doi.org/10.1016/S0042-6989(02)00066-4

Harris, J. M., & Rogers, B. J. (1999). Going against the flow. *Trends in Cognitive Sciences*, *3*(12), 449–450.

Harris, M. G., & Carré, G. (2001). Is optic flow used to guide walking while wearing a displacing prism? *Perception*, *30*(7), 811–818. https://doi.org/10.1068/p3160

Hartley, T., Maguire, E. a., Spiers, H. J., & Burgess, N. (2003). The well-worn route and the path less traveled: Distinct neural bases of route following and wayfinding in humans. *Neuron*, *37*(5), 877–888. https://doi.org/10.1016/S0896-6273(03)00095-3

Herlihey, T. A. (2010). *Optic flow, egocentric direction and walking*. Cardiff University (United Kingdom).

Herlihey, T., & Rushton, S. K. (2012). The role of discrepant retinal motion during walking in the realignment of egocentric space. *Journal of Vision*, *12*(3), 1–11. https://doi.org/10.1167/12.3.4

Hermer, L., & Spelke, E. (1996). Modularity and development: The case of spatial reorientation. *Cognition*, *61*(3), 195–232. https://doi.org/10.1016/S0010-0277(96)00714-7

Hillis, J. M., Ernst, M. O., Banks, M. S., & Landy, M. S. (2002). Combining sensory information: mandatory fusion within, but not between, senses. *Science*, *298*(5598), 1627–1630.

Hothorn, T., Bretz, F., & Westfall, P. (2008). Simultaneous Inference in General Parametric Models. *Biometrical Journal*, *50*(3), 346–363.

Huk, A. C., Dougherty, R. F., & Heeger, D. J. (2002). Retinotopy and functional subdivision of human areas MT and MST. *The Journal of Neuroscience : The Official Journal of the Society for Neuroscience*, *22*(16), 7195–7205. https://doi.org/20026661

Iaria, G., Petrides, M., Dagher, A., Pike, B., & Bohbot, V. D. (2003). Cognitive strategies dependent on the hippocampus and caudate nucleus in human navigation: variability and change with practice. *The Journal of Neuroscience : The Official Journal of the Society for Neuroscience*, *23*(13), 5945–5952.

Ilg, U. J., & Thier, P. (2003). Visual tracking neurons in primate area MST are activated by smooth-pursuit eye movements of an "imaginary" target. *Journal of Neurophysiology*, *90*(3), 1489–1502. https://doi.org/10.1152/jn.00272.2003

Jacobs, J., Weidemann, C. T., Miller, J. F., Solway, A., Burke, J. F., Wei, X.-X., … Kahana, M. J. (2013). Direct recordings of grid-like neuronal activity in human spatial navigation. *Nature Neuroscience*, *16*(9), 1188–1190. https://doi.org/10.1038/nn.3466

Jeffreys, H. (1961). *Theory of Probability*. *Theory of Probability* (Vol. 2). Retrieved from http://ocw.mit.edu/OcwWeb/Mathematics/18-175Spring-2007/LectureNotes/Index.htm

Judge, S. J. (1990). Knowing where you're going. *Nature*, *348*(6297), 115.

Karnath, H.-O. (1997). Spatial orientation and the representation of space with parietal lobe lesions. *Philosophical Transactions of the Royal Society of London. Series B: Biological Sciences*, *352*(1360), 1411–1419. https://doi.org/10.1098/rstb.1997.0127

Kelly, D. M., Spetch, M. L., & Heth, C. D. (1998). Pigeons' (Columba livia) encoding of geometric and featural properties of a spatial environment. *Journal of Comparative Psychology*, *112*(3), 259–269. https://doi.org/10.1037/0735-7036.112.3.259

Kesten, H. (1958). Accelerated Stochastic Approximation. *The Annals of Mathematical Statistics*, *29*(1), 41–59. https://doi.org/10.1214/aoms/1177706705

Kim, N. G., Fajen, B. R., & Turvey, M. T. (2000). Perceiving circular heading in noncanonical flow fields. *Journal of Experimental Psychology. Human Perception and Performance*, *26*(1), 31–56. https://doi.org/10.1037/0096-1523.26.1.31

Koenderink, J. J., & van Doorn, A. J. (1981). Exterospecific component of the motion parallax field. *Journal of the Optical Society of America A, Optics, Image Science, and Vision*, *71*(8), 953–957.

Komatsu, H., & Wurtz, R. H. (1988a). Relation of cortical areas MT and MST to pursuit eye movements. I. Localization and visual properties of neurons. *Journal of Neurophysiology*, *60*(2), 580–603. https://doi.org/10.220.33.5

Komatsu, H., & Wurtz, R. H. (1988b). Relation of cortical areas MT and MST to pursuit eye movements. III. Localization and visual properties of neurons. *Journal of Neurophysiology*, *60*(2), 580–603.

Kropff, E., Carmichael, J. E., Moser, M. B., & Moser, E. I. (2015). Speed cells in the medial entorhinal cortex. *Nature*, *523*(7561), 419–424. https://doi.org/10.1038/nature14622

Krupic, J., Bauza, M., Burton, S., Barry, C., & O'Keefe, J. (2015). Grid cell symmetry is shaped by environmental geometry. *Nature*, *518*(7538), 232–235. https://doi.org/10.1038/nature14153

Kurkin, S., Akao, T., Shichinohe, N., Fukushima, J., & Fukushima, K. (2011). Neuronal activity in medial superior temporal area (MST) during memory-based smooth pursuit eye movements in monkeys. *Experimental Brain Research*, *214*(2), 293–301. https://doi.org/10.1007/s00221-011-2825-6

Landy, M. S., Maloney, L. T., Johnston, E. B., & Young, M. (1995). Measurement and modeling of depth cue combination: in defense of weak fusion. *Vision Research*, *35*(3), 389–412. https://doi.org/10.1016/0042-6989(94)00176-M

Lappe, M. (2000). Computational Mechanisms for Optic Flor Analysis in Primate Cortex. *International Review of Neurobiology*. https://doi.org/10.1016/S0074-7742(08)60745-X

Lappe, M., Bremmer, F., & Van Den Berg, A. V. (1999a). Perception of self-motion from visual flow. *Trends in Cognitive Sciences*, *3*(9), 329–336. https://doi.org/10.1016/S1364-6613(99)01364-9

Lappe, M., Bremmer, F., & Van Den Berg, A. V. (1999b). Reply to Harris and Rogers. *Trends in Cognitive Sciences*, *3*(12), 450. https://doi.org/10.1016/S1364-6613(99)01412-6

Lee, D., & Lishman, J. (1977). Visual Control of Locomotion. *Scandinavian Journal of Psychology*, *18*, 224 230. https://doi.org/10.1111/j.1467-9450.1977.tb00281.x

Lent, D. D., Graham, P., & Collett, T. S. (2010). Image-matching during ant navigation occurs through saccade-like body turns controlled by learned visual features. *Proceedings of the National Academy of Sciences of the United States of America*, *107*(37), 16348–16353. https://doi.org/10.1073/pnas.1006021107

Li, L., & Warren, W. H. (2000). Perception of heading during rotation: sufficiency of dense motion parallax and reference objects. *Vision Research*, *40*(28), 3873–3894. https://doi.org/10.1016/S0042-6989(00)00196-6

Llewellyn, K. R. (1971). Visual guidance of locomotion. *Journal of Experimental Psychology*, *91*(2), 245–61. https://doi.org/doi:10.1037/h0031788

Longuet-Higgins, H. C., & Prazdny, K. (1980). The interpretation of a moving retinal image. *Proceedings of the Royal Society of London, B: Biological Sciences*, *208*(1173), 385–397. https://doi.org/10.1098/rspb.1980.0057

Loomis, J. M., Da Silva, J. a, Fujita, N., & Fukusima, S. S. (1992). Visual space perception and visually directed action. *Journal of Experimental Psychology. Human Perception and Performance*. https://doi.org/10.1037/0096-1523.18.4.906

Loomis, J. M., Klatzky, R. L., Golledge, R. G., Cicinelli, J. G., Pellegrino, J. W., & Fry, P. A. (1993). Nonvisual navigation by blind and sighted: assessment of path integration ability. *Journal of Experimental Psychology. General*, *122*(1), 73–91. https://doi.org/10.1037/0096-3445.122.1.73

Love, J., Selker, R., Marsman, M., Jamil, T., Verhagen, A. J., Ly, A., … others. (2015). JASP. *Computer software](Version 0.6. 6)*.

Maguire, E. A., Burgess, N., Donnett, J. G., Frackowiak, R. S., Frith, C. D., & O'Keefe, J. (1998). Knowing where and getting there: a human navigation network. *Science (New York, N.Y.)*, *280*(5365), 921–924. https://doi.org/10.1126/science.280.5365.921

Maguire, E. A., Gadian, D. G., Johnsrude, I. S., Good, C. D., Ashburner, J., Frackowiak, R. S., & Frith, C. D. (2000). Navigation-related structural change in the hippocampi of taxi

drivers. *Proceedings of the National Academy of Sciences of the United States of America*, *97*(8), 4398–4403. https://doi.org/10.1073/pnas.070039597

Maguire, E. a., Intraub, H., & Mullally, S. L. (2015). Scenes, Spaces, and Memory Traces: What Does the Hippocampus Do? *The Neuroscientist*, 1073858415600389. https://doi.org/10.1177/1073858415600389

Mair, P., & Wilcox, R. R. (2017). Robust statistical methods in R using the WRS2 package. *Journal of Statistical Software*, forthcoming. https://doi.org/10.18637/jss.v000.i00

Mallot, H. A., & Gillner, S. (2000). Route navigating without place recognition: What is recognised in recognition-triggered responses? *Perception*, *29*(1), 43–55.

Marchette, S. A., Vass, L. K., Ryan, J., & Epstein, R. A. (2014). Anchoring the neural compass: coding of local spatial reference frames in human medial parietal lobe. *Nature Neuroscience*, *17*(11), 1598–1606. https://doi.org/10.1038/nn.3834

Markus, E. J., Barnes, C. A., McNaughton, B. L., Gladden, V. L., & Skaggs, W. E. (1994). Spatial information content and reliability of hippocampal CA1 neurons: Effects of visual input. *Hippocampus*, *4*(4), 410–421. https://doi.org/10.1002/hipo.450040404

McGregor, A., Hayward, A., Pearce, J. M., & Good, M. A. (2004). Hippocampal lesions disrupt navigation based on the shape of the environment. *Behavioral Neuroscience*, *118*(5), 1011–21. https://doi.org/10.1037/0735-7044.118.5.1011

McGregor, A., Jones, P. M., Good, M. A., & Pearce, J. M. (2006). Further evidence that rats rely on local rather than global spatial information to locate a hidden goal: reply to Cheng and Gallistel (2005). *J Exp Psychol Anim Behav Process*, *32*(3), 314–321. https://doi.org/Doi 10.1037/0097-7403.32.3.314

Miller, J. F., Neufang, M., Solway, A., Brandt, A., Trippel, M., Mader, I., … Schulze-Bonhage, A. (2013). Neural activity in human hippocampal formation reveals the spatial context of retrieved memories. *Science*, *342*(6162), 1111–1114. https://doi.org/10.1126/science.1244056

Mirman, D. (2014). *Growth curve analysis and visualization using R*. CRC Press Boca Raton, FL.

Mirman, D., Dixon, J. A., & Magnuson, J. S. (2008). Statistical and computational models of the visual world paradigm: Growth curves and individual differences. *Journal of Memory and Language*, *59*(4), 475–494. https://doi.org/10.1016/j.jml.2007.11.006

Mollon, J. D. (1997). "… On the Basis of Velocity Clues Alone": Some Perceptual Themes 1946–1996. *The Quarterly Journal of Experimental Psychology Section A*, *50*(4), 859–878. https://doi.org/10.1080/713755736

Morey, R. D., & Rouder, J. N. (2015). BayesFactor (Version 0.9. 11-3)[Computer software].

Morice, A. H. P., Siegler, I. A., & Bardy, B. G. (2008). Action-perception patterns in virtual ball bouncing: Combating system latency and tracking functional validity. *Journal of Neuroscience Methods*, *169*(1), 255–266. https://doi.org/10.1016/j.jneumeth.2007.11.020

Morrone, M. C., Tosetti, M., Montanaro, D., Fiorentini, A., Cioni, G., Burr, D. C., & Fiorentini, G. C. D. C. B. M. C. M. M. T. D. M. A. (2000). A cortical area that responds specifically to optic flow, revealed by fMRI. https://doi.org/doi:10.1038/81860

Muller, R. U., & Kubie, J. L. (1987). The effects of changes in the environment on the spatial firing of hippocampal complex-spike cells. *Journal of Neuroscience*, *7*(7), 1951–1968.

Nakayama, K. (1985). Extraction of higher order derivatives of the optical velocity vector field: Limitations imposed by biological hardware. In *Brain mechanisms and spatial vision* (pp. 59–71). Springer.

Nakayama, K. (1994). James J. Gibson: An appreciation. *Psychological Review*, *101*(2), 329–335. https://doi.org/10.1037/0033-295X.101.2.329

Newsome, W. T., Wurtz, R. H., & Komatsu, H. (1988). Relation of cortical areas MT and MST to pursuit eye movements. II. Differentiation of retinal from extraretinal inputs. *Journal of Neurophysiology*, *60*(2), 604 LP-620. Retrieved from http://jn.physiology.org/content/60/2/604.abstract

Nichols, T., & Holmes, A. (2003). Nonparametric Permutation Tests for Functional Neuroimaging. *Human Brain Function: Second Edition*, *25*(August 1999), 887–910. https://doi.org/10.1016/B978-012264841-0/50048-2

Niehorster, D. C., Li, L., & Lappe, M. (2017). The accuracy and precision of position and orientation tracking in the HTC vive virtual reality system for scientific research. *I-Perception*, *8*(3), 1–23. https://doi.org/10.1177/2041669517708205

O'Keefe, J. (1976). Place units in the hippocampus of the freely moving rat. *Experimental Neurology*, *51*(1), 78–109. https://doi.org/10.1016/0014-4886(76)90055-8

O'Keefe, J. (1979). A review of the hippocampal place cells. *Progress in Neurobiology*, *13*(4), 419–439. https://doi.org/10.1016/0301-0082(79)90005-4

O'Keefe, J., & Burgess, N. (1996). Geometric determinants of the place fields of hippocampal neurons. *Nature*. https://doi.org/10.1038/381425a0

O'Keefe, J., & Conway, D. H. (1978). Hippocampal place units in the freely moving rat: Why they fire where they fire. *Experimental Brain Research*, *31*(4). https://doi.org/10.1007/BF00239813

O'Keefe, J., & Dostrovsky, J. (1971). The hippocampus as a spatial map. Preliminary evidence from unit activity in the freely-moving rat. *Brain Research*, *34*(1), 171–175. https://doi.org/10.1016/0006-8993(71)90358-1

O'Keefe, J., & Nadel, L. (1978). *The hippocampus as a cognitive map*. Oxford: Clarendon Press.

O'Mara, S. M. (2017). Place Cells: Knowing Where You Are Depends on Knowing Where You're Heading. *Current Biology*, *27*(17), R834–R836. https://doi.org/10.1016/j.cub.2017.06.081

Page, W. K., & Duffy, C. J. (1999). MST neuronal responses to heading direction during pursuit eye movements. *Journal of Neurophysiology*, *81*(2), 596–610. https://doi.org/10.1126/science.273.5281.1544

Pearce, J. M., Good, M. A., Jones, P. M., & McGregor, A. (2004). Transfer of spatial behavior between different environments: Implications for theories of spatial learning and for the role of the hippocampus in spatial learning. *J Exp Psychol Anim Behav Process*, *30*(2), 135–147. https://doi.org/Doi 10.1037/0097-7403.30.2.135

Pearce, J. M., Ward-Robinson, J., Good, M., Fussell, C., & Aydin, A. (2001). Influence of a beacon on spatial learning based on the shape of the test environment. *Journal of Experimental Psychology. Animal Behavior Processes*, *27*(4), 329–344. https://doi.org/10.1037//0097-7403.27.4.329

Perrett, D., Harries, M., Mistlin, A. J., & Chitty, A. J. (1990). Three stages in the classification of body movements by visual neurons.

Peuskens, H., Sunaert, S., Dupont, P., Van Hecke, P., & Orban, G. a. (2001). Human brain regions involved in heading estimation. *The Journal of Neuroscience : The Official Journal of the Society for Neuroscience*, *21*(7), 2451–61. Retrieved from http://www.ncbi.nlm.nih.gov/pubmed/11264319

Pickup, L., Fitzgibbon, A., Gilson, S., & Glennerster, A. (2011). View-based modelling of human visual navigation errors. *IVMSP Workshop, 2011 IEEE 10th*. https://doi.org/10.1109/IVMSPW.2011.5970368

Pinheiro, J., Bates, D., DebRoy, S., Sarkar, D., & R Core Team. (2017). {nlme}: Linear and Nonlinear Mixed Effects Models. Retrieved from https://cran.r-project.org/package=nlme

Pitzalis, S., Galletti, C., Huang, R. S., Patria, F., Committeri, G., Galati, G., … Sereno, M. I. (2006). Wide-field retinotopy defines human cortical visual area v6. *J Neurosci.*, *26*(30), 7962–7973. https://doi.org/10.1523/JNEUROSCI.0178-06.2006

Pitzalis, S., Sereno, M. I., Committeri, G., Fattori, P., Galati, G., Patria, F., & Galletti, C. (2010). Human V6: The medial motion area. *Cerebral Cortex*, *20*(2), 411–424. https://doi.org/10.1093/cercor/bhp112

Quirk, G. J., Muller, R. U., & Kubie, J. L. (1990). The firing of hippocampal place cells in the dark depends on the rat's recent experience. *Journal of Neuroscience*, *10*(6), 2008–2017. Retrieved from http://www.ncbi.nlm.nih.gov/entrez/query.fcgi?cmd=Retrieve&db=PubMed&dopt=Citation&list_uids=2355262

Raffi, M., & Siegel, R. M. (2004). Multiple cortical representations of optic flow processing. In *Optic flow and beyond* (pp. 3–22). Springer.

Ranck, J. B. J. (1984). Head-direction cells in the deep cell layers of dorsal presubiculum in freely moving rats. *Society for Neuroscience Abstracts*, *10*, 599. Retrieved from https://ci.nii.ac.jp/naid/10016936626/en/

Redding, G. M., Clark, S. E., & Wallace, B. (1985). Attention and prism adaptation. *Cognitive Psychology*, *17*(1), 1–25. https://doi.org/10.1016/0010-0285(85)90002-7

Redding, G. M., & Wallace, B. (1996). Adaptive spatial alignment and strategic perceptual-motor control. *Journal of Experimental Psychology. Human Perception and Performance*, *22*(2), 379–394. https://doi.org/10.1037/0096-1523.22.2.379

Regan, D., & Beverley, K. (1982). How do we avoid confounding the direction we are looking and the direction we are moving? *Science*, *215*(4529), 182–194. https://doi.org/10.1126/science.7053572

Rieger, J. H., & Lawton, D. T. (1985). Processing differential image motion. *Journal of the Optical Society of America. A, Optics and Image Science*, *2*(2), 354–360. https://doi.org/10.1364/JOSAA.2.000354

Rieger, J. H., & Toet, L. (1985). Human visual navigation in the presence of 3-D rotations. *Biological Cybernetics*, *52*(6), 377–381. https://doi.org/10.1007/BF00449594

Rieser, J. J., Ashmead, D. H., Talor, C. R., & Youngquist, G. A. (1990). Visual perception and the guidance of locomotion without vision to previously seen targets. *Perception*, *19*(5), 675–689. https://doi.org/10.1068/p190675

Rogers, B. J., & Allison, R. S. (1999). When do we use optic flow and when do we use perceived direction to control locomotion? *Perception ECVP Abstract*, *28*, 0.

Rogers, B. J., & Dalton, C. (1999). The role of (i) perceived direction and (ii) optic flow in the control of locomotion and for estimating the point of impact. In *INVESTIGATIVE OPHTHALMOLOGY & VISUAL SCIENCE* (Vol. 40, pp. S764--S764).

Rouder, J. N., Morey, R. D., Speckman, P. L., & Province, J. M. (2012). Default Bayes factors for ANOVA designs. *Journal of Mathematical Psychology*, *56*(5), 356–374.

Rousseaux, M., Honoré, J., & Saj, A. (2014). Body representations and brain damage. *Neurophysiologie Clinique*, *44*(1), 59–67. https://doi.org/10.1016/j.neucli.2013.10.130

Rowland, D. C., Roudi, Y., Moser, M.-B., & Moser, E. I. (2016). Ten Years of Grid Cells. *Annual Review of Neuroscience*, *39*(1), 19–40. https://doi.org/10.1146/annurev-neuro-070815-013824

Roy, J.-P. P., & Wurtz, R. H. (1990). The role of disparity-sensitive cortical neurons in signalling the direction of self-motion. *Nature*. https://doi.org/10.1038/348160a0

Royden, C. S., Banks, M. S., & Crowell, J. a. (1992). The perception of heading during eye movements. *Nature*. https://doi.org/10.1038/360583a0

Royden, C. S., Crowell, J. A., & Banks, M. S. (1994). Estimating heading during eye movements. *Vision Research*, *34*(23), 3197–3214. https://doi.org/10.1016/0042-6989(94)90084-1

Rushton, S. K. (2004). Egocentric direction and locomotion. In *Optic flow and beyond* (pp. 339–362). Springer.

Rushton, S. K. (2008). Perceptually Guided Action: A Step in the Right Direction. *Current Biology*, *18*(1), 36–37. https://doi.org/10.1016/j.cub.2007.10.064

Rushton, S. K., & Harris, J. M. (2004). The utility of not changing direction and the visual guidance of locomotion. In *Optic flow and beyond* (pp. 363–381). Springer.

Rushton, S. K., Harris, J. M., Lloyd, M. R., & Wann, J. P. (1998). Guidance of locomotion on foot uses perceived target location rather than optic flow. *Current Biology*, *8*(21), 1191–1194. https://doi.org/10.1016/S0960-9822(07)00492-7

Rushton, S. K., & Salvucci, D. D. (2001). An egocentric account of the visual guidance of locomotion. *Trends in Cognitive Sciences*, *5*(1), 6–7. https://doi.org/10.1016/S1364-6613(00)01562-X

Rushton, S., Wen, J., & Allison, R. (2002). Egocentric Direction and the Visual Guidance of Robot Locomotion Background, Theory and Implementation. *Biologically Motivated Computer Vision*, *2525*, 27–36. https://doi.org/10.1007/3-540-36181-2_58

Rutschmann, R. M., Schrauf, M., & Greenlee, M. W. (2000). Brain activation during dichoptic presentation of optic flow stimuli. *Experimental Brain Research*, *134*(4), 533–537. https://doi.org/10.1007/s002210000502

Saj, A., Cojan, Y., Musel, B., Honor??, J., Borel, L., & Vuilleumier, P. (2014). Functional neuro-anatomy of egocentric versus allocentric space representation. *Neurophysiologie*

Clinique, *44*(1), 33–40. https://doi.org/10.1016/j.neucli.2013.10.135

Sargolini, F. (2006). Conjunctive Representation of Position, Direction, and Velocity in Entorhinal Cortex. *Science*, *312*(5774), 758–762. https://doi.org/10.1126/science.1125572

Sargolini, F., Fyhn, M., Hafting, T., McNaughton, B. L., Witter, M. P., Moser, M. B., & Moser, E. I. (2006). Conjunctive representation of position, direction, and velocity in entorhinal cortex. *Science*, *312*(5774), 758–762. https://doi.org/10.1126/science.1125572

Saunders, J. A., & Durgin, F. H. (2011). Adaptation to conflicting visual and physical heading directions during walking. *Journal of Vision*, *11*(3), 15–15. https://doi.org/10.1167/11.3.15

Saunders, J. A., & Ma, K.-Y. (2011). Can observers judge future circular path relative to a target from retinal flow? *Journal of Vision*, *11*(7), 1–17. https://doi.org/10.1167/11.7.16

Save, E., Nerad, L., & Poucet, B. (2000). Contribution of multiple sensory information to place field stability in hippocampal place cells. *Hippocampus*, *10*(1), 64–76. https://doi.org/10.1002/(SICI)1098-1063(2000)10:1<64::AID-HIPO7>3.0.CO;2-Y

Savelli, F., Yoganarasimha, D., & Knierim, J. J. (2008). Influence of boundary removal on the spatial representations of the medial entorhinal cortex. *Hippocampus*, *18*(12), 1270–1282. https://doi.org/10.1002/hipo.20511

Seiffert, A., Somers, D., Dale, A., & Tootell, R. (2003). Functional MRI studies of human visual motion perception: texture, luminance, attention and after-effects. *Cerebral Cortex*, *13*, 340–349. Retrieved from http://cercor.oxfordjournals.org/content/13/4/340.short

Singer, J. D., & Willett, J. B. (2003). *Applied longitudinal data analysis: Modeling change and event occurrence*. Oxford university press.

Smith, A. T., Greenlee, M. W., Singh, K. D., Kraemer, F. M., & Hennig, J. (1998). The processing of first-and second-order motion in human visual cortex assessed by functional magnetic resonance imaging (fMRI). *Journal of Neuroscience*, *18*(10), 3816–3830.

Smith, A. T., Wall, M. B., Williams, A. L., & Singh, K. D. (2006). Sensitivity to optic flow in human cortical areas MT and MST. *European Journal of Neuroscience*, *23*(2), 561–569. https://doi.org/10.1111/j.1460-9568.2005.04526.x

Solstad, T., Solstad, T., Boccara, C. N., Boccara, C. N., Kropff, E., Kropff, E., … Moser, E. I. (2008). Representation of geometric borders in the entorhinal cortex. *Science*,

322(December), 1865–1868. https://doi.org/10.1126/science.1166466

Souman, J. L., & Freeman, T. C. (2008). Motion perception during sinusoidal smooth pursuit eye movements: signal latencies and non-linearities. *Journal of Vision*, *8*(14), 10 1-14. https://doi.org/10.1167/8.14.10\r/8/14/10/ [pii]

Sovrano, V. A., Bisazza, A., & Vallortigara, G. (2003). Modularity as a fish (Xenotoca eiseni) views it: Conjoining geometric and nongeometric information for spatial reorientation. *Journal of Experimental Psychology: Animal Behavior Processes*, *29*(3), 199–210. https://doi.org/10.1037/0097-7403.29.3.199

Spiers, H. J., & Barry, C. (2015). Neural systems supporting navigation. *Current Opinion in Behavioral Sciences*. https://doi.org/10.1016/j.cobeha.2014.08.005

Spiers, H. J., Burgess, N., Hartley, T., Vargha-Khadem, F., & O'Keefe, J. (2001). Bilateral hippocampal pathology impairs topographical and episodic memory but not visual pattern matching. *Hippocampus*, *11*(6), 715–725. https://doi.org/10.1002/hipo.1087

Spiers, H. J., Burgess, N., Maguire, E. A., Baxendale, S. A., Hartley, T., Thompson, P. J., & O'keefe, J. (2001). Unilateral temporal lobectomy patients show lateralized topographical and episodic memory deficits in a virtual town. *Brain*, *124*(12), 2476–2489.

Stackman, R. W., & Taube, J. S. (1998). Firing properties of rat lateral mammillary single units: head direction, head pitch, and angular head velocity. *The Journal of Neuroscience : The Official Journal of the Society for Neuroscience*, *18*(21), 9020–37. https://doi.org/10.3389/fnbeh.2016.00040

Stone, L. S., & Perrone, J. A. (1997). Human heading estimation during visually simulated curvilinear motion. *Vision Research*, *37*(5), 573–590. https://doi.org/10.1016/S0042-6989(96)00204-0

Tanaka, K., Fukada, Y., & Saito, H. A. (1989). Underlying mechanisms of the response specificity of expansion/contraction and rotation cells in the dorsal part of the medial superior temporal area of the macaque monkey. *Journal of Neurophysiology*, *62*(3), 642–56. Retrieved from http://www.ncbi.nlm.nih.gov/pubmed/2769352

Tanaka, K., Hikosaka, K., Saito, H., Yukie, M., Fukada, Y., & Iwai, E. (1986). Analysis of local and wide-field movements in the superior temporal visual areas of the macaque monkey. *Journal of Neuroscience*, *6*(1), 134–144.

Tanaka, K., & Saito, H. (1989). Analysis of motion of the visual field by direction, expansion/contraction, and rotation cells clustered in the dorsal part of the medial superior temporal area of the macaque monkey. *Journal of Neurophysiology*, *62*(3),

626–641.

Taube, J. S. (1995). Head direction cells recorded in the anterior thalamic nuclei of freely moving rats. *The Journal of Neuroscience : The Official Journal of the Society for Neuroscience*, *15*(1 Pt 1), 70–86. https://doi.org/0361-9230(94)00252-5 [pii]

Taube, J. S. (1998). Head direction cells and the neurophysiological basis for a sense of direction. *Progress in Neurobiology*, *55*(3), 225–256. https://doi.org/10.1016/S0301-0082(98)00004-5

Taube, J. S., Muller, R. U., & Ranck, JB, J. B. (1990a). Head-direction cells recorded from the postsubiculum in freely moving rats. I. Description and quantitative analysis. *The Journal of Neuroscience : The Official Journal of the Society for Neuroscience*, *10*(2), 420–35. https://doi.org/10.1212/01.wnl.0000299117.48935.2e

Taube, J. S., Muller, R. U., & Ranck, JB, J. B. (1990b). Head-direction cells recorded from the postsubiculum in freely moving rats. II. Effects of environmental manipulations. *J. Neurosci.*, *10*(2), 436–447. https://doi.org/10.1212/01.wnl.0000299117.48935.2e

Taylor II, R. M., Hudson, T. C., Seeger, A., Weber, H., Juliano, J., & Helser, A. T. (2001). VRPN: a device-independent, network-transparent VR peripheral system. In *Proceedings of the ACM symposium on Virtual reality software and technology* (pp. 55–61).

Thomson, J. A. (1980). How do we use visual information to control locomotion? *Trends in Neurosciences*, *3*(10), 247–250. https://doi.org/10.1016/S0166-2236(80)80076-2

Thomson, J. A. (1983). Is continuous visual monitoring necessary in visually guided locomotion? *Journal of Experimental Psychology: Human Perception and Performance*, *9*(3), 427–443. https://doi.org/10.1037/0096-1523.9.3.427

Tolman, E. C. (1948). Cognitive maps in rats and men. *Psychological Review*, *55*(4), 189–208. https://doi.org/10.1037/h0061626

Tommasi, L., & Polli, C. (2004). Representation of two geometric features of the environment in the domestic chick (Gallus gallus). *Animal Cognition*, *7*(1), 53–59. https://doi.org/10.1007/s10071-003-0182-y

Tootell, R. B., Mendola, J. D., Hadjikhani, N. K., Ledden, P. J., Liu, A. K., Reppas, J. B., … Dale, A. M. (1997). Functional analysis of V3A and related areas in human visual cortex. *The Journal of Neuroscience : The Official Journal of the Society for Neuroscience*, *17*(18), 7060–7078. Retrieved from http://www.ncbi.nlm.nih.gov/pubmed/9278542

Turano, K. A., Yu, D., Hao, L., & Hicks, J. C. (2005). Optic-flow and egocentric-direction

strategies in walking: Central vs peripheral visual field. *Vision Research*, *45*(25–26), 3117–3132. https://doi.org/10.1016/j.visres.2005.06.017

Vallar, G., Lobel, E., Galati, G., Berthoz, A., Pizzamiglio, L., & Le Bihan, D. (1999). A fronto-parietal system for computing the egocentric spatial frame of reference in humans. *Experimental Brain Research*, *124*(3), 281–286. https://doi.org/10.1007/s002210050624

van den Berg, A. V. (1992). Robustness of perception of heading from optic flow. *Vision Research*, *32*(7), 1285–1296. https://doi.org/10.1016/0042-6989(92)90223-6

van den Berg, A. V. (1996). Judgements of heading. *Vision Research*, *36*(15), 2337–2350. https://doi.org/10.1016/0042-6989(95)00247-2

Van Oostende, S., Sunaert, S., Van Hecke, P., Marchal, G., & Orban, G. A. (1997). The kinetic occipital (KO) region in man: an fMRI study. *Cerebral Cortex (New York, NY: 1991)*, *7*(7), 690–701.

Vann, S. D. (2011). A role for the head-direction system in geometric learning. *Behavioural Brain Research*, *224*(1), 201–206. https://doi.org/10.1016/j.bbr.2011.05.033

Vann, S. D., Aggleton, J. P., & Maguire, E. A. (2009). What does the retrosplenial cortex do? *Nature Reviews Neuroscience*, *10*(11), 792–802. https://doi.org/10.1038/nrn2733

Vernon Odom, J., Ghude, P., & Humble, H. (2006). Effect of prism orientation on heading detection in optic flow. *Journal of Modern Optics*, *53*(9), 1363–1369. https://doi.org/10.1080/09500340600619239

Vishton, P. M., & Cutting, J. E. (1995). Wayfinding, displacements, and mental maps: velocity fields are not typically used to determine one's aimpoint. *Journal of Experimental Psychology. Human Perception and Performance*, *21*(5), 978–995. https://doi.org/10.1037/0096-1523.21.5.978

Wall, M. B., & Smith, A. T. (2008). The Representation of Egomotion in the Human Brain. *Current Biology*, *18*(3), 191–194. https://doi.org/10.1016/j.cub.2007.12.053

Wang, R. F., Hermer, L., & Spelke, E. S. (1999). Mechanisms of reorientation and object localization by children: A comparison with rats. *Behavioral Neuroscience*, *113*(3), 475–485. https://doi.org/10.1037/0735-7044.113.3.475

Wann, J., & Land, M. (2000). Steering with or without the flow: Is the retrieval of heading necessary? *Trends in Cognitive Sciences*, *4*(8), 319–324. https://doi.org/10.1016/S1364-6613(00)01513-8

Wann, J., & Land, M. (2001). Heading in the wrong direction. Reply to Fajen and Warren [3]. *Trends in Cognitive Sciences*, *5*(1), 8–9. https://doi.org/10.1016/S1364-

6613(00)01565-5

Wann, J. P., & Swapp, D. K. (2000). Why you should look where you are going. *Nature Neuroscience*, *3*(7), 647–648. https://doi.org/10.1038/76602

Warren, W. H., & Fajen, B. (2004). Behavioral Dynamics of Human Locomotion. *Ecological Psychology*, *16*(1), 61–66. https://doi.org/10.1207/s15326969eco1601

Warren, W. H., & Hannon, D. J. (1988). Direction of self-motion is perceived from optical flow. *Nature*, *336*(November), 162–163. https://doi.org/10.1038/336162a0

Warren, W. H., & Hannon, D. J. (1990). Eye movements and optical flow. *Journal of the Optical Society of America. A, Optics and Image Science*, *7*(1), 160–169. https://doi.org/10.1364/JOSAA.7.000160

Warren, W. H., Kay, B., Zosh, W., Duchon, A., & Sahuc, S. (2001). Optic flow is used to control human walking. *Nature Neuroscience*, *4*(2), 213–216. https://doi.org/10.1038/84054

Warren, W. H., Mestre, D. R., Blackwell, A. W., & Morris, M. W. (1991). Perception of Circular Heading From Optical Flow. *Journal of Experimental Psychology. Human Perception and Performance*, *17*(1), 28–43. https://doi.org/10.1037/0096-1523.14.4.646

Warren, W. H., Morris, M. W., & Kalish, M. (1988). Perception of translational heading from optical flow. *Journal of Experimental Psychology. Human Perception and Performance*, *14*(4), 646–660. https://doi.org/10.1037/0096-1523.14.4.646

Wehner, R., & Räber, F. (1979). Visual spatial memory in desert ants, Cataglyphis bicolor (Hymenoptera: Formicidae). *Cellular and Molecular Life Sciences*, *35*(12), 1569–1571.

Wilkie, R., & Wann, J. (2003). Controlling steering and judging heading: retinal flow, visual direction, and extraretinal information. *Journal of Experimental Psychology: Human*. Retrieved from http://psycnet.apa.org/journals/xhp/29/2/363/

Wilson, M., & McNaughton, B. (1993). Dynamics of the hippocampal ensemble code for space. *Science*, *261*(5124), 1055–1058. https://doi.org/10.1126/science.8351520

Wolbers, T., & Büchel, C. (2015). Dissociable retrosplenial and hippocampal contributions to successful formation of survey representations. *The Journal of Neuroscience : The Official Journal of the Society for Neuroscience*, *25*(13), 3333–3340. https://doi.org/10.1523/JNEUROSCI.4705-04.2005

Wood, R., Harvey, M., & Young, C. (2000). Weighting to go with the flow? *Current Biology: …*, *10*(15), 545–546. https://doi.org/10.1016/S0960-9822(00)00606-0

Wystrach, A., & Beugnon, G. (2009). Ants Learn Geometry and Features. *Current Biology*, *19*(1), 61–66. https://doi.org/10.1016/j.cub.2008.11.054

Xu, Y., Regier, T., & Newcombe, N. S. (2017). An adaptive cue combination model of human spatial reorientation. *Cognition*, *163*, 56–66. https://doi.org/10.1016/j.cognition.2017.02.016

Yoder, R. M., & Taube, J. S. (2014). The vestibular contribution to the head direction signal and navigation. *Frontiers in Integrative Neuroscience*, *8*(April), 32. https://doi.org/10.3389/fnint.2014.00032

Yuen, K. K. (1974). The two-sample trimmed t for unequal population variances. *Biometrika*, *61*(1), 165–170. https://doi.org/10.1093/biomet/61.1.165